ROLE OF CLIMATIC FACTORS AND LAND USE LAND COVER CHANGE ON STREAM FLOW PATTERN OF MAYURAKSHI RIVER BASIN, EASTERN INDIA

A THESIS SUBMITTED IN PARTIAL FULFILLMENT OF THE REQUIREMENTS FOR THE DEGREE OF DOCTOR OF PHILOSOPHY

DAVID DURJOY LAL SOREN
MZU REGISTRATION NO.: 2107597
Ph.D. REGISTRATION NO.: MZU/Ph.D./1727 of 14.11.2020

DEPARTMENT OF GEOGRAPHY AND RESOURCE MANAGEMENT
SCHOOL OF EARTH SCIENCE AND NATURAL RESOURCE MANAGEMENT
SEPTEMBER, 2024

ROLE OF CLIMATIC FACTORS AND LAND USE LAND COVER CHANGE ON STREAM FLOW PATTERN OF MAYURAKSHI RIVER BASIN, EASTERN INDIA

BY

DAVID DURJOY LAL SOREN

Department of Geography and Resource Management

Supervisor

Prof. BROTOTI BISWAS

Submitted

In partial fulfillment of the requirement of the Degree of Doctor of Philosophy in Geography and Resource Management of Mizoram University, Aizawl.

DEPARTMENT OF GEOGRAPHY AND RESOURCE MANAGEMENT
MIZORAM UNIVERSITY, AIZAWL - 796004

Phone: 0389-2330834
Mobile: 8171392579
Email: brototibiswas@yahoo.co.in
brototibiswas@gmail.com

Prof. Brototi Biswas
Professor

Post Box No. 190
Gram: MZU

CERTIFICATE

This is to certify that David Durjoy Lal Soren registered under MZU/Ph.D./1727 of 14.11.2020 is a research scholar working under my supervision on a thesis entitled **"Role of Climatic Factors and Land Use Land Cover Change on Stream Flow Pattern of Mayurakshi River Basin, Eastern India"**

All though his research pursuance, I found David Durjoy Lal Soren very serious, hardworking, and dedicated. He could challenge his tasks with quality of scholarship and was able to carry out his assignment successfully.

I further certify that the thesis in this form is the report of the research scholar's original work. Certain extracts and quotes are duly referred to in an appropriate manner.

I recommend the thesis for due evaluation and recommendation.

Date: **(Prof. B. BISWAS)**

DECLARATION

MIZORAM UNIVERSITY

MARCH, 2025

I **DAVID DURJOY LAL SOREN**, hereby declare that the subject matter of this thesis is the record of work done by me, that the contents of this thesis did not form basis of the award of any previous degree to me or to do the best of my knowledge to anybody else, and that the thesis has not been submitted by me for any research degree in any other University/Institute.

This is being submitted to the Mizoram University for the **Degree of Doctor of Philosophy in Geography.**

(Mr. DAVID DURJOY LAL SOREN)

Candidate

(Prof. CH. UDAYA BHASKARA RAO)

Head

(Prof. B. BISWAS)

Supervisor

Acknowledgment

I would like to express my deepest gratitude to my guide, Prof. Brototi Biswas, for her invaluable guidance, unwavering support, and insightful feedback throughout the course of my PhD journey. Her expertise and encouragement have been instrumental in the successful completion of this research.

I extend my sincere thanks to the Head of the Department of Geography and Resource Management, as well as all the teachers, for their continuous support and for providing a conducive academic environment that greatly contributed to my research endeavours.

I am profoundly grateful to the Chief Engineer, T&BDBO, CWC, Kolkata, and the Executive Engineer of Damodar Division, CWC, Asansol, for providing the essential hydrological data that formed a critical part of this study. Their cooperation and assistance were crucial to the success of my research.

I am deeply indebted to my family members for their unwavering support, patience, and encouragement throughout this arduous journey. Their belief in me provided the strength and motivation needed to persevere and complete this research.

Lastly, I would like to offer my heartfelt thanks to the Almighty God for His blessings and guidance, which have been my source of inspiration and strength throughout this journey.

(**Mr. David Durjoy Lal Soren**)

Contents

Table No.	List of Tables	Page No.
	Chapter- I	
1.1	Tributaries and geographic location	5
1.2	Soil coverage status of Mayurakshi basin of the basin	7
1.3	Geological setup of Mayurakshi basin based on catchment	9
1.4	Hydrological Soil Group	12
1.5	Summary of literature review	14
1.6	Journal and quantity of article	36
1.7	Distribution of article	38
	Chapter- II	
2.1	Tests of Normality	69
2.2	Decadal and long-term rainfall variation	71
2.3	Modified Mann Kendall Statistic and Sen's slope estimation	73
2.4	Change point statistics of the basin	74
2.5	Rainfall seasonality and decadal status	77
2.6	Rainfall anomaly and drought status	79
2.7	Climatic parameters	84
2.8	Trend of Climatic parameters	85
2.9	Change point of temperature	87
2.10	Forecasted rainfall status (2021 to 2030)	88
	Chapter- III	
3.1	Image collection for LULC classification	100
3.2	LULC class description	108
3.3	Accuracy assessment	109
3.4	Error matrix of Accuracy Assessment 1991	109
3.5	Error matrix of Accuracy Assessment 1996	109
3.6	Error matrix of Accuracy Assessment 2002	109
3.7	Accuracy assessment	110
3.8	Error Matrix of Accuracy Assessment 2008	110
3.9	Error Matrix of Accuracy Assessment 2014	111
3.10	Error Matrix of Accuracy Assessment 2020	111
3.11a	LULC status (1991, 1996, 200)	114
3.11b	LULC status (2008, 2014, 2020)	114
3.12	LULC status of lost and gain	114
3.13	Conversion Matrix 1991 – 1996	117
3.14	Conversion Matrix 1996 – 2002	117
3.15	Conversion Matrix 2002 – 2008	117
3.16	Conversion Matrix 2008 – 2014	118
3.17	Conversion Matrix 2014 – 2020	118
13.18	Contingency matrix number of actual 2020 and simulated	121

Chapter 1: INTRODUCTION

1.1 Introduction

Climate change is currently a very important concern. It poses a threat to both bio and non-bio resources. Numerous changes in the environmental and socioeconomic fields are owed to climate change (Croitoru & Minea, 2014). The hydrological responses of the basin are directly related to climate and direct human intervention, like various misuses of water for anthropogenic causes, like industrialization, irrigation, domestic uses, and agriculture (Wang et al., 2021).

The stream flow is impacted by climate change (Su et al., 2016). The primary cause of climate change is an increase in temperature, which is closely related to the cycle of water resources (Bronstert et al., 2002). The continuous accumulation of greenhouse gases is expected to change regional temperatures and precipitation, which have a direct impact on water resources (Nash et al., 1991). The functional relationship among the variables that directly or indirectly influence the runoff was paid attention to by the researchers in the 1970s and 1980s. Thereupon, runoff estimation and future prediction based on the mathematical model became a prime focus for assessing rainfall-runoff relations and water demand for future uses (Zealand et al., 1999). At present, researchers around the globe have focused on mathematical models to estimate the human activity and climate change impact on runoff change (Cao et al., 2015; Kan et al., 2015; Li et al., 2015). At the beginning of the 20th century, runoff response was studied mostly based on geophysical conditions, leading to the development of the paired catchment concept (Langbein, 1949).

Many models and climatic change projections have been developed by scientists for watershed management and future climatic prediction with hydrological responses (Jung et al., 2012; Pourmokhtarian et al., 2012; Boni et al., 2013; Biswas et al., 2019). Various studies have been conducted on modeling scenarios that heavily rely on streamflow regimes while estimating the changes in hydrological response on both local and global scales (Döll and Zhang, 2010; Fung et al., 2011).

The worsening effect of climate change and anthropogenic activity has increased a world-wide water crisis that has been focused on in global hydrological research (IPCC, 2007; Kumar et al., 2020). According to the Fourth Assessment Report of the Intergovernmental Panel on Climate Change (IPCC), the intensity and frequency of precipitation and temperature variations will rise due to climate change and anthropogenic impacts (Parry et al., 2007). The regional and worldwide distribution of water resources, both spatially and temporally, is strongly influenced by climate change and changes in land cover spurred by human activity in the 20th century. (Scanlon et al., 2007; Solomon et al., 2007; Ling et al., 2011). Some of the studies stated a positive correlation between temperature and stream flow (Nijssen et al., 2001; Arnell, 2003; Wang et al., 2011), while on the contrary, high temperatures enhance the evapotranspiration of plants, thereby reducing runoff (Frederick and Major, 1997), whereas some studies stated that climate change decreased streamflow (Yilmaz and Imteaz, 2011; Chang et al., 2014). The change in runoff (either increase or decrease) consequently influences sediment yield and its temporal-spatial distribution (Zhang and Wang, 2007).

It is widely recognized that one of the key factors that will be affected by climate change is the availability of water. The basic concepts of water resource planning encompass stream flow and hydrological process analysis. This basin is an important agro-based area that depends on irrigation for agricultural practice. Thus, the investigation in the present work has an immense bearing on society. For the sake of future management of runoff conditions, the study of the intensity and magnitude of climate change has greater importance to decision-makers (Chang et al., 2014). Climate change impact on runoff and discharge is an important study domain; thus, a proper review of this topic can formulate sustainable knowledge to proceed with further research interest in the ‘climate change impact in stream-flow domain’.

1.2 Statement of Research Problem

This study is framed to assess the impact of climatic variability and land use land (LULC) cover dynamics on the alteration of runoff patterns in the Mayurakshi river basin located in the eastern Indian monsoonal tropical climate. The purpose of

this research is to evaluate the complex interaction of climate change and LULC change patterns on the runoff of the basin. The upper portion of the basin is the extended part of the Chotonagpur plateau, while the lower part of the basin is a plain area with agricultural practices. A lot of changes in climatic conditions and LULC have taken place in the last couple of decades (refer to Chapters 2 and 3). The diversity of topography, its climatic variability, and LULC dynamics have extended to the complex nature of the basin, making it ideal for runoff-related studies of the basin. Many studies have reported that the runoff response varies from region to region, including the conditions of soil, geology, lithology, climate, human interventions, and LULC patterns (Sun et al., 2004; Wang et al., 2013; Mitra et al., 2021). Few studies were conducted in the present study area based on drainage basin morphometry and flood analysis (Islam et al., 2020), hydro-morphological characteristics, and land use modification (Mukhopadhyay et al., 2013). Thus, the study of water resource management and the effect of climate change and LULC dynamics on the runoff is an unknown aspect of the Mayurakshi river basin. Thus, the present study is a plausible attempt to fill this research gap.

1.3 Study Area

The Mayurakshi River system is one of the most important river systems in eastern India. The river originates from Trikut Hill in the Chota Nagpur plateau of Jharkhand state. The basin is located between the coordinates of 23° 63′ 12″ to 24° 51′ 3″ N latitude and 86° 84′ 38″ to 88° 16′ 12″ E longitude, spreading across the states of Jharkhand and West Bengal, covering an area of 5004.99 km^2 (Fig. 1.1). Geologically, the whole area of the upper part of the basin dates back to the Proterozoic eon formation of undivided Precambrian rock. The middle catchment of the basin is most dominantly deposited by laterite and lateritic soil, and the lower catchment of the basin is mostly covered by young and old alluvial soil. The formation of the lower basin can be dated back to the quartanery eon, while the middle portion of the basin is dominated by jurassic cretaceous formation, sparsely dated back to the late carboniferous Permian eon.

The Masanjor Dam, which was commissioned in 1955, is situated in the Mayurakshi river basin in the Dumka district of Jharkhand. It is 2170 feet in length

and stands 155 feet high from its base, with an overflow section extending 225.60 meters. The dam has a storage capacity of 617,000,000 m^3 and a discharge capacity of 4.446 m^3/s. Tilpara Barrage downstream, 29.5 km away from the Masanjor Dam, was commissioned in 1949 on the Mayurakshi River. The Tilpara Barrage was constructed for irrigation and other agricultural activities.

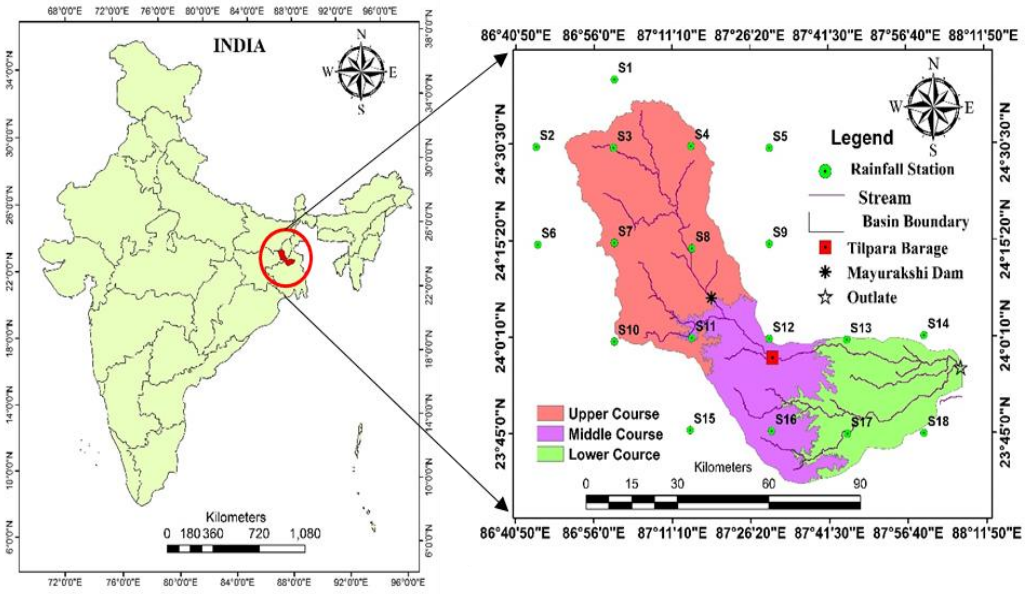

Fig. 1.1: Study area

1.4 Drainage System

The Mayurakshi River is a rain-fed river that originated from Trikut Hill on the Chota Nagpur plateau of Jharkhand state. The river valley consists of many rills and gullies that form a dendritic drainage pattern. The river Mayurakshi flows through two states, Jharkhand and West Bengal. In Jharkhand, it covers three districts: Deoghor, Jamtara, and Dumka. Dumka district comprises most of the tributaries of the upper catchments of the Mayurakshi basin (Table 1.1). In West Bengal state, the Mayurakshi River flows through Biurbhum and Murshidabad districts. The majority of the tributaries of this river remain dry in the summer season since the river relies 80% on monsoon rain. The major tributaries of the upper catchment are Motihara, Tepra, Bhamri, Dhobi, Bhurbhuri, and Pusaru. The largest tributary of the upper catchment is Sidheswari, about 53.89 km long, which

originated at Fatapur in Jamtara district. In the middle course of the basin, there are Bakreswar (63.63 km) and Khuskarini (26.69 km) in West Bengal state. In the lower course, there are two tributaries: Kopai (27.83 km) and Kolya (43.25 km) (Table 1.1).

Table 1.1: Tributaries and geographic location

Sl No	Tributaries	Length (Km)	Origin	District	State	Course
1	Motihara	37.54	Deoghar	Deoghar	Jharkhand	Upper Course
2	Tepra	39.58	Jharmundi	Dumka	Jharkhand	Upper Course
3	Bhamri	14.95	Masalia	Dumka	Jharkhand	Upper Course
4	Dhobi	46.11	Ramghar	Dumka	Jharkhand	Upper Course
5	Bhurbhuri	18.8	Ramghar	Dumka	Jharkhand	Upper Course
6	Pusaru	11.8	Jama	Dumka	Jharkhand	Upper Course
7	Sidheswari	53.89	Fatapur	Jamtara	Jharkhand	Upper Course
8	Khuskarini	26.69	Rajnagar	Birbhum	West Bengal	Middle Course
9	Bakreswar	63.63	Dubrajpur	Birbhum	West Bengal	Middle Course
10	Kopai	27.83	Bolpur	Birbhum	West Bengal	Lower Course
11	Kolya	43.25	Labpur	Birbhum	West Bengal	Lower Course

The average drainage density of the basin is 0.26 km/km^2 with the drainage density ranging between 0.22 to 0.35 km/km^2 in the upper, middle, and lower course of the river basin (Fig. 1.2). The Mayurakshi river basin is considered one of the most flood-prone basins in India. The line density method was applied to better visualize the drainage density of the basin. The middle and lower courses of the basin are mostly high drainage density areas, thereby making them flood-prone zones.

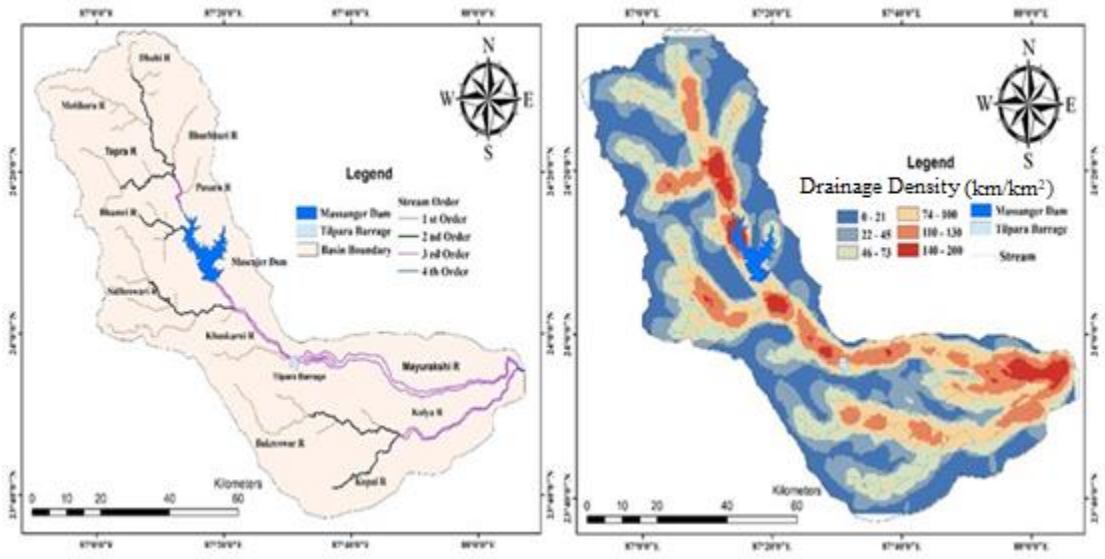

Fig. 1.2: Stream (A) and Drainage density (B) of the basin.

1.5 Soil

The soil of the Mayurakshi basin has been identified as Entisols, Alfisols, and Ultisols (National Remote Sensing Center) (Fig. 1.3). The categories of alfisols are Older Alluvial, Red Lomy, Palue Stulfs Loamy, Red Sandy, and Huplustafs Clayey. The Alfisols order of soil categories dominantly covered 75.86% of the area, followed by Ultisols at 17.87% (laterite) and Entisols at 6.269% (Ustochrents Clayey, Younger Alluvial). As in the individual soil category, Red Sandy (Alfisols) covers 39.68% of the area. Alfisols are clay-enriched soils containing mostly Al- and Fe-iron contents. Alfisols are ordered by soil taxonomy and are dominantly covered in the upper catchment of the basin due to the favorable humid and sub-humid growing conditions of the climate over the basin. The second highest soil coverage is older alluvial soil, which covers 18.97% of the basin area. The older alluvial soil, also known as Bhangar soil, is basically less fertile than the alluvial soil found in the lower portion of Birbhum district. The next dominant soil group is utisols, which are characterized as an acidic, clay-rich, reddish soil not suitable for agriculture but naturally suitable for forestry because of their high concentration of acidity and low retention of moisture. Laterite soil is one of the Utisols taxonomic soils that covers 894.78 km^2 of the middle basin area (Table 1.2). This aluminum and iron-rich soil has developed in the hot and humid weather conditions in the entire Birbhum district

of the basin. Entisols taxonomic soil of Younger Alluvial covered 277.04 km^2 of the lower part of the basin. It is formed by the accumulation of clay, sand, silt, gravel, and organic matter flowing from the upper and middle courses of the basin. This fertile plain in the lower catchment is well supported for kharif and rabi crops.

Table 1.2: Soil coverage status of Mayurakshi basin of the basin

Soil	Area (sq. km)	Percentage
Younger Alluvial (Entisols)	277.04	5.53
Older Alluvial (Alfisols)	949.5	18.97
Laterite (Ultisols)	894.78	17.87
Red Lomy (Alfisols)	84.16	1.68
Ustochrents Clayey (Entisols)	36.36	0.72
Palue Stulfs Loamy (Alfisols)	205.58	4.10
Red Sandy (Alfisols)	1986.18	39.68
Huplustafs Clayey (Alfisols)	571.39	11.41

Source:- NRSC

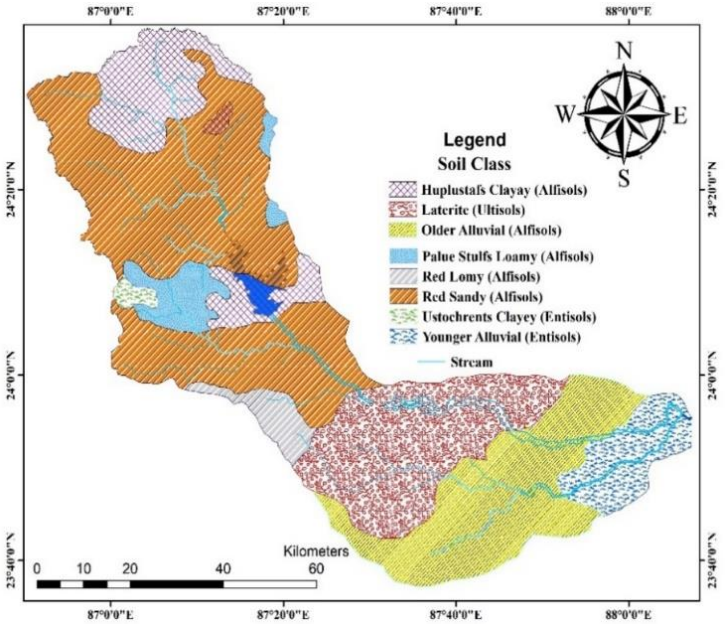

Fig. 1.3: Soil status of Mayurakshi basin

1.6 Geology

Geologically, the whole area of the upper part of the basin dates back to Proterozoic and Phanerozoic eon formations of undivided Precambrian rock. The upper part of the basin administratively belongs to the Dumka district, and geologically, it covered mostly unclassified granite gneiss with enclaves of metamorphic rocks covering about 1407.19 km^2 (26.64%) of the upper part of the basin (Fig. 1.4 and Table 1.3). It is a Chotonagpur gneissic complex from the Proterozoic eon. The south and southwest parts of the upper basin were mostly covered by laterite and lateritic soil, which covered 12.20% of the basin. A narrow strip of sandstone and shale is found in the north-western part of the upper basin area (177.32 km^2), and the north-eastern portion of the basin is covered by basalt and inter-trapped bed-chert (178.38 km^2). The north-western portion is composed of a small patch of 64.54 km^2 (1.22%) of acid-intrusive Granodiorite, Homblend schist, and amphibolite formations of the Proterozoic eon. Very small patches of Augen gneiss, migmatite, and chamokite/acid granulite are strewn over the upper part of the basin (Table 1.3).

The middle catchment of the basin dates back to the Phanerozoic eon of the Mesozoic era in Jurassic to Cretaceous formation. This middle catchment of the basin is most dominantly deposited by laterite and lateritic soil, covering about 385

km^2 (7.29% of the whole basin), followed by siltstone, sandstone, and shale, with alluvium covering 361.68 km^2 (6.85% of the whole basin). Unclassified granite gneiss with enclaves of metamorphic deposition (289.51 km^2) covers the upper part of the middle catchment of the basin. The Rajmahal trap of the Jurassic to Cretaceous period is an important geological deposition of laterite and lateritic soil in the middle catchment. The lower catchment of the basin is mostly covered by young and old alluvial deposition dating back to the Triassic period of the Mesozoic era to the upper Carboniferous period of the Palaeozoic era. These two depositions are found in this lower catchment of the basin: hard clay impregnated with caliche nodules, 451.29 km^2, followed by siltstone, sandstone, and shale with alluvial 635.7 km^2 (Table 1.3).

Table 1.3: Geological setup of Mayurakshi basin based on catchment

Catchment	Geology	Area (sq. km)	Percentage
Upper Catchment	Siltstone, sandstone, Shale with alluvium	12.48	0.24
	Laterite and lateritic soil	644.34	12.20
	Sandstone and shale	177.32	3.36
	Basalt / Inter trappen bed-chert	178.38	3.38
	Homblend schist and amphibolite	64.54	1.22
	Augen gneiss and megmatite	99.99	1.89
	Chamokite / Acid granulite	45.17	0.86
	Unclassified granite gneiss with enclaves of metamorphic	1407.19	26.64
Middle Catchment	Silt stone, sand stone, Shale with alluviam	361.68	6.85
	Hard clay impregnated with caliche nodules	205.72	3.89
	Laterite and lateritic soil	385.00	7.29
	Sandstone and shale	18.31	0.35
	Homblend schist and amphibolite	10.12	0.19
	Chamokite / Acid granulite	18.25	0.35
	Unclassified granite gneiss with enclaves of metamorphic	289.51	5.48
Lower Catchment	Silt stone, sand stone, Shale with alluviam	635.7	58.48
	Hard clay impregnated with caliche nodules	451.29	41.51

Source: Bhukosh

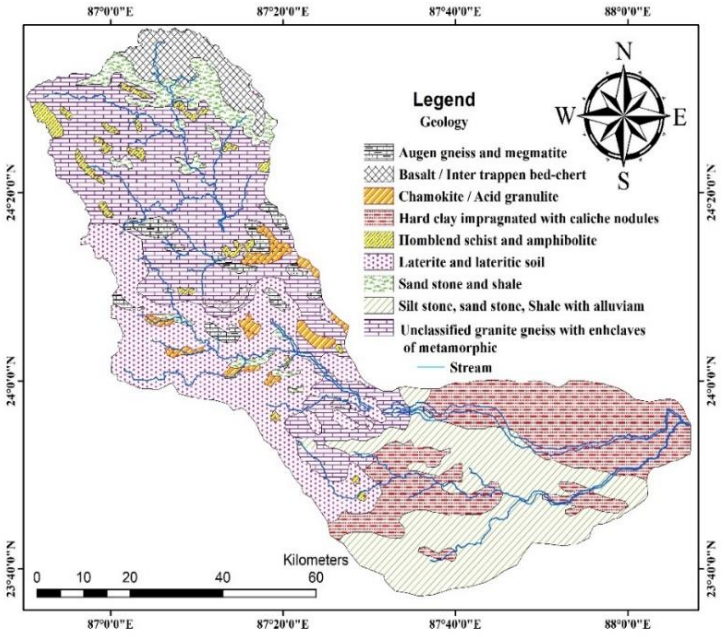

Fig. 1.4: Geological environment of Mayurakshi basin

1.7 Relief

Relief of the upper catchment of the Mayurakshi basin is very undulating and covered with flat-topped isolated hills; most of which are >300 meters (Fig. 1.5). The upper catchment is part of the Deoghar, Jamtara, and Dumka districts, characterized as the fringe of the Chotanagpur plateau covered by undulating relief and isolated hills like *Trikut* pahar (elevation 753 m., 24 29N, 86 51E) in the north west and in the north east, Jangalpur pahar (elevation 377 m., 24°28'48.53"N, 87°14'17.68"E), *Amgachhi* Pahar (elevation 310 m., 24°10'1.00"N, 87° 8'18.29" E), Panjapahari (elevation 311 m., 24° 6'43.10"N, 87°20'11.87"E), Supriya Hill (elevation 185., 24° 6'14.13"N, 87°18'16.77"E 610). The middle catchment of the basin is the portion of Birbhum district of West Bengal state, also known as the Rarh region. It is an eastward extended undulating fringing portion of the Chotonagpur plateau that ranges from 71m to 120m in height. The lower catchment is mostly encompassed by parts of the Birbhum, Burdwan, and Murshidabad districts of West Bengal in the lower-lying floodplain. The lower catchment is characterized as a plain of deposited sand, silt, and clay from the Bakreswar, Kopai, and Mayurakshy rivers.

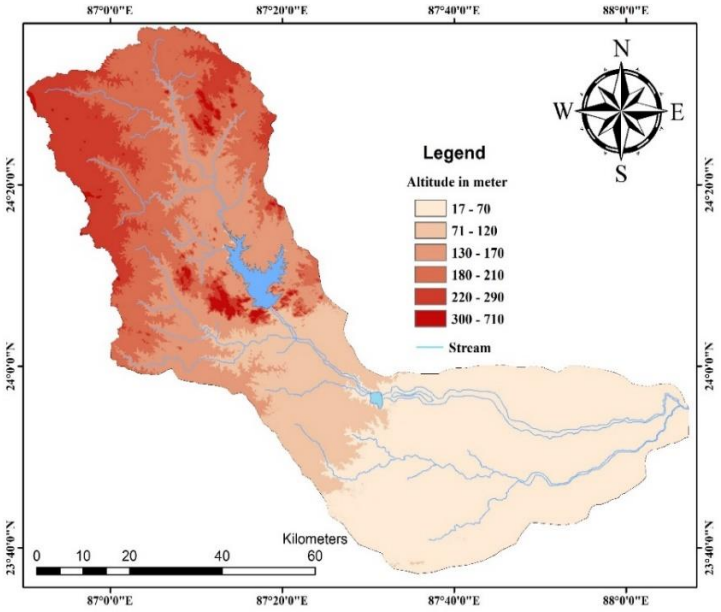

Fig. 1.5: Elevation status of the basin

1.8 Hydrological Soil Groups

Hydrological soil groups (HSGs) are the fundamental soil classification of curve number (CN) initiated by the United States Department of Agriculture (USDA) that includes the texture of the soil to estimate rainfall runoff. The study area covers HSGs - C known for a runoff potential moderately high, D known for high runoff potential, and C/D and D/D known for high runoff potential unless drained. The basin is covered by 71.58% of HSG-C and 23.95% of HSG-C/D, where HSGs D and D/D cover 1.86% and 2.61% of the area, respectively (Fig. 1.6 and Table 1.4).

Table 1.4: Hydrological Soil Groups

HSGs	Area (Sq.km)	Area (%)
C	3582.40	71.58
C/D	1198.67	23.95
D	93.28	1.86
D/D	130.64	2.61

Source: soilgrids.org

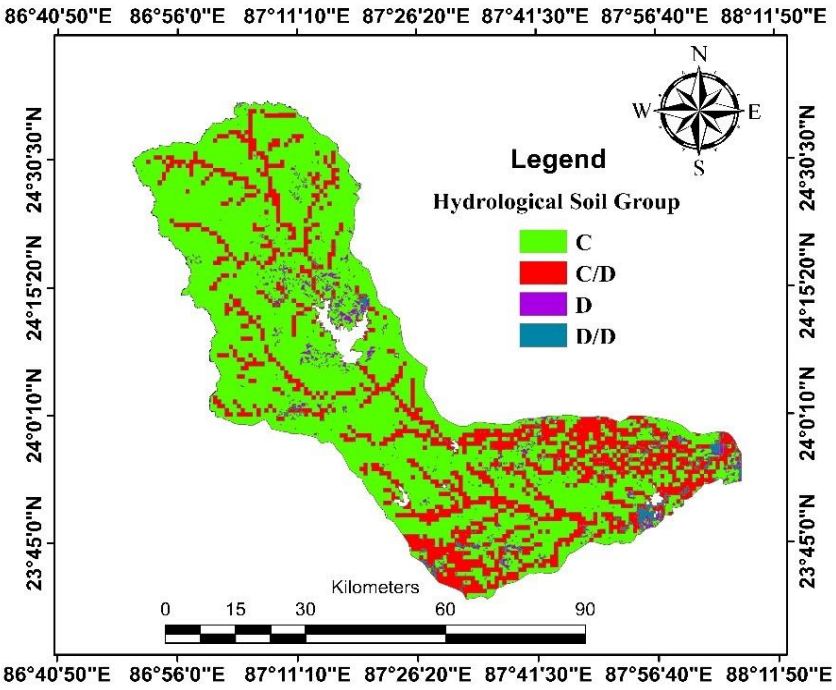

Fig. 1.6: Hydrological Soil Group

1.9 Overview of related studies

1.9.1 Review of literature

A lot of research has studied the runoff responses with respect to climatic parameters and human interference. An extensive literature review has been done to determine the outcome of climate change and its anthropogenic impact on runoff, as well as the methods and findings. The articles were reviewed simultaneously and grouped into clusters (1–5) based on the following topics: (i) climate change effects on runoff; (ii) anthropogenic and climate change impacts on runoff; (iii) effects of climate change on runoff and ecosystems; and (iv) effects of climate change on streamflow and hydropower. (v) Climate change impacts stream flow and sediment yield.

The clustered articles were grouped based on the year of publication, and the articles were summarized systematically based on the author's name and year. The review of the literature was aimed at the purpose of the research conducted, methodology, and key findings. The investigation of climatic variability and its impact on stream flow was aided by the prepared database.

1.9.2 Overview of important literature

The increase in global average air temperature and an increase in potential evaporation have significantly affected the hydrological cycle. This, in turn, has affected the stream flow (IPCC, 2007). Al-Faraj et al. (2014) studied climate change as the reason for drought occurrences. The volume of runoff is an important concern to mitigate drought phenomena in the downstream area. Drought and climate change put adverse pressure on water resource management and considerably increase the level of water paucity in downstream countries (Table 1.5). Müller Schmied (2012) asserted that the main cause of the shift in mean annual runoff is climate change. Climate change's effects on discharge/runoff calibration were investigated by Githui et al., 2009; Phan et al., 2011; Zhang et al., 2012; Li et al., 2015; Oliveira et al., 2017; Qiu et al., 2019; Huo et al., 2013; Hagemann et al., 2013; who used the Soil and Water Assessment Tool (SWAT) as model validation. Gupta et al. (2011) applied the global circulation model and the SCS model to estimate the effect of climate change on runoff. Stream and lake eutrophication might be substantially impacted by climate change in terms of phosphorus transfer and collaboration with changes in nutrient loading, which may strengthen eutrophication symptoms in lakes (Jeppesen et al. 2009). The hydrological model was used to determine the change in runoff induced by both human-caused and natural factors (Lei et al. 2014). Meng et al. (2011) argued that annual potential evaporation was more significant than annual precipitation to reduce runoff. The insight was given to annual runoff change and makes a future runoff change prediction. Based on the future prediction hypothesis, empirical equations are developed and validated in the different watersheds. Narsimlu et al. (2013) found that climate change studies are helpful for the conservation of soil water management planning, crop conservation, and drought tolerance crop management planning. Climate change also influences river ecosystems, species abundance, and ecosystem services (Schneider et al., 2013). Chen and Chen (2014) applied sensitivity analysis to detect the climate change effect on runoff. This method can provide valuable insights into how the hydrological components will respond to future climate change. Tang et al. (2012) studied the changing nature of stream flow by applying the Variable Infiltration

Capacity (VIC) model to the increasing trend of temperature change and change in stream flow that harmed water management and ecology. P. Doll and J. Zhang (2010) studied the effect of climate change on river flow regimes and freshwater ecosystems and concluded that by the end of the 2050s, climate change will affect the ecological characteristics of the river.

Table 1.5: Summary of literature review

SL No	Author(s) and Journal	Purpose	Sample	Method	Key findings
	Cluster 1: Climate change effects on runoff				
1	Githui *et al.,* (2009) Int. J. Climatol	To assess the climatic impact on runoff change.	Western Kenya	Soil and Water Assessment Tool	Assessed the potential future climatic changes. Stream-flow response was not sensitive only to temperature but also depended on population growth and land cover.
2	Jeppesen *et al.,* (2009) J. Environ	To assess Climate change effects on runoff and potential adaptations.	Denmark	Climate change projections, General Circulation Model, Hydrological NAM model	Climate change has a deep impact on phosphorus (P) transport in streams and on lake eutrophication.
3	Roderick *et al.,* (2011) Water Resources Research	To study relating variations in runoff to variations in climatic conditions and catchment properties	Murray-Darling Basin, Southeast Australia	Budyko-type equation	Climate change was attributed to a 10% change in precipitation resulting in 26% change in the runoff which was predicted by using the Intergovernmental Panel on Climate Change AR4 climate model.

4	Yang *et al.,* (2011) Water Resources Research	To examine the climate elasticity of runoff and to assess the effects of climate change on annual runoff	Hai River Basin, China	Climate Elasticity	Evaporation elasticity, precipitation elasticity, and catchment characteristics were very sensitive to climate change. 1% change in precipitation leads to 1.6% to 3.9% change in the runoff, and 1^0C of temperature change leads 2% decrease in the runoff.
5	Bauwens *et al.,* (2011) Hydrol. Earth Syst. Sci	To study hydrological response to climate change	Wallonia, Belgium	Physically Based Model	Physically-based model was used to understand the water-soil-plant relation with climate change impact. The projected climate change trend was a 10% decrease in evapotranspiration could lead to a decrease of 17% in stream flow.
6	Meng *et al.,* (2011) Hydrol. Process.	To assess the effect of climate change on mean annual runoff	Songhua River Basin, China	Schreiber Equation, Penman-Monteith (P-M) Equation, General Circulation Model	Changing the nature of climatic variables like temperature and wind speed increased evapotranspiration and runoff.
7	Gupta *et al.,* (2011) J Indian Soc. Remote Sens.	To study the impact of Climate change on Runoff	India	Soil Conservation Service Curve Number Method	Future prediction analysis indicated a decrease in runoff all over

					India with climate change. Significant runoff reduction was found on the Subarnarekha River, the lower parts of the Ganga, upper parts of the Mahanadi and Bahamani-Baitrani Rivers.
8	Yilmaz *et al.,* (2011) Hydrological Sciences Journal	To assess the impact of climate change on runoff	Euphrates Basin, Turkey	Mann-Kendal Test, Spearman's rho Tests, Distributed Models, Regional Circulation Model	A futuristic climate change database was produced using various hydrological models. The projected model shows a 34%, 13%, 10%, and 28% runoff decline in summer, spring, winter, and autumn respectively.
9	Tang *et al.,* (2012) Global and Planetary Change	To assess the streamflow sensitivity to temperature increases	Salmon River Basin, Idaho	Variable Infiltration Capacity (VIC) Model	The result shows a decrease in stream flow with increasing temperature. The increase of temperature 2 °C and 3 °C decrease streamflow 2% to 6% and 3 to 8%, respectively.
10	D¨oll *et al.,* (2012) Environ. Res. Lett	To evaluate the impact of climate change on mean annual runoff and river flow regimes	A global overview	Water GAP Global Hydrology Model (WGHM)	Anthropogenic factors reduced river discharge. Mean annual runoff will increase by 10%

					on 50% of the global land area
11	Leppi *et al.,* (2012) Climatic Change	To study the impacts of climate change on stream discharge	Central-Rocky Mountain, US	Shapiro-Wilk test, Mann-Kendall Test	The result shows a negative correlation between temperature and discharge. A significant decline in discharge was found over the last half-century.
12	Wu *et al.,* (2012) Quaternary International	To inspect the climatic effects of the Three Gorges Reservoir and simulation of runoff.	Yangtze River, China	Regional Climate Models, Double Nested Method	A significant increase in temperature and a decrease in precipitation over the Three Gorges area.
13	Zhang *et al.,* (2012) Journal of Hydrology	To study the effect of forest harvesting and climatic variability on runoff	Yangtze River Basin, China	Non-parametric Tests (Mann–Kendall, and Spearman), Time Series Cross-Correlation Analysis	The significant break point of annual runoff change was examined in 1969. Forest harvesting had a significant role in the dry season and annual runoff (an increase of 38 mm/yr).
14	Zhang *et al.,* (2012) Journal of Hydrologic Engineering	To examine hydrologic simulation to explore the impacts of climate change on runoff	Huaihe River Basin of China	Variable Infiltration Capacity Model	The increase of annual runoff, both regional shortage of water and flood occurrence was accelerated owing to global warming.
15	Huo *et al.,* (2013) Environ Earth Sci	To assess the impact of climate change on stream flow in a typical debris flow	Jianzhuangcuan Catchment Shaanxi Province, China	Soil and Water Assessment Tool	Future climate change scenario generated from 2020 to 2030. It was concluded

		watershed			that the climate of the study area would become warmer.
16	Luo *et al.,* (2013) Science of the Total Environment	To examine the impact of climate change on hydrology and water quality through watershed modeling approach	California	Soil and Water Assessment Tool	A decrease in stream flow was predicted with reduced precipitation in summers while an increase in stream flow during winter. Modified SWAT model incorporated with CO_2 impacts and future stream flow prediction.
17	Schneider *et al.,* (2013) Hydrol. Earth Syst. Sci.	To study how climate change modified river flow regimes	Europe	Global Hydrology Model WaterGAP3	WaterGAP3 indicated that snow cover will be reduced for the boreal climate zone. River flows will likely be lower in the 2050s.
18	Arnell *et al.,* (2013) Journal of Hydrology	To study the impacts of climate change on river flow regimes	A world view	Coupled Model Intercomparison Project Phase 3	The model scenario (Hadley Centre HadCM3) shows a 47% significant increase in annual runoff across the Equator, eastern Europe, Canada, and high-latitude Siberia, and a decrease of runoff (37%) in the Mediterranean, Central America, Brazil, and central Europe.

19	Hagemann *et al.,* (2013) Earth System Dynamics	To examine the Climate change impact on available water resources	A world view	global climate and hydrology models	The projected result shows a 10% decrease in water resources in parts of Europe, the catchments of the Euphrates/Tigris in the Middle East, Murray in SE Australia, Zhu Jiang in southern China.
20	Janzˇa *et al.,* (2013) Nat Hazards	To assess the impact of projected climate change on the hydrological regime	Upper Socˇa River basin, Slovenia	Distributed Hydrological Model MIKE SHE	The study is based on future predictions (2011–2040, 2041–2070, 2071–2100). Future projection shows an increase of average temperature - 0.9^0C, 02.3^0C, and 3.8^0C respectively, thereby reducing runoff and groundwater recharge.
21	Narsimlu *et al.,* (2013) Water Resour Manage	To examine the future climate change impacts on water resources	Upper Sind River Basin, India	Soil and Water Assessment Tool, Sequential Uncertainty Fitting Algorithm (SUFI2)	The result shows a predicted increase in the annual stream flow in the mid-century and end-century by 16.40% and 93.50% respectively.
22	Crossman *et al.,* (2013) Journal of Great Lakes Research	To study the impact of climate change on hydrology and water quality along with	Lake Simcoe watershed, Canada	Global Circulation Model	The projected IPCC scenario shows increased precipitation during winter and an increase in

		management strategies			temperature in summer throughout the 21st century.
23	Al-Faraj *et al.,* (2014) Water	To examine the sensitivity of surface runoff to drought and climate change	Diyala river basin shared between Iraq and Iran	Meteorological Drought Severity, Streamflow Drought Index, Rainfall-Runoff Model	A decrease in water resources by 17.30 % annually was projected owing to climate change.
24	Giang *et al.,* (2014) Hindawi Publishing Corporation Scientific World Journal	To examine the impact of climate change on water resources	Upper Ca River Watershed in Southeast Asia	Soil and Water Assessment Tool	The result indicated an increase of temperature by 3.4^0C and evaporation in the 2090s. The discharge will increase in the wet season and will decrease in the dry season at a rate of ±25%.
25	Liersch *et al.,* (2014) Hydrol. Earth Syst. Sci.	To study the impact of climate change on streamflow	African river basins	Soil and Water Integrated Model	Results showed a statistical correlation between precipitation and runoff in the Nile valley, and some African regions.
26	Lei *et al.,* (2014) Journal of Hydrology	To study the impact of climate change and vegetation dynamics on runoff in the mountainous region	Haihe River Basin, Northern China	Community Land Model, River Transport Model	The climatic variables of precipitation, solar radiation, air temperature, and wind speed counted as 56%, 14%, 13%, and 5% respectively which accounted for the overall reduction

					in the annual runoff since 1960.
27	Lin et al., (2014) Front. Earth Sci.	To explore changes in runoff and eco-flow	Dongjiang River of the Pearl River Basin, China	Mann-Kendall test , Pettitt-Mann-Whitney Change-Point Statistics, Indicators of Hydrologic Alteration	The trend analysis depicts the increasing rate of annual median flow from 1957 to 2010 with a significant change point between 1970 to 1974 due to climate change and the construction of reservoirs.
28	Oni *et al.,* (2014) Science of the Total Environment	To examine uncertainty assessments and hydrological implications of climate Change	Southern Ontario	Statistical Downscaling Model, Physically-Based Semi-Distributed Rainfall-Runoff Model	Human activities increased the differences in integrated hydrological responses.
29	Yang et al., (2014) Water Resources Research	An assessment of error analysis of the Budyko hypothesis on the contribution of climate change to runoff	Hai River Basin, China	Budyko Hypothesis, Mann-Kendall test	Negative correlation between precipitation and potential evaporation..
30	Chen *et al.,* (2014) Front. Earth Sci	To study the effects of climate fluctuations on runoff	Kaidu River in Northwestern, China	Mann-Kendal Test	The result shows an increasing trend of precipitation and runoff over the past 50 years.
31	Croitoru *et al.,* (2014) Theor Appl Climatol	To study the impact of climate changes on river discharge	Moldavia region, Romania	Mann–Kendall Test, Sen's Slope	The result shows an increase in summer precipitation resulting in increased river discharge in 80% of the rivers. The

					opposite was found in winter owing to reduced precipitation.
32	Yates *et al.,* (2014) International Journal of Water Resources Development	To study the climatic impact on runoff based on an integrated water balance model	Mulberry Basin in Arkansas, USA	WatBal Model, Priestley Taylor Method	An increase in temperature by 1^0C caused a reduction of precipitation by 2%. Change of precipitation ± 10% and ± 20% produced ± 12% and ±23% changes in runoff, respectively.
33	Yang *et al.,* (2014) Journal of Geophysical Research: Atmospheres	To study the climate change and probabilistic scenario of streamflow extremes	Yellow River Basin, China	Artificial Neural Network Downscaling Models	The result showed a decreasing trend of streamflow in the Alpine region and predicted an extreme change in streamflow in the future.
34	Kwadijk and Middelkoop, (2014) Climatic Change	To estimate the climate change on peak discharge variability	Rhine River, Germany	RHINEFLOW Model	With an increase of temperature by 4°C, stream flow is reduced by 6%, and a 20% decrease in precipitation leads to a 30% lower peak flow.
35	Goulden *et al.,* (2014) J. Earth Syst. Sci.	To study mountain runoff vulnerability with increased evapotranspiration and vegetation expansion	upper Kings River basin, Southern California	Climate Projections	Climatic projection shows in 2100 evaporation could increase 28% and river flow will decrease 26%.

36	Stagl *et al.,* (2015) *Water*	To study the impacts of climate change on the hydrological regime	Danube River catchment, Europe	Soil and Water Integrated Model	The result shows that runoff reduces in summer and increases in winter.
37	Vano *et al.,* (2015) Water Resources Research	To study the Seasonal hydrologic responses to climate change	Columbia River basin and its adjacent coastal drainages	Variable Infiltration Capacity (VIC) land-Surface Hydrology Model	The runoff decreasing rate was higher in a warm season by about 74%. Runoff increased in the cold season at the rate of 26%.
38	Uniyal et al., (2015) Water Resour Manage	To assess Climate Change Impact on Water Balance Components	Upper Baitarani River Basin of Eastern India	Soil and Water Assessment Tool	Change in temperature from 1°C to 5°C caused a reduction in the surface runoff by 2.5% to 11%, respectively. While increasing the nature of rainfall 2.5% and 15% suggested increasing runoff from about 6.67 % to 43.42%. A change in evapotranspiration by 5.05% to 11.88% rise would change groundwater recharge by 8.7% to 23.15%, respectively.
39	Zhang *et al.,* (2015) Quaternary International	To study the changes in extreme climate events in eastern China	Huaihe River Basin, eastern China	Penman-Monteith Method, Surface Humid Index, Crop Moisture Index, Keetch and Byram Drought Index, Crop-	The count of the annual rainy day declined; the regional average value of wet events increased by 0.0118

				Specific Drought Index, daily Water stress index, Moisture Deficit Index, Agricultural Reference Index	times/year. The regional extreme drought events had a much negative tendency about 0.0127 times/year.
40	Su *et al.,* (2016) Climatic Change	To examine the impact of climate change on streamflow	Yangtze River Basin, China	General Circulation Model, An analysis of variance (ANOVA)	The projected result shows an increased temperature all over the basin. The simulated result shows a 69% increase in runoff.
41	Sorribas *et al.,* (2016) Climatic Change	To examine the Projections of climate change effects on discharge and inundation	Guyanese and Brazilian shields, and the Amazon plain	General Circulation Model	The projected result shows the increasing trend of precipitation, increased discharge, and inundation of rivers in western and central Amazonia and Peruvian floodplains. The projected results are decreasing discharge in the eastern basin along with decreasing inundation in the Amazon basin.

42	Pumo *et al.*, (2016) Science of the Total Environment	To study the climate change effects on the hydrological regime	Italy	Flow Duration Curves, General Circulation Models, ModABa Hydrological Model	ModABa hydrological model's projection of 2090 depicts an increase in temperature and a reduction of precipitation by about 13% and a reduction of annual runoff by 10% and 20% for the future projections at 2055 and 2090, respectively.
43	Wang *et al.*, (2016) Journal of Hydrology	To study the multiple elasticities of runoff to climate change and catchment characteristics alteration	Thirty River Basin across China	Mann – Kendall Test, Pettitt Test	Among the climatic variables, precipitation played a 48.98% role in runoff. Evapotranspiration and land-use change contributed to a negative impact on runoff. Among 30 catchments, 19 were detected with change points with a 10% level of confidence, and the change point was between the years of 1970 s and 1980 s.
44	Papadimitriou et al., (2016) Hydrol. Earth Syst. Sci	To study high-end climate change impact on runoff and low flows	Europe	JULES a Land Surface Model, Multi-Segment Bias Correction (MSBC) Method	Assessed mean and low hydrological states at 4^0C global warming scenario for the European region. The study predicted the increasing nature

					of the water cycle at higher levels of warming. There were remarkable projected decreases of low flows in the future.
45	Berton *et al.,* (2016) Journal of Hydrology: Regional Studies	To examine the changing climate increases discharge and attenuates its seasonal distribution	Merrimack Watershed, USA	Principal Component Analysis, Factor Analysis, Mann-Kendal Test	The result shows that positive correlation between annual discharge and precipitation.
46	Chang *et al.,* (2017) Nat Hazards	To study the impact of climate change on runoff and uncertainty Analysis	Weihe River Basin, China	TOPMODEL, M-GLUE method, Mann-Kendal Test	The result of the RCP4.5 and RCP8.5 scenarios shows runoff will decrease from 13.3% to 27.7%, respectively.
47	Radchenko *et al.,* (2017) Water Resources	To study Climate Change Impacts on Runoff	Central Asia	General Circulation Model	The simulated result shows significant decreases in summer runoff by 12% to 42% and an increase in winter runoff by 44% to 107%.
48	Donnelly *et al.,* (2017) Climatic Change	To examine the impacts of climate change on European hydrology	Europe	General Circulation Model	The result shows an increasing trend of temperature closely associated with runoff change. More instance of runoff change was found at 1.5°C to 3 °C temperature.
49	Eisner *et al.,* (2017) Climatic	To analyze the climate change impacts	**Multiple	General Circulation Model	The result shows a declining trend of stream flow in the

	Change	on streamflow seasonality			Tagus basin and an increase in winter streamflow in the Rhine basin.
50	Shanka et al., (2017) Environ Pollut Climate Change	To study Climate Change Impacts on Runoff	Gidabo Basin, Ethiopia	Statistical Downscaling Model, General Circulation Model, Soil and Water Assessment Tool	The result shows a significant increase in runoff in the summer season and a high amount of decrease in runoff in the winter season.
51	Das *et al.,* (2018) Hydrological Sciences Journal	To evaluate the potential climate change impact on monsoon flow	Wainganga River Basin, India	Machine Learning Technique	The result predicted a significant decrease in monsoon affecting stream flow.
52	Lv *et al.,* (2018) scientific reports	To study the effects of climate and catchment characteristic change on streamflow	Yellow River, China	Budyko-type equation	The streamflow changed 26.87mm between the period 1978 to 2010. Runoff altered by 91.27% due to changes in watershed characteristics and 6.50% due to climate change.
53	Worqlul *et al.,* (2018) water	To examine the impact of climate change on streamflow hydrology	Upper Blue Nile Basin, Ethiopia	Global Circulation Models	The result predicted an increase of maximum and minimum temperature by 3.6^{o}C to 2.4^{o}C by the end of the 21st century. With increasing temperature, evapotranspiration will increase by 7.8%. The

					hydrological model indicates that stream flow increases by 64% in the dry season and decreases by 19% in the wet season.
54	Kelaiya *et al.,* (2019) International Journal of Bio-resource and Stress Management	To asses the water balance components	Bhadra River Basin, India	Soil and Water Assessment Tool	The result shows that annual evapotranspiration, runoff, and rainfall were 252.9mm, 243.67mm, and 670mm respectively. The annual average rainfall accounted for 36.37% of the annual average runoff.
55	Bhatta *et al.,* (2019) Catena	To assess the climate change impact on the hydrology	Koshi River Basin, Nepal	Soil and Water Assessment Tool	The study predicted the climate from 2030 to 2080. The predicted result shows a decrease in streamflow by 8.5% during the twenty-first century.
56	Qiu *et al.,* (2019) Journal of Hydrology	To study the impact of climate change on watershed systems	Miyun Reservoir Watershed, China	Soil and Water Assessment Tool	The result shows that during the middle, near, and future periods annual runoff changes were −22.17%, −30.14%, −3.97% respectively. The decrease of runoff is associated with an increase in temperature and

					evapotranspiration.
57	Oti *et al.,* (2020) Heliyon	To examine the hydrologic response to climate change	Densu River Basin, Ghana	Water Evaluation and Planning System	The result indicated that with an increase of temperature by 8.23%, there is a decrease of 17% in the precipitation. The increase in temperature and reduction of precipitation results in 58.3% water resource reduction.
58	Bingfei *et al.,* (2020) J. Geogr. Sci.	To examine the differential changes in precipitation and runoff Discharge	Yellow River of China	Standardized Precipitation Index, Mann-Kendal Test,	The result shows that 1989 was the change point of runoff when 14% of stream flow reduction occurred. Variation of precipitation was not strictly consistent with runoff.
59	Srinivas *et al.,* (2020) Stochastic Environmental Research and Risk Assessment	To study the hydroclimatic river discharge and seasonal trends assessment	Ganges River Basin, India	Mann–Kendall Test, Sen's Slope	The study was predicted for 2030, 2040, and 2050. It stated that a gradual decrease in precipitation leads to a significant decrease in river discharge at the rate of 15% to 21%.
60	Koch *et al.,* (2020) Climatic Change	To study climate change and water resource management	Pajeú watershed in north-eastern Brazil	Soil and Water Integrated Model	The study stated that the semi-arid region of Brazil was prone to

					drought.

Cluster 2: Climate change and human impact on runoff

61	Wang *et al.*, (2011) Water Resources Research	To quantify the relative contribution of the climate and direct Human Impact on Mean Annual streamflow	United States	Budyko-type equation	The study stated that climate and human activities have a strong impact on stream flow. Climate exhibits an 18% increase in streamflow. In the arid region climate- and human-induced changes were more severe than in other regions
62	Wang and Hejazi (2011) Water Resour. Res	To quantify the relative contribution of the climate and direct human impacts on mean annual streamflow	United States	Budyko-type equation	Mean annual streamflow increased due to climate change in most of the watersheds. The impact of climate change on annual stream flow was 18%. The human-induced impact on mean annual runoff was heterogeneous in different watersheds.
63	Wang *et al.*, (2012) Quaternary International	To study the role of climate change and human activities on the runoff	Yangtze River, China	Cumulative Anomaly and the Slope Change Catio of Cumulative Quantity (SCRCQ).	The impact of human activities on runoff change was about 90%, while climatic variables were influenced by about 10%.
64	Zhang *et al.*,	To assess of	Huifa River	Soil and Water	Reconstruction of

	(2012) Water Resour Manage	impact of climate change and human activities on runoff	Basin, Northeast China	Assessment Tool	annual runoff from 1965 to 2005 based on calibration and validation of the baseline period between 1956 and 1964. The result indicates a correlation between climatic variables (precipitation and temperature) and runoff coefficients.
65	Wang et al., (2012) Hydrol. Process.	To quantify the impact of climate variability and human activities on runoff changes	Haihe River Basin, China	Mann–Kendall Test, Precipitation–Runoff Double Cumulative Curves Method and Pettitt's Test	The study quantified climate variability and human activities on runoff response across three river basins. The climatic elasticity analysis shows an average decrease of runoff by 38.33% due to climatic variables across the basins. Human activity resulted in about 61.66% runoff change across the three basins.
66	Chen *et al.,* (2013) Theor Appl Climatol	To quantify the effects of climatic variability and human activities on runoff	Kaidu River Basin, North China	Mann–Kendall Test, Mann–Kendall–Sneyers Test, Hydrologic Sensitivity Analysis Method	The runoff trend was divided into a natural period (1960–1993) and a human-induced period (1994–2009) and the change point in annual runoff was identified as the

					year 1993. A significant increase in runoff was recorded and it was concluded that climatic variability was the main contributing factor (90.5%) followed by human activity (9.5%).
67	Chang *et al.,* (2014) Quaternary International	To study the impact of climate change and human activities on runoff	Weihe River Basin, China	Variable Infiltration Capacity Hydrological Model	The study showed a decline of 35% in the runoff of the river basin since the baseline decade (1956). The percentage of runoff change caused by climate change in 1970,1980,1990 and 2000 was 36%, 28%, 53%, and 10%, respectively. The percentage of runoff change caused by human activity was 64%, 72%, 47%, and 90%, respectively.
68	Jiang *et al.,* (2015) Journal of Hydrology	To study the impacts of climate change and human activities on runoff	Weihe River, China	Budyko-type equations, Mann-Kendall Test	The result of the study shows that human activity and climatic factors both were the driving factors in reducing the runoff.
69	Mohammed et al., (2016) Stoch Environ	To assess various models for predicting	Lower Zab River, Iqra	Pettitt, Precipitation-Runoff Double	Alteration of the climatic variable was the prime

	Res Risk Assess	anthropogenic interventions and climate variability on surface runoff		Cumulative Curve, Mann–Kendal, Multi-Model Combination Technique	concern of runoff change, during the year 2003 to 2013. Climate change has resulted in a 66% to 97% reduction of runoff while anthropogenic interventions attributed to about 4% to 34% reduction.
70	Wang *et al.,* (2017) Appl Water Sci	To investigate the causes of change in runoff	Gushan River	Hydrological Simulation Approach	The result shows a reduction of runoff by 52.4 mm during the study period of 1980 to 2013 climate change contributes about 38.5% and human activity contributes 61.5% of total runoff.
71	Wang et al., (2018) J. Earth Syst. Sci.	To Assess the response of runoff to climate change and human activities	Northern Taihang Mountain, China	Mann–Kendall test, Pettitt change-point statistics, Elasticity Coefficient Method	Runoff reduction owing to spring snowmelt and winter snowfall was 59% and 18%, respectively. The significance of annual runoff and precipitation was detected in 1982. The contribution of climate change and human activities on runoff change was 37.5% and 62.5%, respectively.

Cluster 3: Climate change effects on runoff and ecosystem

72	D¨oll *et al.,* (2010) Hydrol-Earth-Syst-sci.	To assess the impact of climate change on freshwater ecosystems and river flow alterations on a global scale.	A global overview	Water GAP Global Hydrology Model	Flow alteration and their spatial-temporal magnitudes were computed
73	Fekete *et al.,* (2010) Global Biogeochem. Cycles	To study ecosystem scenarios with respect to climate and hydrological alterations	A global overview	Global Circulation Model, Water Balance/Transport Model, Millennium Ecosystems Assessment	The future climatic consequence to alternative environmental management policies.

Cluster 4: Climate change impact on stream-flow and hydropower

74	Oliveira *et al.,* (2017) Int. J. Climatol	To assess the climate change impacts on streamflow and hydropower potential	Southeastern Brazil	Soil and Water Assessment Tool	The result shows a significant decrease in runoff in all seasons and a resultant decrease in hydropower from 6.1% to 58.6% throughout the 21st century.
75	Wagner *et al.,* (2017) Environ Earth Sci	To examine the impacts of climate change on streamflow and hydropower Generation	Alpine region	Hydrological Modelling	The result indicates a decrease in runoff in some seasons.

Cluster 5: Climate change impact on streamflow and sediment yield

76	Phan *et al.,* (2011) Water Resources	To study the impact of climate change on Stream discharge and sediment yield	Northern Viet Nam	Soil and Water Assessment Tool	The result predicted for the 2050s as a change in the rate of sediment load and stream discharge

					to be 11.4% and 15.3%, respectively with discharge increasing with sedimentation during the wet season.
77	Li *et al.,* (2015) water	To examine the runoff and sediment yield variations in response to precipitation changes	Loess Plateau, China	Soil and Water Assessment Tool	The result shows sediment yield and runoff increased by 11.54% and 18.36% respectively when precipitation increased by 10% and sediment yield and runoff decreased by 10.05% and 13.36% respectively when precipitation decreased by 10%.

1.9.3 The trend of article publication and journals

Of the 77 articles reviewed from the period 2009 to 2020, the highest number of articles were found to be in the domain of the effect of climate change on runoff and discharge, which accounted for 18.18% of the total in 2014 (Table 1.5). The papers mostly appeared in *Water, Hindawi Publishing Corporation Scientific World Journal, and Hydrol. Earth Syst. Sci, Quaternary International, Journal of Hydrology, Front. Earth Sci, Science of the Total Environment, Water Resources Research, Front. Earth Sci, Theor Appl Climatol, International Journal of Water Resources Development, Journal of Geophysical Research: Atmospheres, Climatic Change, and J. Earth Syst. Sci*. From 2011 to 2013, the same number of articles were taken, which contained 11.69% of articles in each year. The lowest number of articles (2.60%) were found for the years 2009 and 2010 (Table 1.5).

The articles were grouped into five clusters (Table 1.5), as detailed in Methodology. Cluster 1 covered 77.92% of the articles that were reviewed. 14.28% of the articles belonged to Cluster 2 (to understand the anthropogenic influence on runoff). Clusters 3 to 5 underlined the impact of climate change on runoff, ecosystems, stream flow, hydropower, and sediment. This covered 2.5% of the reviewed articles.

Out of 77 articles, the highest percentage was published in the Journal of Climatic Change and Water Resour. Res (7% of each). 6% of the articles were published in the Journal of Hydrology, followed by 4% each in the Journal of Hydrol. Earth Syst. Sci., Quaternary International, and Water. This was followed by 3% of articles in the journals Science of Total Environment, Hydrological Process, and Water Resources Management. Journals of Int. J. Climatol, Hydrol. Process, Hydrological Sciences Journal, Nat Hazards, Theor Appl Climatol, and J. Earth Syst. Sci published 2% articles in each of the journals, while the other journals published only 1% articles in each (Fig. 1.7 and Table 1.6). An increasing trend of article publication based on the topic of the review was found in the journals of Climatic Change, Water Resources. Res, and Journal of Hydrology.

Table 1.6: Journal and quantity of articles

Sl No	Journal	Count	Sl No	Journal	Count
1	Water Resour. Res	7	21	Global and Planetary Change	1
2	Climatic Change	7	22	Journal of Hydrologic Engineering	1
3	Journal of Hydrology	6	23	Earth System Dynamics	1
4	Hydrol. Earth Syst. Sci	4	24	Journal of Great Lakes Research	1
5	Quaternary International	4	25	Hindawi Publishing Corporation Scientific World Journal	1
6	Water	4	26	Front. Earth Sci.	1
7	Science of the Total Environment	3	27	International Journal of Water Resources Development	1
8	Hydrol. Process.	3	28	Journal of Geophysical Research: Atmospheres	1
9	Water Resour Manage	3	29	Stoch Environ Res Risk Assess	1

10	Int. J. Climatol	2	30	Journal of Hydrology: Regional Studies	1
11	Hydrol. Process.	2	31	Appl Water Sci	1
12	Hydrological Sciences Journal	2	32	Water Resources	1
13	Nat Hazards	2	33	Environ Pollut Climate Change	1
14	Theor Appl Climatol	2	34	Scientific reports	1
15	J. Earth Syst. Sci.	2	35	International Journal of Bio-resource and Stress Management	1
16	J. Environ	1	36	Catena	1
17	Hydrol-Earth-Syst-sci.	1	37	Heliyon	1
18	Global Biogeochem.Cycles	1	38	J. Geogr. Sci.	1
19	J Indian Soc Remote Sens	1	39	Stochastic Environmental Research and Risk Assessment	1
20	Environ. Res. Lett	1		**Total**	**77**

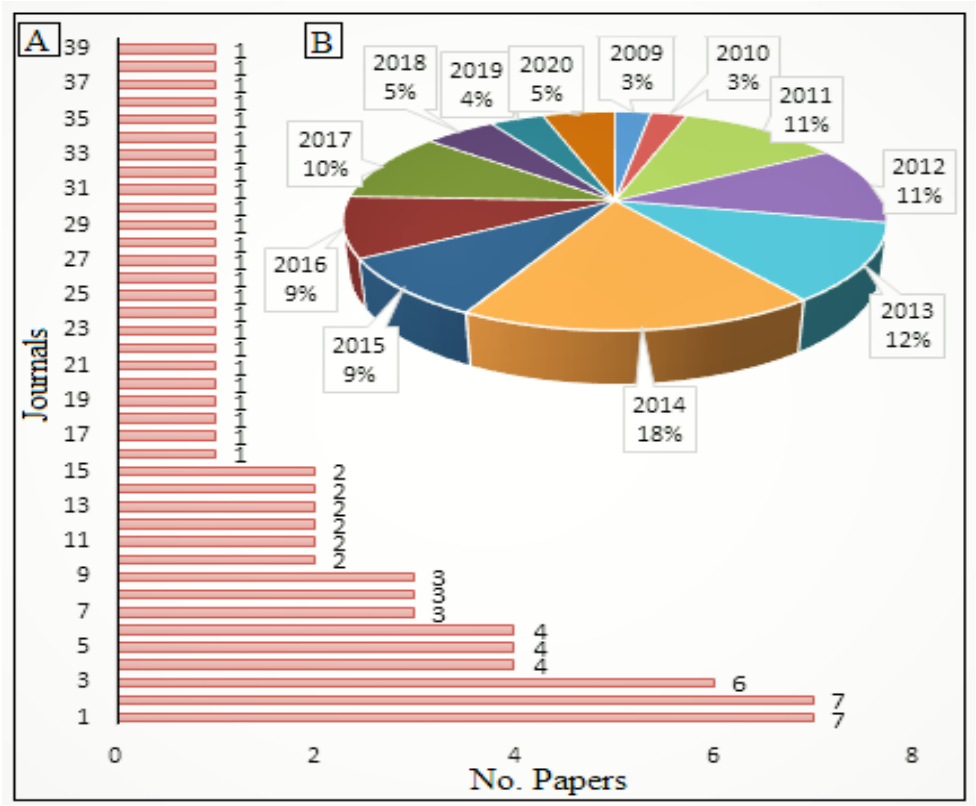

Fig. 1.7: (A) List of journals and number of papers published, (B) Quantity of journals based on year.

1.9.4 Country of origin

The study covered every continent of the globe, with the highest number of articles published from Asia (51%), with China dominating the publications (26 publications), followed by India (6 publications). Nepal, Turkey, Iraq, Taiwan, and Vietnam had one publication each. North America had the 2nd highest publication rate with 15% of the articles, with the United States having 9 publications and Canada and Ontario having 1 each. The third-highest publication on the topic of study is attributed to Europe (14%). Out of 77 articles undertaken for the present study, 5 were based on a global overview; one study was conducted on Iraq and Iran (both as one study region); and 4 studies were conducted on a continental scale, i.e., Southeast Asia, Asia, Africa, and the Alpine region. The details of the studies undertaken have been presented in Fig. 1.8, and Table 1.7.

Table 1.7: Distribution of article

SL NO	Country	Count	SL NO	Country	Count
1	China	26	16	Romania	1
2	United States	9	17	Germany	1
3	India	6	18	Italy	1
4	A global overview	5	19	Nepal	1
5	Europe	4	20	Ghana	1
6	Brazil	3	21	Iraq	1
7	Ethiopia	2	22	Taiwan	1
8	Kenya	1	23	Vietnam	1
9	Denmark	1	24	**Iraq and Iran	1
10	Australia	1	25	**Southeast Asia	1
11	Belgium	1	26	**Africa	1
12	Turkey	1	27	**Asia	1
13	Slovenia	1	28	**Alpine region	1
14	Canada	1	29	**Multiple	1
15	Ontario	1	**Total**		**77**

Note- **Iraq and Iran contained both countries; **Southeast Asia, **Africa, **Asia, **Alpine region covered continents as study region, **Multiple represents Rhine and Tagus in Europe, upper Amazon in South America, upper Mississippi in North America, Lena, Ganges, upper Yellow, and the upper Yangtze in Asia, Blue Nile and Niger in Africa, and Darling in Australia as a study region.

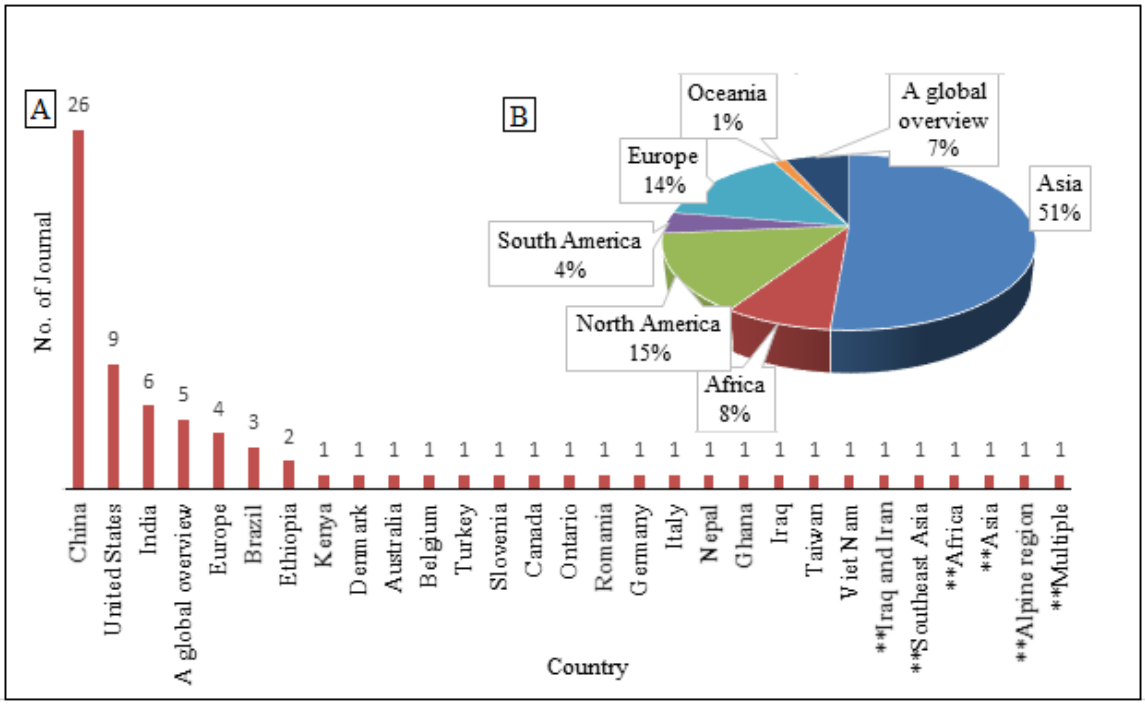

Fig. 1.8: (A) Journal distribution based on country (B) Journal distribution based on the continent

1.9.5 Summary of Findings

The work highlighted how runoff alteration will be impacted by climate change over time. Runoff changes by 26% with a 10% change in precipitation (Jeppesen et al., 2009). Climate change is indicated by a significant increase in temperature and a drop in precipitation, thereby having a major impact on runoff (Wu et al., 2012; Yates et al., 2014; Pumo et al., 2016). An increase in temperature by 4 °C reduces stream flow, leading to a 30% lower peak flow (Kwadijk and Middelkoop, 2014). The relationship between temperature and runoff/discharge is adverse (Leppi et al., 2012; Liersch et al., 2014). The temperature change (10 °C) caused a reduction (2%) of runoff change (Yang et al., 2011), and the increase in

temperature by 2°C and 3°C decreased stream flow by 2% to 6% and 3% to 8%, respectively (Tang et al., 2012). The changes in land use and land cover also had a detrimental effect on runoff (Wang et al., 2016). The projected result for future water resources shows a change in groundwater recharge by 23.15% (Uniyal et al., 2015; Biswas et al., 2018) and a reduction in both runoff and groundwater recharge (Hagemann et al., 2013; Papadimitriou et al., 2016).

Anthropogenic activities have a decisive effect on runoff change (Chang et al., 2014). The anthropogenic role in runoff reduction is more dominant than climatic factors (Wang et al., 2012; Chang et al., 2014; Wang et al., 2017; Wang et al., 2018). In Northern Vietnam and China's Loess Plateau, the SWAT model was used to examine how climate change would impact sediment output (Phan et al., 201; Li et al., 2015).

1.10 Objectives:

1. To estimate the rainfall trend of the Mayurakshi river basin.

2. To assess the land use and land cover dynamics of the basin.

3. To evaluate seasonal streamflow patterns and simulate the runoff pattern of the basin.

4. To assess the role of climate change and land use land cover change on streamflow.

1.11 Research Questions

The research work has been conducted to address the following questions in reference to the study area:

(i) Is there any change in rainfall during the study period?

(ii) What types of land use and land cover changes occurred in the study area?

(iii) What is the impact of climate, land use, and land cover change on the runoff of the basin?

1.12 Methods

The research objectives were solved one by one through a series of methodological steps. Before the rainfall trend and changepoint analysis, the normality of the data was assessed by the Kolmogorov-Smirnov test. The data also underwent autocorrelation tests to confirm that the time-series data has a serial dependency or that the data is independent. Due to the autocorrelated data, the modified Mann-Kendall test (mMK) was applied for the trend analysis, and the magnitude of the trend was measured by Sen's slope. The change point of the rainfall time series has been evaluated by the statistics of Pettitt, Buishand U Statistic, and Standard Normal Homogeneity Test. The rainfall variability of the study area is analyzed by the Rainfall Seasonality Index (RSI), while the drought condition over the study period is measured by the Rainfall Anomaly Index (RAI). The Autoregressive Integrated Moving Average (ARIMA) model was used based on 30 years of time-sequence rainfall data to predict the future rainfall scenario of the basin.

The land use and land cover (LULC) dynamics of the basin are analyzed by the sequential steps of image classification, change detection, and future prediction. The satellite images were classified by the machine learning algorithm Random Forest (RF), and the change in LULC was assessed by the transition matrix. In order to predict the future scenario of LULC, the popular Cellular Automata-Markov model (CA-Markov) was employed. The runoff of the basin is simulated in the Soil and Water Assessment Tool (SWAT), and the model is calibrated and validated, where the calibration and validation are accepted based on the R^2 and Nash-Sutcliffe simulation efficiency (NSE). The climatic and LULC impacts on the runoff were evaluated by developing the models S_{2IPQ} of the simulated average runoff contribution of the basin during the impact period, S_{1NPQ} the simulated average runoff contribution of the basin during the natural period, and S_{3IPCL} the runoff simulation with reference to climate change. In the model (S_{3IPCLQ}), the LULC is constant and referred to as the natural period (S_{1NPQ}), and the climatic components are referred to as the impact period (S_{2IPQ}).

1.13 Data Sources

The rainfall data was collected from the IMD Puna (https://www.imdpune.gov.in/cmpg/Griddata/Rainfall_25_Bin.html). The spatial resolution of this daily gridded rainfall data is 0.25 × 0.25 degrees, and the unit of rain is a millimeter (mm). The data was collected from 1901 to 2020. For image classification, the satellite data was collected from the United States Geological Survey (USGS) portal (http://earthexploration.usgs.gov/). The LULC for the years 1991, 1996, 2002, and 2008 was done using the collected Landsat 5 images and Thematic Mapper (TM). For the years 2014 and 2020, Landsat 8 and Operational Land Imager (OLI) were used. To run the SWAT model, weather datasets, including temperature, humidity, wind speed, and solar radiation, were acquired from NASA Power Access MERRA-2 data (https://power.larc.nasa.gov/data-access-viewer/). The observed discharge data were obtained from the Ministry of Jal Shakti, Central Water Commission Executive Engineer, Damodar Division, CWC, Asansol, under the Government of India.

1.14 Future research

The work can lead researchers in the areas of climatology, agricultural science, and regional planning to undertake further studies on regional climate changes and their effect on agriculture, regional economies, ecosystems, and hydropower production. Further, the changes in LULC can prove to be food for future research in the fields of regional planning and environmental conservation for sustainable policy changes.

1.15 Conclusion

The work can lead researchers in the areas of climatology, agricultural science, and regional planning to undertake further studies on regional climate changes and their effect on agriculture, regional economies, ecosystems, and hydropower production. The study was focused on understanding the impact of climate change, land use, and land cover change (LULC) on the stream flow domain.

Further, the changes in LULC can prove to be food for future research in the fields of regional planning and environmental conservation for sustainable policy changes.

References

Aich, V., Liersch, S., Vetter, T., Huang, S., Tecklenburg, J., Hoffmann, P., Hattermann, F. F. (2014). Comparing impacts of climate change on streamflow in four large African river basins. *Hydrol. Earth Syst. Sci*, 1-14. doi:doi:10.5194/hess-18-1305-2014

Al-Faraj, F., Scholz, M., & Tigkas, D. (2014). Sensitivity of Surface Runoff to Drought and Climate Change: Application for Shared River Basins. *6*, 3033-3048. doi:doi:10.3390/w6103033

Allen, M., & Ingram, J. (2002). Constraints on future climate changes and the hydrologic cycle. *Nature*, 224–232.

Arnell, N. W. (2003). Relative effects of multi-decadal climatic variability and changes in the mean and variability of climate due to global warming: future streamflows in Britain. *Journal of Hydrology*, 195–213.

Arnell, N., & Gosling, S. (2013). The impacts of climate change on river flow regimes at the global scale. *Journal of Hydrology*, 351–364. doi:http://dx.doi.org/10.1016/j.jhydrol.2013.02.010

Biswas B., Ratnaprabha J., Nilima T. (2019), Rainfall Distribution and Trend Analysis for Upper Godavari Basin, India, from 100 Years Record (1911–2010), J. of the Indian Soc. of Remote Sensing, https://doi.org/10.1007/s12524-019-01011-8(0123456789-volV)(0123456789().

Biswas B., Jain S., Rawat S, (2018), Spatio-temporal analysis of groundwater levels and projection of future trend of Agra city, Uttar Pradesh, India, *Arab J Geosci, 1-18* https://doi.org/10.1007/s12517-018-3577-4

Berton, R., Driscoll, C., & Chandler, D. (2016). Changing climate increases discharge and attenuates its seasonal distribution in the northeastern United States. *Journal of Hydrology: Regional Studies*, 164–178. doi:http://dx.doi.org/10.1016/j.ejrh.2015.12.057

Bingfei, H., Chao, J., & Jianxin, S. O. (2020). Differential changes in precipitation and runoff discharge during 1958–2017 in the headwater region of the Yellow River of China. *J. Geogr. Sci., 30*(9), 1401-1418. doi: https://doi.org/10.1007/s11442-020-1789-5

Boini, N., Ashvin K., G., & Baghu R., C. (2013). Assessment of Future Climate Change Impacts on Water Resources of Upper Sind River Basin, India Using SWAT Model. *Water Resour Manage, 27*, 3647–3662. doi: 10.1007/s11269-013-0371-7

Bronstert, A., Niehoff, D., & Burger, G. (2002). Effects of climate and land-use change on storm runoff generation: present knowledge and modeling capabilities. *Hydrological Processes, 16*, 509-529.

Carey, M., Baraer, M., Mark, B., French, A., Bury, J., Young, K., & McKenzie, J. (2013). Toward hydro-social modeling: Merging human variables and the social sciences with climate-glacier runoff models (Santa River, Peru). *Journal of Hydrology*, 1-11. doi:http://dx.doi.org/10.1016/j.jhydrol.2013.11.006

Cauvy-Fraunie´, S., Andino, P., Espinosa, R., Calvez, R., Jacobsen, D., & Dangles, O. (2015). Ecological responses to experimental glacier-runoff reduction in alpine rivers. *Nature Communications*, 1-5. doi: 10.1038/ncomms12025

Chang, J., Wang, Y., Istanbulluoglu, E., Bai, T., Huang, Q., Yang, D., & Huang, S. (2014). Impact of climate change and human activities on runoff in the Weihe River Basin, China. *Quaternary International*, 1-11. doi:http://dx.doi.org/10.1016/j.quaint.2014.03.048

Chang, J., Zhang, H., Wang, Y., & Zhang, L. (2017). Impact of climate change on runoff and uncertainty analysis. *Nat Hazards*, 1-19. doi: 10.1007/s11069-017-2909-0

Chen, H., Fleskens, L., Baartman, J., Wang, F., Moolenaar, S., & Ritsema, C. (2020). Impacts of land use change and climatic effects on streamflow in the Chinese Loess Plateau: A meta-analysis. *Science of the Total Environment*, 134989-135003. doi:https://doi.org/10.1016/j.scitotenv.2019.134989

Chen, Z., & Chen, Y. (2014). Effects of climate fluctuations on runoff in the headwater region of the Kaidu River in northwestern China. *Front. Earth Sci.*, 1-10. doi: 10.1007/s11707-014-0406-2

Chen, Z., Chen, Y., & Li, B. (2013). Quantifying the effects of climate variability and human activities on runoff for Kaidu River Basin in arid region of northwest China. *111*, 537–545. doi:DOI 10.1007/s00704-012-0680-4

Croitoru, A.-E., & Minea, I. (2014). The impact of climate changes on river discharge. *Theor Appl Climatol*, 1-14. doi: 10.1007/s00704-014-1194-z

Crossman, J., Futter, M., Oni, S., Whitehead, P., Jin, L., Butterfield, D., Dillon, P. (2013). Impacts of climate change on hydrology and water quality: Future-proofing management strategies in the Lake Simcoe watershed, Canada. *Journal of Great Lakes Research*, 19–32. doi:http://dx.doi.org/10.1016/j.jglr.2012.11.003

D¨oll, P., & Zhang, J. (2010). Impact of climate change on freshwater ecosystems: a global-scale analysis of ecologically relevant river flow alterations. *Hydrol. Earth Syst. Sci, 14*, 783–799. doi:doi:10.5194/hess-14-783-2010

Daba, M., & You, S. (2020). Assessment of Climate Change Impacts on River Flow Regimes in the Upstream of Awash Basin, Ethiopia: Based on IPCC Fifth Assessment Report (AR5) Climate Change Scenarios. *doi:10.3390/hydrology7040098*, 1-22. doi:doi:10.3390/hydrology7040098

Danneberg, J. (2012). Changes in runoff time series in Thuringia Germany—Mann-Kendall trend test and extreme value analysis. *Adv Geosci, 31*, 31-56. doi:doi:10.5194/adgeo-31-49-2012

Das, J., & Nanduri, U. (2018). Assessment and evaluation of potential climate change impact on monsoon flows using machine learning technique over Wainganga River Basin, India. *Hydrological Sciences Journal*. doi: 10.1080/02626667.2018.1469757

Delcour, I., Spanoghe, P., & Uyttendaele, M. (2015). Literature review: Impact of climate change on pesticide use. *Food Research International*, 7–15. doi:http://dx.doi.org/10.1016/j.foodres.2014.09.030

Döll, P., & Bunn, S. (2014). Impact of Climate Change on Freshwater Ecosystems due to Altered River Flow Regimes. *Cross-Chapter Box*, 143-146.

Döll, P., & Müller Schmied, P. (2010). How is the impact of climate change on river flow regimes related to the impact on mean annual runoff? A global-scale analysis. *Environ. Res. Lett., 7*(1). doi:http://dx.doi.org/10.1088/1748-9326/7/1/014037

Dong, L. H., Xiong, L. H., Yu, K. X., & Li, S. (2012). Research advances in effects of climate change and human activities on hydrology Adv. Water Sci. *2*, 278–285.

Donnelly, C., Greuell, W., Andersson, J., Gerten, D., Pisacane, G., Roudier, P., & Ludwig, F. (2017). Impacts of climate change on European hydrology at 1.5, 2 and 3 degrees mean global warming above preindustrial level. *Climatic Change, 143*, 13–26. doi:DOI 10.1007/s10584-017-1971-7

Eisner, S., Flörke, M., Chamorro, A., Dasgupta, P., Donnelly, C., Huang, J., . . . Krysanova, V. (2017). An ensemble analysis of climate change impacts on streamflow seasonality across 11 large river basins. *Climatic Change, 141*, 401–417. doi: 10.1007/s10584-016-1844-5

Fekete, B., Wisser, D., Kroeze, C., Mayorga, E., Bouwman, L., Wollheim, W., & Vörösmarty, C. (2010). Millennium Ecosystem Assessment scenario drivers (1970–2050): Climate and hydrological alterations. *Global Biogeochemical Cycles*, 1-12. doi:doi:10.1029/2009GB003593

Frederick, K. D., & Major, D. C. (1997). Climate change and water resources,. *Climatic Change, 37*, 7–23.

Giang, P. Q., Toshiki, K., Sakata, M., Kunikane, S., & Vinh, T. Q. (2014). Modeling Climate Change Impacts on the Seasonality of Water Resources in the Upper Ca River Watershed in Southeast Asia. *Hindawi Publishing Corporation The Scientific World Journal*, 1-15. doi:http://dx.doi.org/10.1155/2014/279135

Githui, F., Gitau, W., Mutua, F., & Bauwens, W. (2009). Climate change impact on SWAT simulated streamflow in western Kenya. *Int. J. Climatol*, *29*, 1823–1834. doi: 10.1002/joc.1828

Goulden, M., & Bales, R. (2014). Mountain runoff vulnerability to increased evapotranspiration with vegetation expansion. *Department of Earth System Science, University of California, Irvine*, *111*(39), 14071–14075. Retrieved from www.pnas.org/lookup/suppl/doi:10.

Gupta, P., Panigrahy, S., & Parihar, J. S. (2011). Impact of Climate Change on Runoff of the Major RiverBasins of India Using Global Circulation Model (HadCM3) Projected Data. *J Indian Soc Remote Sens*, *39*(3), 337–344. doi: 10.1007/s12524-011-0101-7

Hagemann, S., Chen, C., Clark, D. B., Folwell, S., Gosling, S. N., Haddeland, I., . . . Wiltshire, A. J. (2013). Climate change impact on available water resources obtained using multiple global climate and hydrology models. *Earth Syst. Dynam*, *4*, 129–144. doi:doi:10.5194/esd-4-129-2013

Hamdi, R., Termonia, P., & Baguis, P. (2011). Effects of urbanization and climate change on surface runoff of the Brussels Capital Region: a case study using an urban soil–vegetation–atmosphere-transfer model. *Int. J. Climatol*, 1959–1974. doi: 10.1002/joc.2207

IPCC. (2007). Climate change 2007. *The Physical Science Basis Report AR4*.

Janzˇa, M. (2013). Impact assessment of projected climate change on the hydrological regime in the SE Alps, Upper Socˇa River basin, Slovenia. *Nat Hazards*, *67*, 1025–1043. doi:DOI 10.1007/s11069-011-9892-7

Jeppesen, E., & Kronvang, B. (2009). Climate Change Eff ects on Runoff , Catchment Phosphorus Loading and Lake Ecological State, and Potential Adaptations. *J. Environ. Qual*, *38*, 1930–1941. doi:doi:10.2134/jeq2008.0113

Jiang, C., Xiong, L., Wang, D., Liu, P., Guo, S., & Xu, C.-Y. (2015). Separating the impacts of climate change and human activities on runoff using the Budyko-type equations with time-varying parameters. *Journal of Hydrology*, 326–338. doi:http://dx.doi.org/10.1016/j.jhydrol.2014.12.060

Jung, I. W., Moradkhani, H., & Chang, H. (2012). Uncertainty assessment of climate change impacts for hydrologically distinct river basins. *J. Hydrol*, 73–87. doi:http://dx.doi.org/10.1016/j.jhydrol.2012.08.002.

Koch, H., Silva, A. C., Liersch, S., Azevedo, J. G., & Hattermann, F. (2020). Effects of model calibration on hydrological and water resources management simulations under climate change in a semi-arid watershed. *Climatic Change*, *163*, 1247–1266.

Kwadjk, J., & Middelkoop, H. (1994). Eastimation of impact of climate change on the peak discharge probability of the river Rhine. *Climatic Change June*, 1-26.

Kumar J.,Biswas B., Walker S *(2020),* Multi-temporal LULC Classification using Hybrid Approach and Monitoring Built-up Growth with Shannon's Entropy for a Semiarid Region of Rajasthan, India, *J. of the Geo. Soc. of India*, Doi: 1 0.1007/s12594-020-1489-x. 95. 626-635

Lei, H., Yang, D., & Huang, M. (2014). Impacts of climate change and vegetation dynamics on runoff in the mountainous region of the Haihe River basin in the past five decades. *Journal of Hydrology*, 786-799. doi:http://dx.doi.org/10.1016/j.jhydrol.2014.02.029

Leppi, J., DeLuca, T., Harrar, S., & Running, S. (2012). Impacts of climate change on August stream discharge in the Central-Rocky Mountains. *Climatic Change, 112*, 997–1014. doi: 10.1007/s10584-011-0235-1

Lettenmaier, D. P., Wood, E. F., & Wallis, J. R. (1994). Hydro-climatological trends in the continental United States1948–88. (7), 586-607.

Li, T., & Gao, Y. (2015). Runoff and Sediment Yield Variations in Response to Precipitation Changes: A Case Study of Xichuan Watershed in the Loess Plateau, China. *Water, 7*, 5638-5656. doi:doi:10.3390/w7105638

Lin, K., Lin, Y., Xiaohong, C., & Fan, L. (2014). Changes in runoff and eco-flow in the Dongjiang River of the Pearl River Basin, China. *Front. Earth Sci.*, 1-11. doi: 10.1007/s11707-014-0434-y

Ling, H. B., Xu, H. L., Shi, W., & Zhang, Q. (2011). Regional climate change and its effects on the runoff of Manas River, Xinjiang, China. *Environ Earth Sci,, 64*(8), 2203–2213.

Luo, Y., Ficklin, D., Liu, X., & Zhang, M. (2013). Assessment of climate change impacts on hydrology and water quality with a watershed modeling approach. *Science of the Total Environment*, 72–82. doi:http://dx.doi.org/10.1016/j.scitotenv.2013.02.004

Lv, X., Zuo, Z., Ni, Y., Sun, J., & Wang, H. (2019). The effects of climate and catchment characteristic change on streamflow in a typical tributary of the Yellow River. *Scintific Report*. doi:https://doi.org/10.1038/s41598-019-51115-x 1

Ma, H., Yang, D., Tan, S. K., Gao, B., & Hu, Q. (2010). Impact of climate variability and human activity on streamflow decrease in the Miyun Reservoir catchment. *Journal of Hydrology*, 317–324. doi:doi:10.1016/j.jhydrol.2010.06.010

Mohammed, R., Scholz, M., Nanekely, A. M., & Mokhtari, Y. (2016). Assessment of models predicting anthropogenic interventions and climate variability on

surface runoff of the Lower Zab River. *Stoch Environ Res Risk Assess*, 1-18. doi: 10.1007/s00477-016-1375-7

Narsimlu, B., Gosain, A., & Chahar, B. (2013). Assessment of Future Climate Change Impacts on Water Resources of Upper Sind River Basin, India Using SWAT Model. *Water Resour Manage* , 3647–3662. doi: 10.1007/s11269-013-0371-7

Nijssen, B., Schnur, R., & Lettenmaier, D. P. (2001). Global retrospective estimation of soil moisture using the variable infiltration capacity land surface model, 1980–93. *Journal of Climate*, *14*, 1790-1808.

Ning, T., Li, Z., & Liu, W. (2016). Separating the impacts of climate change and land surface alteration on runoff reduction in the Jing River catchment of China. *Catena*, *147*, 80–86. doi:http://dx.doi.org/10.1016/j.catena.2016.06.041

Oliveira, V., Mello, C., & Viola, M. (2017). Assessment of climate change impacts on streamflow and hydropower potential in the headwater region of the Grande river basin, Southeastern Brazil. *Int. J. Climatol.*, 1-19. doi: 10.1002/joc.5138

Oni, S., Futter, M., Molot, L., Dillon, P., & Crossman, J. (2014). Uncertainty assessments and hydrological implications of climate change in two adjacent agricultural catchments of a rapidly urbanizing watershed. *Science of the Total Environment*, 326–337. doi:http://dx.doi.org/10.1016/j.scitotenv.2013.12.032

Oti, J. O., Kabo-bah, A., & Ofosu, E. (2020). Hydrologic response to climate change in the Densu River Basin in Ghana. *Heliyon*. doi:https://doi.org/10.1016/j.heliyon.2020.e04722

Papadimitriou, L., Koutroulis, A., Grillakis, M., & Tsanis, I. (2016). High-end climate change impact on European runoff and low flows – exploring the effects of forcing biases. *Hydrol. Earth Syst. Sci*, *20*, 1785–1808. doi:doi:10.5194/hess-20-1785-2016

Parry, ML; Canziani, OF;. (2007). Technical summary Climate change: impacts, adaptation and vulnerability, contribution of Working Group II to the Fourth Assessment Report of the Intergovernmental Panel on Climate Change. (M. Parry, O. Canziani, J. Palutikof, J. van der Linden, & C. Hanson, Eds.) *Cambridge University Press, Cambridge, UK*, 23-78.

Peng, D., Qiu, L., Fang, J., & Zhang, Z. (2016). Quantification of Climate Changes and Human Activities That Impact Runoff in the Taihu Lake Basin, China. *Hindawi Publishing Corporation Mathematical Problems in Engineering*, 1-8. doi:http://dx.doi.org/10.1155/2016/2194196

Phan, D., Wu, C., & Hsieh, S. (2011). Impact of Climate Change on Stream Discharge and Sediment Yield in Northern Viet Nam1. *Water Resources, 38*(6), 827-236. doi:10.1134/S0097807811060133

Pourmokhtarian, A., Driscoll, C. T., Campbell, J. L., & Hayhoe, K. (2012). Modeling potential hydrochemical responses to climate change and increasing CO2atthe Hubbard Brook Experimental Forest using a dynamic biogeochemical model (PnET-BGC). *Water Resour. Res, 48*(13), 1-14. doi:http://dx.doi.org/10.1029/2011WR011228.

Pumo, D., Arnone, E., Francipane, A., Caracciolo, D., & Noto, L. (2017). Potential implications of climate change and urbanization on watershed hydrology. *Journal of Hydrology*, 80–99. doi:http://dx.doi.org/10.1016/j.jhydrol.2017.09.002

Pumo, D., Caracciolo, D., Viola, F., & Noto, L. (2016). Climate change effects on the hydrological regime of small non-perennial river basins. *Science of the Total Environment*, 76–92. doi:http://dx.doi.org/10.1016/j.scitotenv.2015.10.109

Qiu, J., Shen, Z., Leng, G., Xie, H., Hou, X., & Wei, G. (2015). Impacts of climate change on watershed systems and potential adaptation through BMPs in a drinking water source area. *Journal of Hydrology*, 223-235. doi:https://doi.org/10.1016/j.jhydrol.2019.03.074

Radchenko, I., Dernedde, Y., Mannig, B., Frede, H.-G., & Breuer, L. (2017). Climate Change Impacts on Runoff in the Ferghana Valley (Central Asia). *44*(5), 1-24. doi: 10.1134/S0097807817050098

Scanlon, T., Caylor, K., Levin, S., & Rodriguez-Iturbe, I. (2007). Positive feedbacks promote power-law clustering of Kalahari vegetation. *Nature, 449*, 209-2012.

Schneider, C., Laiz´e, C. L., Acreman, M. C., & Fl¨orke, M. (2013). How will climate change modify river flow regimes in Europe? *Hydrol. Earth Syst. Sci, 17*, 325–339. doi:doi:10.5194/hess-17-325-2013

Shanka, A. S. (2017). Evaluation of Climate Change Impacts on Run-Off in the Gidabo River Basin: Southern Ethiopia. *Environment Pollution and Climate Change, 1*(3), 1-13.

Singh A., Rai P k., Deka G., Biswas B., Prasad D., Rai VK (2021), Management of natural resources through integrated watershed management in Nana Kosi micro watershed, district Almora, India, *Eco. Env. & Cons*, 27(5),259-266.

Solomon, S., Qin, D., Manning, M., Marquis, M., Averyt, K., Tignor, M. B., . . . Chen, Z. (2007). Climate Change 2007: The Physical Science Basis, Cambridge University. *Press, Cambridge, 996*.

Sorg, A., Bolch, T., Stoffel, M., Solomina, O., & Beniston, M. (2012). Climate change impacts on glaciers and runoff in Tien Shan (Central Asia). *Climate Change*, 725-732. doi: 10.1038/NCLIMATE1592

Sorribas, M. V., Paiva, R., Melack, J., Bravo, J., Jones, C., Carvalho, L., . . . Costa, M. H. (2016). Projections of climate change effects on discharge and inundation in the Amazon basin. *Climatic Change*, 1-16. doi: 10.1007/s10584-016-1640-2

Srinivas, R., Singh, A. P., Dhadse, K., & Magner, J. (2020). Hydroclimatic river discharge and seasonal trends assessment model using an advanced spatio-temporal model. *Stochastic Environmental Research and Risk Assessment*, 1-16. doi:https://doi.org/10.1007/s00477-020-01780-6

Stagl, J., & Hattermann, F. (2015). Impacts of Climate Change on the Hydrological Regime of the Danube River and Its Tributaries Using an Ensemble of Climate Scenarios. *Water, 7*, 1-14. doi:6139-6172; doi:10.3390/w7116139

Su, B., Huang, J., Zeng, X., Gao, C., & Jiang, T. (2016). Impacts of climate change on streamflow in the upper Yangtze River basin. *Climatic Change*, 1-14. doi: 10.1007/s10584-016-1852-5

Tang, C., Crosby, B., Wheaton, J., & Piechota, T. (2012). Assessing streamflow sensitivity to temperature increases in the Salmon River Basin, Idaho. *Global and Planetary Change*, 32–44. doi:doi:10.1016/j.gloplacha.2012.03.002

Uniyal, B., Jha, M. K., & Verma, A. K. (2015). Assessing Climate Change Impact on Water Balance Components of a River Basin Using SWAT Model. *Water Resour Manage, 29*, 4767–4785. doi: 10.1007/s11269-015-1089-5

Vano, J., Nijssen, B., & Lettenmaier, D. (2015). Seasonal hydrologic responses to climate change in the Pacific Northwest. *Water Resources Research*, 1-18. doi:10.1002/2014WR015909

Wagner, T., Themeßl, M., Schu¨ppe, A., Gobiet, A., Stigler, H., & Birk, S. (2017). Impacts of climate change on stream flow and hydro power generation in the Alpine region. *Environ Earth Sci, 76*(4), 1-24. doi: 10.1007/s12665-016-6318-6

Wang, D., & Hejazi, M. (2011). Quantifying the relative contribution of the climate and direct human impacts on mean annual streamflow in the contiguous United States. *Water Resour. Res, 47*, 1-16. doi: 10.1029/2010WR010283

Wang, G., Zhang, J., Li, X., Bao, Z., Liu, Y., Liu, C., Luo, J. (2017). Investigating causes of changes in runoff using hydrological simulation approach. *Appl Water Sci, 7*, 2245–2253. Doi: 10.1007/s13201-016-0396-1

Wang, J., Gao, Y., & Wang, S. (2018). Assessing the response of runoff to climate change and human activities for a typical basin in the Northern Taihang

Mountain, China. *J. Earth Syst. Sci.*, 1-15. doi:https://doi.org/10.1007/s12040-018-0932-5

Wang, M., Qin, D., Lu, C., & Li, Y. (n.d.). Modeling Anthropogenic Impacts and Hydrological Processes on a Wetland in China. *Water Resour Manage*, 2743–2757. doi: 10.1007/s11269-010-9577-0

Wang, S., Yan, M., Yan, Y., Shi, C., & He, L. (2012). Contributions of climate change and human activities to the changes in runoff increment in different sections of the Yellow River. *Quaternary International*, 66e77. doi:http://dx.doi.org/10.1016/j.quaint.2012.07.011

Worqlul, A. W., Dile, Y. T., Ayana, E. K., Jeong, J., Adem, A. A., & Gerik, T. (2018). Impact of Climate Change on Streamflow Hydrology in Headwater Catchments of the Upper Blue Nile Basin, Ethiopia. *water*, 1-18. doi: 10.3390/w10020120

Wu, J., Gao, X., Giorgi, F., Chen, Z., & Yu, D. (2012). Climate effects of the Three Gorges Reservoir as simulated by a high resolution double nested regional climate model. *Quaternary Internationa*, 27- 36. doi: 10.1016/j.quaint.2012.04.028

Yang, H., Yang, D., & Hu, Q. (2014). An error analysis of the Budyko hypothesis for assessing the contribution of climate change to runoff. *Water Resources Research*, 9620-9630. doi:doi:10.1002/2014WR015451.

Yang, T., Wang, X., Yu, Z., Krysanova, V., Chen, X., Schwartz, F., & Sudicky, E. (2014). Climate change and probabilistic scenario of streamflow extremes in an alpine region. *Journal of Geophysical Research: Atmospheres*, 8535-8550. doi:10.1002/2014JD021824

Yates, D. (2014). WatBal: An Integrated Water Balance Model for Climate Impact Assessment of River Basin Runoff. *International Journal of Water Resources Development, 12*(2), 121-140. doi: 10.1080/07900629650041902

Yilmaz, A. G., & Imteaz, M. A. (2011). Impact of climate change on runoff in the upper part of the Euphrates. *Hydrological Sciences Journal – Journal des Sciences Hydrologiques, 56*(7), 1265-1279.

Zhang, J. Y., & Wang, G. Q. (2007). Research on Impacts of Climate Change on Hydrology and Water Resources. *Science Press: Beijing, China*, 1-9.

Zhang, J. Y., Wang, G. Q., Pagano, T. C., Liu, C. S., HE, M. R., & Liu, L. I. (2012). Using hydrologic simulation to explore the impacts of climate change on runoff in the Huaihe River basin of China. *Journal of Hydrologic Engineering*, 1-28. doi:doi:10.1061/(ASCE)HE.1943-5584.0000581

Zhang, W., Shaoming, P., Cao, L., Cai, X., Zhang, K., Xu, Y., & Wei, X. (2015). Changes in extreme climate events in eastern China during 1960e2013: A case study of the Huaihe

Chapter 2: TREND AND RAINFALL VARIABILITY

2.1 Objective and Chapter Organization

This chapter extensively incorporates rainfall trends, change points, and variability analysis over a 30-year period (1991-2020). Section 2.3 deals with databases and methods applied. Prior to trend and change analysis, the data was preprocessed, and the same has been deliberated in detail in Section 2.3.2, followed by the steps of data preprocessing, visualization, and error correction. To select the suitable statistical technique, the entire dataset went through the Kolmogorov-Smirnov test and the autocorrelation test in sections 2.3.3 and 2.3.4, respectively. The trend of rainfall time series data was evaluated in Section 2.3.5, while Section 2.3.6 incorporated the methods of change point detection. The rainfall variability was analyzed in Section 2.3.7. The future rainfall condition (2021-2030) of the basin has been predicted through the ARIMA model in Section 2.3.8. The results of decadal and long-term rainfall status, change point detection, rainfall seasonality, and rainfall anomalies were analyzed in sections 2.4.3, 2.4.5, and 2.4.6, respectively. The future scenario for the next 10 years is simulated in Section 2.4.8. The previous related studies were reviewed in Section 2.4.9, and the key results were summarized with concluding remarks in Section 2.4.10.

2.2 Introduction

Basin management is the indispensable management of water resources as well as the multi-resource management of a large area or river basin. In the last few decades, the driving factors of hydrological components and the impact of climatic change have resulted in a growing interest in hydrological research (Zalewski 2000; Novotny and Stefan 2007; Clifton et al., 2018). Climatic components, as well as anthropogenic activities like water extraction, water diversification, construction of multipurpose projects, and changing land cover, are the key factors for the change in stream flow pattern (Gao et al., 2013). For the sake of water resource management, climatic parameter alteration must be quantified (Wang et al., 2018). Alteration of the hydrological cycle is directly associated with the changing nature of rainfall that

is directly related to water resources (Gajbhiye et al., 2015). The Indian subcontinent and its surroundings rely on the southwest monsoon, which brings a huge amount of moisture. In the last few decades, the variability and uncertainty of precipitation have become prominent (Long et al., 2021). In recent times, the Indian subcontinent has been facing very high spatiotemporal variability as well as the uncertainty of rainfall. For example, the mean yearly rainfall in Rajasthan (the western part of India) is 100 mm, while the rainfall is >2500 mm in the north-eastern part of India (Indian Water Resource Society, 2016). The changing behavior of climatic vectors, particularly the frequency of rainfall and its quantity, is changing the stream flow pattern, soil moisture content, and groundwater recharge (Islam et al., 2012; Srivastava et al., 2014; Swain et al., 2022a, b).

Climate change is the primary cause of the inconsistency or changing nature of rainfall events, which has exacerbated the dry season, runoff reduction, and food insecurity. Thus, climate change, which causes variability in rainfall, is the primary cause of agriculture's negative impact in many parts of the world (Siraj et al., 2020). The unabated increase in fossil fuel burning and greenhouse gas concentration has resulted in changes to a wide range of climatic components. The abrupt change that can occur in climatic behavior is known as a change point (Stern et al., 2014). Thus, the analysis of climatic variables, particularly rainfall, its changing nature, and trends is the most important way for any region to manage its water resources. In the Indian subcontinent, the study of climate change is a prime concern to understand the precipitation pattern (Jain, 2012).

Many studies have focused on change-point studies at the global and regional levels (Karl et al., 2000; Ahmad et al., 2014; Agarwal et al., 2021). In historical time series data, the Mann-Kendall test, Sen’s slop non-parametric test, and Pettit’s test were widely used for trend analysis, the magnitude of trend, and change point detection (Fu et al., 2007; Salarijazi et al., 2012; Karmeshu, 2012; Das et al., 2021). A standard normal homogeneity test was also applied to evaluate whether the data is homogeneous in long-term time-series data or whether the change has been perceived (Winingaard et al., 2003; Stepanek et al., 2009). Among the parametric methods (assuming that the data is normally distributed), various statistical techniques were also applied to understand the change point detection, such as

Buishand U, Buishand range, standard normal homogeneity, and a log-likelihood-based method (Kang and Yusof 2012; Dhorde and Dhorde 2013; Hussain et al., 2015; Chargui et al., 2018; Pandžić et al., 2019; Militon et al., 2020). Knowledge of change detection and trend analysis will help in understanding the nature of climatic anomalies along with providing proper management techniques (Fischer et al., 2012). Therefore, the study of temporal and spatial variations of rainfall and its long-term time series analysis have a decisive role in understanding the nature of rainfall (Michiels et al., 1992). To understand the trend of the climatic variables, various indices have been successfully used, such as the Precipitation Concentration Index (PCI) (Xuemei et al., 2010; De-Luis et al., 2011; Cui et al., 2017; Oliver, 1980; Michiels et al., 1992), the Rainfall Seasonality Index (Walsh and Lawler, 1981), and the Rainfall Anomaly Index (RAI) (Hernando et al., 2015). This study deals with Mann-Kendall statistics and Sen's slope to determine the trend of rainfall and the magnitude of linear change. If the stations in the study area have different topographical characteristics or are widely placed, then statistical tests are preferred to assess the absolute homogeneity and change point, as a significant association may not occur between them (Ahmed et al., 2020). Hence, the Pettitt Test, Buishand U Statistic, and Standard Normal Homogeneity Test were used to determine the significant change in the time series rainfall data. To evaluate the spatio-temporal variability and seasonality of rainfall, two extensively used and recognized indexes, RSI and RAI, were applied.

The modeling of climate change and its impact on future rainfall events is important for planning water resource management. The prediction of future rainfall is broadly studied based on a dynamic and empirical approach (Swami et al., 2018). The dynamic approaches are physical-based models, whereas the empirical approaches are fuzzy logic, regression, artificial neural networks (ANN), and Autoregressive Integrated Moving Averages (ARIMA) (Narayanan et al., 2016). The ARIMA model has been widely used to forecast future rainfall (Shamsnia et al., 2011; Mahsin et al., 2012), hydrology and river modeling (Cui, 2011), and evapotranspiration (Valipour et al., 2012). The prediction of future rainfall is performed in various states all over India (Narayanan et al., 2013; Chattopadhyay et

al., 2013). Many studies have been done on the river basin scale (Nanda et al., 2013). This present study has employed the ARIMA model to forecast rainfall.

The study area is economically and demographically important. The region is an important agricultural zone for eastern India. Further, the Mayurakshi River water system has a bearing on the region's irrigation, drinking, fishing, and varied other multipurpose uses (Ghosh et al., 2017). The river creates widespread flooding in certain sections of the basin during the rainy season, while over the years it has been reduced to a tame stream during the summer season. Thus, the study wants to find out the role of precipitation and the spatiotemporal character of rainfall in the Mayurakshi basin. The seasonal trend of rainfall was studied to obtain a clear understanding of the future trend, which is required for suitable planning of the river basin.

2.3 Database and Methodology

The database used in this chapter is outlined in this section, the detailed data source and the methodologies are given below:

2.3.1 Data Source

The rainfall data was collected from the India Meteorological Department (IMD) Pune (https://www.imdpune.gov.in/cmpg/Griddata/Rainfall_25_Bin.html). The obtained daily gridded rainfall data (in millimeters) has a high spatial resolution of 0.25 × 0.25 degrees. Rainfall data from 1991 to 2020 for the study area was obtained from the said source.

2.3.2 Data pre-processing: Visualization and error correction

After collecting the rainfall data, the row data set was exported to MS Excel, where it was corrected for missing values, and the stations were filtered to get the required rainfall stations for the study area. A total of 18 stations, covering the entire study area, were assigned names as - S1, S2, S3,... S18 (Fig. 2.1 and Table 2.2). The rainfall data was arranged on a daily, monthly, and annual basis for subsequent analysis.

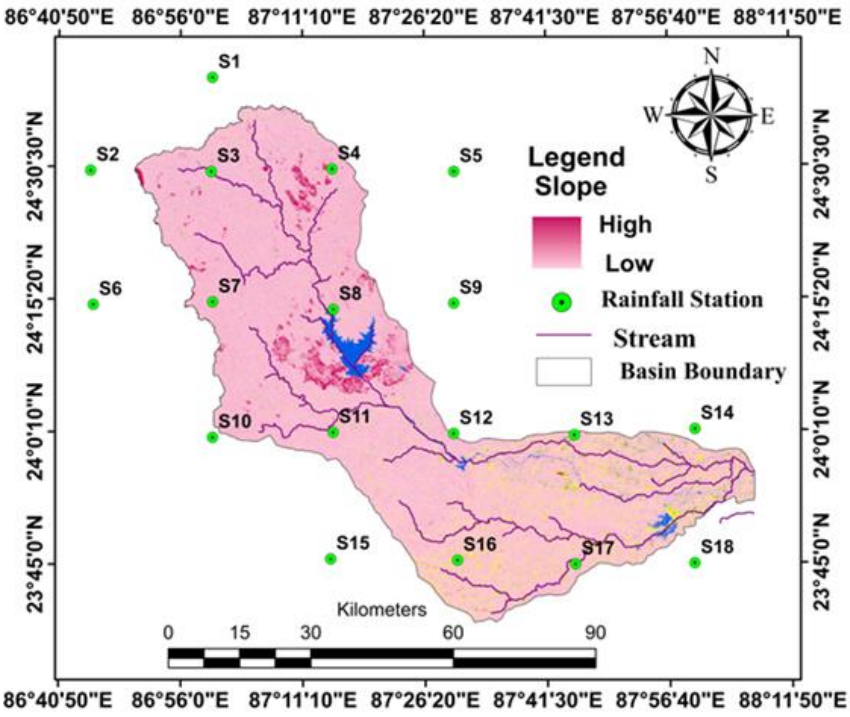

Fig. 2.1: Distribution of rainfall station

2.3.3 Normality test

Before applying appropriate change point detection techniques, it is crucial to assess whether the rainfall data confirms a normal distribution (Ghasemi et al., 2012). If the data exhibits a normal distribution, the Buishand U test and standard normal homogeneity test statistics can be utilized. Conversely, if the data does not follow a normal distribution, the Pettitt test can be employed. The normality of the data was evaluated using the Kolmogorov-Smirnov test with SPSS v26 software.

(i). Kolmogorov-Smirnov Test

The Kolmogorov-Smirnov test, also referred to as the KS test, is a statistical tool utilized to assess whether a given sample conforms to a particular probability distribution. Introduced by Kolmogorov and Smirnov in the 1930s and cited by D'Agostino & Stephens (1986), this test is classified as non-parametric, meaning it does not make assumptions about the data's underlying distribution. It is typically employed when the sample size exceeds 50. The test involves comparing the empirical cumulative distribution function (ECDF) of the sample against the

theoretical cumulative distribution function (CDF) of the target distribution. The test statistic is computed as the maximum absolute difference between these two functions, quantifying how well the sample aligns with the specified distribution (Alice Robson et al., 2000). If the test statistic exceeds the critical value, the null hypothesis is rejected, indicating that the sample does not conform to the normal distribution. Conversely, if the test statistic is smaller, the null hypothesis is retained, suggesting insufficient evidence to conclude that the sample deviates from the normal distribution.

The equation for the Kolmogorov-Smirnov (KS) test statistic is as follows:

$$D = \max|F(x) - S(x)| \quad \text{(Eq.1)}$$

Where: D represents the KS test statistic. F(x) is the theoretical cumulative distribution function (CDF) of the specified distribution. S(x) is the empirical cumulative distribution function (ECDF) of the sample. In this equation, the test statistic D is calculated as the maximum absolute difference between the theoretical CDF and the empirical CDF at each data point. It measures the largest vertical distance between the two cumulative distribution functions, indicating how well the sample aligns with the specified distribution.

2.3.4 Autocorrelation

Autocorrelation is one of the important tests to confirm whether the time series data has a serial dependency or is independent (Uyanto, 2020). It is highly recommended to check the autocorrelation of the dataset prior to trend analysis. In this present study, the autocorrelation was tested by employing ACF.pet in R statistical software (R v 4.1.2) at the K of lag-1 since the rainfall data was yearly data. If the test result confirms that the data belongs to independent series, then the Mann-Kendall test (MK test) is allowed for trend analysis; otherwise, the modified Mann-Kendall test (mMK) is preferred for auto-correlated data.

2.3.5 Methods of trend analysis

(i) Mann-Kendall Statistic

To analyze the trends in time series for long as well as short-term periods, the Mann-Kendall non-parametric test can be the measure to assess the consistent increasing or decreasing trends of the data (Lukas and Khambhammettu 2005; Alhaji et al., 2018). As the Mann-Kendall test is non-parametric, it suits all types of distributions of data and hence has been widely used when compared to other statistical methods to study long-term trends in time series data (Alahacoon and Edirisinghe 2021).

The tested Kendall's statistics (S) of time series data m1, m2, m3. . ., and m_n is estimated by the following equation (Libiseller and Grimvall 2002; Hipel and McLeod 1994).

$$S = \sum_{k=1}^{n-1} \sum_{j=k=1}^{n} sgn(x_J - x_k) \qquad \text{.....} \quad \text{(Eq.2)}$$

$$sgn(x_J - x_k) = \begin{cases} +1 \text{ -------- } (x_J - x_k) > 0 \\ 0 \text{ --------- } (x_J - x_k) = 0 \\ -1\text{--------- } (x_J - x_k) < 0 \end{cases} \text{.....(Eq.3)}$$

When $x_1 \ldots x_{2..} x_3 \ldots x_n$ and n is the time period of study. xj presents the data point at time j. If n is 10 or >10 then Z-transformation is employed as a normal approximation called the Kendall Z-value. To get the value of Z statistics to needs to adapt the variance of *VAR*(*S*) (Chattopadhyay et al., 2018; Aleum and Dioha 2020)

$$VAR(S) = 1/18\left[n(n-1)(2n+5) - \sum_{p-1}^{g} (t_p - 1)(2t_p - 5) \right] \text{.....} \quad \text{(Eq.4)}$$

When n is the number of observations, g is equal trend values, p represents the number of the tide group in the data set, and t_p indicates the number of data values, Sum (Σ) represent the summation of the overall tide group (Agbo and Ekpo 2021).

Calculated $VAR(S)$ computed to calculate Z transformation (Kendall test statistics Z-value) is a follows:

$$Z = \begin{cases} \frac{S-1}{VAR(S)} S > 1 \\ 0, \quad S = 0 \\ \frac{S-1}{VAR(S)} \; S < 0 \end{cases} \ldots\ldots\ldots\ldots\ldots\ldots\ldots\ldots\ldots\ldots\ldots\ldots$$

(Eq.5)

Here Z value represents a standard normal distribution, the negative value of z presents a down word trend and the positive value of Z represents an upward or increasing trend. For testing the significance level α is utilized (a two-tailed test).

(ii) Modified Mann–Kendall Test

The Mann-Kendall statistics give an erroneous result that overestimates or underestimates the Z statistics when the time series data has a significant autocorrelation (Rahman et al., 2017; Sharma and Goyal 2020). In such conditions, researchers prefer the modified Mann-Kendall test (Phuong et al. 2020; Güçlü, 2020) Therefore, the time series data was first tested at the lag-1 significance level to confirm the probability of serial dependency among the time series data. Due to the significant autocorrelation in the data series, modified Mann Kendall (mMK) statistic was used (Hamed and Rao 1998).

The modified Mann-Kendall VAR (S) was estimated by the following equation

$$\text{VAR}(S) = \left(\frac{n(n-1)(2n+5)}{18}\right) \cdot \left(\frac{n}{n_e^*}\right) \ldots\ldots\ldots\ldots\ldots\ldots\ldots\ldots$$

(Eq.6)

The auto-correlation data is adjusted by $\left(\frac{n}{n_e^*}\right)$ correction factor

$$\left(\frac{n}{n_e^*}\right) = 1 + \left(\frac{2}{n^3-3n^2+2n}\right)\sum_{f=1}^{n-1}(n-f)(n-f-1)(n-f-2)\rho_e(f).$$ (Eq.7)

$\rho_e(f)$ signifies the of auto-correlation among the rank of observation, computed as follows

$$\rho(f) = 2\sin\left(\frac{\pi}{6}\rho_e(f)\right)$$ (Eq.8)

(iii) Sen's Slope

Mann-Kendall Statistic provide the inclination (positive or negative) of the considered attribute, but the extent of the inclination is commonly assessed with Sen's Slope. A non-parametric statistic was developed by Sen (1968) to compute the slope and magnitude of linear change. Sen's slope estimates positive and negative slopes, which has been widely used to compute the magnitude of the trend (Alhaji et al., 2018; Kamal and Pachauri, 2019; Biswas et al., 2019). The slope is calculated as follows (Hirsch et al., 1982).

The method of linear trend estimation applied through a linear f (t) equation as

$$F(t) = Qt+B$$ (Eq.9)

Here F(t) represents a time series, that could be increased or decreased where *Q* is the slope and *B* is a constant. The *Q* can be calculated as shown in Eq 10.

$$Q_i = \frac{xj-xk}{j-k} \qquad i = 1,2,3,4,5 \ldots n \; j > k$$ (Eq.10)

Where, x_j and x_k represent the data values at time j and k (j > k) separately. The median of the n value Q_i is determined by the following equation:

$$Qi = \begin{cases} \left[\frac{Qn+1}{2}\right] \ldots\ldots\ldots\ldots\ldots\ldots\ldots\ldots\ldots n \text{ odd} \\ \frac{1}{2}\left[\frac{Qn}{2}\right] + \left[\frac{Qn+2}{2}\right] \ldots\ldots\ldots\ldots n \text{ even} \end{cases}$$

(Eq.11)

When *Qi* is positive it will present an increasing trend, and when *Qi value* is negative will represent a decreasing trend whereas zero value indicates no trend.

2.3.6 Methods of Change Point Detection

(i) Pettitt Test

Single change point detection was developed by Pettitt (1997). This statistical analysis is a nonparametric abrupt change point detection for hydrological and climate time series data (Smadi and Zghoul 2006; Gao et al., 2011; Zarenistanak et al., 2014). It was widely used by Bryson et al. (2012), Dhorde and Zarenistanak (2013); Agha et al., (2017), and many others as stated in Eq- 12, 13, 14.

$$U_k = 2\sum_{i=0}^{n} m_i - k(n+1) \quad \text{……}$$

(Eq.12)

Here m_i represents the rank of i^{th} observation and x_1, x_2, x_3,…, x_n are data points arranged in ascending order, and the value of k is taken from 1,2,3, 4, ……., n

$$K = \max\left|U_k\right| \text{……..…..} \quad \text{(Eq.13)}$$

$$U_k = \sum_{i=1}^{t} \sum_{1j=t+1}^{n} sign\left(x_i - x_j\right) \text{…….……..…} \quad \text{(Eq.14)}$$

The value of K in a series attains maximum by U_k, and a change point appears in the series. The critical value is gotten by:

$$K\alpha=[-1n\alpha(n^3+n^2)/6]^{1/2} \text{…….}$$

(Eq.15)

Here α represents the level of significance that decides the critical value and n is the number of observations of the data point.

(ii) Buishand U Statistic

The Buishand's U test was used to measure the change point detection (Ndione et al., 2017). This statistical test was applied for single change point detection (Buishand 1984). The Buishand U test is formulated as:

$$U = \frac{\sum_{k=1}^{n-1}(S_K / D_X)^2}{n(n+1)} \quad \text{……..……(Eq.16)}$$

Where the terms S_k is cumulative of deducted value from mean, and D^2_x is the standard deviation presented in Eq-17& 18.

$$S_k = \sum_{i=1}^{k}(X_i - \bar{X})$$

……..…….……(Eq.17)

$$D_x^2 = 1/n\sum_{i=1}^{n}(X_i - \bar{X})^2$$

…….……..……(Eq.18)

(iii) Standard Normal Homogeneity Test

Alexandersson (1986) developed standard normal homogeneity tests as a statistical method for detecting a change point in time-series data. This method is widely used to analyze change point detection in rainfall data (Kang and Yusof 2012; Dhored and Zarenistanak 2013). The equations are given below (Alexandersson 1986).

$$Ty = y\bar{z}_1 + (n-y)\bar{z}_2, Y = 1.2,3.....n$$

…….…..…(Eq.19)

Here $T_{(y)}$ statistic is computed to compare the mean value of the 1st year (y) with the last year (n-y), and Z_1 Z_2 computation can be written as below:

$$\bar{Z}_1 = 1/y\sum_{i=1}^{n}(y_1 - \bar{y}/S_q) \quad \text{and} \quad \bar{Z}_2 = 1/n-y\sum_{i=y+1}^{n}(y_1 - \bar{y}/S_q)$$

……. (Eq.20)

Here $\bar{y}$ represents the arithmetic mean value of the ratio and S_q standard deviation of the series. A breaking point in the time series exists when the value of *T* is maximum. To compute the homogeneity critical value is computed as

$$T_o = \max T_y \quad \text{.....(Eq.21)}$$

2.3.7 Methods of Rainfall Variability Analysis

(i) Rainfall Seasonality Index

The relative seasonality of the rainfall regime is expressed by the Rainfall Seasonality Index (RSI). The statistics of relative seasonality refer to the contrast of monthly rainfall throughout the year. This method is significant for describing the precipitation distribution and understanding the seasonal nature of rainfall. The RSI has been computed by using the following formula (Walsh and Lawler 1981)

$$RSI = \frac{1}{\overline{R}} \sum_{n=1}^{n=12} \left| \bar{x}_{ny} - \bar{R}_y / 12 \right| \quad \text{.....}$$

(Eq.22)

where $\bar{x}_{ny}$ measured the rainfall of month n of the specific $_y$ year, and $\overline{R_y} / 12$ measured the total annual rainfall for a specific year $_{y.}$

(ii) Rainfall Anomaly Index

The Rainfall Anomaly Index (RAI) is a ranked-based statistical method to compute the magnitude of anomalies, i.e., positive (+) anomalies and negative (-) anomalies (Gibbs and Maher 1967; Keyantash and Dracup 2002). The ten highest and lowest values are ranked and averaged to formulate the threshold of positive and negative anomalies proposed by Van-Rooy (Van-Rooy 1965). The ten highest and lowest values are ranked and averaged. This could be expected in extreme wet and dry conditions (Shen et al., 2006).

$$\text{RAI} = 3\frac{(\text{P}_\text{i} - \overline{\text{P}})}{(\bar{\text{r}} - \overline{\text{P}})} \quad \text{.....} \quad \text{(Eq.23)}$$

$$\text{RAI} = -3\frac{(\text{P}_\text{i} - \overline{\text{P}})}{(\bar{\text{r}} - \overline{\text{P}})} \quad \text{.....(Eq.24)}$$

Where P_i represents precipitation of the specific year (mm), $\bar{P}$ is the mean rainfall of the time series. $\bar{R}, \bar{r}$ represents the average of ten extreme highest and lowest-ranked precipitations, prefix ±3 used to compute positive and negative anomalies.

2.3.8 Prediction model

(a) ARIMA

The most important approach to time-series analysis, as proposed by Box and Jenkins in 1976 and modified by Box et al. (1994), is abbreviated as ARIMA a numeric weather forecasting empirical approach: - Autoregressive Integrated Moving Average (ARIMA). The model has been used to forecast the rainfall based on the 30 years of rainfall data (1991–2020) in the study area. Previous studies confirm that ARIMA modeling was effective and suitable for predicting future hydrological and meteorological parameters by considering numerous earlier data and random errors (Yurekli et al., 2007; Chattopadhyay et al., 2011). The ARIMA model is a synthesis of ARIMA (p, d, q), i.e., AR (p) autoregressive deals with historical time-series data (rainfall), I (d) differencing, and MA (q) moving average of random value (Phillips and Perron 1988). The ARIMA model was developed with sequential steps of model identification, model estimation, diagnostic check, and forecasting. The model identification deals with the Autocorrelation Function (ACF), Partial Autocorrelation Function (PACF), and Augmented Dickey-Fuller (ADF) statistics to check the stationarity and seasonality of the data (Figs 2.2 (a), (b)). Both statistical tests (ACF and PACF) identified the rainfall data as non-stationary. To get the stationarity of the data and to remove the seasonality of the data, the model is estimated by applying ACF, PACF with model residuals, and log transformation (Figs 2.3 (a), (b)). The Augmented Dickey-Fuller (ADF) result indicates Dickey-Fuller -13.193, at Lag order 7, with a p-value of 0.01 (0.05), indicating that the data is stationary. The model was selected based on Akaike information criteria (AIC = 4118.02) and Bayesian information criteria (BIC = 4125.72) (Akaike 1974; Schwarz 1978). The diagnostic check of model residuals reveals that the data is well-fitted and does not follow any extreme outliers. Based on AIC criteria, the best-fitted model was ARIMA (0,0,0) (1,1,0) [12]. After fitting the fitted model, rainfall is forecasted for ten years (2021–2030) at a 95% significance level. The model was validated by Jung–Box's (1976) statistic of residuals at log 30. The result of the Box-Ljung test p = 0.1134 (>0.05) indicated the model fitted well and was relevant to use for future prediction.

The rainfall prediction ARIMA (p, d, q) model is presented below (Box et al., 2015).

The rainfall prediction ARIMA (p, d, q) model is presented below

The backshift operator (B) expressed as

$$\phi(B)(1-B)^d z_t = \theta(B)a_t \quad \text{(Eq.25)}$$

The p, d, q of the ARIMA model is expressed below (Khashei et al., 2011; Valipour et al., 2016)

$$\bar{z}_t = \phi_1 \bar{z}_t - 1 + \phi_2 \bar{z}_t - 2 + \cdots + \phi_p \bar{z}_t - p + a_t - \theta_1 \bar{z}_t - 1 - \theta_2 \bar{z}_t - 2 - \cdots \theta_q \bar{z}_t - q \ldots \text{(Eq-26)}$$

where $\bar{z}_t = z_t - \mu$, and a_t is represent, the shock expressed in equation ……

The model was determined based on the Akaike information criterion (AIC) and Bayesian information criterion (BIC) expressed below

$$\text{AIC}(p,q) = N\ln(\sigma_\varepsilon^2) + 2(p+q) \quad \text{(Eq.27)}$$

$$BIC = \ln(n)k - 2\ln(\hat{L}) \quad \text{(Eq.28)}$$

Where in ARIMA p and q are logs, $\hat{L}$ is represented by $p(x \mid \psi, M)$, M using ψ as a parameter x represents the observed data and k is the number of the parameter.

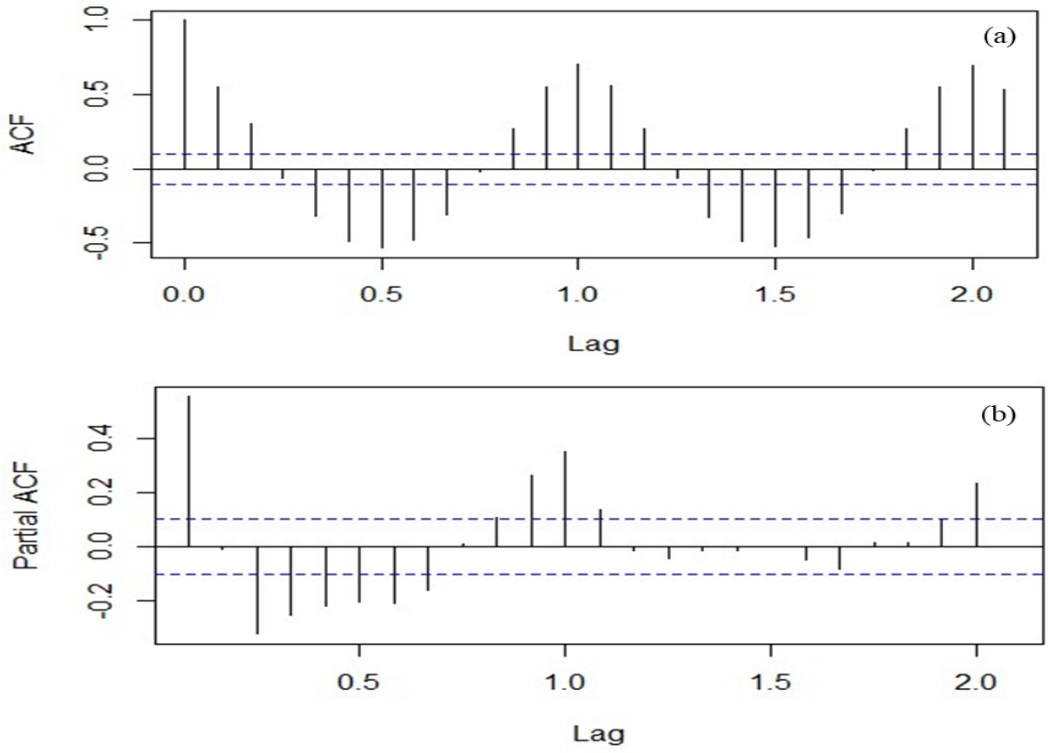

Fig. 2.2: (a) Autocorrelation function (ACF), (b) Partial autocorrelation function (PACF) plot of observed rainfall data

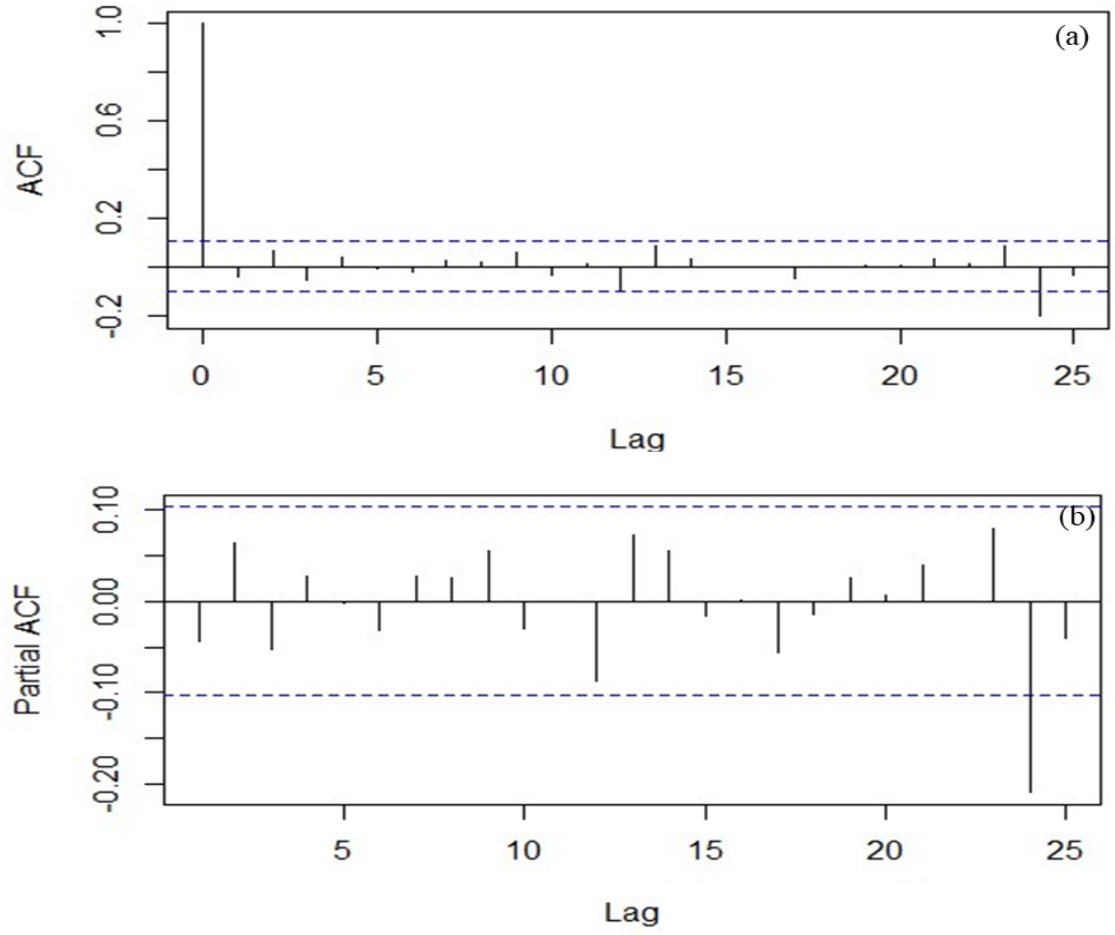

Fig. 2.3: (a) Autocorrelation function (ACF), (b) Partial autocorrelation function (PACF) plot of differencing and deseasonalized the rainfall data

2.3.9 Thematic presentation

(a) Inverse Distance Weighted (IDW)

Inverse distance weighted (IDW) is a deterministic estimation technique that relates the linear combination among nearby estimated points and determines the unknown value (Wu et al., 2016). Schloeder et al. (2001) evaluated various spatial interpolation techniques such as spline, kriging, and IDW. They concluded that the IDW technique gives a satisfactory result. Chen et al. (2012) applied IDW to rainfall data and got a satisfactory result with a high correlation coefficient value. Among the various interpolation methods like inverse distance weighting (IDW), radial basic function (RBF), local polynomial (LP), and global polynomial (GP), IDW was found

to be the most suitable technique for rainfall analysis (Kong and Tong, 2008; Wu et al., 2010). The advantage of this technique is its effectiveness in rainfall analysis. This method is sensitive to the extreme outer layer (Longley et al., 2005). In this present study of 30 years of rainfall data, there was no extreme out layer. The average distance among the stations was 28 km, with the maximum distance being 37.41 km and the minimum distance being 20.22 km. The IDW technique has been applied to create various spatial maps of the rainfall distribution in the study area.

2.4 Results and Discussion

2.4.1 Test of Normality

The 30-year time series rainfall data was tested for normality by employing the Kolmogorov-Smirnov test at a 95% of the confidence interval. The tested result showed that the p-value was greater than 0.05 (α=0.05, df=30, p>0.05) (Table 2.1). That confirmed the data is normally distributed (Fig 2.4).

Table 2.1: Tests of Normality

	Kolmogorov-Smirnov[a]		
	Statistic	df	Sig.
Rainfall	.114	30	.200*

Note: *. This is a lower bound of the true significance.

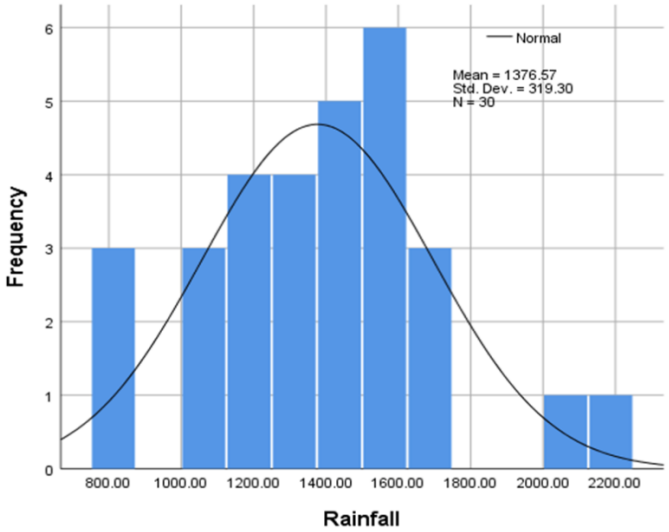

Fig. 2.4: normality plot of rainfall data (1991 - 2020)

2.4.2 Auto correlation test

The rainfall time-series data was checked for autocorrelation where the ACF.pet was 0.40 with the p- 0.02 at a 95% of confident interval. The result proved that the data does not have an autocorrelation and thus modified Mann-Kendall test has been used for the trend analysis of rainfall.

2.4.3 Rainfall Status

The detailed rainfall characteristics of the Mayurakshi basin from 1991 to 2020 have been taken to investigate the changing nature and spatial-temporal variation of rainfall in the basin. The basin covered 18 rainfall stations. The decadal annual and seasonal variability, along with the long-term trend of rainfall, are summarized in the sub-sections below:

(i) Decadal and long-term variation of rainfall

The modified Mann-Kendall statistic has been used to identify the trend of rainfall. The tested mMK of the whole basin shows the variation as well as the effect of climate change. To compute the overall rainfall variation of the basin, the p-value was calculated, which was computed to be >0.05 of the significance level alpha

(0.05). It indicates that in 30 years of long-term rainfall, there is no specific positive or negative trend in the rainfall series, and the trend varies from time to time. In general, negative Kendall's Z (-1.63) and normalized Kendall's tau (-0.20) show a decreasing rainfall trend (Fig. 2.6 and Table 2.3). The magnitude of the trend presented by Sen's slope shows the rainfall of the basin has a strong negative Sen's slope value which is -10.37 mm/year, implies that there is a decreasing or downward trend in rainfall (Fig. 2.6). The basin has 18 rainfall stations except for station S6; all the stations had negative rainfall trends during the whole sampled period. The highest negative magnitude of Sen's slope was found at S3, S4, and S12 (Q = -25.77 mm/year, -23.71 mm/year, and -12.30 mm/year) representing a high magnitude of decreasing rainfall trend. These were followed by negative Z statistics of -2.18, -1.70, and -5.00, respectively. The study found negative normalized Kendall's Z and Sen's slope values distributed throughout the study area. (Fig. 2.7 and Table 2.3).

Table 2.2: Decadal and long-term rainfall variation

Longitude	Latitude	Station	Rainfall (mm)			
			1991-2000	2001-2010	2011-2020	Long-term
87.00	24.75	S1	1354.32	1239.73	1146.57	1285.07
86.75	24.50	S2	1324.11	1281.24	1243.97	1297.40
87.00	24.50	S3	1752.05	1539.25	1355.59	1619.90
87.25	24.50	S4	1885.86	1838.98	1380.41	1717.37
87.00	24.25	S5	1674.31	1544.97	1369.27	1572.63
87.25	24.25	S6	1528.89	1553.95	1297.35	1451.71
87.50	24.25	S7	1660.64	1744.03	1305.31	1542.20
87.00	24.00	S8	1517.80	1446.53	1340.73	1458.77
87.25	24.00	S9	1607.93	1465.52	1344.43	1520.10
87.50	24.00	S10	1558.36	1566.56	1237.19	1451.30
87.75	24.00	S11	1368.12	1345.04	1095.81	1277.35
88.00	24.00	S12	1414.82	1287.93	1028.08	1285.90
87.25	23.75	S13	1602.61	1435.10	1377.65	1527.62
87.50	23.75	S14	1498.86	1413.80	1220.77	1406.16
87.75	23.75	S15	1365.61	1271.42	1106.56	1279.26
88.00	23.75	S16	1252.81	1180.60	1060.33	1188.65
87.50	23.50	S17	1464.92	1386.78	1255.11	1394.99
87.75	23.50	S18	1383.28	1281.80	1120.70	1295.75
	average		**1511.96**	**1434.62**	**1238.10**	**1420.67**
	maximum		**1885.86**	**1838.98**	**1380.41**	**1717.37**
	minimum		**1252.81**	**1180.60**	**1028.08**	**1188.65**
	SD		**160.48**	**170.52**	**114.66**	**140.01**
	CVR		**10.61**	**11.89**	**9.26**	**9.86**

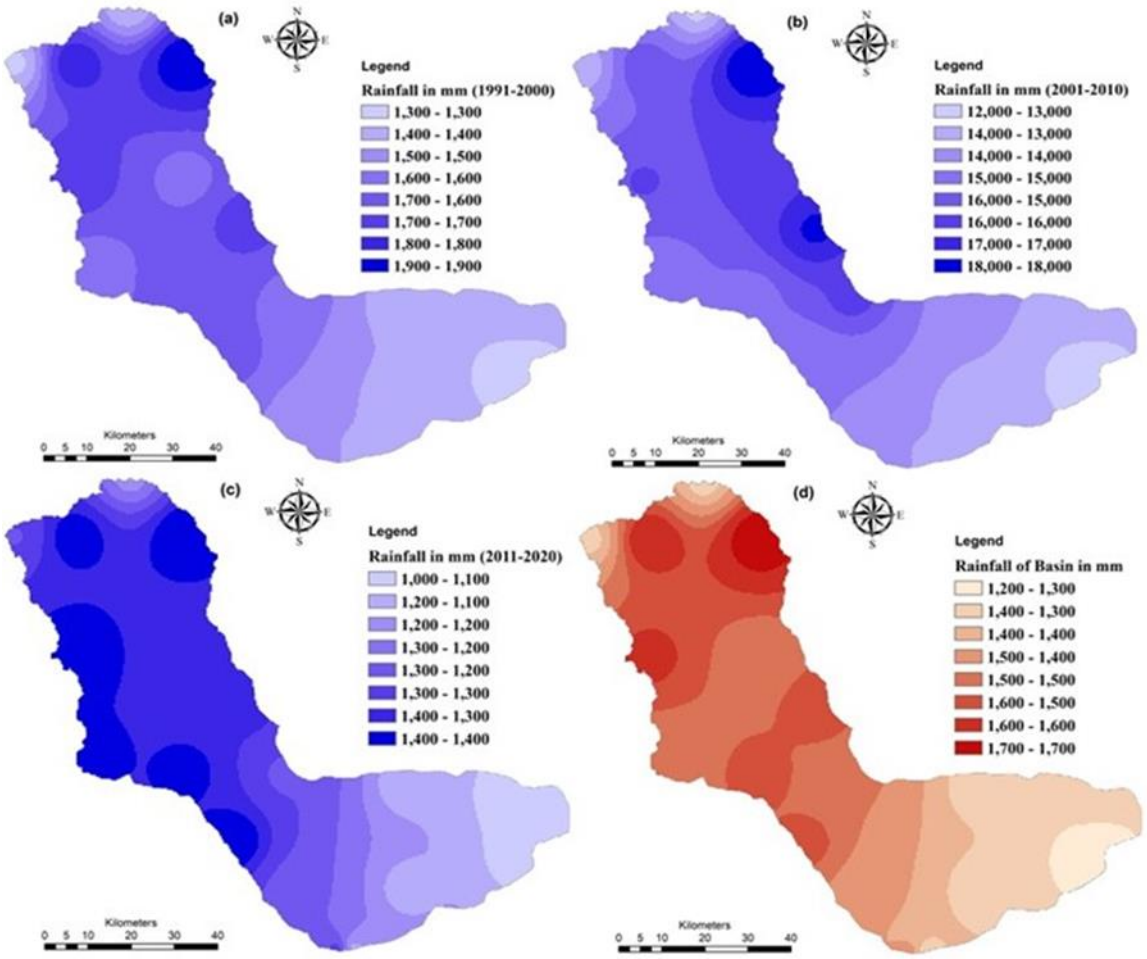

Fig. 2.5: Decadal and long-term spatial rainfall variation (a) 1st decade, (b) 2nd decade, (c) 3rd decade, (d) long-term basin average

2.4.4 Trend of rainfall

The modified Mann-Kendall statistic has been used to identify the trend of rainfall. The tested mMK of the whole basin shows the variation as well as the effect of climate change. To compute the overall rainfall variation of the basin, the p-value was calculated, which was computed to be >0.05 of the significance level alpha (0.05). It indicates that in 30 years of long-term rainfall, there is no specific positive or negative trend in the rainfall series, and the trend varies from time to time. In general, negative Kendall's Z (-1.63) and normalized Kendall's tau (-0.20) show a decreasing rainfall trend (Fig. 2.6 and Table 2.3). The magnitude of the trend presented by Sen's slope shows the rainfall of the basin has a strong negative Sen's

slope value which is -10.37 mm/year, implies that there is a decreasing or downward trend in rainfall (Fig. 2.6). The basin has 18 rainfall stations except for station S6; all the stations had negative rainfall trends during the whole sampled period. The highest negative magnitude of Sen's slope was found at S3, S4, and S12 (Q = -25.77 mm/year, -23.71 mm/year, and -12.30 mm/year) representing a high magnitude of decreasing rainfall trend. These were followed by negative Z statistics of -2.18, -1.70, and -5.00, respectively. The study found negative normalized Kendall's Z and Sen's slope values distributed throughout the study area. (Fig. 2.7 and Table 2.3).

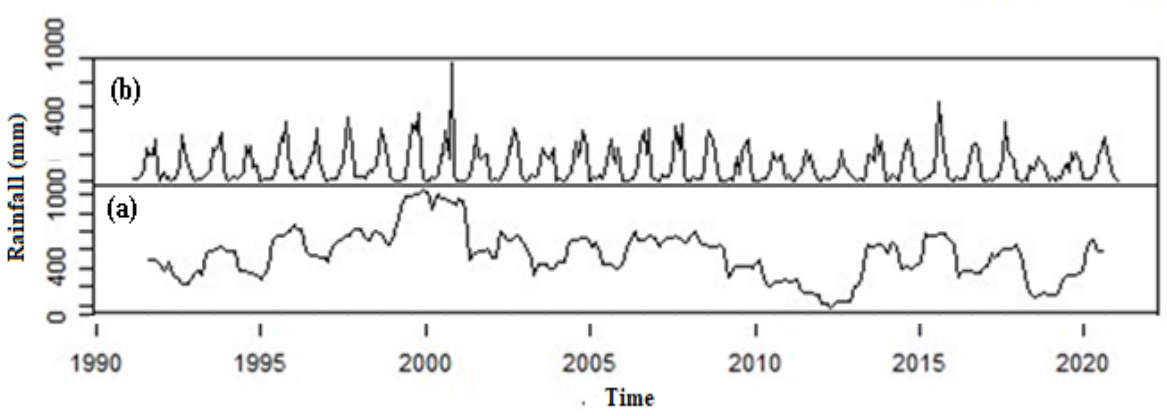

Fig. 2.6: (a)Rainfall trend (b) seasonal variation

Table 2.3: Modified Mann Kendall Statistic and Sen's slope estimation

Station	Normalized Test (Z)	Kendall's tau	p-value (Two-tailed)	Sen's slope (Q value mm/year)
Basin	-1.63	-0.20	0.103	-10.37
S1	-1.89	-0.25	0.059	-14.31
S2	-0.50	-0.07	0.617	-3.98
S3	-2.18	-0.28	0.030	-25.77
S4	-1.70	-0.20	0.089	-23.71
S5	-1.23	-0.20	0.219	-12.14
S6	0.11	0.02	0.910	1.30
S7	-0.69	-0.10	0.492	-10.68
S8	-0.21	-0.03	0.830	-5.40
S9	-1.18	-0.15	0.239	-10.07
S10	-0.89	-0.14	0.374	-9.23
S11	-0.86	-0.11	0.392	-9.70
S12	-5.00	-0.37	0.000	-21.30
S13	-1.64	-0.21	0.101	-12.37

S14	-2.00	-0.26	0.046	-17.20
S15	-1.61	-0.21	0.108	-12.18
S16	-1.74	-0.15	0.083	-6.88
S17	-1.58	-0.23	0.113	-11.73
S18	-1.64	-0.21	0.101	-13.86

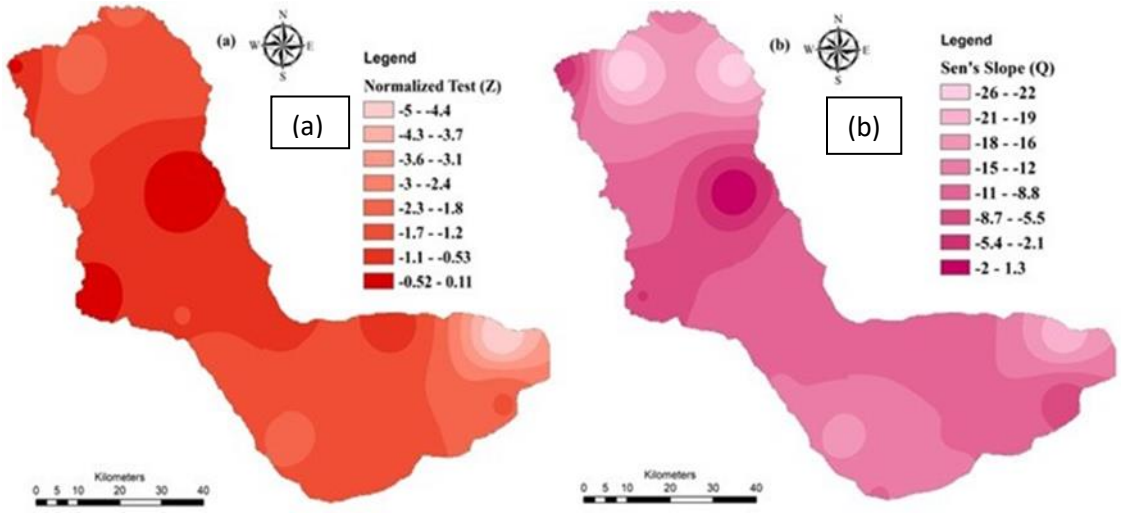

Fig. 2.7: Normalized Z (a) Sen's slope Q (b)

2.4.5 Change point of annual rainfall

Statistical methods like Pettitt's test, the SNHT test, and Buishand's test were applied to detect the homogeneity and change point of rainfall. The tests confirmed that the change point of the basin was in 2008. The tested mathematical models show that the computed p-value is lower than the significant level $\propto = 0.05$ at 95 % of the confidence interval, indicating a change in rainfall during the 30-year study period. For the individual rainfall stations tested, models presented a breakpoint of annual rainfall at stations S1, S4, S10, S14, and S18 in 2008 and at S3 in 2007, which was around the middle of the taken time period (Table 2.4). For stations, S12 Pettitt's test indicated that the change point was in 2002, while according to the SNHT test and Buishand's U test, it was in 2009 (Table 2.4). The tested change-point models (Pettitt's test, SNHT test, Buishand's test) show the computed p-value was greater than the significant level $\propto = 0.05$ at 95% of the confident interval at 61.11% of the stations (S2, S5, S6, S7, S8, S9, S11, S13, S15, S16, S17), indicating there was no significant change in rainfall during the study period.

Table 2.4: Changepoint statistics of the basin

Station	Pettitt's test			SNHT test			Buishand's test		
	U	t	p 95%	T0	t	P 95%	Q	t	P 95%
Basin	138	2008	0.033	8.1931	2008	0.0435	0.531	2008	0.027
S1	124	2008	0.073	6.171	2008	0.143	0.456	2008	0.047
S2	95	2007	0.287	4.502	2007	0.325	0.226	2007	0.225
S3	153	2007	0.013	10.269	2007	0.012	0.809	2007	0.004
S4	154	2008	0.012	10.045	2008	0.013	0.594	2008	0.020
S5	114	2008	0.122	4.295	2008	0.362	0.286	2008	0.151
S6	94	1996	0.299	4.809	1996	0.285	0.240	2008	0.201
S7	120	2008	0.090	6.378	2008	0.130	0.321	2008	0.114
S8	78	2008	0.541	3.443	2008	0.525	0.248	2008	0.188
S9	116	2008	0.011	5.855	2008	0.167	0.472	2008	0.010
S10	136	2008	0.037	7.599	2008	0.041	0.406	2008	0.046
S11	107	2019	0.171	4.781	2009	0.293	0.284	2009	0.156
S12	148	2002	0.018	9.995	2009	0.014	0.846	2009	0.002
S13	118	2008	0.100	5.347	2000	0.218	0.366	2000	0.082
S14	140	2008	0.030	7.872	2008	0.054	0.540	2008	0.027
S15	140	2002	0.195	4.801	2008	0.285	0.393	2008	0.070
S16	90	2002	0.350	3.497	2002	0.510	0.263	2002	0.169
S17	128	2008	0.059	6.148	2008	0.145	0.418	2008	0.059
S18	112	2008	0.035	6.216	2008	0.137	0.011	2008	0.034

2.4.6 Rainfall seasonality index

The long-term (30-year) rainfall seasonality in each year of individual stations in the basin was computed to reveal the nature of rainfall seasonality. The overall computed rainfall seasonality revealed that two classes of RSI existed across the basin (<0.19: “very equable” and 0.20-0.39: “equable indefinite weather”). At stations S12 and S15, a greater percentage of the sampled years (60.00%) were computed to have “very equitable” rainfall throughout the year. The RSI was counted as “very equitable” and “equitable” in definite weather in 50.00% of the sampled years at 44.44% of the stations throughout the year (Table 2.5). At stations S5, S8, and S10, the RSI was computed as “equitable” in definite weather in 53.33% of sampled years. The decadal RSI revealed that only in the 1st decade at S18 RSI was “very equitable” (<0.19), while in the 1st, 2nd, and 3rd decades, RSI was 0.20-0.39, i.e., “equable” in definite weather across the study area (Table 2.5). The RSI was calculated as “equitable” in definite weather for the decadal character of basin rainfall for 43.33% of the years. The spatially high intensity of RSI between 0.20 and 0.39 was found in the upper basin in the 1^{st} decade and the 2^{nd} decade in the middle and upper parts of the basin, whereas in the 3^{rd} decade, the southern part of the middle and lower basin experienced RSI >0.20 (Fig. 2.8). The rainfall received in the study area is monsoonal rain. The rainfall seasonal character of the upper and middle basins is nearly the same as it is situated in the plateau region, and orographic conditions prevail. while in the plain region of the lower basin area, there is much difference between “very equable” and “equable” in definite weather rainfall, i.e., in average, “very equable” (56.67%) and “equable” in definite weather rainfall (43.33% of the sampled years). The absence of a topographic barrier could be the reason for rainfall uncertainty in the region.

Table 2.5: Rainfall seasonality and decadal status

Station	RSI Class (Year in percent)		RSI decadal average		
	Very equable (<0.19)	Equable in definite weather (0.20-0.39)	1991-2000	2001-2010	2011-2020
Basin	56.67	43.33	0.20	0.20	0.22
S1	53.33	46.67	0.20	0.20	0.24
S2	50.00	50.00	0.23	0.20	0.24
S3	50.00	50.00	0.22	0.20	0.23
S4	50.00	50.00	0.20	0.20	0.22
S5	46.67	53.33	0.22	0.21	0.24
S6	56.67	43.33	0.20	0.23	0.20
S7	53.33	46.67	0.21	0.21	0.21
S8	46.67	53.33	0.21	0.22	0.24
S9	50.00	50.00	0.19	0.22	0.23
S10	46.67	53.33	0.20	0.21	0.24
S11	50.00	50.00	0.20	0.19	0.24
S12	60.00	40.00	0.20	0.19	0.22
S13	50.00	50.00	0.20	0.20	0.24
S14	53.33	46.67	0.20	0.20	0.24
S15	60.00	40.00	0.20	0.18	0.23
S16	56.67	43.33	0.21	0.19	0.22
S17	50.00	50.00	0.20	0.21	0.23
S18	50.00	50.00	0.17	0.20	0.27

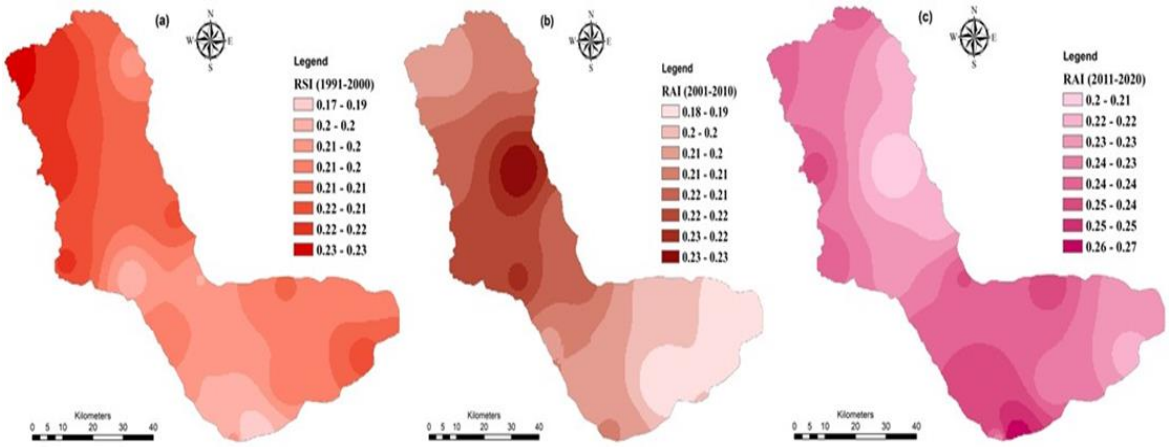

Fig. 2.8: RSI decadal average (a) 1st decade, (b) 2nd decade, (c) 3rd decade

2.4.7 Rainfall anomaly index

Based on RAI, the events of the dry and rainy conditions in the basin were evaluated. In the overall 30 years, the temporal characteristic of rainfall was found to be extremely wet in 16.67% of the years, with the categories of very wet, moderately wet, slightly wet, and slightly dry in 10 % of the sampled years, and 6.67% of the years were recorded as having extremely dry conditions across the basin. The temporal character of RAI represents extremely wet (>3.00) and extremely dry (<-3.00) conditions in 13.33% of the years at S1, S5, S10, S12, and S14 throughout the basin.

The highest percentage of near-normal rainfall anomalies occurred at S11 and S13 in 26.67% and 23.33% of years, respectively, and at S1, S7, and S17 in 20 % of the counted years. The very dry condition of RAI was found in 23.33% of the sampled years at S7 and 20 % of the sampled years at S6, and S13. Similar precipitation variability was classified as moderately dry in 13.33% of the sampled years at S1, S2, S8, S11, S13, S15, S17, and S18. In general, the basin experienced extremely wet and extremely dry conditions in 16.67% and 6.67% of the sampled years, and near-normal conditions were recorded in only 6.67% of the years (Table 2.6).

In the context of spatial-temporal variation, RAI perceived that the years 2009–2014 had an extreme drought condition and 1999–2000 had an extreme wet condition for the basin (Fig. 2.9). At stations S7, S9, S10, S11, S12, S15, and S16, extreme dry conditions were recorded from 2011 to 2012 (Fig. 2.9). Except for stations S7, S12, S16, and S18, extremely wet conditions were recorded from 1999 to 2000 through RAI (Fig. 2.9).

Table 2.6: Rainfall anomaly and drought status

Station	Class description (RAI) & years in percentage									Drought year (%)
	Extremely Wet	Very Wet	Moderately Wet	Slightly Wet	Near Normal	Slightly Dry	Moderately Dry	Very Dry	Extremely Dry	
	>3.00	2.00 to 2.99	1.00 to 1.99	0.50 to 0.99	0.49 to -0.49	-0.50 to -0.99	-1.00 to -1.99	-2.00 to -2.99	<-3.00	
Basin	16.67	10.00	10.00	10.00	6.67	10.00	16.67	13.33	6.67	50.00
S1	13.33	3.33	13.33	3.33	20.00	10.00	13.33	6.67	16.67	50.00
S2	13.33	6.67	13.33	13.33	0.00	13.33	13.33	13.33	13.33	53.33
S3	10.00	13.33	6.67	6.67	10.00	10.00	20.00	6.67	16.67	60.00
S4	13.33	6.67	20.00	6.67	6.67	0.00	16.67	10.00	20.00	53.33
S5	13.33	0.00	10.00	23.33	0.00	3.33	20.00	16.67	13.33	53.33
S6	10.00	10.00	13.33	10.00	3.33	3.33	16.67	20.00	13.33	56.67
S7	13.33	6.67	3.33	10.00	20.00	10.00	3.33	23.33	10.00	56.67
S8	10.00	6.67	10.00	10.00	13.33	3.33	13.33	16.67	16.67	56.67
S9	10.00	6.67	10.00	10.00	13.33	10.00	10.00	13.33	16.67	50.00
S10	13.33	10.00	16.67	0.00	0.00	20.00	16.67	10.00	13.33	60.00
S11	10.00	6.67	16.67	3.33	26.67	0.00	13.33	10.00	13.33	53.33
S12	13.33	10.00	20.00	6.67	6.67	6.67	20.00	3.33	13.33	50.00
S13	10.00	3.33	13.33	0.00	23.33	3.33	13.33	20.00	13.33	53.33
S14	13.33	13.33	10.00	6.67	10.00	6.67	16.67	10.00	13.33	53.33
S15	13.33	6.67	13.33	13.33	16.67	6.67	13.33	6.67	10.00	46.67
S16	10.00	6.67	23.33	3.33	13.33	13.33	20.00	0.00	10.00	46.67
S17	16.67	3.33	13.33	6.67	20.00	6.67	13.33	0.00	20.00	60.00
S18	13.33	3.33	20.00	20.00	10.00	0.00	13.33	10.00	10.00	43.33

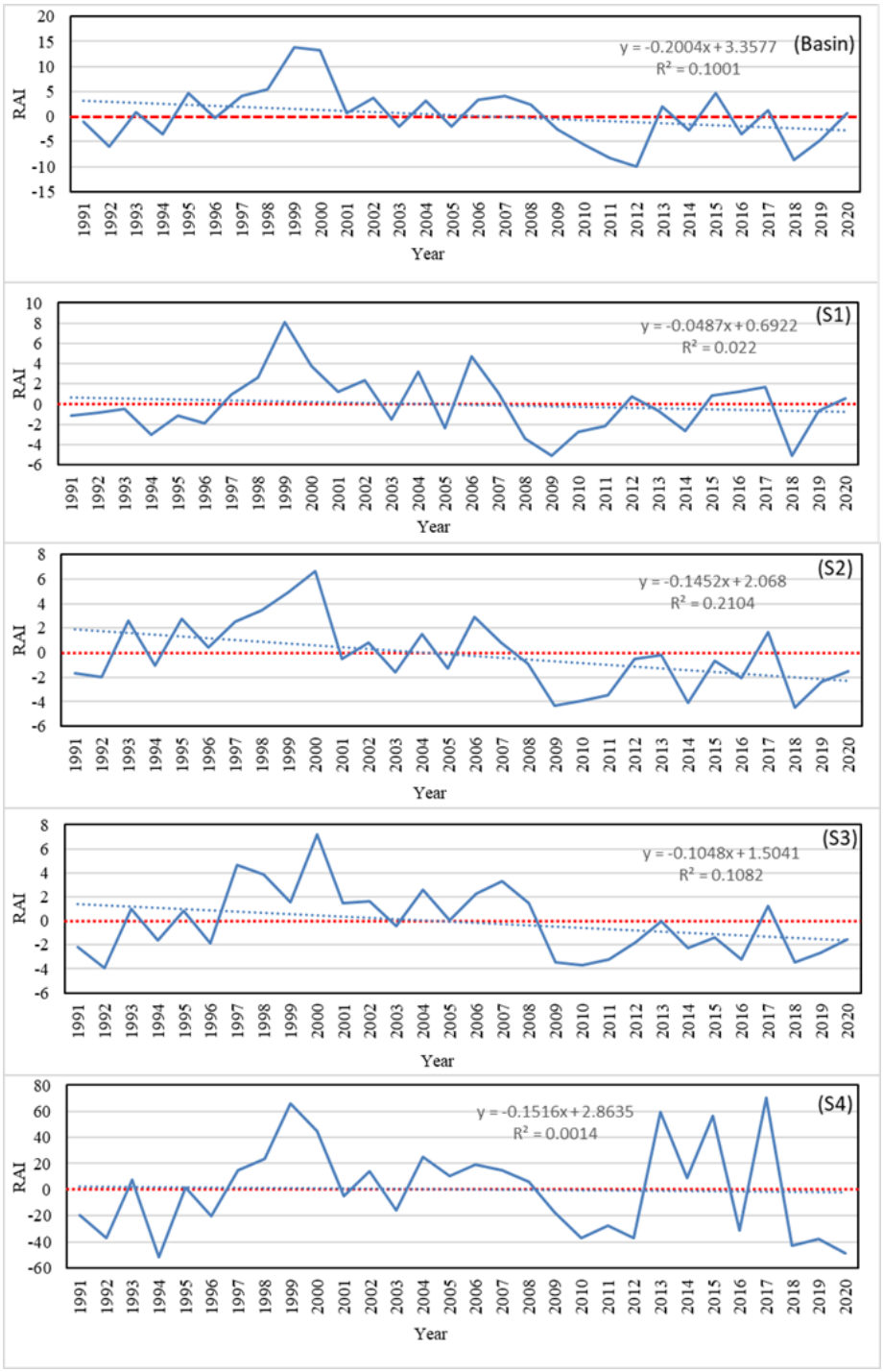
(Basin)
y = -0.2004x + 3.3577
R² = 0.1001
(S1)
y = -0.0487x + 0.6922
R² = 0.022
(S2)
y = -0.1452x + 2.068
R² = 0.2104
(S3)
y = -0.1048x + 1.5041
R² = 0.1082
(S4)
y = -0.1516x + 2.8635
R² = 0.0014
RAI
Year

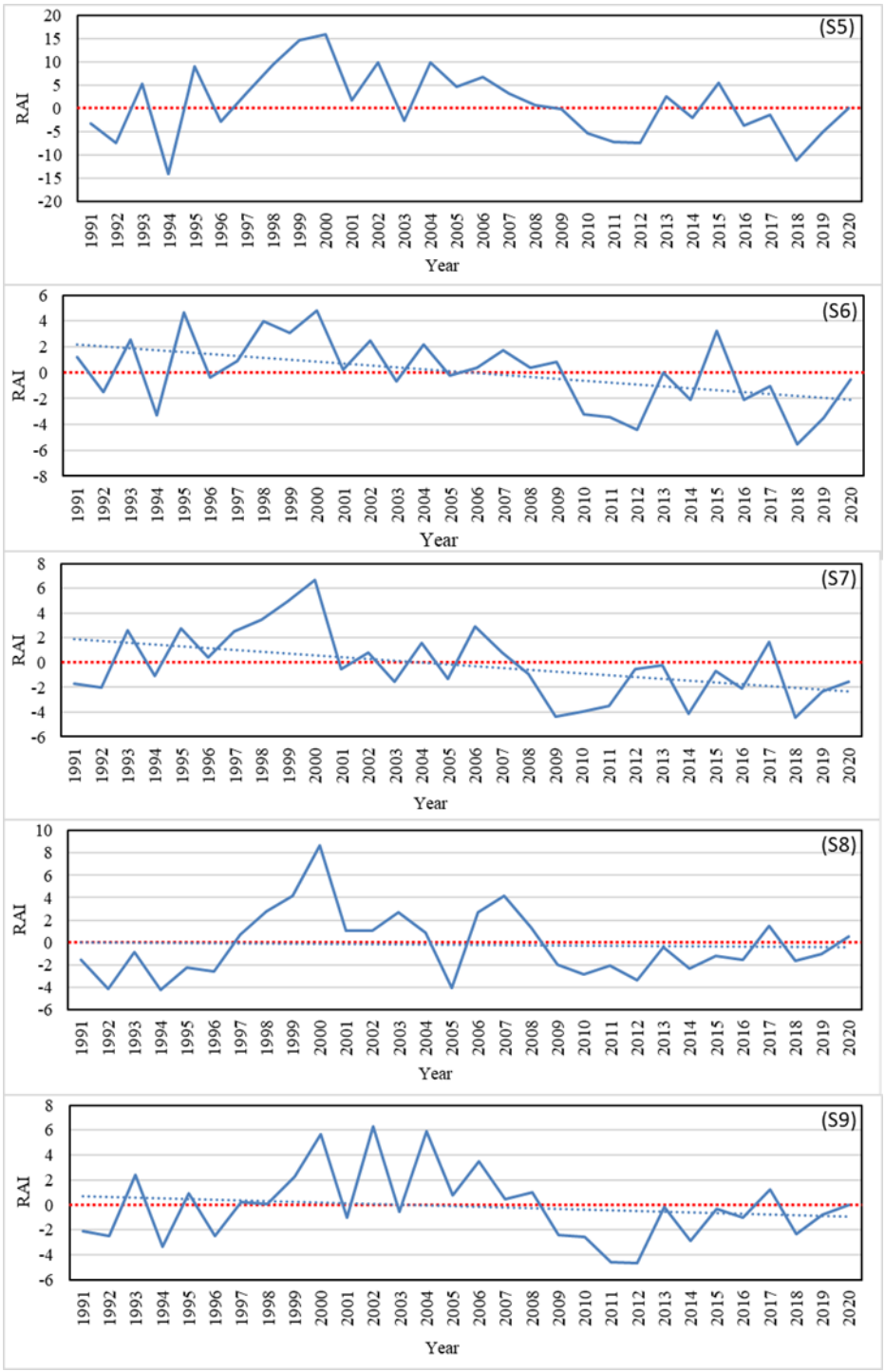
(S5)
RAI
Year
(S6)
RAI
Year
(S7)
RAI
Year
(S8)
RAI
Year
(S9)
RAI
Year

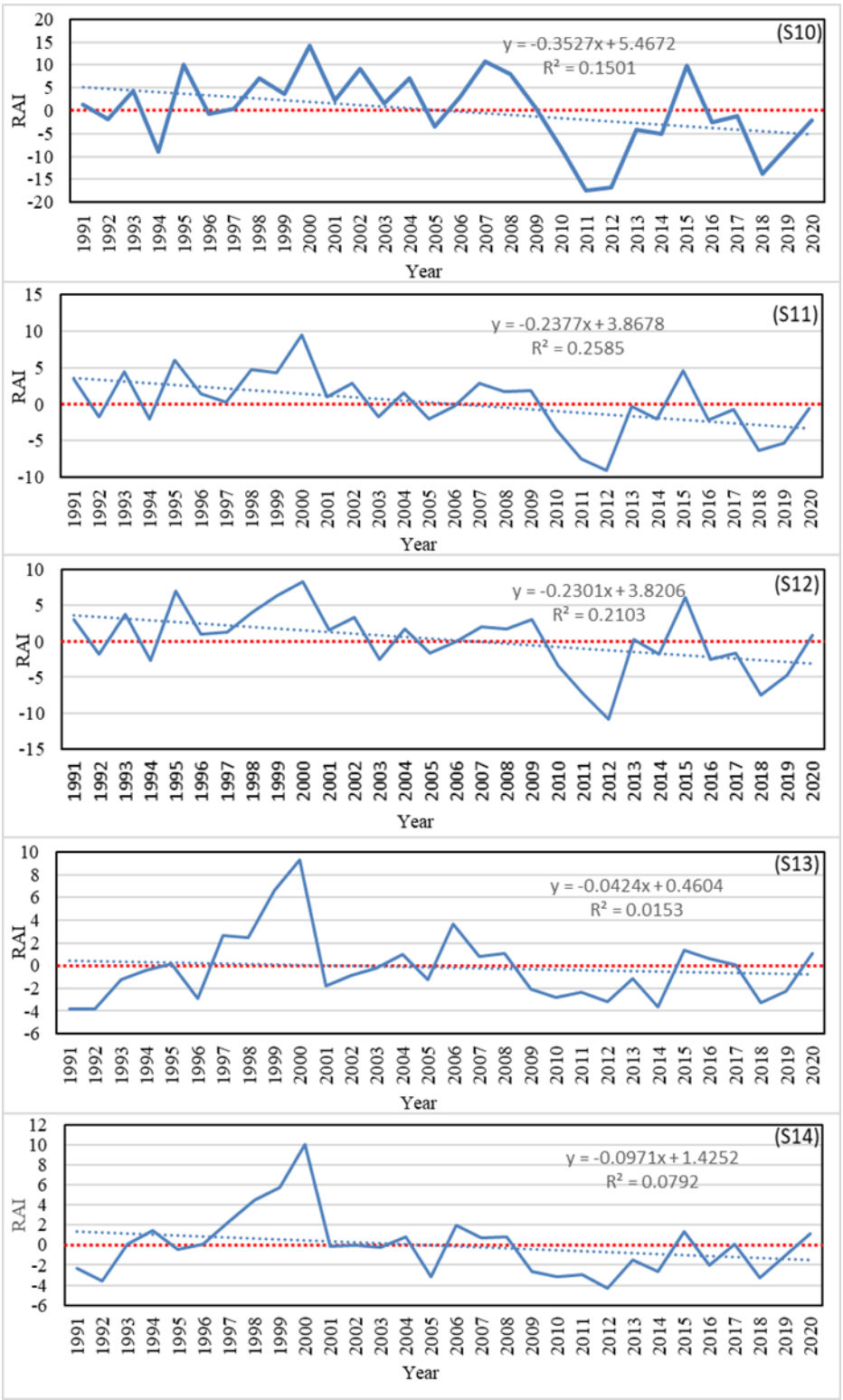
(S10)
y = -0.3527x + 5.4672
R² = 0.1501
RAI
Year
(S11)
y = -0.2377x + 3.8678
R² = 0.2585
RAI
Year
(S12)
y = -0.2301x + 3.8206
R² = 0.2103
RAI
Year
(S13)
y = -0.0424x + 0.4604
R² = 0.0153
RAI
Year
(S14)
y = -0.0971x + 1.4252
R² = 0.0792
RAI
Year

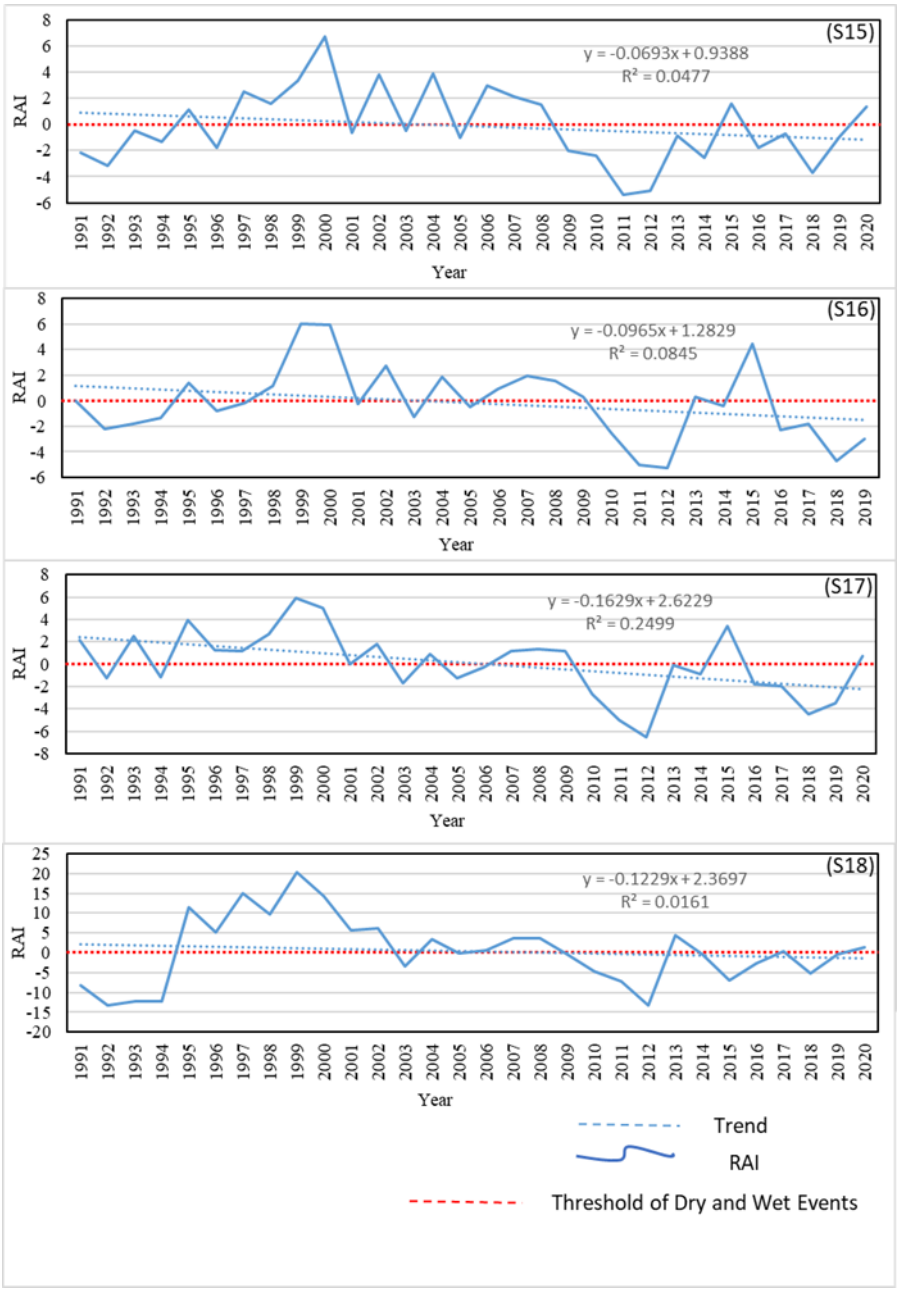

Fig. 2.9: Wet and dry condition of individual stations

2.4.8 Temperature, Wind speed, Solar radiation, and Humidity variability

In the long-term average of a 30-year time period, the average of climatic components such as temperature, wind speed, solar radiation, and humidity were recorded as 32.23 ± 0.63 ℃, 1.9 ± 0.12 m/s, 90.40 ± 5.00 W/m^2, and 63.44 ± 5.48 respectively (Table 2.7). During the study period, the basin received a maximum temperature of 33.80℃, the temperature varied from time to time, in overall

conditions from 1991 to 2020, the temperature followed a slightly increasing trend (Fig. 2.10a) seconded by a significant Kendall's P value of 0.05 with its normalized test (Z) and Kendall's tau of 1.89, 0.24 respectively. The increasing trend in temperature was 0.03 ^{0}C at the annual rate. The maximum and minimum wind speed conditions during the study period were 2.25 m/s and 1.72 m/s with an average of 1.99 m/s. During the whole study period, wind speed experienced a significant (P = <0.05) decreasing trend (Fig. 2.10b), and the magnitude of the decreasing wind speed was -0.007 m/s annually with its normalized test (Z) and Kendall's tau accounted for -2.29 and -0.37, respectively (Tables 2.7 and 2.8). The maximum and minimum solar radiation recorded 99.78 W/m^2 and 82.25 W/m^2 respectively, a very low decreasing rate of solar radiation recorded (-0.44 W/m^2 annually) during the whole study period. The maximum and minimum humidity were 73.59 % and 49.37 % respectively. The humidity followed a decreasing trend with a magnitude of -0.43% annually. Among the climatic parameters, a significant increase in temperature is found, while the rest of the parameters (wind speed, solar radiation, and humidity) were recorded as decreasing in nature over the study period. With increasing temperatures, rainfall, humidity, and wind speed have decreased with time.

Table 2.7: Climatic parameters

Year	Temperature (C)	Wind Speed (m/s)	Solar Radiation (W/m^2)	Humidity (%)
1991	31.66	2.08	95.01	73.59
1992	32.23	2.17	95.76	66.78
1993	31.93	2.21	99.78	65.69
1994	32.08	2.25	95.07	68.53
1995	32.92	2.25	97.98	64.37
1996	32.53	2.13	97.35	63.98
1997	32.13	2.02	96.84	64.12
1998	31.41	1.98	95.56	67.06
1999	32.30	2.01	98.34	63.13
2000	31.43	1.95	96.75	67.44
2001	32.82	1.94	87.83	63.84
2002	32.37	1.90	87.15	62.96
2003	31.34	1.93	88.30	69.41
2004	31.17	1.96	89.39	68.80
2005	31.74	1.92	87.36	66.77
2006	32.28	1.81	88.13	65.31

2007	31.83	1.90	87.35	66.72
2008	31.91	1.72	86.30	66.34
2009	32.01	1.89	88.29	65.77
2010	31.90	1.97	89.16	63.40
2011	31.90	1.90	84.67	64.71
2012	32.22	2.10	87.64	63.75
2013	31.78	2.08	85.34	67.90
2014	32.28	1.98	86.74	59.97
2015	32.06	1.96	83.80	53.71
2016	33.80	1.98	92.67	56.35
2017	33.01	1.92	84.80	53.46
2018	33.10	1.89	90.22	55.16
2019	33.52	2.02	86.28	49.37
2020	33.20	1.84	82.25	54.76
Long-term Average	32.23	1.99	90.40	63.44
SD	0.63	0.12	5.00	5.48

Table 2.8: Trend of Climatic parameters

Parameter	Normalized Test (Z)	Kendall's tau	p-value (Two-tailed)	Sen's slope (Q value)
Temperature	1.89	0.24	0.058	0.03
Wind speed	-2.92	-0.37	0.003	-0.007
Solar radiation	-4.31	-0.55	-0.55	-0.44
Humidity	-2.18	-0.28	-0.55	-0.43

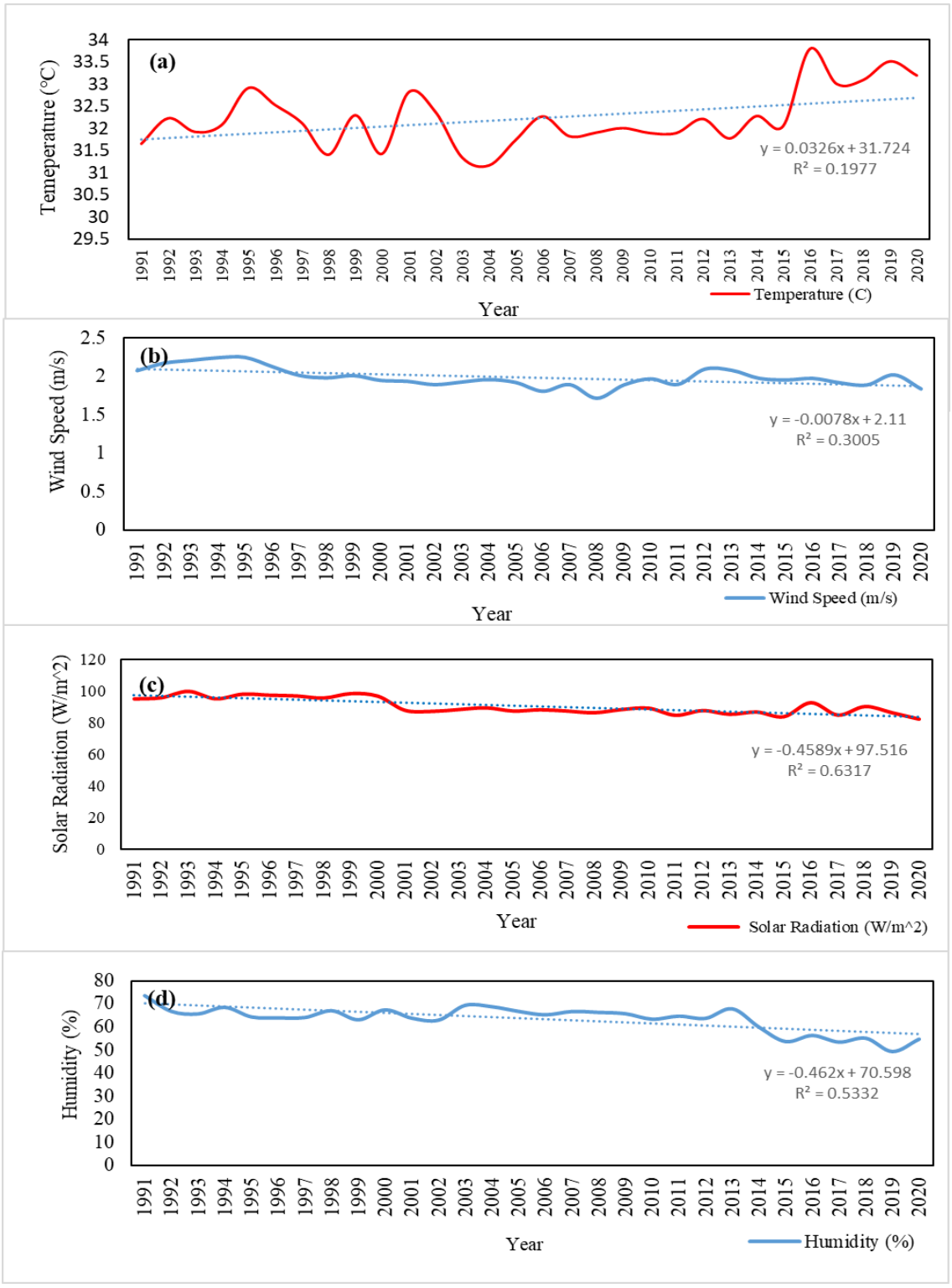

Fig. 2.10: Trend of (a) temperature, (b) Wind Speed (c) Solar Radiation, (d) Humidity

2.4.9 Change point of temperature

At present climate change is attributed to increasing temperatures as it has also been found in the IPCC 2003 report. The temperature of the study area increased by 0.03^0C/year. Statistical methods like the SNHT test, and Buishand's test were applied to detect the homogeneity and change point of temperature. The tests confirmed that the change point of temperature was in 2015 confirmed by the SNHT test, and Buishand's test. The tested mathematical models show that the computed p-value is lower than the significant level $\propto = 0.05$ at 95 % of the confidence interval, indicating a change in temperature during the 30-year study period.

Table 2.9: Change point of temperature

Parameter	SNHT test			Buishand's test		
	T0	t	P 95%	Q	t	P 95%
Temperature	17.36	2015	<0.05	0.72	2015	<0.05

2.4.10 Rainfall Forecasting

The forecasted annual rainfall of the Mayurakshi basin shows an average of 1303.38 ± 19.99 mm of rainfall with a maximum and minimum of 1335.28 mm, and 1251.84 mm respectively, from January 21st, 2021 to December 30th, 2030. The forecasted rainfall shows very little variability of rainfall (CV 1.53) for the next 10 years and the trend line depicts a linear positive trend for the rainfall of the basin. The predicted highest rainfall is estimated for 2022, and the lowest annual rainfall is for 2021 (Table 2.9).

Table 2.10: Forecasted rainfall status (2021 to 2030)

Yeas	Rainfall (mm)
2021	1251.84
2022	1335.28
2023	1292.56
2024	1314.43
2025	1303.23
2026	1308.97
2027	1306.03
2028	1307.54
2029	1306.76
2030	1307.16
Average	1303.38
Maximum	1335.28
Minimum	1251.84
SD	19.99
CV	1.53

ARIMA (0, 0, 0) (1, 1, 0) [12] was applied to forecast the annual and monthly rainfall. The forecasted time series was plotted in Fig. 2.11 and the monthly seasonal character was plotted in Fig. 2.12 with a 95% confidence level. The rainfall result shows that there was consistency in annual rainfall of around 1300 mm for the next 10 years (Fig. 2.11, 2.12 and Table 2.10). The validated Box-Ljung test result of p = 0.1134 (> 0.05) indicated that the model fit well and that the seasonal pattern of monthly rainfall fit reasonably well.

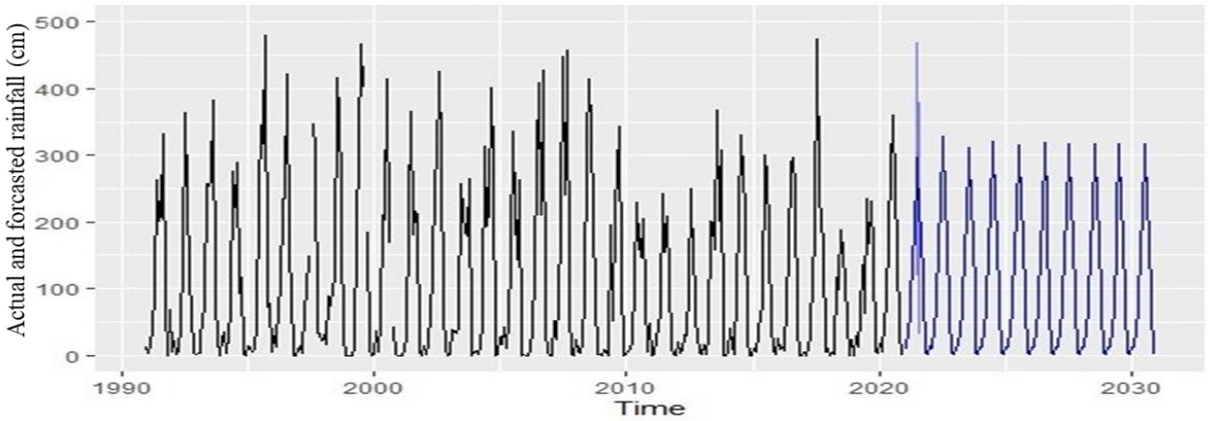

Fig. 2.11: forecasted seasonal rainfall ARIMA (0.0,0) (0,1,1) [12] blue line indicates 95% confidence limit

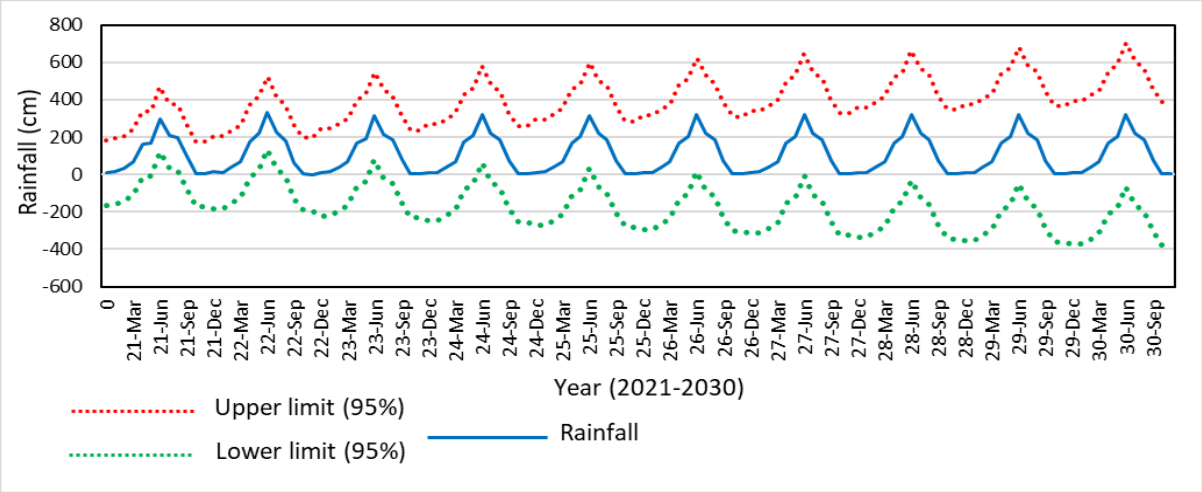

Fig. 2.12: forecasted rainfall data with 95% confidence limit

2.4.11 Comparison of the findings with other works

Mondal et al. (2016) investigated a negative trend in water presence frequency and wetland hydrological dynamics of the lower Mayurakshi River. Islam et al. (2020) studied the flood-prone areas and the contribution of tributaries to flood intensity in lower basin areas of the Mayurakshi River based on morphometric parameters. They concluded that such flood occurrences are mostly a result of the region's flashy precipitation patterns on the Chotanagpur Plateau. The present study also found that decadal and long-term high rainfall occurs in the upper part of the basin covered by the Chotanagpur Plateau (Fig. 2.5). Pal et al. (2021) investigated the annual and monthly water balances of the Mayurakshi basin using the parameters of evapotranspiration, rainfall, runoff, and soil moisture. The result of their study shows annual and seasonal water deficit and surplus conditions. Pre-monsoon months recorded a reverse state, whereas monsoonal months recorded a surplus water balance state. Biswas et al. (2016) worked on the statistically significant relationships among the variables of upstream water level, discharge, inflow, and rainfall. This study evaluated the role of rainfall on drought, discharge, and flood conditions in the rainy season. Previous studies established a negative trend in water presence frequency and wetland hydrological dynamics owing to the uncertainty of rainfall patterns. The present study also found 50 % drought years during the entire study period of 30 years.

The previous studies were conducted mostly on water dynamics, flood intensity, the influence of rainfall on drought and flooding, and annual and seasonal water deficits. However, the present work is a detailed analysis of rainfall patterns' changing nature and trend analysis in the spatiotemporal domain to understand the present and past conditions of rainfall variability and its changing behavior. The previous works lacked the goal of the present work. The decreasing pattern of rainfall was evaluated along with its seasonal variability through RSI and trend analysis statistics. The rainfall anomaly and drought status were also evaluated through RAI. The rainfall forecasting for the next ten years was done using the fitted model ARIMA (0,0,0) (1,1,0) [12]. This work can provide important insights into the rainfall condition of the basin for future planning and water resource management strategies.

2.5 Concluding remarks

The present study focused on the spatiotemporal character of rainfall in the Mayurakshi river basin. The decadal characteristics and long-term average rainfall show that the spatial concentration of high rainfall was in the upper and middle parts of the basin (1500 to 1700 mm). In general, the basin's maximum and minimum rainfall were 1717.37 mm and 1188.65 mm respectively, with a mean annual rainfall of 1420.67 ± 140.01 mm. The long-term spatially high concentration of rainfall was recorded in the upper and middle basin areas, and the low rainfall concentration was recorded in most of the lower parts of the basin. An overall negative Kendall's Z (-1.63), normalized Kendall's tau (-0.20), and Sen's slope value (-10.37 mm/year) proved a decreasing rainfall trend in the basin. The decadal nature of rainfall also indicates a decreasing nature of rainfall over the basin. Statistical methods like Pettitt's test, the SNHT test, and Buishand's U test were applied to detect the homogeneity and change point of rainfall. The tests confirmed that the change point of rainfall in the basin was in 2008. Based on RAI, the temporal characteristics of basin rainfall were found to be extremely wet in 16.67% of the years; moderately dry, slightly wet, and slightly dry in 16.67% of the sampled years. 10% of the sampled years and 6.67% of the years were recorded as extremely dry across the basin. ARIMA evidence indicated an average of 1303.38 ± 19.99 mm of rainfall with

the very least variability (CV 1.53) and a decreasing trend for the next 10 years over the basin. All the micro-level information gathered from this study will augment basin management and the planning of water resources in the basin, thereby helping the planners and scientists with crop management and regional planning.

References

Agarwal, S., AS, S., & Singh, S. P. (2021). Analysis and Interpretation of Rainfall Trend using Mann-Kendall's and Sen's Slope Method. *Indian Journal of Ecology, 48*(2), 453-457.

Agbo, E. P., & Ekpo, C. M. (2021). *Trend Analysis of the Variations of Ambient Temperature Using Mann-Kendall Test and Sen's Estimate in Calabar, Southern Nigeria* (1734). Journal of Physics: Conference Series. doi:doi:10.1088/1742-6596/1734/1/012016

Agha, O. M., Bağçacı, S., & Şarlak, N. (2017). *Homogeneity Analysis of Precipitation Series in North Iraq* (Vol. 5). IOSR Journal of Applied Geology and Geophysics (IOSR-JAGG). doi: 10.9790/0990-0503025763

Ahmad, A., Tang, D., Wang, T. F., Wang, M., & Wagan, B. (2014). Precipitation Trends over Time Using Mann-Kendall and Spearman's rho Tests in Swat River Basin, Pakistan. *Hindawi Publishing Corporation Advances in Meteorology*, 1-16. doi:http://dx.doi.org/10.1155/2015/431860

Akaike, H. (1974). A new look at the statistical model identification. *19*(6), 716–723. doi: 10.1109/tac.1974.1100705

Alahacoon, N., & Edirisinghe, M. (2021). Spatial Variability of Rainfall Trends in Sri Lanka from 1989 to 2019 as an Indication of Climate Change. *ISPRS Int. J. Geo-Inf, 10*(2), 84. doi:https://doi.org/10.3390/ijgi10020084

Alemu, Z. A., & Dioha, M. O. (2020). *Climate change and trend analysis of temperature: the case of Addis Ababa, Ethiopia* (Vol. 9). Alemu and Dioha Environ Syst Res. doi:https://doi.org/10.1186/s40068-020-00190-5

Alexandersson, H. (1986). A Homogeneity Test Applied to Precipitation Data. *Journal of Climatology, 6*(6), 661-675. doi:https://doi.org/10.1002/joc.3370060607.

Alhaji, U. U., Yusuf, A. S., Edet, C. O., Oche, C. O., & Agbo, E. P. (2018). *Trend Analysis of Temperature in Gombe State Using Mann Kendall Trend Test* .Journal of Scientific Research & Reports. doi: 10.9734/JSRR/2018/42029

Alhaji, U., Yusuf, A., Edet, C., Oche, C., & Agbo, E. P. (2018). *Trend analysis of temperature in Gombe state using Mann-Kendall Trend test.* 20(1)). Journal of Scientific Research and Reports. doi:https://doi.org/10.9734/JSRR/2018/42029

Ana F., M., Mehdi, M., & Dolores Ugarte, U. (2020). On the Performances of Trend and Change-Point Detection Methods for Remote Sensing Data. *remote sensing*, 1-25. doi:10.3390/rs12061008

Box, G., Jenkins, G. M., Reinsel , G. E., & Ljung, G. L. (2015). Time Series Analysis: Forecasting and Control (Fifth Edition) Wiley Series in Probability and Statistics. *John Wiley & Sons publishing*.

Bryson, C., Richard, E., & Adrian, W. (2012). *Trend estimation and change point detection in individual climatic series using flexible regression methods*. J Geophys Res. doi: 10.1029/2011JD017077

Buishand, T. (1984). *Test for Detecting a Shift in the Mean of Hydrological Time Series* (Vol. 73). Journal of Hydrology. doi:https://doi.org/10.1016/0022-1694(84)90032-5

Chargui, S., Jaberi, A., Cudennec, C., Lachaal, F., Calvez, R., & Slimani, M. (2018). Statistical detection and no-detection of rainfall change trends and breaks in

semiarid Tunisia— 50+ years over the Merguellil agro-hydro-climatic reference basin. *Arabian Journal of Geosciences*, 1-14. doi:https://doi.org/10.1007/s12517-018-4001-9

Chattopadhyay, G., Chakraborty, P., & Chattopadhyay, S. (2012). *Mann–Kendall trend analysis* (110). Theor Appl Climatol. doi https://DOI10.1007/s00704-012-0617-y.

Chattopadhyay, S., Jhajharia, D., & Chattopadhyay, G. (n.d.). Univariate modeling of monthly maximum temperature time series over northeast India: neural network versus Yule-Walker equation based approach. *Meteorol. Appl*, 70-82.

Chen, F.-W., & Liu, C.-W. (2012). Estimation of the spatial rainfall distribution using inverse distance weighting (IDW) in the middle of Taiwan. *Paddy Water Environ, 10*(3), 209–222. https://doi: 10.1007/s10333-012-0319-1

D'Agostino, R. B., & Stephens, M. A. (1986). Goodness-of-Fit Techniques. *Marcel Dekker, New York.*

Das, J., Mandal, T., Rahman, A. S., & Saha, P. (2021). Spatio-temporal characterization of rainfall in Bangladesh: an innovative trend and discrete wavelet transformation approaches. *Theoretical and Applied Climatology*. doi:https://doi.org/10.1007/s00704-020-03508-6

Dhorde, A. G., & Dhorde, M. (2013). Three-way approach to test data homogeneity: An analysis of temperature and precipitation series over southwestern Islamic Republic of Iran. *J. Ind. Geophys. Union, 17*(3), 233-242.

Dhorde, A. G., & Zarenistanak, M. (2013). *Three-way approach to test data homogeneity: An analysis of temperature and precipitation series over southwestern Islamic Republic of Iran* (17). J. Indian Geophys. Union.

Dhorde, A., & Zarenistanak, M. (2013). *Three-way approach to test data homogeneity: An analysis of temperature and precipitation series over southwestern Islamic Republic of Iran* (17). J. Ind. Geophys. Union.26-35

Fischer, T., Gemmer, M., Liu, L., & Su, B. (2012). Change-points in climate extremes in the Zhujiang River basin, South China, 1961–2007. *Climatic Change, 110*, 783–799. doi:https://doi.org/10.1007/s10584-011-0123-8

Fu, G., Charles, S., Viney, N., Chen, S., & Wu, Q. (2007). Impacts of climate variability on stream-flow in the Yellow River Hydrol Process. *21*(25), 3431–3439.

Gajbhiye, S., Meshram, C., Singh, S. K., Srivastava, P. K., & Islam, T. (2015). Precipitation trend analysis of Sindh River basin, India, from 102-year record (1901–2002). *Atmospheric Science Letters, 17*(1), 71-77.

Gao, P., Mu, X., Wang, F., & Li, R. (2010). *Changes in streamflow and sediment discharge and the response to human activities in the middle reaches of the Yellow River* (15). Hydrol Earth Syst Sci.1-12

Ghasemi, A., & Zahediasl, S. (2012). . Normality tests for statistical analysis: a guide for non-statisticians. *International journal of endocrinology and metabolism, 10*(2), 486-291.

Gibbs, W., & Maher, J. (1967). Rainfall deciles as drought indicators. *Bureau of Meteorology Bulletin 48*.20-28

Güçlü, Y. (2020). Improved visualization for trend analysis by comparing with classical Mann-Kendall test and ITA. *J Hydrol*, 584:124674. doi:https://doi.org/10.1016/j.jhydrol.2020.124674

Hamed, K. H., & Rao, A. R. (1998). A modified Mann-Kendall trend test for autocorrelated data. *Journal of Hydrology, 204*(1-14), 182-196. doi: https://doi.org/10.1016/S0022-1694(97)00125-X

Hipel, K., & McLeod, A. (1994). Time Series Modelling of Water Resources and Environmental Systems. *Development in water science (1st Edition) Elsevier Publishing*.

Hirsch, R. M., Slack, J. R., & Smith , R. A. (n.d.). Techniques of trend analysis for monthly water quality data. *Water Resources Research, 18*(1), 107-121. doi: https://doi.org/10.1029/WR018i001p00107

Hussain, F., Nabi, G., & Boota, M. W. (2015). Rainfall trend analysis by using the mann-kendall test & sen's slope estimates: a case study of district chakwal rain gauge, barani area, northern Punjab province, Pakistan. *Sci.Int. (Lahore), 27*(4), 3159-3165.

Indian Water Resource Society. (2016). Retrieved from http://www.iwrs.org.in/iwr.htm.

IPCC. (2020). *Climate change and biodiversity.* IPCC Technical Paper V. Retrieved from https://www.ipcc.ch/pdf/technicalpapers/climate-changes-biodiversity-en.pdf

Islam, T., Rico-Ramirez, M., Han, D., Srivastava, P., & Ishak, A. M. (2012). Performance evaluation of the TRMM precipitation estimation using ground-based radars from the GPM validation network. *Journal of Atmospheric and Solar-Terrestrial Physics , 77*, 194–208.

Jain, S., & Kumar, V. (2012). Trend analysis of rainfall and temperature data for India. *Curr Sci, 102*(1), 37–49.

Kamal, N., & Pachauri, S. (2019). *Mann-Kendall, and Sen's Slope estimators for precipitation trend analysis in north-eastern states of India* (177). International Journal of Computer Applications.36-41

Kang, H. M., & Yusof, F. (2012). Homogeneity Tests on Daily Rainfall Series in Peninsular Malaysia. *Int. J. Contemp. Math. Sciences, 7*(1), 9 - 22.

Kang, M. H., & Yusof, F. (2012). *Homogeneity Tests on Daily Rainfall Series in Peninsular Malaysia* (7). Int. J. Contemp. Math. Sciences.

Karl, T., Knight, R., & Baker, B. (2000). The record-breaking global temperaturesof 1997 and 1998: evidence for an increase in the rate of global warming? *Geophysical Research Letters, 27*(5), 719–722. doi:https://doi.org/10.1029/1999GL010877.

Karmeshu, N. (2012). Trend Detection in Annual Temperature and Precipitation using the Mann Kendall Test—A Case Study to Assess Climate Change on Select States in the Northeastern United States. *Master of Environment Studies Capstone project, University of Pennsylvania USA*. Retrieved from http://repository.upenn.edu/mes_capstones/47

Keyantash, J., & Dracup, J. (2002). The Quantification of Drought, An Evaluation of Drought Indices. *Bulletin of the American Meteorological Society, 83*, 1167-1180.

Kong, Y. F., & Tong, W. W. (2008). Spatial exploration and interpolation of the surface precipitation data. *Geograph Res, 27*(5), 1097–1108.

Libiseller, C., & Grimvall, A. (2002). Performance of partial Mann–Kendall tests for trend detection in the presence of covariates. *Environmetrics, 13*(1), 71-84. doi: https://doi.org/10.1002/env.507

Long, S.-M., & Li, G. (2021). Model Uncertainty in the Projected Indian Summer Monsoon Precipitation Change under Low-Emission Scenarios. *Atmosphere*, 1-7. Retrieved from https://doi.org/10.3390/atmos12020248

Lukas, R., & Khambhammettu, P. (2005). Mann-Kendall Analysis for the Fort Ord Site. *HydroGeoLogic, Inc.*, 1-6.

Ndione, D. M., Sambou, S., Sane, M. L., Kane, S., Leye, I., Tamba, S., & Cisse, M. T. (2017). *Statistical Analysis for Assessing Randomness, Shift and Trend in Rainfall Time Series under Climate Variability and Change: Case of Senegal* (5). Journal of Geoscience and Environment Protection. doi:DOI: 10.4236/gep.2017.513003

Pandžić, K., Kobold, M., Oskoruš, D., Biondić, B., Biondić, R., Bonacci, O., . . . Curić, O. (2019). Standard normal homogeneity test as a tool to detect change points in climate-related river discharge variation: case study of the Kupa River Basin. *Hydrological Sciences Journal*, 1-16. doi: 10.1080/02626667.2019.1686507

Pettitt, A. N. (1997). A Non-Parametric Approach to the Change-Point Problem. *Journal of the Royal Statistical Society. Series C (Applied Statistics), 28*(2), 126-135. . doi:https://doi.org/10.2307/2346729

Phuong, D., Tram, V., Nhat, T., Ly, D., & Loi, N. (2020). Hydro-meteorological trend analysis using the Mann-Kendall and innovative-Şen methodologies: a case study. *Int J Glob Warming, 20*(2), 145–164. doi:https://doi.org/10.1504/IJGW.2020.105385

Rahman, M., Yunsheng, L., & Sultana, N. (2017). Analysis and prediction of rainfall trends over Bangladesh using Mann–Kendall, Spearman's rho tests and ARIMA model. *Meteorol Atmos Phys, 129*(4), 409–424. doi:https://doi.org/10.1007/s00703-016-0479-4

Robson, & Alice, J. (2002). Evidence for trends in UK flooding." Philosophical Transactions of the Royal Society of . *Physical and Engineering Sciences*, 1327-1343.

Salarijazi, M., Ali, M. A., Adib, A., & Daneshkhan, A. (2012). Trend and change-point detection for the annual stream-flow series of the Karun River at the Ahvaz hydrometric station. *Afr J Agric Reserv, 7*(32), 4540–4552.

Schloeder, C., Zimmerman, N., & Jacobs, M. (2001). Comparison of methods for interpolating soil properties using limited data. . *Soil Science Society of America Journal*, 470–479.

Schwarz, G. (1978). Eastimating a dimention of a model. *The Annel of Statics, 6*(2), 461-464.

Sen, P. (1968). *Estimates of the regression coefficient based on Kendall's tau* (63). Journal of the American Statistical Association.51-59

Sharma, A., & Goyal, M. (2020). Assessment of the changes in precipitation and temperature in Teesta River basin in Indian Himalayan region under climate

change. *Atmos Res*, 27-38, doi:https://doi.org/10.1016/j.atmosres.2019.104670

Shen, S., Dai, Q., Yin, H., & Howard, A. (2006). Statistical Analysis of Drought Indices and Drought Monitoring for Alberta. *Canada*, pp GC41A-1037.

Siraj, K. T., Muhammed, A., Bam, S., & Addisu, S. (2020). Long Years Comparative Climate Change Trend Analysis In Terms Of Temperature, Coastal Andhra Pradesh, India. *International Journal of Scientific Research in Science and Technology, 2*(7), 2-14.

Smadi, M. M., & Zghoul, A. (2006). *A sudden change in rainfall characteristics in Amman, Jordan during the mid 1950's* (2). Am. J. Environ. Sci.20-29

Srivastava, P. K., Han, D., Rico-Ramirez, M. A., & Islam, T. (2014). Sensitivity and uncertainty analysis of mesoscale model downscaled hydro-meteorological variables for discharge prediction. *Hydrological Processes, 28*, pp. 4419–4432.

Stepanek, P., & Zahradnek, P. (2009). Data quality control and homogenization of air temperature and precipitation series in the area of Czech Republic in the period of 1961-2007. *Int J Global Energy.* doi:doi:10.1504/IJGGI.2009.030657

Stern, D. I., & Kaufmann, R. K. (2014). Anthropogenic and natural causes of climate change. *Climatic Change, 122*(2), pp. 257–269.

Van-rooy, M. (1965). A Rainfall Anomaly Index (RAI), Independent of the Time and Space. *Notos, 14*, 43-48.

Walsh, R., & Lawle, D. (1998). Rainfall Seasonality: Description, Spatial Patterns And Change Through Time. *Department of Geography, University College of Swansea, Department of Geography, University of Birmingham*, 201-208.

Winingaard, J., Kleink, A. T., & Konnen, G. (2003). Homogeneity of 20th Century European Daily Temperature and Precipitation Series. *Int J Climatol, 23*, :679–692.

Wu, L., Wu, X. J., Xiao, C. C., & Tian, Y. (2010). On temporal and spatial error distribution of five precipitation interpolation models. *Geogr Geo-Inf Sci, 26*(3), 19-24.

Wu, Y.-H., & Hung, M.-C. (2016). *Comparison of Spatial Interpolation Techniques Using Visualization and Quantitative Assessment.* Application of Spatial Statistics. IntechOpen.5(4), 56-61. doi:http://dx.doi.org/10.5772/65996

Yürekli, K., Simsek, H., Cemek, B., & Karaman, S. (2007). Simulating climatic variables by using a stochastic approach. *Building and Environment, 42*(10), 3493-3499. doi:https://doi.org/10.1016/j.buildenv.2006.10.046

Zarenistanak, M., Dhorde, G. D., & Kripalani, R. H. (2014). *Trend analysis and change point detection of annual and seasonal precipitation and temperature series over southwest Iran* (123),21-30. J. Earth Syst. Sci.

Chapter 3: THE LAND USE AND LAND COVER DYNAMICS

3.1 Objective and Chapter Organization

In this chapter, an extensive analysis of land use and land cover (LULC) spanning 30 years (1991 - 2020) has been conducted to investigate the dynamic change in the land use pattern of the basin. The study period is divided into distinct segments, as outlined in Section 3.5, to facilitate change detection. Section 3.2 focuses on the relevant literature about LULC, while Section 3.3.2 provides an in-depth explanation of the popular machine learning approach used for LULC classification, namely Random Forest (RF). The accuracy of the image classification is assessed in sections 3.3.3 and 3.4.1, and the findings are subsequently utilized in the change detection process described in section 3.5. To evaluate the future scenario of LULC in the basin, the CA-Markov model is employed, as explained in Section 3.3.4, with suitable driving forces derived from auxiliary data, as detailed in Section 3.3.5. The output model is validated against the actual LULC data of 2020 in Section 3.6.1, and the future prediction of LULC for the year 2032 has been presented in Section 3.6.2. The key results are summarized in Section 3.7, followed by concluding remarks in Section 3.8.

3.2 Introduction

The earth's surface cover encompasses various elements such as soils, grass, vegetation, water, and human settlements, while land use refers to the specific purposes served by these elements, such as agriculture, wildlife habitat, residential areas, and recreational spaces. Global environmental change is increasingly concerned with significant alterations in land use and land cover (LULC) (Pandian et al., 2014). The ongoing population growth, escalating demand for natural resources, climate factors, and changing land use and land cover contribute to this issue. In the present decade, land use and land cover alteration have emerged as critical environmental concerns worldwide (Guan et al., 2011). Consequently, LULC alteration is of utmost importance in various locations across the globe (Sleeter et al., 2013; Taelman et al., 2016). The increase in land use and land cover changes is

driven by both human activities and natural phenomena (Javed et al., 2012; Alam et al., 2019). Understanding the data derived from the detection of land use and land cover changes, along with their magnitude and dimensions, is crucial for sustainable development, ecosystem preservation, land conservation management, water resource balance, and basin management planning (Tewabe and Fentahun, 2020). The dynamic nature of land uses and land cover can significantly impact regional climate, ecosystem stability, water balance, streamflow, and socioeconomic practices (Kindu et al., 2013; Hyandye and Martz, 2017). Utilizing time-series analysis to detect changes in land use and land cover and leveraging the resulting information is essential for effective long-term land use management (Gashaw et al., 2017). Land use and land cover changes are intertwined with the historical process of human land utilization (Ahmad, 2014). In other words, these changes reflect the results and nature of natural and socio-economic characteristics influenced by humans over time and space. Population growth plays a significant role in land use change, with excessive population growth being one of the key factors (Lambin et al., 2003). India, the second-most populated country in the world, experiences a high growth rate of 17.64 percent (Census of India 2011). This study conducted on the Mayurakshi River Basin, which includes parts of West Bengal and the relatively less populated state of Jharkhand, emphasizes the effects of land use changes on resource accessibility, including soil, vegetation, and water (Ahmad, 2014). Land use and land cover have a direct impact on groundwater level, overall runoff, and evapotranspiration, LULC change is a significant global issue due to its repercussions on natural and socio-economic resources (Hurni et al., 2005; Akpoti et al., 2016). Understanding the interaction between human activities, changes in landscape patterns, and natural phenomena is crucial for effective land management and the development of decision support systems (Rawat & Kumar, 2015). Continuous alterations in land use and land cover have adverse effects on climatic trends and socio-economic dynamics, leading to increased local and global hazards such as landslides and droughts (Sewnet, 2015; Chakilu & Moges, 2017). Human-induced factors play a more significant role in land use and land cover changes than natural phenomena, influencing food supply and potentially leading to socio-political consequences (Turner et al., 2007; Uma et al., 2021).

The conversion of vegetation cover zones into agricultural land and urban areas due to climate change and population growth has become a significant driver of environmental degradation, including adverse effects on rainfall-runoff relationships (Leach & Coulibaly, 2019). Numerous studies have focused on modeling land use and land cover change and its impact on runoff in various regions (Porter-Bolland et al., 2007; Umar et al., 2021). Remote sensing data plays a crucial role in detecting land use changes and is an essential source of information for decision support systems (Tewabe & Fentahun, 2020). Understanding land use, land cover change, and making future predictions is vital for studying forest fragmentation, biodiversity loss, earth-atmosphere interactions, and future management plans (Chen et al., 2000; Olson et al., 2008; Dayamba et al., 2016).

Various techniques are commonly employed to evaluate land use and land cover dynamics such as change detection, principal component analysis, vector analysis, image overlay, individual classification and post-classification analysis, image rationing, NDVI index, and land cover statistics comparisons (Han et al., 2009). Several studies have been conducted on land use and land cover change and future predictions using models such as Markov chain (Guan et al., 2014; Wang et al., 2020; Munthali et al., 2020), cellular automata (Verburg et al., 2006; Mishra and Rai, 2016; Anand et al., 2018), CLUE (Han et al., 2015), and agent-based (Xie et al., 2007). The key aspect of change detection is quantifying the transformation of land use classes into other classes (Han et al., 2009; Yirsaw et al., 2017). Therefore, future predictions of land use and land cover changes are based on transition probability matrices from one period to another (Hyandye and Martz, 2017). The Markov-CA approach is often employed as a convenient method for projecting future scenarios. Thus, detailed land use and land cover (LULC) dynamics were executed to get the present and future scenarios of the basin.

3.3 Database and Methods

This section outlines the comprehensive database and methodologies utilized in this research. A thorough exploration of the database and the methods employed in this chapter is presented in this section.

3.3.1 Data Source

In order to determine the LULC classification and change detection of the Mayurakshi basin from 1991 to 2020, historical images were collected from open-source available satellite data from the United States Geological Survey (USGS) portal (http://earthexploration.usgs.gov/). For the years 1991, 1996, 2002, and 2008, the LULC maps were obtained by classifying the satellite images with Landsat 5, Thematic Mapper (TM), and for the years 2014 and 2020, Landsat 8, Operational Land Imager (OLI), followed by paths 139 and raw 43, 44 (Table 3.1). To eliminate cloud disturbance, images with 5% cloud coverage were collected (Jain and Sharma, 2019). Before LULC classification, QGIS 3.16 and ArcGIS 10.8 software were used for geometric correction and atmospheric correction to convert the DN values from radiance to reflectance. To get better clarity, image enhancement techniques were applied, and mosaicking, masking, and clipping were performed to get the study area.

Table 3.1: Image collection for LULC classification

Year	Satellite	Sensor	Acquisition	Path/Raw	Datum/UTM	Claude Cover	Resolution
1991	Landsat5	TM	1991-8-12	139/43 & 139/44	WGS84/45N	<5%	30m
1996	Landsat5	TM	1996-8-20	139/43 & 139/44	WGS84/45N	<5%	30m
2002	Landsat5	TM	2002-7-14	139/43 & 139/44	WGS84/45N	<5%	30m
2008	Landsat5	TM	2008-8-25	139/43 & 139/44	WGS84/45N	<5%	30m
2014	Landsat8	OLI	2014-9-16	139/43 & 139/44	WGS84/45N	<5%	30m
2020	Landsat8	OLI	2020-8-17	139/43 & 139/44	WGS84/45N	<5%	30m

3.3.2 Random Forest

Random Forest (RF) is a machine learning algorithm developed by Breiman (2001) commonly used for regression, classification, and prediction of land use and land cover (LULC). The RF is non-parametric in nature, has high accuracy of classification, and is capable of handling high data dimensionality (Avic et al., 2022).

The random forest algorithm has several hyper-parameters that need to be tuned for optimal performance, including the number of trees, the depth of each tree, and the number of features used in each split. Additionally, the input features must be carefully selected and preprocessed to ensure that they are relevant and informative for the classification task. The number of trees combined to make a random forest, where each of them plays the role of casting one vote for the most common class to be assigned to the input data (Adam et al., 2014; Vahid et al., 2015). The RF algorithm works by building a multitude of decision trees at training time and outputting the class that is the mode of the classes (classification) or mean prediction (regression) of the individual trees. The numerous binary classification trees were run through the bagging or bootstrapping samples, and the replacement was extracted from the original observation. The samples that are excluded from bootstrap samples are called out-of-bag (OOB) samples. Based on the training data subset, the RF model increases the number of trees. The OOB helps to determine the misclassification error as well as the importance of variable estimation (Vahid et al., 2015). The split of entropy is calculated based on the bootstrap samples, and the classification splits with no pruning of the lower diversity of classification trees; thus, the lower bias is archived in the classification (Rodriguez-Galiano et al., 2011; Vahid et al., 2015). Several studies have been conducted on RF and have demonstrated that it is the best method that is not sensitive to overtraining or noise (Rodriguez-Galiano et al., 2011).

The following equation summarizes the Random Forest algorithm for LULC classification:

$y = f(x_1, x_2, x_3,x_4,x_5 ..., x_n)$……..(Eq.1)

where:

y is the LULC class

x_1, x_2, x_3,x_4,x_5 ..., x_n are the input features (e.g. Water, Vegetation, Bare-Land, Agriculture, Built-up, etc.) f is the function that combines the outputs of multiple decision trees to make the final prediction.

3.3.3 Accuracy Assessment

The accuracy assessment plays a crucial role in evaluating the precision of LULC classes. This assessment involves comparing the classified map with reference or ground truth data to determine the level of agreement or disagreement between the two. To quantify the accuracy assessment, metrics such as Producer's Accuracy (PA) and User's Accuracy (UA) are calculated for each land use or land cover class. These metrics provide valuable insights into the reliability and quality of the LULC classification results for specific classes (Mishra et al., 2018).

PA measures the ratio of correctly classified pixels for a particular LULC class to the total number of reference pixels for that class (Eq. 2). It indicates the likelihood that a pixel from the reference data belongs to a specific class and is accurately classified in the classified map (Jamali et al., 2019). Commission Error (CE) or Producer's Error (PE) refers to the occurrence of an incorrect classification of a pixel into a specific LULC class in the classified map. In other words, it represents a false positive error where a class is present in the map but should not be there according to the reference data.

UA measures the ratio of correctly classified pixels for a specific LULC class to the total number of pixels classified as that class in the classified map (Eq. 3). It indicates the probability that a pixel labeled as a particular class in the map is indeed a member of that class in the reference data (Mishra et al., 2018). Omission Error (OE) or User's Error (UE) occurs when a pixel is mistakenly excluded or missed from a specific LULC class in the classified map, representing a false negative error. In this case, a class is absent from the map but should be present based on the reference data.

The most commonly used metric for LULC accuracy assessment is Overall Accuracy (OA), which calculates the ratio of correctly classified pixels of LULC classes to the total number of pixels in the study area. OA provides an overall measure of accuracy for the entire classification. It is calculated using the following equation (Eq. 4)

The Kappa index of agreement, also known as Cohen's Kappa coefficient, is a statistical measure widely used to assess the agreement between the classified map and reference data in LULC classification (Hamad et al., 2018; Nguyen et al., 2020).

The Kappa index takes into account the agreement that would be expected by chance alone, providing a more robust measure of accuracy. The equation to calculate the Kappa index of agreement in LULC classification is as follows (Eq. 5). The Kappa index ranges from 0 to 1, with different interpretations: A value of 1 indicates perfect agreement between the classified map and reference data. A value of 0 indicates no agreement between the classified map and reference data. It is one of the suitable indices for the measurement of accuracy and a value > 0.85 is considered a standard threshold value (Yan et al. 2015). The interpretation of Kappa values is subjective, but commonly used thresholds include: Kappa < 0.20: Poor agreement, 0.20 ≤ Kappa < 0.40: Fair agreement, 0.40 ≤ Kappa < 0.60: Moderate agreement, 0.60 ≤ Kappa < 0.80: Substantial agreement, Kappa ≥ 0.80: Almost perfect agreement

$$PA=(\sum NT_c)/(\sum NT_{rp})*100 \quad \text{(Eq. 2)}$$

$$UA=(\sum NT_c)/(\sum NT_{cp})*100 \quad \text{(Eq. 3)}$$

$$OA = \frac{\sum_{i=1}^{nc} e_{ii}}{NT} \times 100 \quad \text{(Eq. 4)}$$

$$\check{K} = \frac{(NT \times \sum_{i=1}^{nc} e_{ii}) - \text{Pe}}{(NT)^2 - \text{Pe}} \quad \text{were, } NT = \sum_{i=1}^{nc} \sum_{j=1}^{nc} e_{ij} \quad \text{(Eq. 5)}$$

In these equations:

PA = Producer's Accuracy in percentage, UA = User's Accuracy in percentage $OA =$ overall accuracy in percentage, $\check{K}$ = Kappa index, NT_c = number of correctly classified pixels for a specific class, NT_{rp} = number of reference pixels for that class, NT_{cp} = number of classified pixels for that class, $nc =$ total number of class, $e_{it} =$ element in, i^{th} row and i^{th} column, $NT =$ total number of samples, $e_{ij} =$ element in i^{th} row and j^{th} column, P_e = represents the expected proportion of agreement due to chance. It is calculated by multiplying the marginal totals of the reference and classified data for each LULC class summing them up, and then dividing by the total number of pixels squared.

By considering these accuracy metrics, it becomes possible to assess the accuracy of LULC classes, identify potential errors, and determine areas where improvements may be needed in the classification process.

3.3.4 CA-Markov model

In order to predict future LULC changes, the CA-Markov model is suitable to simulate LULC classes from one time to another and predict future LULC conditions. The Markov Chain Model (MCM) is a statistical model that predicts the probability of transitioning from one LULC to another over time, based on historical data. The MCM works on the principle of the transition probability matrix. The transition probability matrix is the likelihood of pixels of one LULC class to move to another LULC class within the next time period, i.e., time 1 ($t+_1$) to time 2 ($t+_n$). The MCM contains the stochastic potentiality of changing the behavior of random variables over time (Amponsah et al., 2021; Munthali et al., 2020; Khwarahm et al., 2021). The model assumes that the probability of transitioning from one LULC class to another is dependent only on the current ($t+_1$) LULC type, and not on any previous ($t-_1$), or future ($t+_n$) LULC types. This is known as the Markov property, which states that the future (LULC) state of a system depends only on its ($t+_1$), state, and not on any ($t-_1$) states.

The MCM can be used to simulate LULC changes over time by iteratively applying the transition probability matrix to the ($t+_1$) LULC map to generate a new LULC map for the next desired time step. The model can be calibrated and validated by using ($t+_1$) LULC and used to project ($t+_n$) LULC scenarios.

The MCM model can be represented mathematically as follows:

$$P\_j(t+1) = \Sigma\_i \; P\_i(t) * T\_ij \quad \text{(Eq. 6)}$$

where P_j(t+1) is the probability of being in LULC type j at the time t+1, given the current LULC type at the time t; P_i(t) is the probability of being in LULC type i at the time t, and T_ij is the probability of transitioning from LULC type i to future LULC type j.

The matrix T is typically estimated from historical data. The diagonal elements of T represent the probabilities of remaining in the same LULC type, while the off-diagonal elements represent the probabilities of transitioning to another LULC type.

MCM has widely been used in the simulation of future LULC prediction (Munthali et al., 2020; Wang et al., 2020), but it does not provide the distribution and allocation of spatial changes of LULC over time (Yang et al., 2012). The cellular automata (CA) model, when incorporated with MCM, has the ability to compute a non-linear, complex spatial distribution of LULC classes (Mishra and Rai 2016). The Automata CA model for LULC change is a spatially explicit model that simulates the dynamics of LULC at fine resolution using a set of simple rules. The model operates on a regular grid of cells, where each cell represents a location on the landscape and is assigned a particular LULC type. The model operates based on the principle of iteratively updating the state of each grid cell based on a set of transition rules that are defined according to the characteristics of the LULC types being simulated. The transition rules of CA work on the present LULC cell status ($t+_1$) and the neighboring cells are based on the past LULC status ($t+_2$) (Hamad et al., 2018; Liping et al., 2018). Thus, the CA-MCM makes a combination to produce the transition probability matrix remove the gap in spatial dimension defining barriers, and simulate the future LULC (Beroho et al., 2023; Khwarahm et al., 2020).

The CA model for LULC change can be represented mathematically as follows:

$L\_ij(t+_1) = F(L\_ij(t), N\_ij(t))$…….(Eq. 7)

where L_ij(t+1) is the LULC type of cell (i,j) at time $t+_1$, L_ij(t) is the LULC type of the same cell at time t, and N_ij(t) is the neighborhood of cell (i,j) at time t. The function F specifies the transition rules that determine how the LULC type of a cell changes over time, based on its current LULC type and the LULC types of its neighbors.

The neighborhood N_ij(t) is typically defined as a set of adjacent cells surrounding the cell (i,j) at time t. The size and shape properties of the neighborhood can vary based on the specific application and spatial scale of the model. The transition rules specified by the function F can also vary depending on the ($t+_1$) data availability.

The CA model for LULC change can be implemented using computer software that simulates the dynamics of LULC over time, based on the transition rules specified by the function F. The model can be calibrated and validated using historical LULC data and used to project ($t+_n$) LULC scenarios.

3.3.5 Driving Factors

The inclusion of driving factors to comprehend plausible deep knowledge about the LULC transition is very important to predict future LULC status. However, there is no universally predefined set of driving factors that can reliably predict future LULC status (Shafizadeh-Moghadam et al., 2013; Osman et al., 2019; Hasan et al., 2020; Chaturvedi, 2021; Lai et al., 2022). This study incorporated four specific driving factors: slope, elevation, road proximity, and city center proximity (Fig. 3.1). The slope factor was derived from a 30 m digital elevation model (DEM) provided by the US Geological Survey (USGS), while the elevation map was also generated from the DEM. Both slope and elevation play crucial roles in influencing LULC patterns. Steep slopes and high elevations are generally unsuitable for agriculture and settlement, whereas flat regions are more favorable for agricultural activities and human settlements (Jantz et al., 2004). The road network was downloaded from the shapefile of the Road Open Street Map (https:// www. open street map. org/) and city center drown point data from Google Earth. From a social perspective, proximity to roads is vital for ensuring socio-economic sustainability, promoting urban densification, and facilitating access to goods and services (Ji et al., 2014). Additionally, the proximity to the city center is pivotal as it serves as a hub for health, education, and socio-economic advantages, which significantly influence LULC in any given location (Linard et al., 2012). These driving factors demonstrate a plausible influence on the status of LULC changes.

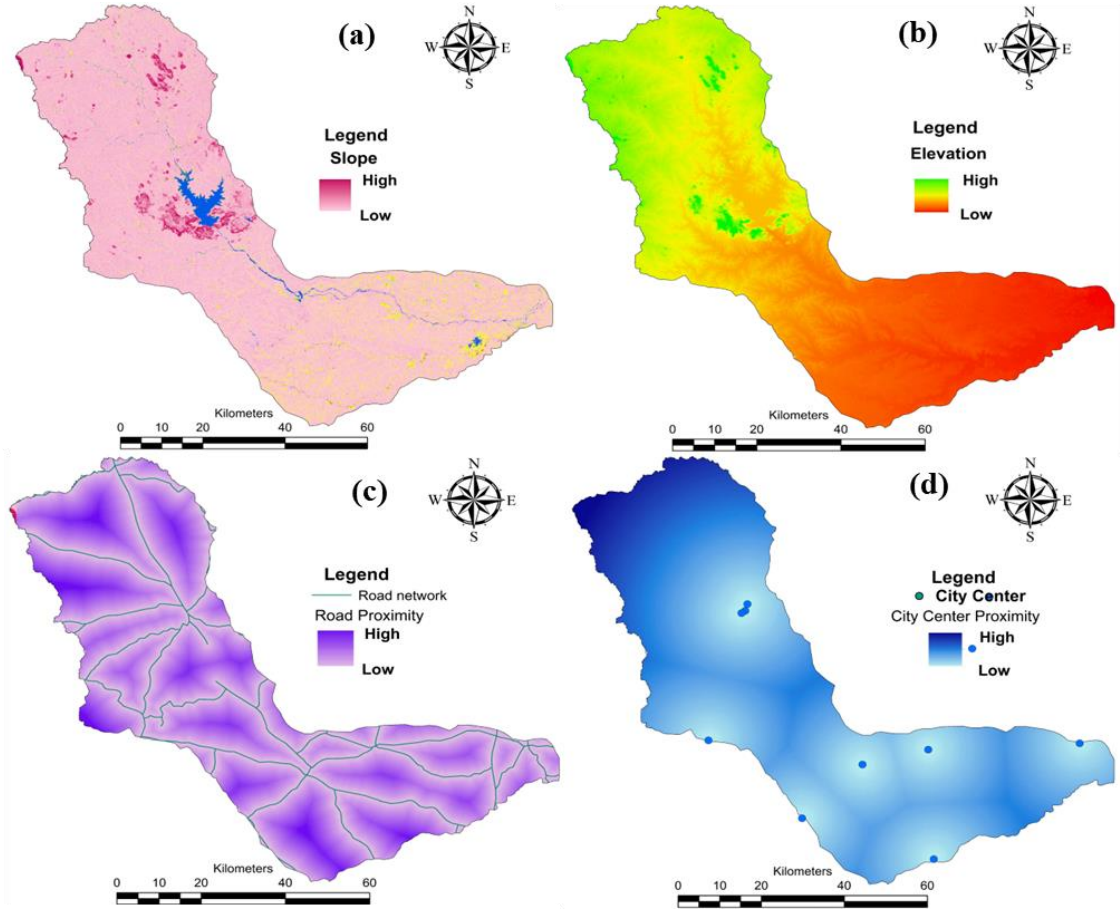

Fig. 3.1: Driving factors, a- Slope, b- Elevation, c- Road network, d- City center

3.3.6 LULC classes

This study incorporated five LULC classes that fulfilled all categories of LULC in the study area. The classes identified in this study are:

1. Water: it comprises dams and reservoirs, rivers, ponds, and wetlands as water bodies;

2. Vegetation: the natural vegetation cover area, planted orchard, and sparse vegetation cover area come under this category;

3. Bare-land: open ground with no vegetation cover, fallow open ground not used for agriculture; the ground left after opencast mining is accounted for as bare-land;

4. Agriculture: the arable land used for agriculture and;

5. Built-up: the residential built-up area, commercial, and industrial areas (Table 3.2).

From each LULC class, more than 120 spatial training signatures were collected. The Random Forest (RF) machine learning algorithm is applied to get LULC classification.

Table 3.2: **LULC class description**

CULC Class	ID	Description
Water	1	Dam/Reservoir, Pond, river, and wetlands
Vegetation	2	Natural vegetation areas and plantations
Bare-land	3	Open ground with no vegetation, bare rock, relinquished ground of open cast mining
Agriculture	4	Arable land
Built-up	5	Residential built-up, Commercial, and institutional areas

3.4 Results and Discussion

3.4.1 Accuracy Report

The accuracy of the classified LULC is evaluated using various metrics, such as the confusion matrix, including Usear Accuracy (UA), Producer Accuracy (PA), Overall Accuracy (OA), and Kappa coefficients. To analyze the changes in LULC over a 30-year period (1991, 1996, 2002, 2008, 2014, and 2020), the images were classified every six years. For accuracy assessment, a total of 180, 156, and 210 ground control points were considered for the years 1991, 1996, and 2002, respectively. These ground control points were obtained from historical images of Google Earth and aerial photography. The accuracy was assessed individually for each LULC category, and the results are presented in Table 3.3 and Table 3.7. The diagonal values of the error matrix represent the correctly classified points between the classified LULC maps and the ground truth at the corresponding number of validation points: 165, 140, and 187 for the years 1991, 1996, and 2002, respectively (Tables 3.4,3.5, and 3.6). The PA ranged from 49.44% to 89.47% for 1991, 66.67% to 97.22% for 1996, and 86.67% to 94.59% for 2002. The UA ranged from 88.89% to 94.44% for 1991, 72.73% to 92.50% for 1996, and 83.33% to 92.86% for 2002. The OA and Kappa coefficients for the years 1991, 1996, and 2002 were 91.67%, 89.74%, 89.05%, and 0.89, 0.86, 0.86, respectively (Table 3.3).

Table 3.3: Accuracy assessment

	1991		1996		2002	
Class Name	**PA**	**UA**	**PA**	**UA**	**PA**	**UA**
Water	94.12%	88.89%	95.83%	92.00%	88.64%	92.86%
Vegetation	94.44%	94.44%	84.09%	92.50%	86.67%	92.86%
Bar-Land	89.19%	91.67%	92.50%	92.50%	89.74%	83.33%
Agriculture	89.47%	94.44%	97.22%	87.50%	86.67%	92.86%
Built-up	91.43%	88.89%	66.67%	72.73%	94.59%	83.33%
Overall Accuracy	91.67%		89.74%		89.05%	
Kappa Statistics	0.89		0.86		0.86	

Table 3.4: Error matrix of Accuracy assessment 1991

LULC class	Water	Vegetation	Bar-land	Agriculture	Built-up	Total
Water	32	0	0	4	0	36
Vegetation	2	34	0	0	0	36
Bar-land	0	0	33	0	3	36
Agriculture	0	1	1	34	0	36
Built-up	0	1	3	0	32	36
Total	34	36	37	38	35	180

Table 3.5: Error matrix of Accuracy assessment 1996

LULC class	Water	Vegetation	Bar-land	Agriculture	Built-up	Total
Water	23	1	0	0	1	25
Vegetation	1	37	1	1	0	40
Bar-land	0	0	37	0	3	40
Agriculture	0	5	0	35	0	40
Built-up	0	1	2	0	8	11
Total	24	44	40	36	12	156

Table 3.6: Error matrix of Accuracy assessment 2002

LULC class	Water	Vegetation	Bar-land	Agriculture	Built-up	Total
Water	39	1	1	1	0	42
Vegetation	1	39	0	1	1	42
Bar-land	2	2	35	2	1	42
Agriculture	1	1	1	39	0	42
Built-up	1	2	2	2	35	42
Total	44	45	39	45	37	210

The contingency matrix was assessed for the years 2008, 2014, and 2020, taking into account the ground validation points recorded as 210, 156, and 184, respectively (Tables 3.8, 3.9, and 3.10). Out of the selected validation points, there were 186, 143, and 167 accurately matched points between the classified LULC classes and the ground truth. The evaluation of accuracy levels revealed that the PA and UA for 2008 and 2014 varied between 86.36% and 95.12%, 72.73% and 96.00%, 83.33% and 92.86%, and 88.89% and 92.50%, respectively. For the year 2020, the PA and UA ranged from 87.50% to 95.45% and 87.50% to 92.11% respectively. The overall accuracy (OA) for 2008, 2014, and 2020 was determined to be 88.57%, 91.67%, and 90.76% respectively. Additionally, the computed Kappa coefficients were 0.85, 0.89, and 0.88 for the respective years (Table 3.7).

Table 3.7: Accuracy assessment

	2008		2014		2020	
Class Name	**PA**	**UA**	**PA**	**UA**	**PA**	**UA**
Water	95.12%	92.86%	96.00%	88.89%	95.45%	87.50%
Vegetation	86.36%	90.48%	90.24%	92.50%	91.30%	91.30%
Bar-Land	82.61%	90.48%	94.87%	92.50%	92.11%	92.11%
Agriculture	85.37%	83.33%	92.50%	92.50%	89.13%	89.13%
Built-up	94.74%	85.71%	72.73%	88.89%	87.50%	93.33%
Overall Accuracy	88.57%		91.67%		90.76%	
Kappa Statistics	0.85		0.89		0.88	

Table 3.8: Error matrix of Accuracy assessment 2008

LULC class	Water	Vegetation	Bar-land	Agriculture	Built-up	Total
Water	39	1	1	1	0	42
Vegetation	1	38	1	2	0	42
Bar-land	0	1	38	1	2	42
Agriculture	1	2	4	35	0	42
Built-up	0	2	2	2	36	42
Total	41	44	46	41	38	210

Table 3.9: Error matrix of Accuracy assessment 2014

LULC class	Water	Vegetation	Bar-land	Agriculture	Built-up	Total
Water	24	0	0	0	1	25
Vegetation	1	37	1	2	0	41
Bar-land	0	1	37	1	0	39
Agriculture	1	2	0	37	0	40
Built-up	1	0	2	0	8	11
Total	27	40	40	40	9	156

Table 3.10: Error matrix of Accuracy assessment 2020

LULC class	Water	Vegetation	Bar-land	Agriculture	Built-up	Total
Water	21	1	0	2	0	24
Vegetation	1	42	0	2	1	46
Bar-land	0	0	35	1	2	38
Agriculture	0	3	1	41	1	46
Built-up	0	0	2	0	28	30
Total	22	46	38	46	32	184

3.4.2 LULC Status

The LULC of the Mayurakshi basin was assessed over a period of 30 years, at intervals of six years (1991, 1996, 2002, 2008, 2014, and 2020). The study area encompassed various LULC classes, including water, vegetation, barren land, agriculture, and built-up (Table 3.2). The dominant land use in the basin was agriculture, particularly in the lower basin area, which comprised a fertile river plain predominantly used for agricultural activities (Figs. 3.2, and 3.3). In 1991, agricultural land covered an area of 2460.06 km^2 (49.15%), which increased to 2644.82 km^2 (52.48%) in 1996, and in 2002, agricultural land decreased by 2429.85 km2 (48.55%). Except for 2002, agricultural land has continuously increased in 2008, 2014, and 2020 by 2469.85 km2, 3215.69 km^2, and 3533.81 km^2 (49.35%, 64.25%, and 70.61%) (Tables 3.11a, 3.11b, and Fig. 3.4). In the whole study period, agricultural land dominated in terms of its area and the nature of the conversion of the other LULC classes into agricultural land. The status of agricultural land between the years 1991 and 1996 was 184.76 km^2 (3.69% area gain) between 1996 and 2002, 4.30 % area lost between 2002 and 2008, 0.80 % area gained between 2008 and

2014, 745.84 km^2 (14.90% area gain), and 318.12 km^2 (6.36% area gain) between 2014 and 2020 (Table 3.12 and Fig. 3.4, Fig. 3.5).

The second-most dominant LULC class in the Mayurakshi basin was vegetation cover. In 1991, the area covered by vegetation was 1023.56 km^2 (20.45%) and counted as the 3rd dominant LULC class, which increased to 993.94 km^2 (19.86%) and jumped to the 2nd dominant LULC class in 1996, 829.18 km^2 (16.57%) in 2014, and in 2020 it was covered by 16.57%, 15.57% (Tables 3.11a, 11b). The vegetation cover exhibited a slight increase of 3.10% and 2.80% between the years of 1996–2002 and 2002–2008, but overall, it experienced a continuous decline throughout the study period. Specifically, it decreased by 29.62 km^2 (0.59%) between 1991 and 1996, by 460.20 km^2 (9.19%) between 2008 and 2014, and by 49.68 km^2 (0.99%) between 2014 and 2020 (Tables 3.12 and Fig. 3.4, Fig. 3.5).

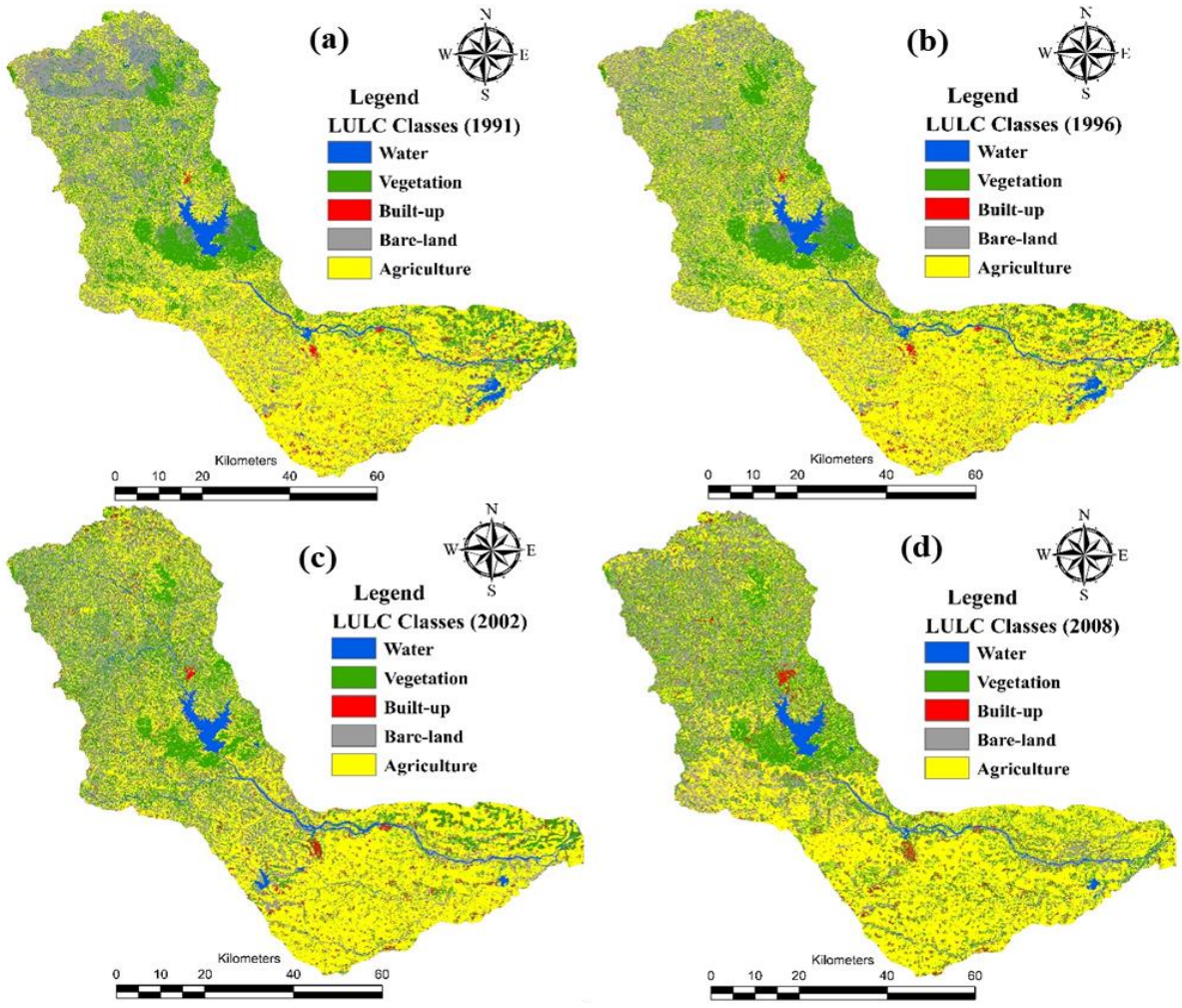

Fig. 3.2: LULC a-1991, b-1996, 2002, c-2008

The third dominant LULC class in the basin was bare-land, predominantly found in the upper part of the basin, which is characterized by plateau areas. In 1991, 2008, and 2020, bare land accounted for 22.96% (1149.33 km^2), 18.01% (901.53 km^2), and 5.18% (259.37 km^2) of the area, respectively (Tables 3.11a, 11b). The only increase in bare land occurred between 1996 and 2002, amounting to 140.12 km^2 (2.80%). However, bare land underwent a decreasing trend as it was converted into agricultural land and built-up areas. The years 1991 to 1996 witnessed a decrease of 166.42 km^2 (3.33%), followed by a decrease of 221.50 km^2 (4.43%) between 2002 and 2008, and a decrease of 257.79 km^2 and 394.36 km^2 (5.15% and 7.88%) between 2008 and 2014 and 2014 and 2020, respectively. During the study period, the built-up area experienced an overall increase; in 1991, it covered an area of 107.82 km^2, accounting for 2.15% of the total area. By 2002, the built-up area had expanded to 145.38 km^2 (2.91%), and in 2020, it had reached 272.30 km^2 (5.44%).

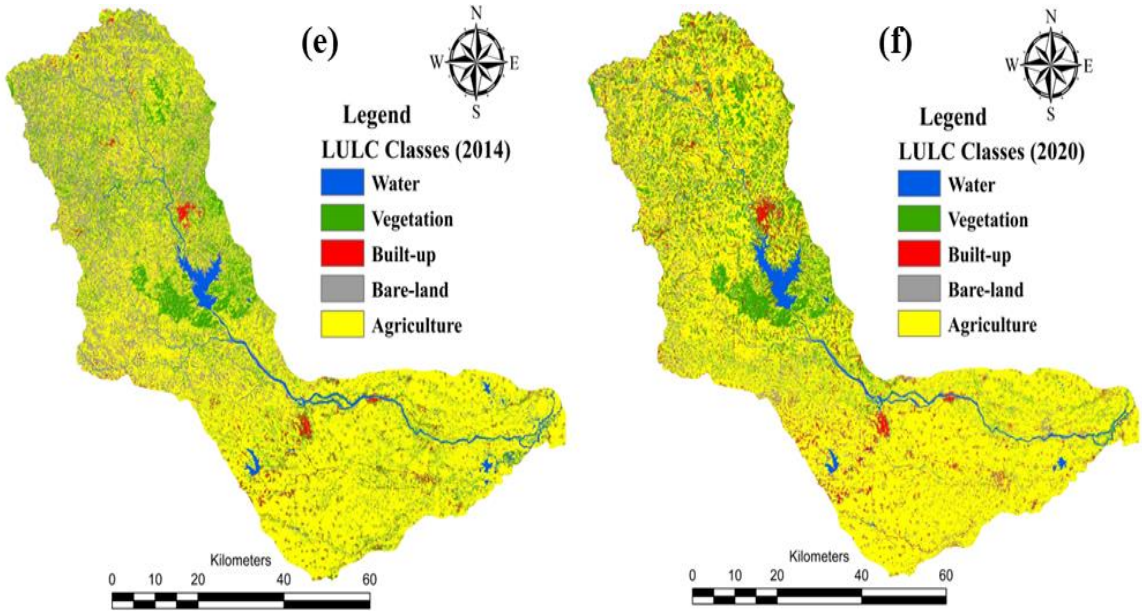

Fig. 3.3: LULC e-2014, f-2020

Table 3.11a: LULC status (1991, 1996, 200)

	Area in km^2					
LULC Class	**1991**	**Area (%)**	**1996**	**Area (%)**	**2002**	**Area (%)**
Water	264.22	5.28	267.67	5.35	157.16	3.14
Vegetation	1023.56	20.45	993.94	19.86	1149.12	22.96
Bare-land	1149.33	22.96	982.91	19.64	1123.03	22.44
Agriculture	2460.06	49.15	2644.82	52.84	2429.85	48.55
Built-up	107.82	2.15	115.65	2.31	145.83	2.91

Table 3.11b: LULC status (2008, 2014, 2020)

	Area in km^2					
LULC Class	**2008**	**Area (%)**	**2014**	**Area (%)**	**2020**	**Area (%)**
Water	181.66	3.63	149.34	2.98	160.01	3.20
Vegetation	1289.38	25.76	829.18	16.57	779.50	15.57
Bare-land	901.53	18.01	643.74	12.86	259.37	5.18
Agriculture	2469.85	49.35	3215.69	64.25	3533.81	70.61
Built-up	162.58	3.25	167.05	3.34	272.30	5.44

Table 3.12: LULC status of lost and gain

LULC Class	**1991to 1996**	**%**	**1996 to 2002**	**%**	**2002 to 2008**	**%**	**2008 to 2014**	**%**	**2014 to 2020**	**%**
Water	+3.46	+0.07	-110.52	-2.21	+24.50	+0.49	-32.32	-0.65	+10.67	+0.21
Vegetation	-29.62	-0.59	+155.18	+3.10	+140.26	+2.80	-460.20	-9.19	-49.68	-0.99
Bare-land	-166.42	-3.33	+140.12	+2.80	-221.50	-4.43	-257.79	-5.15	-394.36	-7.88
Agriculture	+184.76	+3.69	-214.97	-4.30	+40.00	+0.80	+745.84	+14.90	+318.12	+6.36
Built-up	+7.82	+0.16	+30.19	+0.60	+16.74	+0.33	+4.47	+0.09	+115.25	+2.30

Note: symbol '+' indicates area increased or gained, '-' indicates area lost or decreased.

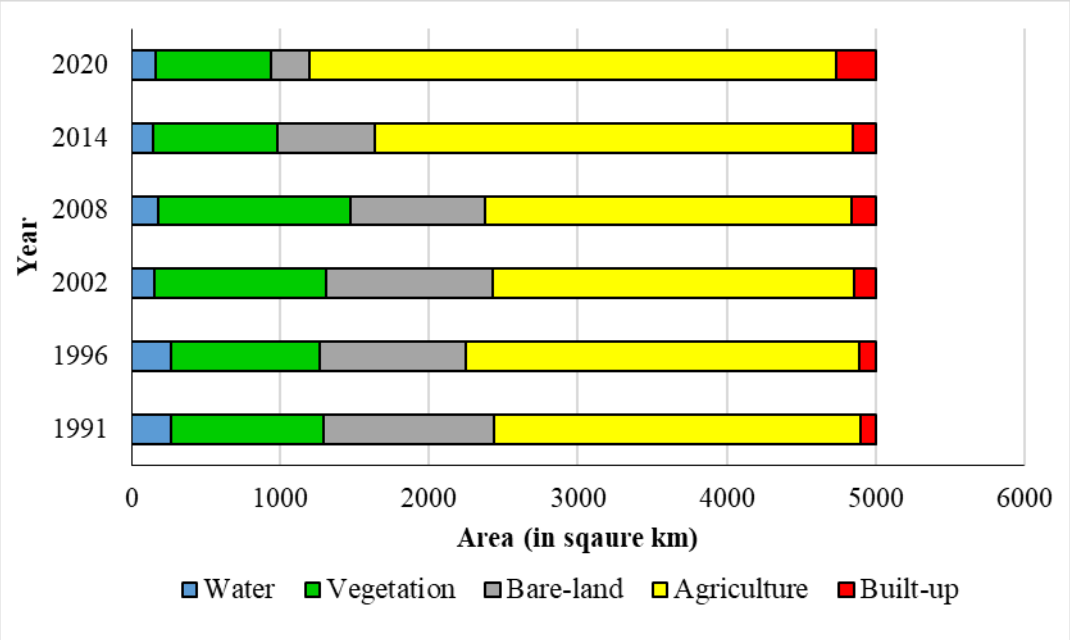

Fig. 3.4: LULC status (1991-2020)

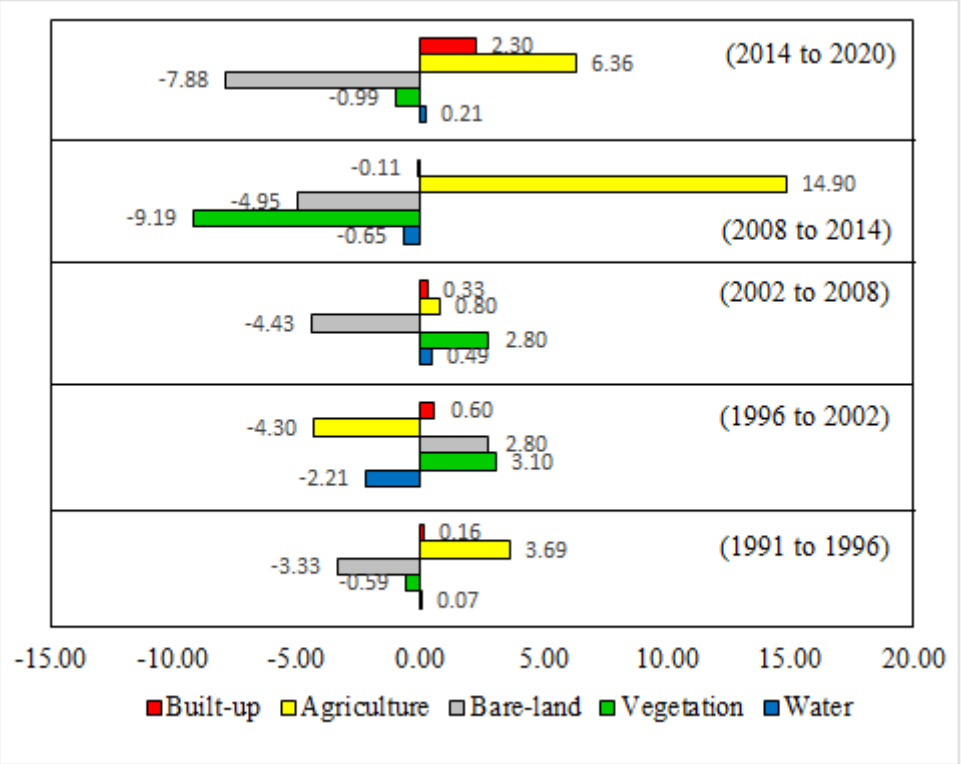

Fig. 3.5: Gain and lost status in percentage (1991-2020)

3.5 LULC Change detection

The basin underwent LULC change detection and land use and land cover conversion analyses spanning from 1991 to 2020. The analysis employed change vector analysis of a conversion matrix at five distinct stages: the first study period (1991–1996), the second study period (1996–2002), the third study period (2002–2008), the fourth study period (2008–2014), and the fifth study period (2014–2020). Throughout the entire study period, the conversion matrix revealed significant changes and transitions in LULC. Notably, during the first study period, the water body, agricultural land, and built-up areas increased by 0.07%, 3.69%, and 0.16%, respectively (Table 3.12). Additionally, the area of 3.72 km^2, 1.78 km^2 of bare land (Plate 1,2), and agriculture were converted into the water class. Moreover, 154.05 km^2 and 78.07 km^2 of bare land and vegetation contributed to the agricultural land. The built-up areas experienced a substantial increase of 7.82 km^2 during the first study period, with contributions of 7.70 km^2 and 4.78 km^2 from bare land and vegetation, respectively (Table 3.13).

In the second study period, vegetation increased by 3.10% (1150.09 km^2), predominantly contributed by agricultural land and bare land (472.64 km^2) and 272.02 km^2, where 4.30% of agriculture classes decreased by 2429.75 km^2, while bare-land and built-up classes increased from 1325.68 km^2 to 1079.09 km^2, 42.82 km^2 to 182.67 km^2, respectively (Table 3.14). In the third study period, water, vegetation, agriculture, and built-up areas increased by 183.02 km^2 (0.49%), 2368.95 km^2 (2.80%), 2469.73 km^2 (0.80%), and 162.37 km^2 (0.33%), respectively (Tables 3.12–15). Notably, the vegetation class received significant contributions from agriculture and bare land of 526.12 km^2 and 140.10 km^2, and the agricultural class received significant contributions from vegetation and bare land of 397.06 km^2 and 310.60 km^2, respectively (Table 3.15).

Table 3.13: Conversion Matrix 1991 – 1996

LULC Class (km^2)	Water	Vegetation	Bare-land	Agriculture	Built-up	Total
Water	261.79	0.13	1.42	0.76	0.06	264.17
Vegetation	0.80	940.40	0.02	78.07	4.78	1024.06
Bare-land	3.72	3.48	980.41	154.05	7.71	1149.38
Agriculture	1.78	46.67	0.23	2410.13	0.74	2459.54
Built-up	0.17	3.80	0.01	1.15	102.71	107.84
Total	268.26	994.49	982.09	2644.15	116.00	5004.99

Table 3.14: Conversion Matrix 1996 – 2002

LULC Class (km^2)	Water	Vegetation	Bare-land	Agriculture	Built-up	Total
Water	97.73	3.34	12.33	30.53	2.41	146.34
Vegetation	8.24	397.12	57.99	323.23	29.26	815.84
Bare-land	25.87	272.02	699.71	291.10	36.98	1325.68
Agriculture	23.98	472.64	308.34	1770.08	99.28	2674.32
Built-up	1.66	4.98	1.62	14.82	19.75	42.82
Total	157.48	1150.09	1079.99	2429.75	187.67	5004.99

Table 3.15: Conversion Matrix 2002 – 2008

LULC Class (km^2)	Water	Vegetation	Bare-land	Agriculture	Built-up	Total
Water	122.38	6.11	17.24	11.47	0.41	157.60
Vegetation	6.31	574.07	129.54	397.06	42.00	1148.98
Bare-land	13.96	140.10	613.77	310.60	44.41	1122.84
Agriculture	38.36	526.12	127.88	1718.08	19.36	2429.80
Built-up	2.01	42.62	12.42	32.53	56.20	145.77
Total	183.02	1289.03	900.84	2469.73	162.37	5004.99

Between 2008 and 2014, there was a significant loss of area in vegetation and bare land, amounting to 1015.16 km^2 to 831.31 km^2, and 1295.10 km^2 to 656.22 km^2 respectively. During the fourth study period, the agriculture class increased from 2529.54 km^2 to 3214.12 km^2. In the agriculture LULC class, vegetation and bare land contributed 583.62 km^2 and 516.03 km^2 of the area, respectively (Table 3.16).

In the final study period (2014–2020), bare land continued to significantly decrease, mirroring the trends observed in the fourth study period. However,

agriculture experienced an increase of 6.36% (3988.62 km^2). The transition of the area from water, vegetation, bare land, and built-up to agriculture accounted for 47.34 km^2, 501.33 km^2, 451.41 km^2, and 90.63 km^2, respectively. Furthermore, the transition of the area from water, vegetation, bare land, and agriculture to built-up was 1.64 km^2, 17.82 km^2, 30.51 km^2, and 29.43 km^2, respectively. (Table 3.17).

Table 3.16: Conversion Matrix 2008 – 2014

LULC Class (km^2)	Water	Vegetation	Bare-land	Agriculture	Built-up	total
Water	88.76	2.38	14.06	17.80	1.16	124.16
Vegetation	16.33	355.75	35.73	583.62	23.72	1015.16
Bare-land	22.20	214.30	499.23	516.03	43.33	1295.10
Agriculture	22.33	253.50	101.80	2088.73	63.18	2529.54
Built-up	0.19	5.38	5.39	7.94	22.14	41.04
total	149.81	831.31	656.22	3214.12	153.53	5004.99

Table 3.17: Conversion Matrix 2014 – 2020

LULC Class (km^2)	Water	Vegetation	Bare-land	Agriculture	Buil-tup	Total
Water	99.21	1.81	3.59	47.34	1.64	153.60
Vegetation	3.29	298.73	9.59	501.33	17.82	830.76
Bare-land	16.82	64.48	91.25	451.41	30.51	654.46
Agriculture	15.17	244.68	25.76	2897.90	29.43	3212.94
Built-up	1.40	15.45	6.11	90.63	39.63	153.23
Total	135.89	625.16	136.30	3988.62	119.03	5004.99

Plate 1: Bare land at up-stream (Ahilpur pur, Dumka)

Plate 2: Bare land and gully erosion at up-stream (Nagabadi, Dumka)

Plate 3: Bare land and gully erosion at mid-stream (Palom, Dumka)

Plate 4: Crop-land (at Sonamukhi, Birbhum)

3.6 LULC Prediction

3.6.1 Model validation

The CA-Markov model was employed to estimate the future LULC, considering various driving factors such as slope, elevation, road proximity, and city center (Fig. 3.1). The accuracy of the simulated LULC was assessed by comparing it with the actual LULC data from 2020. The evaluation results demonstrated an impressive overall accuracy of 93.16% and a Kappa agreement of 0.85 (Table 3.18). These findings indicate a perfect agreement between the simulated and actual LULC, affirming the reliability of the model. Moreover, the comparison between the actual and simulated results was analysed by pairing the respective LULC data (Table 3.20 and Fig. 3.6). The percentages of water, vegetation, bare-land, agriculture, and built-up LULC classes were as follows: 3.20%, 15.57%, 5.18%, 70.61%, and 5.44 % for the actual results and 3.22%, 15.71%, 5.25%, 70.37%, and 5.46 % for the simulated results, respectively. Notably, the vegetation and agriculture classes exhibited the highest rates of change (RC) and percentage of change (PC) at 7.00%, -12.04%, and 0.14%, -0.24% respectively. Overall, considering the Kappa agreement and comparison Tables 19 and 20, the model demonstrated considerable accuracy in predicting future LULC, enabling the estimation of the LULC for the year 2032.

Table 3.18: Contingency matrix number of actual 2020 and simulated 2020

	LULC Class (km^2)	**2020 Simulated**					
		Water	**Vegetation**	**Bare-land**	**Agriculture**	**Built-up**	**total**
2020 Actual	**Water**	158.78	0.16	0.13	0.79	0.17	160.02
	Vegetation	0.33	772.08	1.01	4.42	1.65	779.50
	Bare-land	0.29	0.64	255.72	2.01	0.71	259.37
	Agriculture	1.74	11.39	5.02	3512.53	3.13	3533.81
	Built-up	0.23	2.23	0.81	2.03	267.00	272.29
	Total	161.37	786.50	262.70	3521.77	272.65	5004.99

Table 3.19: Accuracy between actual 2020 and simulated 2020 LULC

LULC Class	UA	PA
Water	56.53 %	56.20 %
Vegetation	90.93 %	92.05 %
Bare-land	69.83 %	69.95 %
Agriculture	97.87 %	97.44 %
Built-up	76.35 %	73.91 %
Overall Accuracy	93.16 %	
Kappa Statistics	0.85	

Table 3.20: Comparison between actual (2020) and simulated (2020)

LULC Class	2020 (Original)	Area (%)	2020 (Simulated)	Area (%)	RC	PC
Water	160.01	3.20	161.37	3.22	1.36	0.02
Vegetation	779.50	15.57	786.50	15.71	7.00	0.14
Bare-land	259.37	5.18	262.70	5.25	3.32	0.07
Agriculture	3533.81	70.61	3521.77	70.37	-12.04	-0.24
Built-up	272.30	5.44	272.65	5.46	0.36	0.02

Note* RC = Rate of change, PC = Percentage of change.

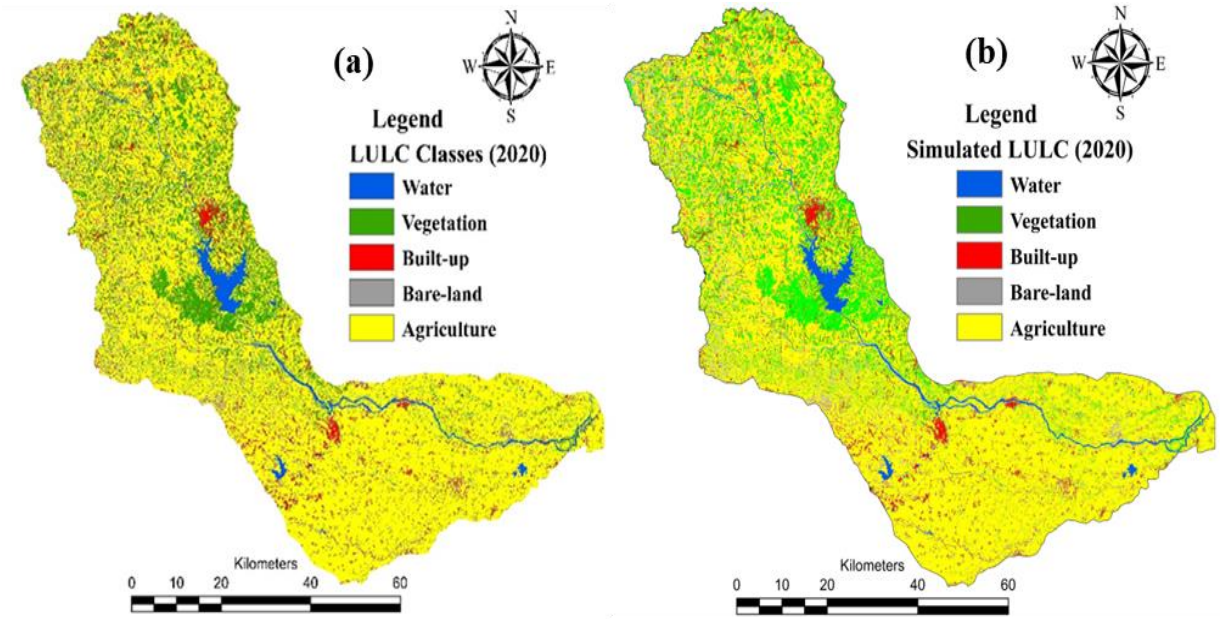

Fig. 3.6: a- Actual 2020 and, b- simulated 2020

3.6.2 Future LULC status and conversion probability

According to the CA-Markov model, the estimated future LULC for 2032 (Fig. 3.7) indicates that agriculture will dominate the study area, covering 70.35% of the area. However, compared to 2020 (70.61%), agricultural land will decrease by 12.89 km^2 (Table 3.19 and 3.20). The second dominant LULC class will be vegetation, covering an area of 788.18 km^2, which will see a slight increase of 0.03%. Bare-land and built-up areas are expected to increase by 0.05% (Table 3.20).

The conversion probabilities for the water class in 2032 are computed as follows: 0.15% from bare-land, 0.04%, 0.06% from vegetation and agriculture, and 0.08% from built-up areas (Table 3.23). The expected vegetation cover will be 788.18 km^2, with contributions of 15.48 km^2 and 2.24 km^2 from agriculture and built-up areas respectively (Table 3.22). The probability of transitioning from water, vegetation, and bare-land to agriculture is estimated at 0.80%, 0.90%, and 0.94%, respectively.

Table 3.21: LULC status of 2032

LULC Class	2032	
	Area (km^2)	(%)
Water	161.38	3.22
Vegetation	788.18	15.75
Bare-land	262.12	5.24
Agriculture	3520.92	70.35
Built-up	272.40	5.44

Table 3.22: Conversion Matrix 2020 - 2032

Land use types	Water	Vegetation	Bare-land	Agriculture	Built-up	Total
Water	158.43	0.09	0.08	1.28	0.13	160.01
Vegetation	0.31	769.99	0.59	7.00	1.61	779.50
Bare-land	0.38	0.37	255.16	2.44	1.01	259.37
Agriculture	2.04	15.48	5.27	3507.64	3.38	3533.81
Built-up	0.20	2.24	1.02	2.56	266.27	272.30
Total	161.38	788.18	262.12	3520.92	272.40	5004.99

Table 3.23: Conversion Probability 2020 – 2032 in percentage

LULC Class	Water	Vegetation	Bare-land	Agriculture	Built-up
Water	99.02	0.06	0.05	0.80	0.08
Vegetation	0.04	98.78	0.08	0.90	0.21
Bare-land	0.15	0.14	98.38	0.94	0.39
Agriculture	0.06	0.44	0.15	99.26	0.10
Built-up	0.08	0.82	0.38	0.94	97.78

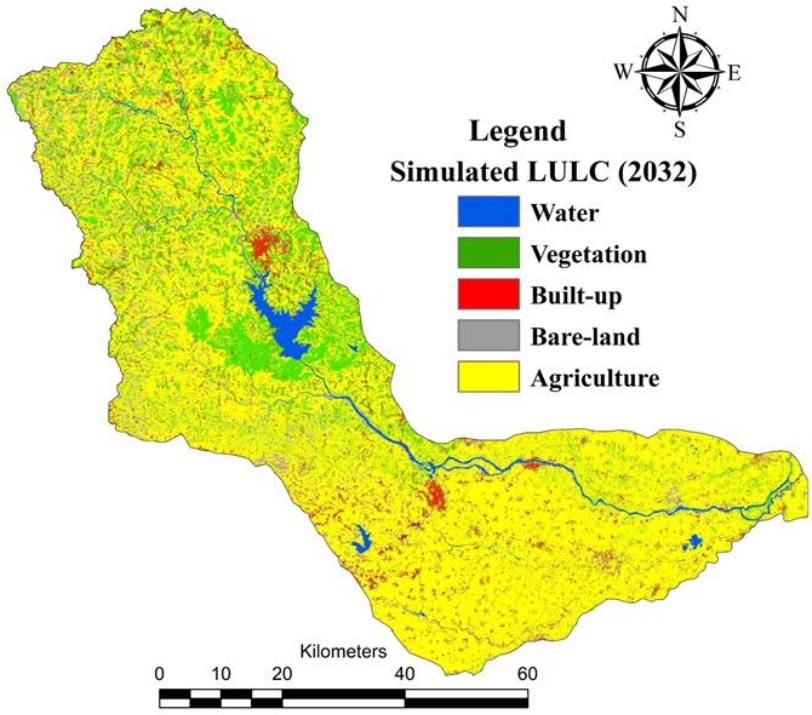

Fig. 3.7: Predicted LULC 2032

3.7 Summary

The analysis of LULC changes over a 30-year study period provided insights into the changing trend and pattern of LULC in the basin. Initially, in 1991, the upper part of the basin consisted mostly of bare land, while the lower basin area was predominantly agricultural. Over time, the bare land was transformed into agricultural land, thereby significantly altering the landscape. In 1991, the agricultural land covered an area of 2460.06 km^2 (49.15%), which increased to 3533.81 km^2 (70.60%) by 2020. Similarly, the built-up area exhibited a consistent

upward trend throughout the study period. In 1991, 2008, and 2020, the built-up area accounted for 2.15%, 3.25%, and 5.44%, respectively.

Conversely, vegetation cover experienced a declining trend over the 30-year span. In 1991, vegetation covered 20.45% of the basin, which increased to 25.76% in 2008 and further dropped to 16.67% and 15.57% in 2014 and, 2020. The analysis revealed that during the first study period, 0.80 km^2 of vegetation and 3.27 km^2 of bare land were converted into water bodies. In the second study period, 1.42 km^2 of water bodies and 78.07 km^2 of vegetation were transformed into bare-land and agriculture. In the final study period, 47.34 km^2 of water, and 298.73 km^2 of vegetation underwent conversion into agriculture and built-up areas. Based on an overall accuracy of 93.16% and a Kappa agreement of 0.85, the future LULC prediction for 2032 indicates that agriculture will be the dominant land cover class, spanning 3520.92 km^2. It will be followed by vegetation covering an area of 788.18 km^2 and built-up areas occupying 272.40 km^2. It is projected that from 2020 to 2032, agricultural land will experience a marginal decline of 0.26%.

3.8 Concluding Remarks

The present chapter aims to provide a concise overview of the evolving land use and land cover patterns in the Mayurakshi basin. The analysis employed popular LULC mapping techniques (RF) and change detection methods, supplemented by the algorithms of the Artificial Neural Network CA-Markov model, to explore future scenarios. Over the period from 1991 to 2020, significant transformations were observed in the basin's land use composition. Initially, the upper region exhibited undulating terrain and bare land, which gradually gave way to agricultural fields. Throughout the study duration, there was an increase in agricultural and built-up areas, while water bodies, vegetation cover, and bare-land areas decreased. The natural vegetation on the plateau in the upper part of the basin experienced a decline, whereas the lower basin area saw the introduction of planted vegetation cover. These detailed LULC findings are instrumental in understanding the runoff characteristics of the basin. Furthermore, future projections of LULC offer insights into the anticipated scenario for the basin. Therefore, this comprehensive analysis of LULC

status, dynamic patterns, and future predictions holds immense value for effective basin management and environmental preservation. Local communities can utilize this knowledge and integrate it into their planning endeavors to ensure sustainable basin management in the years to come.

References

Adam, E., Mutanga, O., Odindi, J., & M. Abdel-Rahman, E. (2014). Land-use/cover classification in a heterogeneous coastal landscape using RapidEye imagery: evaluating the performance of random forest and support vector machines classifiers. *International Journal of Remote Sensing, 35*(10), 3440–3458. doi:http://dx.doi.org/10.1080/01431161.2014.903435

Ahmad, S. (2014). Land use change detection using remote sensing and artificial neural network: Application to Birjand, Iran. *Computational Ecology and Software, 4*(276), 50-68. Retrieved from http://www.iaees.org/publications/journals/ces/onlineversion.asp

Akpoti, K., Antwi, E. O., & Kabo-Bah, A. T. (2016). Impacts of rainfall variability, land use and land cover change on stream flow of the black Volta Basin, West Africa. *Hydrology, 3*(3), 26. doi:https://doi.org/10.3390/ hydrology3030026

Alam, A., Bhat, M. S., & Maheen, M. (2019). Using landsat satellite data for assessing the land use and land cover change in Kashmir valley. *GeoJournal, 88*, 1529–1543.

Amponsah, C., Kozubowski, T., & Panorska, A. (2021). A general stochastic model for bivariate episodes driven by a gamma sequence. *J Stat Distrib App, 8*(7), 38-45 doi:https://doi.org/10.1186/s40488-021-00120-5

Anand, J., Gosain, A. K., & Khosa, R. (2018). Prediction of land use changes based on Land Change Modeler and attribution of changes in the water balance of Ganga basin to land use change using the SWAT model. *Science of the Total Environment, 644*, 503–519.

Anand, J., Gosain, A. K., & Khosa,, R. (2018). Prediction of land use changes based on Land Change Modeler and attribution of changes in the water balance of Ganga basin to land use change using the SWAT model. *Science of the Total Environment, 644*, 503–519.

Avci, C., Budak, M., Yagmur, N., & Balcik, F. B. (2022). Comparison between random forest and support vector machine algorithms for LULC classification. *International Journal of Engineering and Geosciences, 8*(1), 1-10. doi: 10.26833/ijeg.987605

Beroho, M., Briak, H., Cherif, E., Boulahfa, I., Ouallali, A., Mrabet, R., & Aboumaria, K. (2023). Future Scenarios of Land Use/Land Cover (LULC) Based on a CA-Markov Simulation Model: Case of a Mediterranean Watershed in Morocco. *Remote Sensing, 15*(14), 1162-1172.

Bock, A. R., Farmer, W. H., & Hay, L. E. (2018). Quantifying uncertainty in simulated streamflow and runoff from a continental scale monthly water balance model. *Advances in Water Resources*, 122.20-31

Chakilu, G., & Moges, M. (2017). Assessing the land use/cover dynamics and its impact on the low flow of Gumara Watershed, Upper Blue Nile Basin, Ethiopia. *Hydrol Current Res, 7*(2).55-61

Chaturvedi, V. (2021). Urban land use planning. *In: Encyclopedia*.15-25, doi:https:// encyc loped ia. pub/ entry/ 14975

Dayamba, S. D., Djoudi, H., Zida, M., Sawadogo, L., & Verchot, L. (2016). Biodiversity and carbon stocks in different land use types in the Sudanian Zone of Burkina Faso, West Africa. *Agriculture, Ecosystems & Environment, 226*, 61-72.

Fu, B., Chen, L., Ma, K., Zhou, H., & Wang, J. (2000). e relationships between land use and soil conditions in the hilly area of the loess plateau in northern Shaanxi, China. *Catena, 39*(1), 69–78.

Gashaw, T., Tulu, T., Argaw, M., & Worqlul, A. W. (2017). Evaluation and prediction of land use/land cover changes in the Andassa watershed, Blue Nile Basin, Ethiopia. *Environmental Systems Research , 6*(1), 17.

Guan, D., Li, H., Inohae, T., Su, T., Nagaie, T., & Hokao, K. (2011). Modeling urban land use change by the integration of cellular automaton and Markov model. *Ecological Modelling, 222*, 3761-3772.

Guan, D., Li, H., Inohae, T., Su, W., Nagaie, T., & Hokao, K. (2011). Modeling urban land use change by the integration of cellular automaton and Markov model. *Ecological Modelling*(222), 3761–3772.

Guan, D., Lin, X., Gao, W., Su, W., & Hokao, K. (2014). Dynamic evolvement assessment and forecast of land use based on geographic information system Lowland Technology International. *16*(1), 36–44.

Hamad, R., Balzter, H., & Kolo, K. (2018). Predicting land use/land cover changes using a CA-Markov model under two different scenarios. *Sustainablity, 10*(10), 33-47

Hamad, R., Balzter, H., & Kolo, K. (2018). Predicting Land Use/Land Cover Changes Using a CA-Markov Model under Two Different Scenarios. *Sustainability, 10*(3421), 1-23. doi:doi:10.3390/su10103421

Han, J., Hayashi, Y., Cao, X., & Imura, H. (2009). Evaluating land-use change in rapidly urbanizing China: Case study of Shanghai. *Journal of Urban Planning and Development, 135*(4), 166–171. doi:https://doi.org/10. 1061/(ASCE)0733- 9488(2009)135:4(166)

Hasan, S., Shi, W., Zhu, X., Abbas, S., & Khan, H. (2020). Future simulation of land use changes in rapidly urbanizing South China based on land change modeler and remote sensing data. *Sustainability, 12*(11), 4350. doi:https:// doi. org/ 10. 3390/ su121 14350

Hurni, H., Tato, K., & Zeleke, G. (2005). The implications of changes in population, land use, and land management for surface runoff in the upper Nile basin area of Ethiopia. *Mountain Research and Development, 25*(2), 147–154. doi:https://doi.org/10.1659/0276-4741 (2005)025[0147:TIOCIP]2.0.CO;2

Hyandye, C., & Martz, L. W. (2017). Markovian and cellular automata land-use change predictive model of the Usangu Catchment. *International Journal of Remote Sensing*, *38*(1), 64–81.

Jain, G., & Sharma, S. (2019). Spatio-temporal analysis of urban growth in selected small, medium, and large Indian cities. *Geocarto Int, 34*(8), 887–908. doi:https:// doi. org/ 10. 1080/ 10106 049. 2018. 14504 50

Jamali, A. (2019). Evaluation and comparison of eight machine learning models in land use/land cover mapping using Landsat 8 OLI: a case study of the northern region of Iran. *SN Applied Sciences, 1*(1448), 1-11. doi:https://doi.org/10.1007/s42452-019-1527-8

Jantz, C., Goetz, S., & Shelley, M. (2004). Using the SLEUTH urban growth model to simulate the impacts of future policy scenarios on urban land use in the Baltimore-Washington Metropolitan Area. *Environ Plan B Plan Des, 31*(2), 251-271.

Javed, A., Jamal, S., & Khandey, M. Y. (2012). Climate change induced land degradation and socio-economic deterioration: a remote sensing and gis based case study from Rajasthan, India. *Journal of Geographic Information System, 4*(3).60-69

Ji, W., Wang, Y., Zhuang, D., Song, D., Shen, X., Wang, W., & Li, G. (2014). Spatial and temporal distribution of expressway and its relationships to land cover and population: a case study of Beijing, China. *Transp Res D Transp Environ, 32*(3), 86–96. doi:https:// doi. org/ 10.1016/j. trd. 2014. 07. 010

Jiang, Z., Sharma, A., & Johnston, F. (2019). Assessing the sensitivity of hydro climatological change detection methods to model uncertainty and bias. *Advances in Water Resources,* 134.12-26

John, R., & John, M. (2019). Adaptation of the visibility graph algorithm for detecting time lag between rainfall and water level fluctuations in Lake Okeechobee. *Advances in Water Resources, 10*, 134-145

Khwarahm, N., Najmaddin, P., Ararat, K., & Qader, S. (2021). Past and future prediction of land cover land use change based on earth observation data by the CA–Markov model: a case study from Duhok governorate, Iraq. *Arabian*

Journal of Geosciences, 14(1544), 1-14. doi:https://doi.org/10.1007/s12517-021-07984-6

Khwarahm, N., Qader, S., Ararat, K., & Al-Quraish, A. (2020). Predicting and mapping land cover/land use changes in Erbil/Iraq using CA-CAMarkov. *Earth Science Informatics*, 1-14.

Kindu, M., Schneider, T., Teketay, D., & Knoke, T. (2013). Land use/land cover change analysis using object-based classification approach in Munessa-Shashemene landscape of the Ethiopian highlands. *Remote Sensing, 5*(5), 2411–2435.

Kreuter, U. P., Harris, H. G., Matlock, M. D., & Lacey, R. E. (2001). Change in ecosystem service values in the San Antonio area, Texas. *Ecological Economics, 39*(3), 333–346.

Lai, Z., Chen, C., Chen, J., Wu, Z., Wang, F., & Li, S. (2022). Multi-scenario simulation of land-use change and delineation of urban growth boundaries in County Area: a case study of Xinxing County, Guangdong Province. *Land, 11*(9), 1598-1610. doi:https:// doi. org/ 10. 3390/land1 10915 98

Lambin, E. F., Geist, H. J., & Lepers, E. (2003). Dynamics of land-use and land-cover change in tropical regions. *Annual Review of Environment and Resources, 28*, 205–241. doi:https://doi.org/10.1146/annurev.energy.28.050302.105459

Leach, J. M., & Coulibaly, P. (2019). An extension of data assimilation into the short-term hydrologic forecast for improved prediction reliability. *Advances in Water Resources, 134*, 89-97.

Li, X., & Yeh, A. G. (2004). Analyzing spatial restructuring of land use patterns in a fast growing region using remote sensing and GIS. *Landscape and Urban Planning*, *69*(4), 335-354.

Linard, C., Gilbert, M., Snow, R., Noor, A., & Tatem, A. (2012). Population distribution, settlement patterns and accessibility across Africa in 2010. *PLoS ONE, 7*(2), 31743. doi:https:// doi. org/ 10. 1371/ journ al. pone. 00317 43

Liping, C., Yujun, S., & Saeed, S. (2018). Monitoring and predicting land use and land cover changes using remote sensing and GIS techniques a case study of a hilly area, Jiangle, China. *PLoS One*, 13:e0200493.

Lu, D., Mausel, P., Brondizio, E., & Moran, E. (2003). Change detection techniques. *International Journal of Remote Sensing, 25*, 2365-2401.

Mishra, V., & Rai, P. (2016). A remote sensing aided multi-layer perceptron-Markov chain analysis for land use and land cover change prediction in Patna district (Bihar), India. *Arab J Geosci, 9*(294),25-38

Mishra, V., Rai, P., Prasad, R., Punia, M., & Nistor, M.-M. (2018). Prediction of spatio-temporal land use/land cover dynamics in rapidly developing Varanasi district of Uttar Pradesh, India, using geospatial approach: a comparison of hybrid models. *Applied Geomatics*, 1-20. doi:https://doi.org/10.1007/s12518-018-0223-5

Munthali, M., Mustak, S., Adeola, A., Botai, J., Singh, S., & Davis, N. (2020). Modelling land use and land cover dynamics of Dedza district of Malawi using hybrid Cellular Automata andMarkov model Remote. *Society and Environment*, 17-31

Nguyen, H. T., Doan, T. M., Tomppo, E., & E. McRoberts, R. (2020). Land Use/Land Cover Mapping Using Multitemporal Sentinel-2 Imagery and Four Classification Methods—A Case Study from Dak Nong, Vietnam. *remote sensing*, 1-27.

Olson, J. M., Alagarswamy, G., & Andresen, J. A. (2008). Integrating diverse methods to understand climate-land interactions in East Africa. *Geoforum, 39*(2), 898–911.

Osman, T., Shaw, D., & Kenawy, E. (2019). An integrated land use change model to simulate and predict the future of greater Cairo metro metropolitan. *J Land Use Sci, 13*(6), 565–584. doi:https:// doi. org/ 10.1080/ 17474 23X. 2019. 15818 49

Pandian, M., Rajagopa, N., Sakthivel, G., & Amrutha, D. E. (2014). Land use and land cover change detection using remote sensing and gis in parts of Coimbatore and Tiruppur districts, Tamil Nadu, India. *International Journal of Remote Sensing & Geoscience (IJRSG), 3*(1), 14-20.

Pijanowski, B., Brown, D., Shellito, B., & Manik, G. (2002). Using neural networks and GIS to forecast land use changes: a land transformation model Computers,. *Environment and Urban Systems, 26*, 553-575.

Porter-Bolland, L., Ellis, E. A., & Gholz, H. L. (2007). Land use dynamics and landscape history in La Montaña, Campeche, Mexico. *Landscape and Urban Planning, 82*(4), 198–207.

Rawat, J., & Kumar, M. (2015). Monitoring land use/cover change using remote sensing and GIS techniques: A case study of Hawalbagh block, district Almora, Uttarakhand, India. *The Egyptian Journal of Remote Sensing and Space Science, 18*(1), 77–84. doi:https://doi. org/10.1016/j.ejrs.2015.02.002

Rodriguez-Galiano, V., Ghimire, B., Rogan, J., Chica-Olmo, M., & Rigol-Sanchez, J. (2011). An assessment of the effectiveness of a random forest classifier for land-cover classification. *ISPRS Journal of Photogrammetry and Remote Sensing*, 93–104.

Sewnet, A. (2015). Land use/cover change at infra Watershed, Northwestern Ethiopia. *Journal of Landscape Ecology, 8*(1), 69–83. doi:https://doi.org/10.1515/jlecol-2015-0005

Shafizadeh, M., & Helbich, M. (2013). Spatiotemporal urbanization processes in the megacity of Mumbai, India: a Markov chains-cellular automata urban growth model. *Appl Geogr, 40*, 140–149. doi:https:// doi. org/ 10. 1016/j. apgeog. 2013. 01. 009

Sleeter, M. B., Sohl, T. L., & Loveland, T. R. (2013). Land-cover change in the conterminous United States from 1973 to 2000. *Global Environmental Change, 23*(4), 733–748.

Szumacher, I., & Pabjanek, P. (2017). Temporal changes in ecosystem services in European cities in the continental biogeographical region in the period from 1990–2012. *Sustainability, 9*(4), 665.

Taelman, S. E., Schaubroeck, T., Meester, S. D., Boone, L., & Dewulf, J. (2016). Accounting for land use in life cycle assessment: the value of NPP as a proxy indicator to assess land use impacts on ecosystems. *Science of the Total Environment, 550*, 143–156.

Tewabe, D., & Fentahun, T. (2020). Assessing land use and land cover change detection using remote sensing in the Lake Tana Basin, Northwest Ethiopia. *Cogent Environmental Science*, 1-11. doi:https://doi.org/10.1080/23311843.2020.1778998

Turner, B. L., Lambin, E. F., & Reenberg, A. (2007). The emergence of land change science for global environmental change and sustainability. *PNAS, 104*, 20666 - 20671.

Uma, D. A., Ramli, M. F., Tukur, A. I., Jamil, N. R., & Zaudi, M. A. (2021). Detection and prediction of land use change impact on the streamflow regime in Sahelian river basin, northwestern Nigeria. *H2Open Journal, 4*(1), 92-113. doi:doi: 10.2166/h2oj.2021.065

Vahid, E., Saeid, H., Ahmad, M., & Abbas, A. (2015). Land cover mapping based on random forest classification of multitemporal spectral and thermal images. *Environ Monit Assess*, 1-14. doi:DOI 10.1007/s10661-015-4489-3

Verburg, P. H., Overmars, K. P., Huigen, M. G., de Groot, W. T., & Veldkamp, A. (2006). Analysis of the effects of land use change on protected areas in the Philippines. *Applied Geography, 26*(2), 153–173.

Wang, S., Gebru, B., Lamchin, M., Kayastha, R., & Lee, W. (2020). Land use and land cover change detection and prediction in the Kathmandu District of Nepal using remote sensing and GIS. *Sustainablity, 12*(3925).103-129

Wei, H., Fan, W., Ding, Z., Weng, B., Xing, K., Wang, X., Dong, X. (2017). Ecosystem services and ecological restoration in the Northern Shaanxi Loess

Plateau, China, about climate fluctuation and investments in natural capital. *Sustainability, 9*(2), 99-115.

Wu, Y., Li, S., & Yu, S. (2016). Monitoring urban expansion and its effects on land use and land cover changes in Guangzhou city, China. *Environmental Monitoring and Assessment, 188*(1), 54-68

Yang, X., Zheng, X.-Q., & Lv, L.-N. (2012). A spatiotemporal model of land use change based on ant colony optimization, Markov chain, and cellular automata. *Ecol Model, 233*, 11-19.

Yirsaw, E., Wu, W., Shi, X., Temesgen, H., & Bekele, B. (2017). Land use/land cover change modeling and the prediction of subsequent changes in ecosystem service values in a coastal area of China, the Su-Xi-Chang region. *Sustainability, 9*(7), 1204-1220

Zheng, W. H., Shen, G. Q., Wang, H., & Hong, J. (2015). Simulating land use change in urban renewal areas: a case study in Hong Kong. *Habitat International, 46*, 23-34.

Chapter 4: TO EVALUATE THE SEASONAL STREAMFLOW PATTERN AND SIMULATE THE RUNOFF PATTERN OF THE BASIN

4.1 Objective and Chapter Organization

This chapter extensively incorporates runoff simulation calibration and validation over a 30-year period. Section 4.3 deals with the database and method prior to the simulation and validation of the SWAT model. The details of model building and mandatory datasets are outlined in sections 4.3.1 Dataset for the SWAT model, 4.3.2 SWAT model, 4.3.3 SWAT Soil Input Data Preparation, and 4.3.4 for Model Calibration and Validation. The flow pattern of the streams is highlighted in Section 4.5. The runoff of the natural period and the impact period are simulated and validated in sections 4.6 and 4.7. The key result was summarized with concluding remarks in Section 4.8.

4.2 Introduction

The exploration of hydrological modeling is crucial for effective water resource management, driven by its implications for biodiversity preservation and meeting the growing human demand on Earth. The sustenance of both human societies and the ecosystem is intricately tied to the availability and quality of water (Milly et al., 2005). Technological advancements have led to significant changes in LULC, with human activities increasingly disrupting the natural environment, making it highly susceptible to climate change (Huntington, 2006). Runoff dynamics are influenced by various factors, with LULC and climate being pivotal among them. Notably, alterations in runoff are not solely attributed to LULC changes on the Earth's surface; direct human interventions, such as reservoir operations and irrigation, have accounted for a 2.1% reduction in global discharge from 1981 to 2000 (Biemans et al., 2011). The global temperature has risen by 0.85 °C, according to the fourth report of the IPCC (Pachauri et al., 2014). Consequently, distinguishing between the impacts of human activities and climatic factors on runoff is a fundamental focus of hydrological research (Hulme et al., 1999).

Numerous tools and techniques have evolved and have been employed in hydrological research, including climate elasticity (Yang et al., 2008), the time trend method (Zhang et al., 2013), hydrological modeling (Li et al., 2009), Budyko-coupled elasticity (Liang et al., 2013), and the paired catchment method (Huang et al., 2003). Among these models, the Soil and Water Assessment Tool (SWAT) stands out as a widely used and popular model, applied in numerous studies for runoff simulation. This chapter primarily focuses on the calibration and validation of runoff simulation using the well-established models SWAT and SWAT CUP (Soil and Water Assessment Tool-Calibration and Uncertainty Programming) (Hossain et al. 2020)

4.3 Database and Methods

A thorough exploration of the database and the methods employed in this chapter has been presented in this section.

4.3.1 Dataset for the SWAT model

The necessary dataset for this study was sourced from diverse outlets. Rainfall data, crucial for the research, was obtained from IMD Puna (https://www.imdpune.gov.in/cmpg/Griddata/Rainfall_25_Bin.html). The data furnished by this platform features exceptionally high spatial resolution, providing daily gridded rainfall data at 0.25 × 0.25 degrees with the unit of measurement in millimeters (mm). Other mandatory weather datasets, including temperature, humidity, wind speed, and solar radiation, were acquired from NASA Power Access MERRA-2 data (https://power.larc.nasa.gov/data-access-viewer/). These datasets were assessed at a 0.5 × 0.5-degree interval. The specific point dataset needed for simulating the runoff model aimed for precision at a 0.25 × 0.25 interval. To achieve this goal, the NASA Power Access data was processed through kernel smoothing interpolation. The resulting dataset with the desired interval (0.25 × 0.25) was aligned with IMD point latitude and longitude, forming the basis for running the runoff model. Elevation data was sourced from the Digital Elevation Model (DEM), while historical images were collected from openly available satellite data via the United States Geological Survey (USGS) portal (http://earthexploration.usgs.gov/).

The LULC map was classified by the Random Forest (RF) machine learning algorithm, as detailed in Chapter 3, Section 3.3.2. To validate the model, observed discharge data were obtained from the Ministry of Jal Shakti, Central Water Commission Executive Engineer, Damodar Division, CWC, Asansol, under the Government of India.

4.3.2 SWAT model

The Soil and Water Assessment Tool (SWAT) stands as a sophisticated, physically-based model designed for runoff simulation, sediment yield measurement, vegetation growth, and nutrient circulation. Originating from the "Agricultural Research Centre of the United States Department of Agriculture" (USDA), SWAT evolved from the "Simulator for Water Source in Rural Basins" (SWRRB). This GIS-based application is compatible with various GIS platforms, such as QSWAT, VISWAT, MSWAT, and ArcSWAT. Detailed information about the application can be found in the SWAT documentation available at http://swatmodel.tamu.edu/. To operate the SWAT model, essential datasets encompass soil texture, DEM, land use/land cover, precipitation, humidity, solar radiation, wind speed, temperature data for modeling, and observed discharge for calibration and validation. The basin is categorized into sub-basins, and the model delineates hydrologic response units (HRUs) within each sub-basin. For evapotranspiration calculations, the model employs the Priestly-Taylor, Hargreaves, and Penman-Monteith methods. The water balance equation is a fundamental component of the model's functionality (Hosseini et al. 2020).

$$SW_t = SW_o + \sum_{i=1}^{t} (Rv - Qs - Wseepage - E^t - Q^{tgw}) \quad \text{.....(Eq.1)}$$

Where,

SWt is soil humidity, SWo is base humidity, Rv is the volume of rainfall (mm), Qs is runoff, and Wseepage is water percolation under the soil profile per day in millimeters. E^t is evapotranspiration per day in millimeters, and Q^{tgw} is the amount of base flow per day in millimeters.

4.3.3 SWAT Soil Input Data Preparation

Soil input is an important parameter of SWAT modeling to simulate the runoff. The soil data is categorized into physical properties and chemical properties. The SWAT inputs of physical properties such as percentage of sand, silt, clay, bulk density, course fragment, and organic carbon density have a major impact on the movement of air and water through the soil. The initial soil chemical level is determined by soil chemical properties such as soil PH. The physical properties are mandatory, and the chemical properties are optional. The required SWAT soil inputs are given below.

Table 4.1: List of variables for SWAT soil input data

SL.NO	Variables	Remarks
1	**Hydrological Soil Group**	Hydrological Soil Group (HSG) is the classification system of soil based on its ability to absorb and transmit water, widely being used for hydrological studies. The classification system was proposed by the United States Natural Resources Conservation Service (NRCS), is a part of the Soil Conservation Service (SCS) Curve Number (CN) method. The HSG initially categorized four primary hydrological soil groups. These are group A represents high infiltration, group B represents moderate infiltration, group C represents slow Infiltration and group D represents Very Slow Infiltration.
2	**Maximum rooting depth**	The maximum rooting depth is the depth of the soil layer to be taken as an input of the maximum depth of the soil layer considered for the computation of runoff measurement.
3	**Depth of soil from the surface to the bottom of the layer**	The depth of soil from the surface to the bottom of the layer is the depth of soil layers from the surface to the bottom of the individual layers in centimeters. Depth by layer is given below 0 – 5 cm depth 5-15 cm depth 15-30cm depth 30-60cm depth 60-100cm depth 100-200cm depth
4	**Moist bulk density**	The moist bulk density expresses the ratio of the porous material per unit volume or mass of a soil, the volume could be occupied as solids and pores at a specific moisture content. The moist bulk density is expressed in the unit of kilograms per cubic meter (kg/m^3) or as grams

		per cubic centimeter (g/cm³), The moisture content of the soil is an important factor because it affects the permeability as well as the weight of the material for a given volume.
5	**Availability of the water in the soil layer**	Available Water Capacity (AWC) refers to the amount of water in a soil layer that can be stored and is available for plants to uptake. The AWC is determined by Field Capacity (FC) and Wilting Point (WP). The FC refers to the amount of water in the soil retained against the pull of gravity or after the downward movement of the water. It is the condition when the soil is moist enough to adequately supply water for the plants. The WP is the point when soil loses its adequate moisture condition and water is tightly bound with soil and not enough to uptake for plants. The AWC is estimated by Dijkerman, 1988 as follows AWC = (θ33–θ1500) ……..…(Eq.2) θ33 = 0.3697–0.0035*S……. (Eq.2.1) θ1500 = 0.0074 + 0.0039*C……. (Eq.2.2) In these equations AWC= Available Water Capacity, θ33 = soil water content at field capacity, θ1500 = soil water content at wilting point, C = Clay in percentage, and S = Sand in percentage.
6	**Saturated hydraulic conductivity**	Saturated hydraulic conductivity is referring the porous medium of rock or soil under saturated conditions. It is a coefficient of water movement at the saturated condition of the soil under the influence of gravity. The saturated hydraulic conductivity is influenced by factors of porosity of the soil, grain size distribution, soil structure, and compaction history. The standard units to measure saturated hydraulic conductivity are inches per hour (in/hr) or millimeters per hour (mm/hr) or centimeters per second (cm/s) or meters per second (m/s). To calculate the saturated hydraulic conductivity formula used Cosby et al. (1984). Ks = 60.96*10 ^ (−0.6 + 0.0126*S − 0.0064*C)…… (Eq.3) In this equation Ks = saturated hydraulic conductivity, S = Sand in percentage, C = Clay in percentage.
7	**Organic carbon content in the soil**	Soil organic carbon content refers to the presence of carbon content in the soil or sediment. For soil organic carbon is a major component of organic matter that includes animal and plant decomposed residuals. The decomposed residuals are important in determining the moisture retention and fertility of the soil.
8	**Percentage of clay**	The percentage of clay content in the soil is an important

	content in the soil	soil input, the clay layers are included by depth as given below 0 – 5 cm Percentage of clay 5-15 cm Percentage of clay 15-30cm Percentage of clay 30-60cm Percentage of clay 60-100cm Percentage of clay 100-200cm Percentage of clay
9	**Percentage of silt content in the soil**	The percentage of silt content in the soil is an important soil input, the silt layers are included by depth as given below 0 – 5 cm Percentage of silt 5-15 cm Percentage of silt 15-30cm Percentage of silt 30-60cm Percentage of silt 60-100cm Percentage of silt 100-200cm Percentage of silt
10	**Percentage of sand content in the soil**	The percentage of sand content in the soil is an important soil input, the silt layers are included by depth as given below 0 – 5 cm Percentage of sand 5-15 cm Percentage of sand 15-30cm Percentage of sand 30-60cm Percentage of sand 60-100cm Percentage of sand 100-200cm Percentage of sand
11	**Coarse fragment content**	The coarse fragment content of the soil is the non-soil particles typically including pebbles, gravels, and rocks that are larger than the soil particles. The presence of coarse fragments in the soil influences the soil structure.
12	**Moist soil albedo**	Soil albedo is a proportional measurement of solar radiation that is reflected by the soil. Moist soil albedo refers to the albedo of the soil when it is moist or has some level of near-field capacity moisture content. The soil albedo value ranges from 0 to 1, Where 1 represents the surface is totally reflective, and 0 represents a completely absorptive surface. The albedo of moist soil can vary based on several factors including moisture content, soil type, soil composition, and vegetation cover. To compute the moist soil albedo formula used Wang et al. (2005) Albedo = 0.1807 + 0.1019*exp(−3.53*θ33) ……. (Eq.4) θ33 is given in variable 5

13	**USLE equation soil erodibility**	The Universal Soil Loss Equation (USLE) is an empirical equation widely used to predict soil erosion. The key factor (K) is soil erodibility proposed by Williams (1995). The K factor is the probability of soil erosion based on its properties. The unit of K is expressed as tons per acre per hour per inch of rainfall (tons/acre/hr/inch) or the unit depends on the formulation of the equation being used. The USLE is computed as proposed by Williams (1995). $USLE=E_S \times E_{C-T} \times E_{OC} \times E_{HS}$ …….... (Eq.5) $E_S=0.2+0.3\times\exp[-0.256\times S\times(1-T\div100)]$ …… (Eq.5.1) $E_{C-T}=[T/(C+T)]^{0.3}$…….……..... (Eq.5.2) $E_{OC}=1-(0.25\times OC/\ (OC+\ \exp\ [\ (0.72-2.95\times OC)]$ ……... (Eq.5.3) $E_{HS}=1-\{0.7\times(1-S\div100)$ $\div[(1-S\div100)+\exp(-5.51+22.9\times(1-S\div100)]$……. (Eq.5.4) OC = Organic carbon, EOC = represents the effectiveness of cover, EHS=Erosion Hazard Score, S = Percentage of sand, C = Percentage of clay, T = Percentage of silt

(Source of variables are drawn from SWAT manual documentation)

4.3.4 Model Calibration and Validation

The Sequential Uncertainty Fitting (SUFI-2) is used for the calibration and validation of hydrological models in the SWAT Calibration and Uncertainty Program (SWAT-CUP vs. 5.1.2). SWAT-CUP is specifically designed to handle the uncertainty associated with model parameters during the calibration process. Calibration involves adjusting the model parameters to make the simulated outputs match the observed data as closely as possible. The calibration and validation were performed using the fitted parameters taken from SWAT-CUP (Tables 4.2, and 4.5). The natural period calibrated from 1991 to 2002 and 2003 to 2008 was validated. The impact period 2009–2015 is calibrated, and 2016–2020 data is used for model validation. The model's performance was finally evaluated by R^2 and Nash-Sutcliffe simulation efficiency (NSE) (Hosseini et al. 2020).

$$R^2 = \left\{ \frac{\sum_{i=1}^{n} (O_i - O_{\text{ave}}) \times (P_i - P_{\text{ave}})}{\left[\sum_{i=1}^{n} (O_i - O_{\text{ave}})^2\right]^{0.5} \times \left[\sum_{i=1}^{n} (P_i - P_{\text{ave}})^2\right]^{0.5}} \right\}^2 \text{ ..... (Eq.6)}$$

$$ENS = 1 - \frac{\sum_{i=1}^{n} (O_i - P_i)^2}{\sum_{i=1}^{n} (O_i - \bar{O}_i)^2} \text{ ..... (Eq.7)}$$

Where

Oi is the observed value, Pi is the predicted value, N is the total sample, Õi is the observed mean value, O_{ave}, and P_{ave} are the observed and predicted average.

4.4 Masanjor Dam and Tilpara Barage

The Masanjor Dam, also known as the Canada Dam, is situated on the Mayurakshi River basin in the Dumka district of Jharkhand, India (Plate 5,7). Commissioned in 1955, it spans the river basin, strategically placed after the drainage of the plateau region. The dam measures approximately 2170 feet in length and stands 155 feet high from its base, with an overflow section extending 225.60 meters. Designed with a discharge capacity of 4.446 m^3/s and a storage capacity of 617,000,000 cubic meters, the dam maintains a full reservoir level of 121.34 meters and a flood level of 122.56 meters. Apart from its impressive engineering, the Masanjor Dam serves a pivotal role in water storage and irrigation. Creating a reservoir, it stores water for diverse purposes, releasing it during the crop-growing season to support crucial agricultural activities in the region.

The Tilpara Barrage was constructed to harness the water resources of the Mayurakshi River for irrigation and other agricultural activities (Plate 6,8). The barrage was commissioned in 1949 on the Mayurakshi River. The length of the barrage is 309 meters. The barrage plays a crucial role in facilitating irrigation by controlling the flow of water and ensuring a regulated and reliable water supply for agricultural purposes.

Plate 5: Masanjor Dam at up-stream

Plate 6: Tilpara Barage at mid-stream

Plate 7: Mayurakshi at the upper course (at Vijay pur, Dumka)

Plate 8: Mayurakshi at the middle course (at Lalia pur, Birbhum)

Plate 9: Mayurakshi at the middle course (at Sundarpur pur, Murshidabad)

Plate 10: Tributary Bhurbhuri in summer season

4.5 The seasonal stream flow patterns

The basin's stream flow is illustrated using the observed discharge data from 1991 to 2020. The peak runoff in the basin occurs during the rainy season, characterized by rainfall from the southwest monsoon between June and September, known as India's monsoon season. Analysis of the rainfall seasonal pattern, as computed by RSI (Chapter 1, Table 1.5), indicates RSI index categories of, “very equitable” and "equitable in definite weather," contributing to monsoonal discharge peaks in June, July, August, and September over the study period (Fig. 4.1). Apart from the rainy season, the watershed experiences low discharge. The basin relays its 80% of its discharge from monsoonal rainfall, thus the monsoonal discharge pattern is considered to evaluate the seasonal variation of discharge. In the overall seasonal flow, the Mann Kendall statistic showed that the computed p-value was >0.05 of the significance level alpha (0.05). It indicates that in a monsoonal discharge pattern, there is no specific positive or negative trend in the discharge, the trend varies from time to time. Sen’s slope (-0.76 mm/year) showed a very gentle decreasing monsoonal discharge pattern over the study period of the basin (Table 4.2, Fig. 4.1). Over the study period, pick seasonal discharge recorded 66.45 m^3/s in 1992, followed by 66.45, 61.12, 61.11 m^3/s in 2008,2004,2015 respectively. The low seasonal discharge of the basin recorded 22.13 m^3/s followed by 25.35, 26.67, and 28.45 m^3/s in the years 2010, 2018, and 1998 respectively (Table 4.3, Fig. 4.1).

Table 4.2: Trend of seasonal discharge

Station	Normalized Test (Z)	Kendall's tau	p-value	Sen's slope (Q value mm/year)
Basin	0.017	0.004	>0.05	-0.762

Table 4.3: Monsoonal discharge pattern

Years	Discharge of monsoon (m^3/s)	Years	Discharge of monsoon (m3/s)
1991	28.45	2006	45.46
1992	66.45	2007	62.59
1993	27.00	2008	66.45
1994	50.08	2009	57.09
1995	54.58	2010	25.35
1996	30.75	2011	65.53
1997	45.00	2012	22.13
1998	50.08	2013	29.10
1999	47.82	2014	33.54
2000	44.46	2015	61.11
2001	38.62	2016	55.04
2002	55.76	2017	36.28
2003	59.95	2018	26.70
2004	61.12	2019	31.66
2005	54.58	2020	56.49

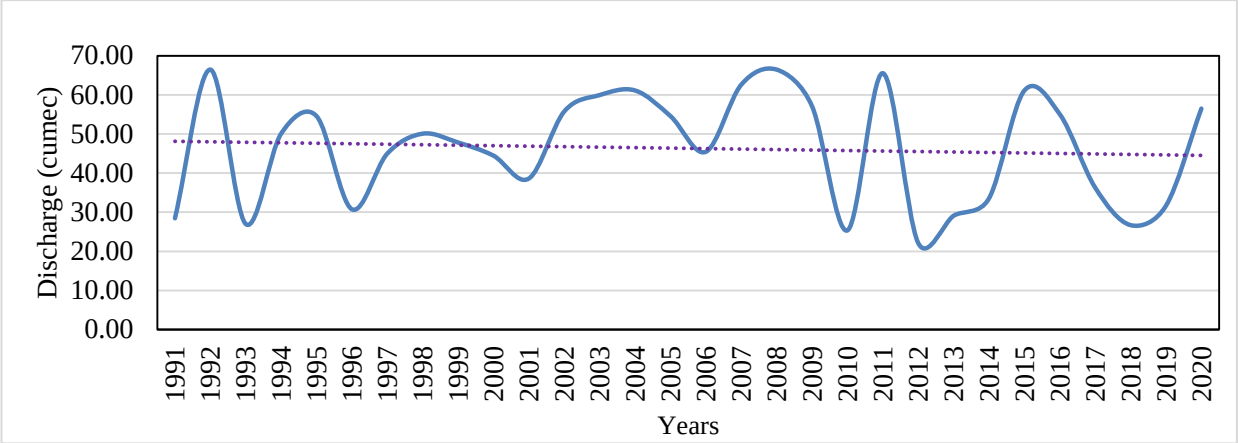

Fig. 4.1: Seasonal trend

4.6 Runoff Simulation of Natural Period

The study period was divided into two segments using change point analysis, as detailed in Chapter 1 (Reference: Change point of annual rainfall 2.4.5). The response of basin runoff relies on various factors, including soil characteristics, slope, LULC, elevation, and climatic elements such as rainfall, humidity, temperature, and wind speed. To simulate runoff during the natural period from 1991 to 2008, parameters outlined in Table 2 were considered, including their best-fitted values. The range of values, both maximum and minimum, for the basin, was also highlighted. For the natural period moisture condition II curve number, baseflow recession constant, delay time for aquaria recharge, the threshold water level in the shallow aquifer for base flow, soil evaporation compensation coefficient, and surface runoff lag coefficient were determined as 0.0275, 0.44375, 169.125, 0.5125, 0.98375, and 0.798437, respectively. The parameters for the runoff simulation model are summarized in Table 2. The model was calibrated and validated using observed discharge data for the natural period. Calibration involved using 13 years (1991–2003) of simulated and observed data, while the next 5 years were used for validation. The validated model for the natural period demonstrated satisfactory performance with R^2 (Fig. 3) and NES values of 0.83 and 0.80, respectively.

Table 4.4: Fitted parameter (1991-2008)

Parameter Name	Fitted Value	Min value	Max value
CN2.mgt	0.0275	-0.2	0.2
ALPHA_BF.gw	0.44375	0	1
GW_DELAY.gw	169.125	30	450
GWQMN.gw	0.5125	0	2
GW_REVAP.gw	0.18875	0	0.2
ESCO.hru	0.98375	0.8	1
CH_N2.rte	0.219375	0	0.3
CH_K2.rte	66.71875	5	130
ALPHA_BNK.rte	0.51875	0	1
SOL_AWC(..).sol	0.19375	-0.2	0.4
SOL_K(..).sol	0.61	-0.8	0.8
SOL_BD(..).sol	0.510625	-0.5	0.6
SFTMP.bsn	-0.5625	-5	5
SURLAG.bsn	0.798437	0.05	24

Table 4.5: Description of fitted parameter

Parameter Name	Description
CN2.mgt	Moisture condition II curve number
ALPHA_BF.gw	Baseflow Recession constant
GW_DELAY.gw	Delay time for aquaria recharge
GWQMN.gw	The threshold water level in the shallow aquifer for base flow
GW_REVAP.gw	Revamp coefficient
ESCO.hru	Soil evaporation compensation coefficient
CH_N2.rte	Manni's "n" value for the main channel
CH_K2.rte	Effective hydraulic conductivity in the main channel
ALPHA_BNK.rte	Baseflow alpha factors for bank storage
SOL_AWC.sol	Available water capacity of the soil layer
SOL_K.sol	Saturated hydraulic conductivity
_SOL_BD.sol	Soil moist bulk density
SFTMP.bsn	Mean air temperature at which precipitation is equally likely to be rain as snow/ freezing rain (^{0}C)
SURLAG.bsn	Surface runoff lag coefficient

Source: -SWAT theoretical documentation

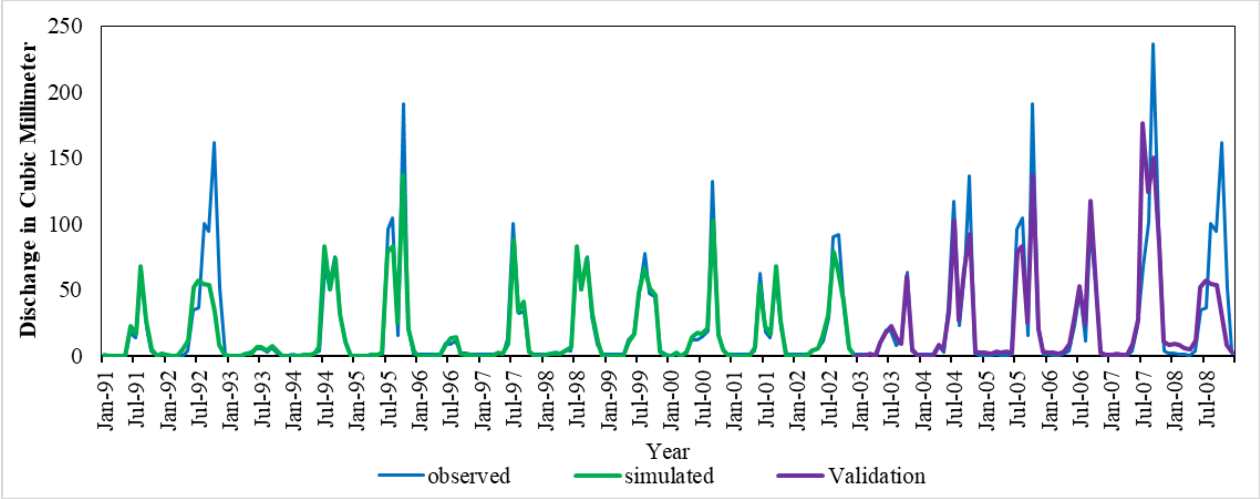

Fig. 4.2: Calibration and validation (1991-2008)

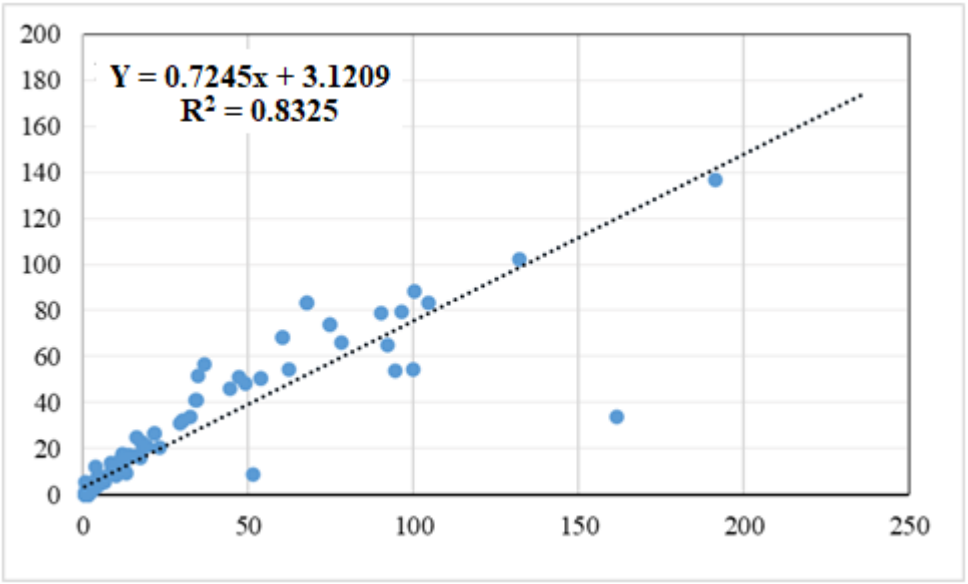

Fig. 4.3: R^2 of Natural Period

Table 4.6: Calibrated and validated discharge (m^3/s) from 1991 to 2008

Date	observed	simulated	Date	observed	simulated
Jan-1991	0.50	0.59	Jan-2000	0.91	0.00
Feb-1991	0.50	0.06	Feb-2000	1.29	2.44
Mar-1991	0.52	0.00	Mar-2000	0.90	0.34
Apr-1991	0.51	0.42	Apr-2000	3.55	2.51
May-1991	0.55	0.02	May-2000	12.38	14.56
Jun-1991	17.84	22.38	Jun-2000	11.91	17.62
Jul-1991	13.77	16.82	Jul-2000	14.50	16.59
Aug-1991	60.47	68.41	Aug-2000	19.26	21.10
Sep-1991	21.73	26.73	Sep-2000	132.16	102.40
Oct-1991	3.63	4.80	Oct-2000	17.29	15.99
Nov-1991	0.76	0.27	Nov-2000	4.20	5.03
Dec-1991	2.01	1.69	Dec-2000	1.28	0.01
Jan-1992	0.92	1.00	Jan-2001	1.07	0.00
Feb-1992	0.52	0.00	Feb-2001	0.99	0.00
Mar-1992	0.51	0.24	Mar-2001	0.97	0.04
Apr-1992	0.80	5.32	Apr-2001	0.99	0.00
May-1992	3.68	11.98	May-2001	3.98	6.55
Jun-1992	34.71	51.85	Jun-2001	62.38	54.15
Jul-1992	36.61	56.87	Jul-2001	17.84	22.38
Aug-1992	100.10	54.26	Aug-2001	13.77	16.82
Sep-1992	94.39	53.73	Sep-2001	60.47	68.41
Oct-1992	161.64	33.61	Oct-2001	21.73	26.73
Nov-1992	51.39	8.57	Nov-2001	1.66	0.22
Dec-1992	0.52	0.95	Dec-2001	1.24	0.01
Jan-1993	0.54	0.07	Jan-2002	1.06	0.06
Feb-1993	0.52	0.01	Feb-2002	1.30	0.07
Mar-1993	0.87	0.40	Mar-2002	1.27	0.04
Apr-1993	1.83	1.83	Apr-2002	4.83	4.04
May-1993	2.73	1.83	May-2002	5.72	6.15
Jun-1993	25.27	6.96	Jun-2002	11.28	15.11
Jul-1993	30.19	6.63	Jul-2002	29.27	31.04
Aug-1993	20.99	4.28	Aug-2002	90.36	79.04
Sep-1993	35.02	7.55	Sep-2002	92.14	64.98
Oct-1993	2.50	3.24	Oct-2002	34.53	41.13
Nov-1993	0.64	0.01	Nov-2002	6.32	5.62
Dec-1993	0.54	0.49	Dec-2002	1.62	0.18
Jan-1994	0.96	0.35	Jan-2003	1.37	0.01
Feb-1994	0.90	0.05	Feb-2003	1.34	0.29
Mar-1994	0.87	0.59	Mar-2003	1.64	1.76
Apr-1994	0.86	0.79	Apr-2003	1.34	0.00

May-1994	2.23	1.97	May-2003	11.69	10.23
Jun-1994	3.95	6.80	Jun-2003	19.96	17.38
Jul-1994	67.66	83.41	Jul-2003	19.25	23.17
Aug-1994	53.81	50.28	Aug-2003	7.95	13.18
Sep-1994	74.90	74.11	Sep-2003	12.79	9.18
Oct-1994	30.17	31.98	Oct-2003	63.31	60.15
Nov-1994	8.66	11.26	Nov-2003	4.27	5.11
Dec-1994	0.72	0.29	Dec-2003	1.68	0.20
Jan-1995	0.67	0.00	Jan-2004	1.52	0.55
Feb-1995	0.67	0.24	Feb-2004	1.31	0.09
Mar-1995	0.69	0.26	Mar-2004	1.32	0.25
Apr-1995	1.05	0.69	Apr-2004	8.20	8.27
May-1995	1.23	0.82	May-2004	2.78	5.25
Jun-1995	1.17	2.98	Jun-2004	36.91	32.66
Jul-1995	96.49	79.41	Jul-2004	117.43	102.20
Aug-1995	104.62	83.36	Aug-2004	23.36	26.66
Sep-1995	16.02	24.90	Sep-2004	66.78	66.10
Oct-1995	191.25	137.00	Oct-2004	136.40	92.61
Nov-1995	23.02	20.40	Nov-2004	2.33	3.29
Dec-1995	1.61	3.09	Dec-2004	0.91	2.51
Jan-1996	1.18	0.04	Jan-2005	0.69	2.47
Feb-1996	1.11	0.02	Feb-2005	0.58	2.07
Mar-1996	1.08	0.01	Mar-2005	1.55	3.40
Apr-1996	1.47	0.51	Apr-2005	0.75	2.51
May-1996	1.29	0.43	May-2005	0.73	3.08
Jun-1996	10.01	7.92	Jun-2005	1.17	2.98
Jul-1996	38.12	13.76	Jul-2005	96.49	79.41
Aug-1996	40.21	13.97	Aug-2005	104.62	83.36
Sep-1996	34.69	1.86	Sep-2005	16.02	24.90
Oct-1996	2.01	1.13	Oct-2005	191.25	137.00
Nov-1996	1.67	1.10	Nov-2005	23.02	20.40
Dec-1996	1.17	0.00	Dec-2005	1.61	3.09
Jan-1997	1.11	0.00	Jan-2006	1.09	2.72
Feb-1997	1.10	0.00	Feb-2006	0.89	2.42
Mar-1997	1.26	0.08	Mar-2006	0.76	2.01
Apr-1997	1.98	2.44	Apr-2006	1.93	3.68
May-1997	1.94	1.59	May-2006	3.46	9.67
Jun-1997	13.20	9.21	Jun-2006	23.37	32.21
Jul-1997	100.35	88.13	Jul-2006	50.23	52.77
Aug-1997	32.50	33.84	Aug-2006	11.25	23.44
Sep-1997	33.93	41.26	Sep-2006	96.98	117.30
Oct-1997	2.90	3.51	Oct-2006	55.40	51.33
Nov-1997	1.20	0.01	Nov-2006	1.42	2.30

Dec-1997	1.07	0.48	Dec-2006	0.87	0.93
Jan-1998	1.31	0.85	Jan-2007	0.65	0.78
Feb-1998	1.71	1.49	Feb-2007	0.86	1.84
Mar-1998	1.69	3.01	Mar-2007	0.66	0.83
Apr-1998	1.80	2.00	Apr-2007	0.76	0.58
May-1998	4.67	4.49	May-2007	3.70	9.53
Jun-1998	3.95	6.80	Jun-2007	54.23	27.90
Jul-1998	67.66	83.41	Jul-2007	75.34	176.20
Aug-1998	53.81	50.28	Aug-2007	70.34	124.00
Sep-1998	74.90	74.11	Sep-2007	61.25	150.50
Oct-1998	30.17	31.98	Oct-2007	65.29	84.03
Nov-1998	8.66	11.26	Nov-2007	4.22	11.23
Dec-1998	1.65	0.39	Dec-2007	2.12	8.08
Jan-1999	1.34	0.00	Jan-2008	1.80	9.48
Feb-1999	1.24	0.00	Feb-2008	1.18	8.29
Mar-1999	1.18	0.00	Mar-2008	0.97	5.80
Apr-1999	1.17	0.00	Apr-2008	0.80	5.32
May-1999	12.19	11.26	May-2008	3.68	11.98
Jun-1999	16.70	17.04	Jun-2008	34.71	51.85
Jul-1999	49.20	48.30	Jul-2008	36.61	56.87
Aug-1999	78.12	66.06	Aug-2008	100.10	54.26
Sep-1999	47.24	50.90	Sep-2008	94.39	53.73
Oct-1999	44.62	46.02	Oct-2008	161.64	33.61
Nov-1999	3.64	3.41	Nov-2008	51.39	8.57
Dec-1999	1.12	0.01	Dec-2008	3.46	2.49

4.7 Runoff Simulation of Impact Period

The runoff of the impact period is simulated and outlined in Table 6. The simulation of the impact period was run by the best-fit parameters of base flow recession constant, the delay time for aquaria recharge, the threshold water level in the shallow aquifer for base flow, revamp coefficient, soil evaporation compensation coefficient, base flow alpha factors for bank storage, and surface runoff lag coefficients of 0.50, 156.00, 0.18, 0.50, and 2.45, respectively (Table 4.7). All the parameters for the runoff simulation model of the impact period are summarized in Table 5, and the parameter description is outlined in Table 3. The model was calibrated and validated using observed discharge data for 2009–2020. Calibration involved using 8 years (2009–2020) of simulated and observed data, while the next 4

years were used for validation. The validated model for the impact period demonstrated satisfactory performance with R^2 (Fig. 4.5) and NES values of 0.89 and 0.87, respectively.

Table 4.7: Fitted parameter (2009-2020)

Parameter Name	Fitted Value	Min value	Max value
CN2.mgt	0.00	-0.20	0.20
ALPHA_BF.gw	0.50	0.00	1.00
GW_DELAY.gw	156.00	30.00	450.00
GWQMN.gw	0.60	0.00	2.00
GW_REVAP.gw	0.18	0.00	0.20
ESCO.hru	0.94	0.80	1.00
CH_N2.rte	0.15	0.00	0.30
CH_K2.rte	42.50	5.00	130.00
ALPHA_BNK.rte	0.50	0.00	1.00
SOL_AWC(..).sol	0.22	-0.20	0.40
SOL_K(..).sol	-0.32	-0.80	0.80
SOL_BD(..).sol	0.49	-0.50	0.60
SFTMP.bsn	-2.00	-5.00	5.00
SURLAG.bsn	2.45	0.05	24.00

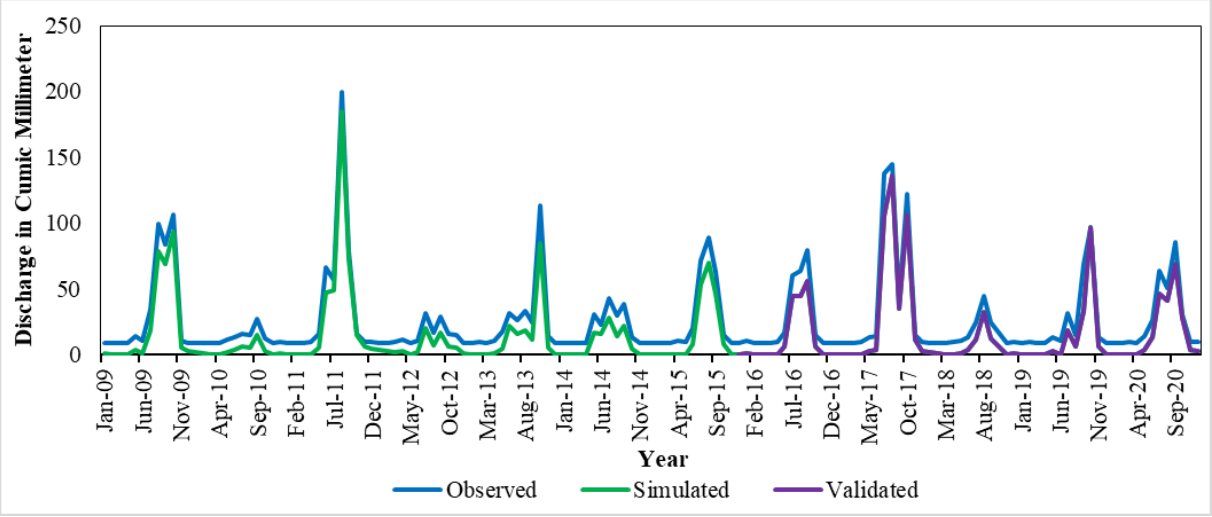

Fig. 4.4: Calibration and validation (2009-2020)

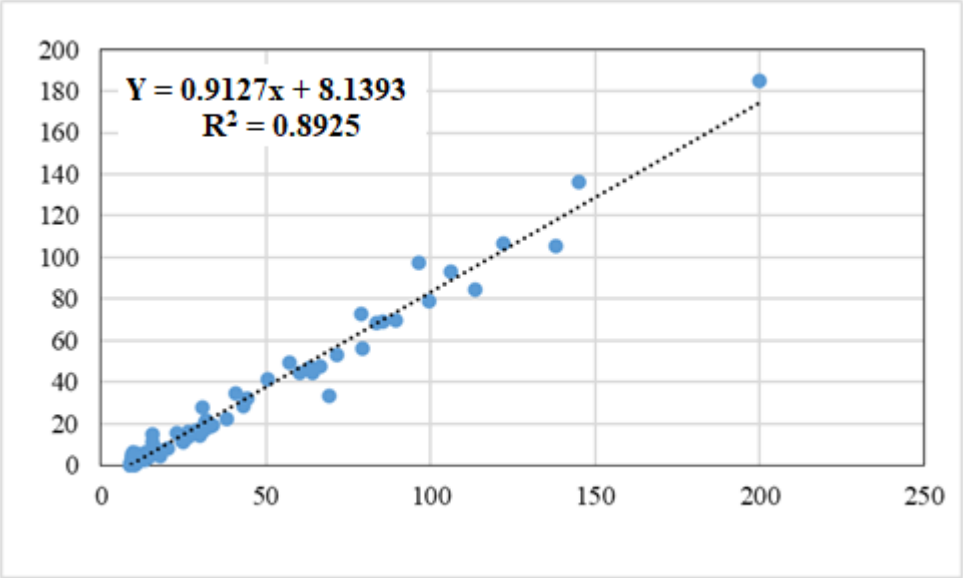

Fig. 4.5: R^2 of Impact Period

Table 4.8: Calibrated and validated discharge (m^3/s) from 2009 to 2020

Date	Observed	Simulated	Date	Observed	Simulated
Jan-2009	9.12	1.06	Jan-2015	9.12	0.06
Feb-2009	9.08	0.37	Feb-2015	9.04	0.00
Mar-2009	9.29	0.11	Mar-2015	9.16	0.04
Apr-2009	9.20	0.04	Apr-2015	10.52	0.56
May-2009	13.86	3.79	May-2015	10.04	0.29
Jun-2009	11.00	1.25	Jun-2015	20.12	8.23
Jul-2009	33.85	18.92	Jul-2015	71.69	53.27
Aug-2009	99.72	78.88	Aug-2015	89.38	69.76
Sep-2009	83.79	68.70	Sep-2015	63.26	46.70
Oct-2009	106.05	93.23	Oct-2015	15.53	8.12
Nov-2009	10.79	5.30	Nov-2015	9.27	0.28
Dec-2009	9.39	3.01	Dec-2015	9.10	0.16
Jan-2010	9.23	2.18	Jan-2016	11.04	1.38
Feb-2010	9.17	1.42	Feb-2016	9.26	0.06
Mar-2010	9.12	0.50	Mar-2016	9.04	0.00
Apr-2010	9.09	0.02	Apr-2016	9.03	0.00
May-2010	11.37	1.89	May-2016	9.78	0.09
Jun-2010	25.37	4.01	Jun-2016	16.49	6.11
Jul-2010	20.34	6.65	Jul-2016	60.12	44.36
Aug-2010	28.36	5.65	Aug-2016	64.04	44.64
Sep-2010	27.35	15.27	Sep-2016	79.49	56.30
Oct-2010	12.45	3.28	Oct-2016	14.86	6.19

Nov-2010	9.30	0.61	Nov-2016	9.35	0.60
Dec-2010	10.01	1.17	Dec-2016	9.14	0.26
Jan-2011	9.09	0.21	Jan-2017	9.06	0.02
Feb-2011	9.04	0.00	Feb-2017	9.03	0.00
Mar-2011	9.05	0.00	Mar-2017	9.08	0.00
Apr-2011	10.15	0.59	Apr-2017	9.79	0.33
May-2011	16.16	5.83	May-2017	13.19	2.79
Jun-2011	66.68	47.70	Jun-2017	29.30	4.13
Jul-2011	57.27	49.44	Jul-2017	39.35	105.30
Aug-2011	59.21	185.10	Aug-2017	35.69	136.20
Sep-2011	78.96	72.72	Sep-2017	40.81	34.82
Oct-2011	15.62	14.69	Oct-2017	22.00	106.40
Nov-2011	9.87	6.28	Nov-2017	15.44	11.29
Dec-2011	9.54	4.99	Dec-2017	9.62	3.31
Jan-2012	9.38	3.93	Jan-2018	9.36	2.42
Feb-2012	9.27	2.78	Feb-2018	9.25	1.59
Mar-2012	9.50	1.86	Mar-2018	9.20	0.72
Apr-2012	11.72	3.08	Apr-2018	9.80	0.60
May-2012	9.17	0.49	May-2018	10.47	1.52
Jun-2012	11.11	2.19	Jun-2018	13.08	3.70
Jul-2012	31.56	20.44	Jul-2018	24.44	11.74
Aug-2012	17.09	7.59	Aug-2018	44.50	32.16
Sep-2012	28.74	16.69	Sep-2018	24.77	12.46
Oct-2012	16.37	6.75	Oct-2018	16.68	6.20
Nov-2012	15.15	5.54	Nov-2018	9.40	0.70
Dec-2012	9.22	0.88	Dec-2018	9.93	0.92
Jan-2013	9.09	0.42	Jan-2019	9.11	0.13
Feb-2013	9.54	0.37	Feb-2019	9.54	0.29
Mar-2013	9.04	0.00	Mar-2019	9.08	0.00
Apr-2013	10.40	0.98	Apr-2019	9.44	0.12
May-2013	17.92	4.44	May-2019	13.08	3.14
Jun-2013	32.00	21.74	Jun-2019	10.37	0.71
Jul-2013	26.49	15.89	Jul-2019	31.60	18.90
Aug-2013	33.13	18.62	Aug-2019	15.44	6.40
Sep-2013	24.78	11.34	Sep-2019	69.24	33.48
Oct-2013	113.70	84.30	Oct-2019	96.34	97.25
Nov-2013	14.15	5.87	Nov-2019	13.68	5.99
Dec-2013	9.30	0.68	Dec-2019	9.25	0.56
Jan-2014	9.11	0.21	Jan-2020	9.10	0.14
Feb-2014	9.46	0.20	Feb-2020	9.15	0.02
Mar-2014	9.05	0.00	Mar-2020	9.60	0.10
Apr-2014	9.16	0.00	Apr-2020	9.34	0.01
May-2014	30.94	16.90	May-2020	14.51	3.96

Jun-2014	22.82	15.65	Jun-2020	26.29	13.74
Jul-2014	43.13	28.52	Jul-2020	63.76	46.49
Aug-2014	30.02	14.43	Aug-2020	50.45	41.20
Sep-2014	38.20	21.96	Sep-2020	85.44	69.29
Oct-2014	13.51	4.66	Oct-2020	30.82	27.75
Nov-2014	9.27	0.36	Nov-2020	9.98	4.22
Dec-2014	9.10	0.17	Dec-2020	9.52	3.15

4.8 Concluding Remarks

The basin experiences its peak runoff during the monsoonal rainy season. Before conducting an assessment of the impact of climate and land use land cover, the study period was segmented into two phases: the natural period (1991–2008) i.e before the step change point of rainfall, and the impact period (2009–2020) i.e after the change point of rainfall. The natural period refers to the time period where there is a homogeneity or no significant increase or decrease in rainfall, After the step change in rainfall (2008) it followed a decreasing pattern that is considered an impact period. Calibration for the natural period spanned 13 years (1991–2003), with the subsequent 5 years allocated for validation, resulting in a satisfactory model performance indicated by R^2 and NES values of 0.83 and 0.80, respectively. Calibration for the impact period covered 8 years (2009–2020), and the subsequent 4 years were designated for validation. The validated model for the impact period exhibited commendable performance, with R^2 and NES values of 0.89 and 0.87, respectively. Consequently, the model was developed to assess the influence of climate change and land use land cover change in the basin.

References

Biemans, H., Haddeland, I., Kabat, P., Ludwig, F., Hutjes, R., Heinke, J., Gerten, D. (2011). Impact of reservoirs on river discharge and irrigation water supply during the 20th century. *Water Resour. Res.*, 47.87-95

Hosseini, S. H., & Khaleghi, M. R. (2020). Application of SWAT model and SWAT-CUP software in simulation and analysis of sediment uncertainty in arid and semi-arid watersheds (case study: The Zoshk–Abardeh watershed). *Modeling Earth Systems and Environment, 6*(4), 2003-2013.

Huang, M., Zhang, L., & Gallichand, J. (2003). Runoff responses to afforestation in a watershed of the Loess Plateau, China. *Hydrol. Process, 17*, 2599–2609. doi:doi:10.1002/hyp.1281

Hulme, M., Barrow, E., Arnell, N., Harrison, P., Johns, T., & Downing, E. (1999). Relative impacts of human-induced climate change and natural climate variability. *Nature, 397*, 688–691.

Huntington, T. (2006). Evidence for intensification of the global water cycle: Review and synthesis. *J. Hydrol, 319*, 83–95.

Li, Z., Liu, W., Zhang, X., & Zheng, F. (2009). Impacts of land use change and climate variability on hydrology in an agricultural catchment on the Loess Plateau of China. *J. Hydrol, 377*, 35–42. doi:doi:10.1016/j.jhydrol.2009.08.007

Liang, K., Liu, C., Liu, X., & Song, X. (2013). Impacts of climate variability and human activity on streamflow decrease in a sediment concentrated region in the Middle Yellow River. *Stochastic Environmental Research and Risk Assessment, 27*(7), 741-1749. doi:doi: 10.1007/s00477-013-0713-2

Milly, P., Dunne, K., & Vecchia, A. (2005). Global pattern of trends in streamflow and water availability in a changing climate. *Nature, 438*, 347–350.

Pachauri, R., Allen, M., Barros, V., Broome, J., Cramer, W., Christ, R., Dasgupta, P. (2014). Contribution of Working Groups I, II and III to the fifth assessment report of the Intergovernmental Panel on Climate Change.In Climate Change 2014. *Synthesis Report; IPCC: Geneva, Switzerland*, ISBN 9291691437.

Yang, H., D Yang, Lei, Z., & F. Sun. (2008). New analytical derivation of the mean annual water-energy balance equation. *Water Resour. Res, 44*,78-85, doi:doi:10.1029/2007WR006135.

Zhang, J., Wang, G., Pagano, T., Jin, J., Liu, C., He, R., & Li, Y. (2013). Using hydrologic simulation to explore the impacts of climate change on runoff in the Huaihe River Basin of China. *J Hydrol Eng, 18*, 1393–1399.

Chapter 5: THE ROLE OF CLIMATE CHANGE AND LAND USE LAND COVER CHANGE ON STREAMFLOW

5.1 Objective and Chapter Organization

In this chapter, the impact of climate and LULC on basin runoff is investigated, and the methodology to separate the climatic impact and LULC on runoff is outlined in Section 5.3.1. The result and discussion of the simulation of *TQ* at the natural period are briefly explained in Section 5.4.1., and the detailed simulation of *TQ* at the impact period and simulated climatic impact is given in Section 5.4.2, while Section 5.4.3 deals with a comparative analysis of rainfall and *TQ*. Section 5.4.4 deals with the impact of LULC and climate on runoff and the concluding remarks outlined in Section 5.5.

5.2 Introduction

The hydrological process is significantly influenced by climatic parameters and Land Use/Land Cover. Numerous studies have delved into the hydrological changes resulting from shifts in LULC patterns (Guo et al., 2008; Dong et al., 2015; Li et al., 2017). Alterations in LULC have a profound impact on groundwater recharge, evapotranspiration, interception, and soil moisture content (Zhang et al., 2001; Woldesenbet et al., 2017; Gashaw et al., 2018). The distribution pattern of LULC in a watershed plays a pivotal role in governing surface runoff and sediment yield (Kumar, 2018). The changing LULC, primarily driven by population growth and ecological footprint stress, is a central concern. Studies concur that an increase in vegetation cover and agricultural land significantly amplifies runoff in the watershed (Bosch and Hewlett, 1982; Fang et al., 2013; Teklay et al., 2018).

The influence of climate change and escalating human demands for ecological footprints intensify hydrological extremes, impacting food, water resource management, and land management vulnerabilities (Bronstert et al., 2002). Understanding the interplay between LULC and climate is pivotal in hydrological studies, particularly in simulating rainfall-runoff models (Joorabian et al., 2017).

Runoff characteristics are not solely influenced by rainfall and LULC but also hinge on watershed features such as slope, soil, wind speed, and solar radiation (Dong et al., 2015; Yang et al., 2017).

Currently, climate change exerts a profound influence on LULC alterations, and this impact manifests in surface runoff, making it a crucial focus for hydrologists (Jia et al., 2010; Nosetto et al., 2010). In the nexus between climate change and LULC, climate emerges as the primary driver for changes in surface runoff and groundwater recharge, while the influence of LULC, encompassing factors like population growth and economic development, is relatively indirect (Liu and Andersson, 2004). The widely adopted SWAT model is employed globally to assess the impact of climate and LULC on surface runoff alterations (Kiros et al., 2015; Gyamfi et al., 2016; Himanshu et al., 2017; Shooshtaria, 2017; Yan, 2017). This chapter aims to evaluate runoff changes and determine the relative influence of LULC and climate on the Mayurakshi river basin's runoff.

5.3 Database and Methodology

The database used in this chapter is briefly outlined in the section, and the details of the methodology are given below:

5.3.1 Methodology

The impact of climate change and land use and land cover change on runoff is assessed by quantifying the surface runoff of the watershed (SUR_Q), lateral flow (LAT_Q), and groundwater (GW_Q) contribution to the stream. The average contribution of SUR_Q, LAT_Q, and GW_Q is taken to evaluate the impact of climate and LULC over the study period of the Mayurakshi river basin. During the study period, time series rainfall change was accounted for in 2008 by the statistics of the Pettitt test, Buishand U test, and Standard Normal Homogeneity test (reference: Chapter 2, Section 2.3.6). Thus, the whole study period is broken into two segments based on the step change in rainfall. Based on the step change result, the study period from 1991 to 2008 is considered the natural period, whereas from 2009 to 2020 is the interference period. The method to separate climatic and human activity (LULC change) is used by many of the studies known as the hydrological model (Devia et

al., 2015; Xu et al., 1999). The model is modified and mathematically presented in Eqs. 2, 3, 4, and 6. The impact accounted for the combinations of the different scenarios or simulations. The first simulation represents the natural period, assuming the climatic variables were in an equitable condition, where climate and LULC are applied to the natural or reference period to simulate the model. The second simulation presents the impact period, where the climate and LULC are applied to the interference or impact period. To quantify the climatic impact, we applied the LULC of the natural period and the climate of the impact period to simulate the model.

Currently, climate change exerts a profound influence on LULC alterations, and this impact manifests in surface runoff, making it a crucial focus for hydrologists (Jia et al., 2010; Nosetto et al., 2010). In the nexus between climate change and LULC, climate emerges as the primary driver for changes in surface runoff and groundwater recharge, while the influence of LULC, encompassing factors like population growth and economic development, is relatively indirect (Liu and Andersson, 2004). The widely adopted SWAT model is employed globally to assess the impact of climate and LULC on surface runoff alterations (Kiros et al., 2015; Gyamfi et al., 2016; Himanshu et al., 2017; Shooshtaria, 2017; Yan, 2017). This chapter aims to evaluate runoff changes and determine the relative influence of LULC and climate on the Mayurakshi river basin's runoff. The hydrological model is used by the researchers to simulate and separate climatic and LULC impact by Ma et al, 2009; Fan et al, 2010 equations are given below.

$$T_Q = \Sigma SUR_Q + LAT_Q + GW_Q \,/\, 3 \quad \text{(Eq.1)}$$

$$TD_Q = S_{2IPQ} - S_{1NPQ} \quad \text{(Eq.2)}$$

$$CL_{IQ} = S_{3IPCLQ} - S_{1NPQ} \quad \text{(Eq.3)}$$

$$LULC_{IQ} = S_{2IPQ} - S_{3IPCL} \quad \text{(Eq.4)}$$

Where,

SUR_Q is the surface flow of the watershed, LAT_Q is the lateral flow contribution to the stream flow of the basin, and GW_Q is the groundwater contribution to the stream. T_Q is the total average contribution of SUR_Q, LAT_Q, and GW_Q to the runoff of the watershed. TD_Q is the total difference in runoff, S_{2IPQ} is the simulated average runoff contribution of the basin during the impact period, S_{1NPQ} is the simulated average runoff contribution of the basin during the natural period, CL_{IQ} is the impact of climate change stream flow, $LULC_{\mathrm{IQ}}$ is the impact of LULC on stream flow. S_{3IPCL} is the runoff simulation with reference to climate change, where the LULC is constantly referred to natural period (S_{1NPQ}), and the climatic components are referred to impact period (S_{2IPQ}).(**Unite of measurement is MASF/y : M: Monthly, A: Average, SF: Stream Flow, /y: per year)

5.4 Results and Discussion

5.4.1 Simulation of T_Q at Natural Period

The simulation of T_Q including SUR_Q, LAT_Q, and GW_Q for the S_{1NPQ} is 137.85 mm. In the total natural period, a greater amount of T_Q was in the year 2007 (T_Q 410.51 mm) with a greater contribution of SUR_Q and GW_Q amounting to 361.18mm and 42.63mm. The minimum T_Q occupied in 1993 (T_Q 19.63 mm) and a low T_Q contribution in the watershed prevailed at the beginning of the natural period (1991 - 1995) (Table 5.1 and Fig. 5.1). At the timeframe of 1996 - 2008 (except 2003) a greater amount of T_Q was recorded. The SUR_Q is an important contributor to the T_Q of the watershed. The contribution of SUR_Q was low at the beginning of the natural period after 1995 the SUR_Q contribution to T_Q notably increased and the trend of T_Q followed a positive increasing trend during the S_{1NPQ} of the watershed (Fig. 5.1).

Table 5.1: Runoff simulation (MASF/y) of S_{1NPQ}

Year	SUR_Q (mm)	LAT_Q (mm)	GW_Q (mm)	T_Q
1991	49.85	2.93	1.5	54.28
1992	19.25	1.3	2.13	22.68
1993	15.27	1.9	2.46	19.63

1994	43.59	1.8	4.05	49.44
1995	42.98	2.63	2.64	48.25
1996	112.59	1.87	2.13	116.59
1997	110.45	4.25	4.21	118.91
1998	157.88	5.42	3.58	166.88
1999	141.85	5.09	1.5	148.44
2000	114.99	4.89	3.9	123.78
2001	106.73	5.09	10.3	122.12
2002	145.48	4.85	2.7	153.03
2003	79.06	4.05	5.61	88.72
2004	209.22	5.58	8.61	223.41
2005	222.1	5.13	16.83	244.06
2006	172.44	5.16	11.7	189.3
2007	361.18	6.7	42.63	410.51
2008	146.1	5.01	30.09	181.2
S_{INPQ}				137.85

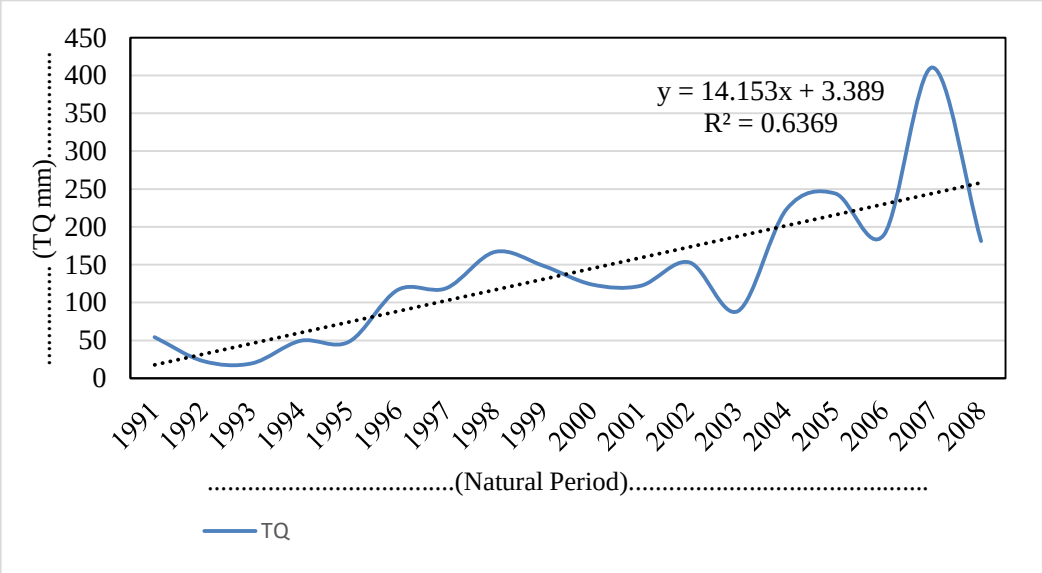

Fig. 5.1: T_Q Natural period

5.4.2 Simulation of T_Q at Impact Period and Simulated Climatic Impact

The T_Q of the basin during the S_{2IPQ} (2009 to 2020) was recorded at 127.65mm, and the maximum and minimum T_Q documented in 2011 and 2010 were 283.34mm, and 44.9mm respectively. Contrary to S_{1NPQ} during the period of S_{2IPQ} the T_Q showed a downward trend (Fig. 5.2). The prime contributor SUR_Q to T_Q

accounted maximum in 2011 (259.24mm) and a minimum in 2010 (26.34) mirroring the T_Q of 2011 and 2010 (Table 5.2). During the S_{2IPQ} maximum contribution of LAT_Q and GW_Q recorded 0.90mm and 23.20mm similar to the SUR_Q contribution to the T_Q of the watershed. The impact of climatic components (S_{3IPCL}) is evaluated where the contribution of T_Q on the watershed was 68.19. The individual contributions of SUR_Q, LAT_Q, and GW_Q were 65.35mm, 0.59mm, and 2.24mm respectively (Table 5.2).

Table 5.2: Runoff simulation (MASF/y) of S_{2IPQ}

Year	SUR_Q (mm)	LAT_Q (mm)	GW_Q (mm)	T_Q
2009	199.7	0.52	21.01	221.23
2010	26.34	0.71	17.85	44.9
2011	259.24	0.9	23.2	283.34
2012	43.56	0.74	15.15	59.45
2013	118.17	0.75	2.44	121.36
2014	77.49	0.82	0.13	78.44
2015	126.66	0.76	0.01	127.43
2016	111.94	0.76	0	112.7
2017	151.23	0.91	11.51	163.65
2018	46.88	0.78	7.15	54.81
2019	122.68	0.68	0.69	124.05
2020	136.07	0.9	3.5	140.47
S_{2IPQ}				127.65
	Simulated climatic impact			
	SUR_Q (mm)	LAT_Q (mm)	GW_Q (mm)	T_Q
S_{3IPCLQ}	65.35	0.59	2.24	68.19

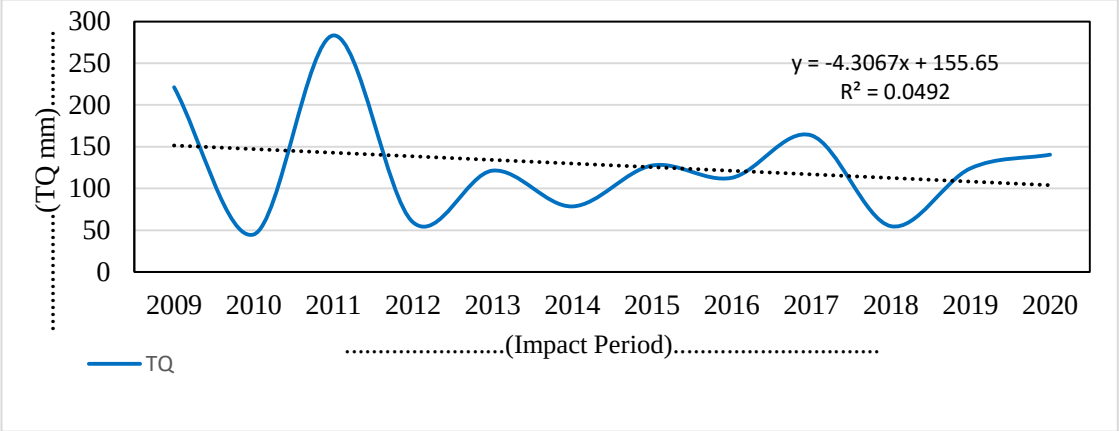

Fig. 5.2: *TQ* Impact period

5.4.3 Comparative analysis of rainfall and T_Q

The rainfall and T_Q of the basin are juxtaposed to analyze the correlation between rainfall patterns and basin runoff patterns. The rainfall and T_Q of the basin are paired to make a comparison of them. In the 30 years of rainfall, the maximum and minimum rainfall were 2128.99 mm and 770.00 mm with an average of 1376.57 mm ± 313.93 mm. The T_Q time series over the study period accounted for an average of 133.77 mm ± 80.08 mm with a maximum and minimum of 410.51 mm and 19.63 mm (Table 5.3). To compute the overall rainfall variation of the basin regarding the natural period and impact period, the computed p-value was >0.05 at the significance level of alpha α= 0.05 for the natural period as well as for the impact period. It indicates that in both time frames, there is no specific positive or negative trend in the rainfall series and the trend varies from time to time. In the natural period Kendall's Z (1.28) and normalized Kendall's tau (0.28) indicate an increasing rainfall trend, whereas in the impact period Kendall's Z (-0.3) and normalized Kendall's tau (-0.07) show a decreasing rainfall trend (Table 5.4 and Fig. 5.3). The T_Q variation is computed for the natural period and the impact period. In the natural period Kendall's Z was 2.25 and normalized Kendall's tau was 0.48 with a computed p-value of 0.02 and the Sen's slope is 10.69 mm/year indicating an increasing T_Q trend. In the impact period, Kendall's Z -0.18 and normalized Kendall's tau -0.05 with the Sen's slope of -1.39 mm/year indicate a decreasing trend of T_Q during the impact period (Table 5.4 and Fig. 5.3).

Table 5.3: Rainfall and T_Q (mm)

Year	Rainfall (mm)	T_Q (mm)	Year	Rainfall (mm)	T_Q (mm)
1991	1315.13	54.28	2006	1560.45	189.3
1992	1011.55	22.68	2007	1599.02	410.51
1993	1427.14	19.63	2008	1506.70	181.2
1994	1158.26	49.44	2009	1221.79	221.23
1995	1627.27	48.25	2010	1031.07	44.9
1996	1361.95	116.59	2011	871.40	283.34
1997	1598.04	118.91	2012	770.00	59.45
1998	1667.80	166.88	2013	1481.17	121.36
1999	2128.99	148.44	2014	1209.49	78.44
2000	2097.20	123.78	2015	1634.67	127.43
2001	1409.63	122.12	2016	1167.39	112.7
2002	1576.80	153.03	2017	1446.96	163.65
2003	1253.11	88.72	2018	843.58	54.81
2004	1553.25	223.41	2019	1096.57	124.05
2005	1255.88	244.06	2020	1414.79	140.47

Table 5.4: Trend and Sen's slope estimation

Station	**Normalized Test (Z)**	**Kendall's tau**	**p-value (Two-tailed)**	**Sen's slope (Q value)**
Rainfall Natural Period	1.28	0.28	0.20	43.47
Rainfall Impact Period	-0.3	-0.07	0.76	-5.87
T_Q Natural Period	2.25	0.48	0.02	10.69
T_Q Impact Period	-0.18	-0.05	0.85	-1.39

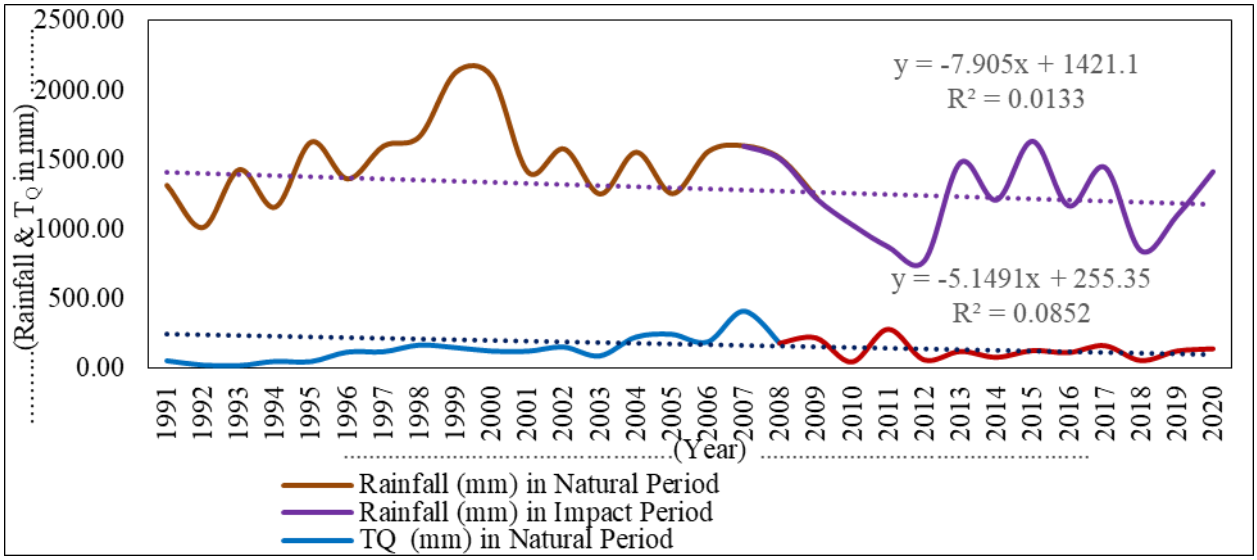

Fig. 5.3: Long-term rainfall and T_Q status

5.4.4 Role of LULC and Climate on stream flow

Climate variability, especially rainfall, and LULC, are the most effective factors that directly control stream flow. In the 30 years of the time period, the basin was characterized by a dynamic nature of climatic variability and LULC change as well. In terms of climatic variability, at the very beginning of the 1st decade of the study period (1991–2000), the basin received low rainfall, and in 1997, the basin started to receive a continuous upward graph of rainfall, with a peak rainfall of 2128.99 mm. Overall, the first decade of the study period accounted for an upward rainfall trend (reference: Chapter 2 Section 2.4.4). After that, the rainfall decreased continuously followed by a downward trend in the 2nd and 3rd decades (Table 2.3). The step change in rainfall accounted for by the statistics of Pettitt's test, the SNHT test, and Buishand's test confirmed that the rainfall change point of the basin was in 2008 (reference: Chapter 2 section 2.4.5). The LULC of the basin at the beginning of the agricultural land was 49.15% and it continuously increased to 70.61% in 2020, the built-up area also increased over the study period, in 1991 it was 2.15% and increased to 5.44% at the end of the study period (2020). The increase of built-up area is one of the accelerating agents of the runoff pattern for the basin. The step change of rainfall and the continuous decreasing of rainfall seconded by Sen's slope (Q) is -12.21 mm/year indicating a decreasing trend of rainfall over the study period

(reference: Chapter 2 Table 2.3, Fig. 2.6). The comparison between the rainfall pattern and the streamflow is paired to examine the rainfall and streamflow characteristics over the study period (Table 5.3). Both followed a decreasing trend (Fig. 5.3). The magnitude of the rainfall trend in the natural period was (Sen's slope) Q = 43.47 mm/year and it was followed by a negative magnitude of Q = -5.87 mm/year in the impact period, mirroring the decreasing trend as well as rainfall.The T_Q pattern computed in natural period Q = 10.69 mm/year and impact period was Q = -1.39 mm/year. The computed result of the decreasing pattern of rainfall reflected the decreasing nature of $T_{Q.}$ Thus it indicates the negative role of climate on stream flow in this basin. In the S_{1NPQ} the surface runoff was 125.06 mm and percolation to the shallow aquifer and recharge to the deep aquifer was 8.88 mm and 0.44 mm respectively. The the contribution of return flow to the stream flow was 8.35 mm (Fig.5.4). The runoff decreased in the impact period (S_{2IMPQ}) accounted for 118.33 mm and percolation to the shallow aquifer and recharge to deep aquifer accounted 6.43 mm and 0.32 mm, with the contribution of return flow to the stream was 6.10 mm (Fig. 5.5). The contribution of $SUR_{Q,}$ LAT_Q, GW_Q is presenting the overall scenario of the streamflow pattern of the basin, that has been taken by computing the monthly average stream flow/ year (MASF/y) of T_Q scenario. Thus the scenarios of S_{1NPQ}, S_{2IPQ}, S_{3IPCLQ} presents the basic stream flow scenarios of the basin under different conditions of climatic variability and LULC dynamics over the 30-year study period. The impact of $LULC_{IQ}$ on streamflow, 59.47 mm indicating the positive role of LULC on streamflow acceleration of the basin. On the other hand, the impact of climate change (CL_{IQ}) is -69.69 mm, the negative value (-) of CL_{IQ} indicating the role of climate on the stream flow pattern is negative, thus when LULC plays a positive role on the stream flow, at the same time the climatic phenomena playing negative influence on streamflow acceleration of the basin. This scenario of the climatic and LULC impact on streamflow was also the same during the periods of S_{1NPQ}, S_{2IPQ}, thus the computed TD_Q was -10.19 mm which indicates a decrease in stream flow over the study period. Also the impact of $LULC_{IQ}$ and CL_{IQ} values to be found at 59.47 mm and -69.66 mm, where the difference between $LULC_{IQ}$ and CL_{IQ} is -10.19 mm mirroring the same difference of TD_Q (Table 5.5).

Thus it is proved that the streamflow decreased by the rate of 10.19 mm where the negative (-) CL_{IQ} assigned the responsibility of streamflow reduction is caused by the climate change on the basin, and the same is found in the step change of climate at the section of Chapter 2 section 2.4.4. & 2.2.5. The computed value of Eq 2,3,4 revealed that climatic factors played a negative role in reducing streamflow of the basin at the rate of 10.19 mm/year with the same evidence has been proved in Chapter 2 Section 2.4.4. & 2.2.5 and Chapter 5 Table 5.5.

Table 5.5: Impact assessment of Climate and LULC on runoff scenario

Simulated and measured impact	Values (mm/year)
S_{1NPQ}	137.85
S_{2IPQ}	127.66
S_{3IPCL}	68.19
TD_Q	-10.19
CL_{IQ}	-69.66
$LULC_{IQ}$	59.47

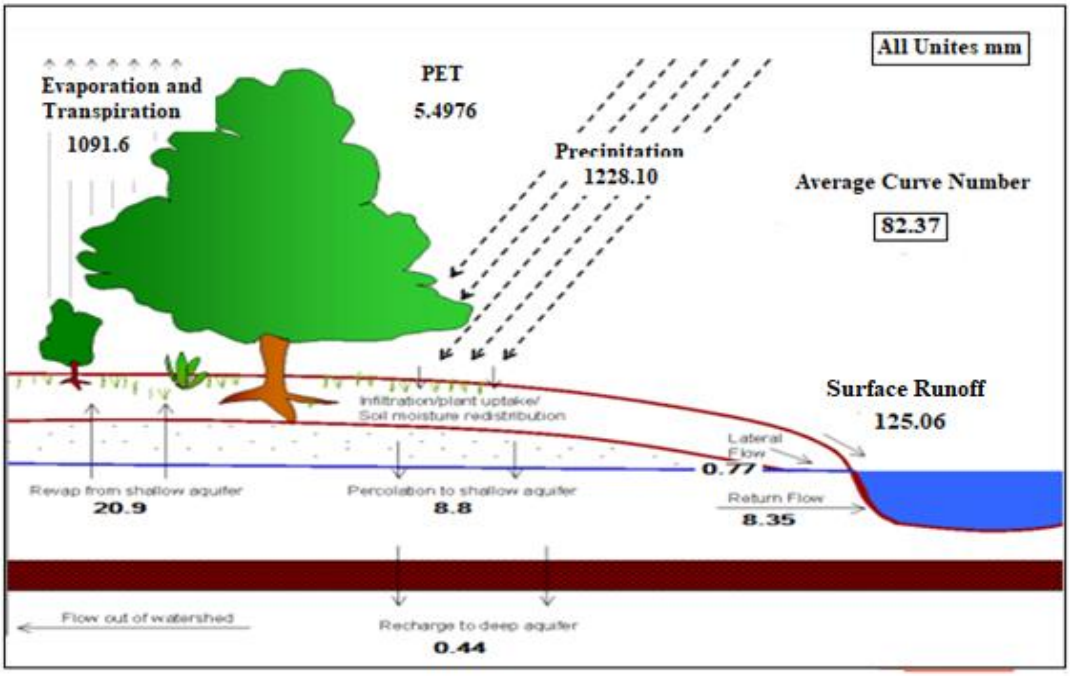

Fig. 5.4: Simulated SUR_Q of S_{1NPQ}

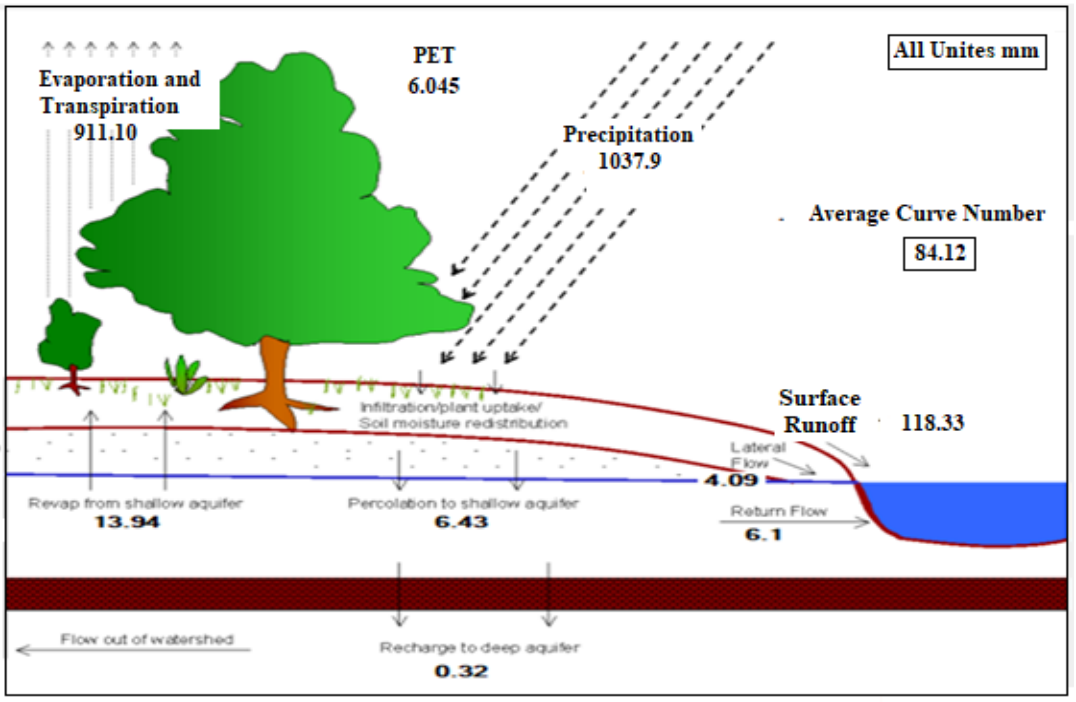

Fig. 5.5: Simulated SUR_Q of S_{2IPQ}

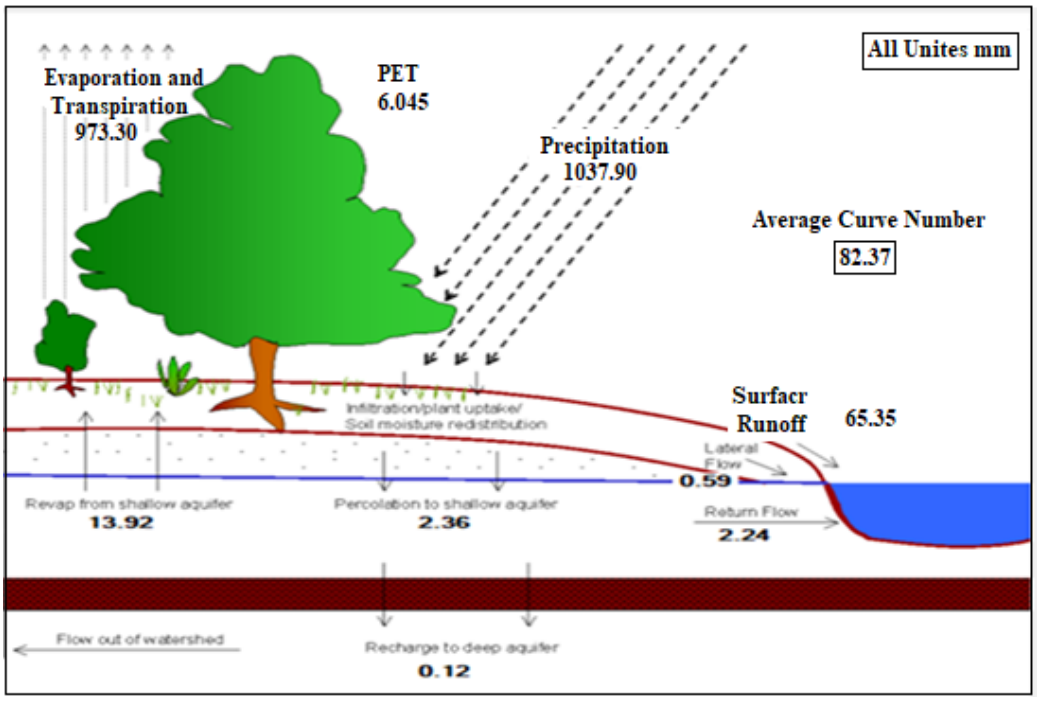

Fig. 5.6: Simulated SUR_Q of S_{3IPCLQ}

5.5 Concluding remarks

In the natural period, T_Q was 137.85 mm and in the impact period, T_Q reduced and counted as 127.66 mm. There is a linear relation that has been found in rainfall pattern and T_Q, with a decreasing trend of rainfall the streamflow pattern was also recorded. The surface runoff in the natural period was 125.06 mm and in the impact period, it was 118.33 mm. The simulated outcome due to the climatic interference revealed that with the constant LULC and the change in climatic factors, the surface runoff accounted for 65.35 mm. The total change of -10.19 mm of T_Q indicates a decrease in stream flow over the study period.

References

Bosch, J., & Hewlett, J. (1982). A review of catchment experiments to determine the effect of vegetation changes on water yield and evapotranspiration. *J. Hydrol., 55(1-4)*, 3-23.

Bronstert, A., Niehoff, D., & Bürger, G. (2002). Effects of climate and land-use change on storm runoff generation: present knowledge and modeling capabilities. *Hydrol. Process*, *16*(2), 509-529.

Devia, G., Ganasri, B., & Dwarakish, G. (2015). Review on hydrological models. *Aquat. Procedia, 4*, 1001–1007.

Dong, L., Xiong, L., Lall, U., & Wang, J. (2015). The effects of land use change and precipitation change on direct runoff in Wei River watershed, China. *Water Sci. Technol, 71*(2), 289–295.

Dong, L., Xiong, L., Lall, U., & Wang, J. (2015). The effects of land use change and precipitation change on direct runoff in Wei River watershed, China. *Water Sci. Technol, 71*(2), 289–295.

Fang, X., Ren, L., Li, Q., Zhu, Q., Shi, P., & Zhu,, Y. (2013). Hydrologic response to land use and land cover changes within the context of catchment-scale spatial information. *J. Hydrol. Eng, 18*, 1539–1548.

Gashaw, T., Tulu, T., Argaw, M., & Worqlul, A. (2018). Modeling the hydrological impacts of land use/land cover changes in the Andassa watershed, Blue Nile Basin, Ethiopia. *Sci.Total Environ, 619-620*, 1394–1408.

Guo,, H., Hu, Q., & Jiang, T. (2008). Annual and seasonal streamflow responses to climate and land-cover changes in the Poyang Lake basin, China. *j.Hydrol, 355*(1-14), 106-122.

Gyamfi, C., Ndambuki, J., & Salim, R. (2016). Application of SWAT model to the Olifants Basin: calibration, validation, and under uncertainty analysis. Journal of Water Resource and Protection. *Journal of Water Resource and Protection*, 397–410. doi:doi:10.4236/jwarp.2016.83033.

Himanshu, S., Pandey, A., & Shrestha, P. (2017). Application of SWAT in an Indian river basin for modeling runoff, sediment and water balance. *Environmental Earth Sciences, 76*(3). 20-33,https://doi::10.1007/s12665-016-6316-8.

Jain, S., Tyagi, J., & Singh, V. (2010). Simulation of runoff and sediment yield for a Himalayan watershed using SWAT model. *Journal ofWater Resource&Protection, 2*(3), 267–281.

Joorabian, S., Kamran, S., Gholamalifard, M., Azari, M., Serrano-Notivoli, R., & Ignacio López-Moreno, J. (2017). Impacts of future land cover and climate change on the water balance in northern Iran. *Hydrological Sciences Journal*, 2150-3435.

Kiros, G., Shetty, A., & Nandagiri, L. (2015). Performance evaluation of SWAT model for land use and land cover changes under different climatic condition: A Review. *Hydrology Current Research*(6), 216. https//doi::10.4172/2157-7587.1000216.

Kumar, H. (2018). Investigation of impacts of land use/land cover change on water availability of Tons River Basin, Madhya Pradesh, India. *Modeling Earth Systems and Environment*. https//:doi:10.1007/s40808-018-0425-1.

Li, G., Zhang, F., Jing, Y., Liu, Y., & Sun, G. (2017). Response of evapotranspiration to changes land use and land cover and climate in China during 2001–2013. *Sci. Total Environ.*, 256–265.

Liu, X., & Andersson, C. (2004). Assessing the impact of temporal dynamics on land-use change modeling. *Computers Environment & Urban Systems, 28*(1-12), 107–124.

Ma, X., Xu, J., Luo, Y., Prasad Aggarwal, S., & Li, J. (2009). Response of hydrological processes to land-cover and climate changes in Kejie watershed, south-west China. *Hydrol. Process, 23*, 1179–1191. https//doi: 10.1002/hyp.7233

Nosetto,, M., Jobbagy,, E., & Paruelo, J. (2010). Land-use change and water losses: the case of grassland afforestation across a soil textural gradient in central Argentina. *Global Change Biology, 11*(7), 1101–1117.

Shooshtaria, S. (2017). Impacts of future land cover and climate change on the water balance in northern Iran. *Hydrological Sciences jOURNAL*. https//doi:10.1080/02626667.2017.1403028.

Woldesenbet, T., Elagib, N., Ribbe, L., & Heinrich, J. (2017). Hydrological responses to land use/cover changes in the source region of the Upper Blue Nile Basin, Ethiopia. *Sci.Total Environ., 575*, 724–741.

Xu, C. (1999). Climate change and hydrologic models: A review of existing gaps and recent research developments. *Water Resour. Manag, 13*, 369–382.

Yang, L., Feng,, Q., Yin, Z., Wen, X., Si, J., Li,, C., & Deo, R. (2017). Identifying separate impacts of climate and land use/cover change on hydrological processes in upper stream of Heihe River, Northwest China. *Hydrol. Process, 31*(5), 1100–1112.

Zhang, L., Dawes, W., & Walker, G. (2001). Response of mean annual evapotranspiration to vegetation changes at catchment scale. *Water Resour. Res., 37*(3), 701–708.

Chapter 6: FINDINGS AND CONCLUSION

6.1 Major findings

6.1.1 Major findings of the first objective

The Mayurakshi river basin is one of the important agricultural belts of eastern India. The work was conducted to understand the dynamic change of climate and LULC of the basin and its impact on the streamflow. In the last 30 years' study period, the maximum and minimum rainfall was 1717.37 mm,1188.65 mm, and the long-term average rainfall was recorded as 1420.67mm. The characteristics of rainfall in the 1st decade (1991-2000) varied, with a maximum of 1885.86 mm, a minimum of 1252.81 mm, and an average of 1511.96 ± 160.48 mm. In the 1st decade, a continuous upward trend of rainfall was recorded. In the 2nd decade (2001-2010), the mean annual rainfall was 14346.22 ± 170.52 mm. In the 3rd decade (2011-2020), the basin received low rainfall (1380.41 mm) as compared to the 1st and 2nd decades. High rainfall concentrations were recorded in the northeastern part of the upper and middle basin areas in the whole study period. The basin experienced a decreasing trend of rainfall, the magnitude of the trend presented by Sen's slope shows the rainfall of the basin has a strong negative Sen's slope value which is -10.37 mm/year, implying that there is a decreasing or downward trend in rainfall. In the 30 years, the rainfall pattern change point was detected in 2008 and was confirmed by the step change point detection. In the long term period, the average values of various climatic components were recorded as follows: temperature at 32.23 ± 0.63 ^{0}C, wind speed at 1.9 ± 0.12 m/s, solar radiation at 90.40 ± 5.00 W/m², and humidity at 63.44 ± 5.48 %. During the study period, the basin experienced a maximum temperature of 38.80 ℃. From 1991 to 2020, temperature showed a slightly increasing trend, supported by a significant Kendall's P value of 0.05, with a normalized test (Z) value of 1.89 and a Kendall's tau of 0.24. The temperature has shown an increase by 0.03 ^{0}C during the study period. The temporal characteristics of the basin rainfall was found to be extremely wet during 16.67% of the years; moderately dry, slightly wet, and slightly dry in 16.67% of the sampled years, while 6.67% of the years were recorded as extremely dry. The rainfall was forecasted

through ARIMA model which indicated an average rainfall condition of 1303.38 ± 19.99 mm/year, with the very least variability (CV 1.53) and a decreasing trend for the next 10 years over the basin.

6.1.2 Major findings of the second objective

In 1991 (1st study period) agricultural land was covered by 49.15% and vegetation cover covered 20.45% area. During the second study period, vegetation expanded by 3.10% (1150.09 km²), mainly due to the contribution from agricultural land and bare land 472.64 km² and 272.02 km², respectively. However, agricultural areas saw a 4.30% decrease, shrinking by 2429.75 km², while bare land and built-up areas grew from 1325.68 km² to 1079.09 km² and from 42.82 km² to 182.67 km², respectively. In the third study period, there were increases in water bodies (183.02 km² or 0.49%), vegetation (2368.95 km² or 2.80%), agricultural land (2469.73 km² or 0.80%), and built-up areas (162.37 km² or 0.33%). During the fourth study period, the agricultural land expanded from 2,529.54 km² to 3,214.12 km². Within this agriculture land use and land cover category, vegetation contributed for 583.62 km², while bare land contributed 516.03 km². During the final study period (2014–2020), bare land continued to decline significantly, reflecting the trends observed in the fourth study period. In contrast, agricultural land increased by 6.36% (3988.62 km²). The LULC transition to agriculture class included 47.34 km² from water, 501.33 km² from vegetation, 451.41 km² from bare land, and 90.63 km² from built-up areas. Additionally, the transition to built-up areas included 1.64 km² from water, 17.82 km² from vegetation, 30.51 km² from bare land, and 29.43 km² from agricultural land. In 2020 the dominant LULC of the basin was agricultural land covered by 70.60% of the area and the second dominant LULC class was vegetation, covered by 15.57% of the area. The built-up area experienced a continuously increasing trend, in 1991 it was 2.15% and in 2020 increased by 5.44%. The water class was covered by 5.28% in 1991 but has decreased by 3.20% of the area in 2020. The future LULC of 2032 indicates that agriculture will remain the dominant land cover class, spanning 3520.92 km^2. It will be followed by vegetation class covering an area of 788.18 km^2 and built-up areas occupying 272.40 km^2. The trend of the seasonal discharge pattern

was -0.762 mm/year indicating a gentle rate of decreasing pattern in monsoonal discharge.

6.1.3 Major findings of the third objective

The hydrological parameters determined for the simulation of runoff in the natural period were moisture condition II the curve number, base-flow recession constant, delay time for aquifer recharge, threshold water level in the shallow aquifer for base flow, soil evaporation compensation coefficient, and surface runoff lag coefficient. The values are 0.0275, 0.44375, 169.125, 0.5125, 0.98375, and 0.798437, respectively. The validated model for the natural period demonstrated satisfactory performance with R^2 and NES values of 0.83 and 0.80, respectively.

The values for various hydrological parameters in impact period were determined as follows: the curve number for natural period moisture condition II was 0.0275, the base-flow recession constant was 0.44375, the delay time for aquaria recharge was 169.125, the threshold water level in the shallow aquifer for base-flow was 0.5125, the soil evaporation compensation coefficient was 0.98375, and the surface runoff lag coefficient was 0.798437. The validated model for the impact period showed satisfactory performance, with R^2 and NES values of 0.89 and 0.87, respectively.

6.1.4 Major findings of the fourth objective

The simulated T_Q of S_{1NPQ} was 137.85 mm. From 1996 to 2008 a greater amount of T_Q was recorded. The simulated S_{2IPQ} *was* 127.65 mm. During the period of $S_{2IPQ,}$ the T_Q showed a downward trend. The impact of the decreasing trend of rainfall caused a decrease in T_Q on the watershed was 68.19 mm. The computed TD_Q between the natural period and the impact period was -10.19 mm/year which indicates a decrease in stream flow over the study period. The CL_{IQ} of -69.66 indicated the negative impact of climate on streamflow.

6.2 Conclusion

This study focused on a detailed examination of rainfall variability and LULC changes over time, aiming to investigate the runoff conditions in the basin and the influence of both climatic and LULC change impacts on basin runoff. The study identified a significant change in both precipitation patterns and LULC. The pattern of precipitation step change occurred in 2008 after the breaking point, when rainfall followed a decreasing trend (-12.21 mm/year). The runoff model employed in this analysis shed light on the fact that, based on the watershed's characteristics (slope, soil, aspect, elevation, climate, and LULC) and the role of relative control between climate and LULC on stream flow, climate played a negative influence on runoff conditions. The findings revealed that at the constant LULC, changes in climate will be caused by the runoff yield of 68.19 mm. Consequently, the runoff decreased by -10.19 mm/year from the natural period to the interference period, exhibiting a negative relative contribution of climatic factors to the stream flow of the basin. The observed reduction in runoff is attributed to climate change, specifically the declining nature of precipitation. This comprehensive study on the interplay of climate and LULC holds significant value for effective basin management and environmental conservation. As the study area is one of the important agricultural belts of eastern India, it is very important to know the impact of climate and LULC on stream flow patterns, which is a very precious aspect of land management and sustainable water resource management. The local communities, planners, and government can leverage this knowledge to integrate sustainable practices into their planning efforts and ensure responsible basin management for the future.

6.3 Recommendations

The study area suffers from the problems of environment-degrading livelihood, environment-degrading agricultural practices, loss of ecological balance, climate change, rampant forest cover loss, and loss of water bodies. Restoration of environmental balance and the sustainable development of "Life on Earth" is the main aim of Sustainable Development Goals (SDGs). The Central government and state government should work hand in hand in the study area to restore the SDGs

such as ecological imbalance and check the rampant deforestation in the study area while maintaining and encouraging a sustainable livelihood. "Ministry of Environment, Forest and Climate Change, (MoEFCC)" can provide some necessary solutions towards the problem through its schemes and policies like "National Afforestation Programme, (NAP)", "Green India Mission (GIM)", " Compensatory Afforestation Fund Management and Planning Authority, (CAMPA)", and " National Mission for a Green India (GIM) ". Further "National Agroforestry Policy (NAP)" under the "Ministry of Agriculture and Farmers' Welfare, (MoAFW)", "Mahatma Gandhi National Rural Employment Guarantee Act, (MGNREGA)" under the "Mahatma Gandhi National Rural Employment Guarantee Act, (MGNREGA)", and "National Forest Policy, (NFP) 1988", under the "Ministry of Food and Agriculture, (MFA)" are aimed to protect the environment. The above-mentioned policies could be implemented to protect the SDGs, like Sustainable Development Goal 12 (SDG 12), to ensure sustainable consumption and production patterns to achieve the sustainable management and efficient use of natural resources, Sustainable Development Goal 13 (SDG 13), to limit and adapt to climate change, to "Take urgent action to combat climate change and its impacts", and Sustainable Development Goal 15 (SDG 15), to "Protect, restore and promote the sustainable use of terrestrial and forest ecosystems, combat desertification, and halt and reverse land degradation and halt biodiversity loss" of the study area which are at risk.

The study revealed that water bodies have been reduced from time to time. To restore the water bodies and sustainable agriculture towards attaining Sustainable Development Goal 2 (SDG 2, to "End hunger, achieve food security and improved nutrition and promote sustainable agriculture"), the government should take steps toward the wetland management program through the "Wetlands Management for Biodiversity and Climate Protection Project, (WMBCPP)" and "National Plan for Conservation of Aquatic Ecosystems (NPCA)" under the "Ministry of Environment, Forest and Climate Change (MoEFCC)", " National Water Mission (NWM)", and " Atal Bhujal Yojana, (Atal Jal)", under the "Ministry of Jal Shakti", and "Pradhan Mantri Krishi Sinchai Yojana, (PMKSY)" under the "Ministry of Agriculture and Farmers' Welfare" these will be helpful towards attaining the respective goals if

implemented. The environmental awareness programs like environmental education and awareness, conservation of natural resources programs for the local people could play an important role in restoring sustainable management of water, soil, forests, and the environment.

6.4 Strength and weakness

The obtained daily gridded rainfall data has a high spatial resolution of 0.25 × 0.25 degrees. The rainfall data from 1991 to 2020 for the study area was obtained from the source of India Meteorological Department (IMD) Pune was quite satisfactory. The LULC classification incorporated with Random Forest Machine Learning algorithm that achieved a satisfactory level of classification accuracy. The SWAT model is configured with important thirteen soil parameters of: Hydrological Soil Group, Maximum rooting depth, Depth of soil from the surface to the bottom of the layer, Moist bulk density, Availability of the water in the soil layer, Saturated hydraulic conductivity, Organic carbon content in the soil, Percentage of clay content in the soil, Percentage of silt content in the soil, Percentage of sand content in the soil, Coarse fragment content, Moist soil albedo, USLE equation soil erodibility. These are calculated by using various equations (Table 1, Chapter 4) to achieve a high accuracy level. The calibration and validation of the model achieved a satisfactory level on R^2 (The validated model for the natural period demonstrated satisfactory performance with R^2 and NES values of 0.83 and 0.80, respectively and the validated model for the impact period showed satisfactory performance, with R^2 and NES values of 0.89 and 0.87, respectively). Thus the SWAT model attempted a satisfactory level of strength towards the evaluation of climatic and LULC impact on streamflow.

To get a better accuracy level in rainfall analysis higher resolution data is expected, the data used for weather parameters had a spatial resolution of 0.25 × 0.25 degrees, where the rainfall analysis could be achieved at a micro level of precision with high-resolution data for all weather parameters like rainfall, temperature, humidity, solar radiation, and wind speed. The LULC is mapped by 30m × 30m spatial resolution. The centinal data provides 10m × 10m spatial resolution, it is a

satisfactory level of special resolution for LULC mapping and LULC change analysis. The centinal data is not available from 1991 and is also not available for every region. Where LULC change detection algorithm should be performed on the same spatial resolution. Due to the unavailability of centinal database, the LULC was mapped with 30m × 30m of spatial resolution. The soil input parameters are computed in 250m of spatial resolution where to achieve a greater accuracy level much more accuracy is expected.

BIO-DATA

Name: David Durjoy Lal Soren

Father's Name: Bishnu Lal Soren

Date of Birth: 29/01/1991

Sex: Male

Marital Status: Unmarred

Address: Vill-Titpur, PO+PS- Bamangola, Dist- Malda (WB)

Contact: 9647346113

Email: devid.dls.king@gmail.com

Educational Qualification

Qualification	Year	Board
M.P	2007	West Bengal Board of Secondary Education
H.S	2009	West Bengal Board Higher of Secondary Education
B.A	2012	University of Gour Banga
M.A	2014	University of Gour Banga
B.ED	2015	University of Gour Banga
NET	2017	West Bengal College Service Commission
SET	2017	University of Grant Commission

Paper publications (Related to the thesis topic)

1. Land/use land /cover dynamics and future scenario of Mayurakshi river basin by random forest and CA–Markov model (2024), International Journal of Environmental Science and Technology, https://doi.org/10.1007/s13762-024-06006-8

2. A Comprehensive Review on the Impact of Climate Change on Streamflow: Current Status and Perspectives, River Conservation and Water Resource Management, (2023), ISSN 2198-3550, https://doi.org/101007/978-981-99-2605-3.

Seminars attended

1. Two Days International Seminar on Climate Change: Environmental Sustainability and Application of Geospatial Technology. Organized by the Department of Geography in Collaboration with IQAC Prof. Sayed Nurul Hasan College, Farakka, Murshidabad, West Bengal, India. (18^{th} – 19^{th} January 2023), An Assessment of the Mayurakshi River Basin's Climatic Variability.

2. National Level Seminar on India at 75: looking behind and beyond. Organized by the Department of Political Science, A.B.N. Seal College, Cooch Behar, West Bengal, India. The impact of climate change on stream flow: A review.

PARTICULARS OF THE CANDIDATE

NAME OF THE CANDIDATE	**: David Durjoy Lal Soren**
DEGREE	**: Doctor of Philosophy**
DEPARTMENT	**: Geography & Resource Management**
TITLE OF THE THESIS	**: Role of Climatic Factors and Land Use Land Cover Change on Stream Flow Pattern of Mayurakshi River Basin, Eastern India.**
DATE OF ADMISSION	**: 14/11/2020**

APPROVAL OF RESEARCH PROPOSAL:

1. **DEPARTMENTAL RESEARCH COMMITTEE : 07/04/2021**
2. **BOARD OF STUDIES : 09/04/2021**
3. **SCHOOL BOARD : 05/05/2021**

MZU REGISTRATION NO.	**: 2107597**
Ph.D REGISTRATION NO & DATE	**: MZU/Ph.D./1727 of 14.11.2020**
EXTENSION	**: (N.A)**

Head

Department of Geography and Resource Management

ABSTRACT

ROLE OF CLIMATIC FACTORS AND LAND USE LAND COVER CHANGE ON STREAM FLOW PATTERN OF MAYURAKSHI RIVER BASIN, EASTERN INDIA

AN ABSTRACT SUBMITTED IN PARTIAL FULFILLMENT OF THE REQUIREMENTS FOR THE DEGREE OF DOCTOR OF PHILOSOPHY

DAVID DURJOY LAL SOREN
MZU REGISTRATION NO.: 2107597
Ph.D. REGISTRATION NO.: MZU/Ph.D./1727 of 14.11.2020

DEPARTMENT OF GEOGRAPHY AND RESOURCE MANAGEMENT
SCHOOL OF EARTH SCIENCE AND NATURAL RESOURCE MANAGEMENT
MARCH, 2025

ROLE OF CLIMATIC FACTORS AND LAND USE LAND COVER CHANGE ON STREAM FLOW PATTERN OF MAYURAKSHI RIVER BASIN, EASTERN INDIA

BY

DAVID DURJOY LAL SOREN

Department of Geography and Resource Management

Supervisor

Prof. BROTOTI BISWAS

Submitted

In partial fulfillment of the requirement of the Degree of Doctor of Philosophy in Geography and Resource Management of Mizoram University, Aizawl.

1. Introduction

Climate change is currently a very important concern. It poses a threat to both bio and non-bio resources. Numerous changes in the environmental and socioeconomic fields are owed to climate change (Croitoru & Minea, 2014). The hydrological responses of the basin are directly related to climate and direct human intervention, like various misuses of water for anthropogenic causes, like industrialization, irrigation, domestic uses, and agriculture (Wang et al., 2021).

The stream flow is impacted by climate change (Su et al., 2016). The primary cause of climate change is an increase in temperature, which is closely related to the cycle of water resources (Bronstert et al., 2002). The continuous accumulation of greenhouse gases is expected to change regional temperatures and precipitation, which have a direct impact on water resources (Nash et al., 1991). The functional relationship among the variables that directly or indirectly influence the runoff was paid attention to by the researchers in the 1970s and 1980s. Thereupon, runoff estimation and future prediction based on the mathematical model became a prime focus for assessing rainfall-runoff relations and water demand for future uses (Zealand et al., 1999). At present, researchers around the globe have focused on mathematical models to estimate the human activity and climate change impact on runoff change (Cao et al., 2015; Kan et al., 2015; Li et al., 2015). At the beginning of the 20th century, runoff response was studied mostly based on geophysical conditions, leading to the development of the paired catchment concept (Langbein, 1949).

Many models and climatic change projections have been developed by scientists for watershed management and future climatic prediction with hydrological responses (Jung et al., 2012; Pourmokhtarian et al., 2012; Boni et al., 2013; Biswas et al., 2019). Various studies have been conducted on modeling scenarios that heavily rely on streamflow regimes while estimating the changes in hydrological response on both local and global scales (Döll and Zhang, 2010; Fung et al., 2011). The worsening effect of climate change and anthropogenic activity has increased a world-wide water crisis that has been focused on in global hydrological research

(IPCC, 2007; Kumar et al., 2020). According to the Fourth Assessment Report of the Intergovernmental Panel on Climate Change (IPCC), the intensity and frequency of precipitation and temperature variations will rise due to climate change and anthropogenic impacts (Parry et al., 2007). The regional and worldwide distribution of water resources, both spatially and temporally, is strongly influenced by climate change and changes in land cover spurred by human activity in the 20th century. (Scanlon et al., 2007; Solomon et al., 2007; Ling et al., 2011). Some of the studies stated a positive correlation between temperature and stream flow (Nijssen et al., 2001; Arnell, 2003; Wang et al., 2011), while on the contrary, high temperatures enhance the evapotranspiration of plants, thereby reducing runoff (Frederick and Major, 1997), whereas some studies stated that climate change decreased streamflow (Yilmaz and Imteaz, 2011; Chang et al., 2014). The change in runoff (either increase or decrease) consequently influences sediment yield and its temporal-spatial distribution (Zhang and Wang, 2007).

It is widely recognized that one of the key factors that will be affected by climate change is the availability of water. The basic concepts of water resource planning encompass stream flow and hydrological process analysis. This basin is an important agro-based area that depends on irrigation for agricultural practice. Thus, the investigation in the present work has an immense bearing on society. For the sake of future management of runoff conditions, the study of the intensity and magnitude of climate change has greater importance to decision-makers (Chang et al., 2014). Climate change impact on runoff and discharge is an important study domain; thus, a proper review of this topic can formulate sustainable knowledge to proceed with further research interest in the ‘climate change impact in stream-flow domain’.

2. Statement of Research Problem

This study is framed to assess the impact of climatic variability and land use land (LULC) cover dynamics on the alteration of runoff patterns in the Mayurakshi river basin located in the eastern Indian monsoonal tropical climate. The purpose of this research is to evaluate the complex interaction of climate change and LULC change patterns on the runoff of the basin. The upper portion of the basin is the

extended part of the Chotonagpur plateau, while the lower part of the basin is a plain area with agricultural practices. A lot of changes in climatic conditions and LULC have taken place in the last couple of decades. The diversity of topography, its climatic variability, and LULC dynamics have extended to the complex nature of the basin, making it ideal for runoff-related studies of the basin. Many studies have reported that the runoff response varies from region to region, including the conditions of soil, geology, lithology, climate, human interventions, and LULC patterns (Sun et al., 2004; Wang et al., 2013; Mitra et al., 2021). Few studies were conducted in the present study area based on drainage basin morphometry and flood analysis (Islam et al., 2020), hydro-morphological characteristics, and land use modification (Mukhopadhyay et al., 2013). Thus, the study of water resource management and the effect of climate change and LULC dynamics on the runoff is an unknown aspect of the Mayurakshi river basin. Thus, the present study is a plausible attempt to fill this research gap.

3. Study Area

The Mayurakshi River system is one of the most important river systems in eastern India. The river originates from Trikut Hill in the Chota Nagpur plateau of Jharkhand state. The basin is located between the coordinates of 23° 63′ 12″ to 24° 51′ 3″ N latitude and 86° 84′ 38″ to 88° 16′ 12″ E longitude, spreading across the states of Jharkhand and West Bengal, covering an area of 5004.99 km^2 (Fig. 1.). Geologically, the whole area of the upper part of the basin dates back to the Proterozoic eon formation of undivided Precambrian rock. The middle catchment of the basin is most dominantly deposited by laterite and lateritic soil, and the lower catchment of the basin is mostly covered by young and old alluvial soil. The formation of the lower basin can be dated back to the quartanery eon, while the middle portion of the basin is dominated by jurassic cretaceous formation, sparsely dated back to the late carboniferous Permian eon.

The Masanjor Dam, which was commissioned in 1955, is situated in the Mayurakshi river basin in the Dumka district of Jharkhand. It is 2170 feet in length and stands 155 feet high from its base, with an overflow section extending 225.60 meters. The

dam has a storage capacity of 617,000,000 m^3 and a discharge capacity of 4.446 m^3/s. Tilpara Barrage downstream, 29.5 km away from the Masanjor Dam, was commissioned in 1949 on the Mayurakshi River. The Tilpara Barrage was constructed for irrigation and other agricultural activities.

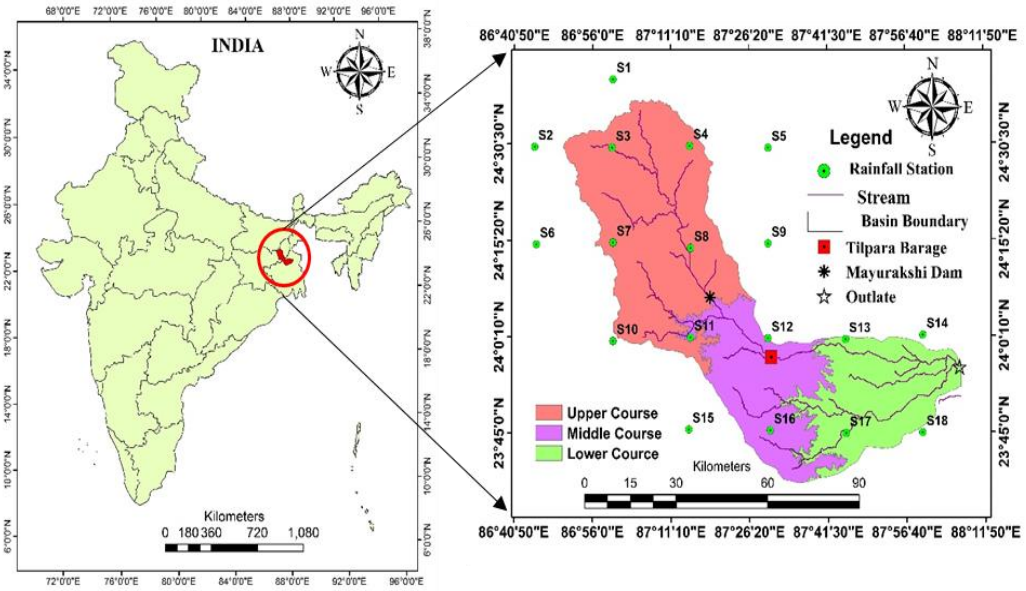

Fig. 1. Study area

4. Objectives:

1. To estimate the rainfall trend of the Mayurakshi river basin.

2. To assess the land use and land cover dynamics of the basin.

3. To evaluate seasonal streamflow patterns and simulate the runoff pattern of the basin.

4. To assess the role of climate change and land use land cover change on streamflow.

5. Research Questions

The research work has been conducted to address the following questions in reference to the study area:

(i) Is there any change in rainfall during the study period?

(ii) What types of land use and land cover changes occurred in the study area?

(iii) What is the impact of climate, land use, and land cover change on the runoff of the basin?

6. Methods

The research objectives were solved one by one through a series of methodological steps. Before the rainfall trend and changepoint analysis, the normality of the data was assessed by the Kolmogorov-Smirnov test. The data also underwent autocorrelation tests to confirm that the time-series data has a serial dependency or that the data is independent. Due to the autocorrelated data, the modified Mann-Kendall test (mMK) was applied for the trend analysis, and the magnitude of the trend was measured by Sen's slope. The change point of the rainfall time series has been evaluated by the statistics of Pettitt, Buishand U Statistic, and Standard Normal Homogeneity Test. The rainfall variability of the study area is analyzed by the Rainfall Seasonality Index (RSI), while the drought condition over the study period is measured by the Rainfall Anomaly Index (RAI). The Autoregressive Integrated Moving Average (ARIMA) model was used based on 30 years of time-sequence rainfall data to predict the future rainfall scenario of the basin.

The land use and land cover (LULC) dynamics of the basin are analyzed by the sequential steps of image classification, change detection, and future prediction. The satellite images were classified by the machine learning algorithm Random Forest (RF), and the change in LULC was assessed by the transition matrix. In order to predict the future scenario of LULC, the popular Cellular Automata-Markov model (CA-Markov) was employed. The runoff of the basin is simulated in the Soil and Water Assessment Tool (SWAT), and the model is calibrated and validated, where the calibration and validation are accepted based on the R^2 and Nash-Sutcliffe simulation efficiency (NSE). The climatic and LULC impacts on the runoff were evaluated by developing the models S_{2IPQ} of the simulated average runoff contribution of the basin during the impact period, S_{1NPQ} the simulated average

runoff contribution of the basin during the natural period, and S_{3IPCL} the runoff simulation with reference to climate change. In the model (S_{3IPCLQ}), the LULC is constant and referred to as the natural period (S_{1NPQ}), and the climatic components are referred to as the impact period (S_{2IPQ}).

7. Data Sources

The rainfall data was collected from the IMD Puna (https://www.imdpune.gov.in/cmpg/Griddata/Rainfall_25_Bin.html). The spatial resolution of this daily gridded rainfall data is 0.25 × 0.25 degrees, and the unit of rain is a millimeter (mm). The data was collected from 1901 to 2020. For image classification, the satellite data was collected from the United States Geological Survey (USGS) portal (http://earthexploration.usgs.gov/). The LULC for the years 1991, 1996, 2002, and 2008 was done using the collected Landsat 5 images and Thematic Mapper (TM). For the years 2014 and 2020, Landsat 8 and Operational Land Imager (OLI) were used. To run the SWAT model, weather datasets, including temperature, humidity, wind speed, and solar radiation, were acquired from NASA Power Access MERRA-2 data (https://power.larc.nasa.gov/data-access-viewer/). The observed discharge data were obtained from the Ministry of Jal Shakti, Central Water Commission Executive Engineer, Damodar Division, CWC, Asansol, under the Government of India.

8. Future research

The work can lead researchers in the areas of climatology, agricultural science, and regional planning to undertake further studies on regional climate changes and their effect on agriculture, regional economies, ecosystems, and hydropower production. Further, the changes in LULC can prove to be food for future research in the fields of regional planning and environmental conservation for sustainable policy changes.

9. Major findings

9.1. Major findings of the first objective

The Mayurakshi river basin is one of the important agricultural belts of eastern India. The work was conducted to understand the dynamic change of climate and LULC of the basin and its impact on the streamflow. In the last 30 years' study period, the maximum and minimum rainfall were 1717.37 mm, 1188.65 mm, and the long-term average rainfall was recorded as 1420.67 mm. The characteristics of rainfall in the 1st decade (1991-2000) varied, with a maximum of 1885.86 mm, a minimum of 1252.81 mm, and an average of 1511.96 ± 160.48 mm. In the 1st decade, a continuous upward trend of rainfall was recorded. In the 2nd decade (2001-2010), the mean annual rainfall was 14346.22 ± 170.52 mm. In the 3rd decade (2011-2020), the basin received low rainfall (1380.41 mm) as compared to the 1st and 2nd decades. High rainfall concentrations were recorded in the northeastern part of the upper and middle basin areas in the whole study period. The basin experienced a decreasing trend of rainfall, the magnitude of the trend presented by Sen's slope shows the rainfall of the basin has a strong negative Sen's slope value, which is -10.37 mm/year, implies that there is a decreasing or downward trend in rainfall. In the 30 years, the rainfall pattern change point was detected in 2008 and was confirmed by the step change point detection. In the long term period, the average values of various climatic components were recorded as follows: temperature at 32.23 ± 0.63^{0}C, wind speed at 1.9 ± 0.12 m/s, solar radiation at 90.40 ± 5.00 W/m^2, and humidity at 63.44 ± 5.48 %. During the study period, the basin experienced a maximum temperature of 38.80^{0}C. From 1991 to 2020, temperature showed a slightly increasing trend, supported by a significant Kendall's P value of 0.05, with a normalized test (Z) value of 1.89 and a Kendall's tau of 0.24. The temperature has shown an increase by 0.03 ^{0}C during the study period. The temporal characteristics of the basin rainfall were found to be extremely wet during 16.67% of the years; moderately dry, slightly wet, and slightly dry in 16.67% of the sampled years, while 6.67% of the years were recorded as extremely dry. The rainfall was forecasted through ARIMA model which indicated an average rainfall condition of 1303.38 ±

19.99 mm/year, with the very least variability (CV 1.53) and a decreasing trend for the next 10 years over the basin.

9.2. Major findings of the second objective

In 1991 (1st study period), agricultural land was covered by 49.15% and vegetation cover covered 20.45% area. During the second study period, vegetation expanded by 3.10% (1150.09 km²), mainly due to the contribution from agricultural land and bare land 472.64 km² and 272.02 km², respectively. However, agricultural areas saw a 4.30% decrease, shrinking by 2429.75 km², while bare land and built-up areas grew from 1325.68 km² to 1079.09 km² and from 42.82 km² to 182.67 km², respectively. In the third study period, there were increases in water bodies (183.02 km² or 0.49%), vegetation (2368.95 km² or 2.80%), agricultural land (2469.73 km² or 0.80%), and built-up areas (162.37 km² or 0.33%). During the fourth study period, the agricultural land expanded from 2,529.54 km² to 3,214.12 km². Within this agriculture land use and land cover category, vegetation contributed 583.62 km², while bare land contributed 516.03 km². During the final study period (2014–2020), bare land continued to decline significantly, reflecting the trends observed in the fourth study period. In contrast, agricultural land increased by 6.36% (3988.62 km²). The LULC transition to agriculture class included 47.34 km² from water, 501.33 km² from vegetation, 451.41 km² from bare land, and 90.63 km² from built-up areas. Additionally, the transition to built-up areas included 1.64 km² from water, 17.82 km² from vegetation, 30.51 km² from bare land, and 29.43 km² from agricultural land. In 2020 the dominant LULC of the basin was agricultural land, covered by 70.60% of the area and the second dominant LULC class was vegetation, covered by 15.57% of the area. The built-up area experienced a continuously increasing trend, in 1991 it was 2.15% and in 2020 it increased by 5.44%. The water class was covered by 5.28% in 1991 but has decreased by 3.20% of the area in 2020. The future LULC of 2032 indicates that agriculture will remain the dominant land cover class, spanning 3520.92 km^2. It will be followed by vegetation class covering an area of 788.18 km^2 and built-up areas occupying 272.40 km^2. The trend of the seasonal discharge pattern was -0.762 mm/year, indicating a gentle rate of decreasing pattern in monsoonal discharge.

9.3. Major findings of the third objective

The hydrological parameters determined for the simulation of runoff in the natural period were moisture condition II the curve number, base-flow recession constant, delay time for aquifer recharge, threshold water level in the shallow aquifer for base flow, soil evaporation compensation coefficient, and surface runoff lag coefficient. The values are 0.0275, 0.44375, 169.125, 0.5125, 0.98375, and 0.798437, respectively. The validated model for the natural period demonstrated satisfactory performance with R^2 and NES values of 0.83 and 0.80, respectively.

The values for various hydrological parameters in the impact period were determined as follows: the curve number for natural period moisture condition II was 0.0275, the base-flow recession constant was 0.44375, the delay time for aquaria recharge was 169.125, the threshold water level in the shallow aquifer for base-flow was 0.5125, the soil evaporation compensation coefficient was 0.98375, and the surface runoff lag coefficient was 0.798437. The validated model for the impact period showed satisfactory performance, with R^2 and NES values of 0.89 and 0.87, respectively.

9.4. Major findings of the fourth objective

The simulated T_Q of S_{1NPQ} was 137.85 mm. From 1996 to 2008 a greater amount of T_Q was recorded. The simulated S_{2IPQ} *was* 127.65 mm. During the period of $S_{2IPQ,}$ the T_Q showed a downward trend. The impact of the decreasing trend of rainfall caused a decrease in T_Q on the watershed was 68.19 mm. The computed TD_Q between the natural period and the impact period was -10.19 mm/year which indicates a decrease in stream flow over the study period. The CL_{IQ} of -69.66 indicated the negative impact of climate on streamflow.

10. Recommendations

The study area suffers from the problems of environment-degrading livelihood, environment-degrading agricultural practices, loss of ecological balance, climate change, rampant forest cover loss, and loss of water bodies. Restoration of environmental balance and the sustainable development of "Life on Earth" is the main aim of Sustainable Development Goals (SDGs). The Central government and

state government should work hand in hand in the study area to restore the SDGs such as ecological imbalance and check the rampant deforestation in the study area while maintaining and encouraging a sustainable livelihood. "Ministry of Environment, Forest and Climate Change, (MoEFCC)" can provide some necessary solutions towards the problem through its schemes and policies like "National Afforestation Programme, (NAP)", "Green India Mission (GIM)", " Compensatory Afforestation Fund Management and Planning Authority, (CAMPA)", and " National Mission for a Green India (GIM) ". Further "National Agroforestry Policy (NAP)" under the "Ministry of Agriculture and Farmers' Welfare, (MoAFW)", "Mahatma Gandhi National Rural Employment Guarantee Act, (MGNREGA)" under the "Mahatma Gandhi National Rural Employment Guarantee Act, (MGNREGA)", and "National Forest Policy, (NFP) 1988", under the "Ministry of Food and Agriculture, (MFA)" are aimed to protect the environment. The above-mentioned policies could be implemented to protect the SDGs, like Sustainable Development Goal 12 (SDG 12), to ensure sustainable consumption and production patterns to achieve the sustainable management and efficient use of natural resources, Sustainable Development Goal 13 (SDG 13), to limit and adapt to climate change, to "Take urgent action to combat climate change and its impacts", and Sustainable Development Goal 15 (SDG 15), to "Protect, restore and promote the sustainable use of terrestrial and forest ecosystems, combat desertification, and halt and reverse land degradation and halt biodiversity loss" of the study area which are at risk.

11. Conclusion

This study focused on a detailed examination of rainfall variability and LULC changes over time, aiming to investigate the runoff conditions in the basin and the influence of both climate and LULC change impacts on basin runoff. The study identified a significant change in both precipitation patterns and LULC. The pattern of precipitation step change occurred in 2008 after the breaking point, when rainfall followed a decreasing trend (-12.21 mm/year). The runoff model employed in this analysis shed light on the fact that, based on the watershed's characteristics (slope, soil, aspect, elevation, climate, and LULC) and the role of relative control between climate and LULC on stream flow, climate played a negative influence on runoff

conditions. The findings revealed that at the constant LULC, changes in climate will be caused by the runoff yield of 68.19 mm. Consequently, the runoff decreased by -10.19 mm/year from the natural period to the interference period, exhibiting a negative relative contribution of climatic factors to the stream flow of the basin. The observed reduction in runoff is attributed to climate change, specifically the declining nature of precipitation. This comprehensive study on the interplay of climate and LULC holds significant value for effective basin management and environmental conservation. As the study area is one of the important agricultural belts of eastern India, it is very important to know the impact of climate and LULC on stream flow patterns, which is a very precious aspect of land management and sustainable water resource management. The local communities, planners, and government can leverage this knowledge to integrate sustainable practices into their planning efforts and ensure responsible basin management for the future.

The study revealed that water bodies have been reduced from time to time. To restore the water bodies and sustainable agriculture towards attaining Sustainable Development Goal 2 (SDG 2, to "End hunger, achieve food security and improved nutrition and promote sustainable agriculture"), the government should take steps toward the wetland management program through the “Wetlands Management for Biodiversity and Climate Protection Project, (WMBCPP)” and "National Plan for Conservation of Aquatic Ecosystems (NPCA)" under the “Ministry of Environment, Forest and Climate Change (MoEFCC)”, " National Water Mission (NWM)", and " Atal Bhujal Yojana, (Atal Jal)", under the "Ministry of Jal Shakti", and "Pradhan Mantri Krishi Sinchai Yojana, (PMKSY)" under the "Ministry of Agriculture and Farmers' Welfare" these will be helpful towards attaining the respective goals if implemented. The environmental awareness programs like environmental education and awareness, conservation of natural resources programs for the local people could play an important role in restoring sustainable management of water, soil, forests, and the environment.

References

Aich, V., Liersch, S., Vetter, T., Huang, S., Tecklenburg, J., Hoffmann, P., Hattermann, F. F. (2014). Comparing impacts of climate change on streamflow in four large African river basins. *Hydrol. Earth Syst. Sci*, 1-14. doi:doi:10.5194/hess-18-1305-2014

Al-Faraj, F., Scholz, M., & Tigkas, D. (2014). Sensitivity of Surface Runoff to Drought and Climate Change: Application for Shared River Basins. *6*, 3033-3048. doi:doi:10.3390/w6103033

Allen, M., & Ingram, J. (2002). Constraints on future climate changes and the hydrologic cycle. *Nature*, 224–232.

Arnell, N. W. (2003). Relative effects of multi-decadal climatic variability and changes in the mean and variability of climate due to global warming: future streamflows in Britain. *Journal of Hydrology*, 195–213.

Arnell, N., & Gosling, S. (2013). The impacts of climate change on river flow regimes at the global scale. *Journal of Hydrology*, 351–364. doi:http://dx.doi.org/10.1016/j.jhydrol.2013.02.010

Biswas B., Ratnaprabha J., Nilima T. (2019), Rainfall Distribution and Trend Analysis for Upper Godavari Basin, India, from 100 Years Record (1911–2010), J. of the Indian Soc. of Remote Sensing, https://doi.org/10.1007/s12524-019-01011-8(0123456789-volV)(0123456789().

Biswas B., Jain S., Rawat S, (2018), Spatio-temporal analysis of groundwater levels and projection of future trend of Agra city, Uttar Pradesh, India, *Arab J Geosci, 1-18* https://doi.org/10.1007/s12517-018-3577-4

Berton, R., Driscoll, C., & Chandler, D. (2016). Changing climate increases discharge and attenuates its seasonal distribution in the northeastern United States. *Journal of Hydrology: Regional Studies*, 164–178. doi:http://dx.doi.org/10.1016/j.ejrh.2015.12.057

Bingfei, H., Chao, J., & Jianxin, S. O. (2020). Differential changes in precipitation and runoff discharge during 1958–2017 in the headwater region of the Yellow River of China. *J. Geogr. Sci.*, *30*(9), 1401-1418. doi: https://doi.org/10.1007/s11442-020-1789-5

Boini, N., Ashvin K., G., & Baghu R., C. (2013). Assessment of Future Climate Change Impacts on Water Resources of Upper Sind River Basin, India Using SWAT Model. *Water Resour Manage, 27*, 3647–3662. doi: 10.1007/s11269-013-0371-7

Bronstert, A., Niehoff, D., & Burger, G. (2002). Effects of climate and land-use change on storm runoff generation: present knowledge and modeling capabilities. *Hydrological Processes, 16*, 509-529.

Carey, M., Baraer, M., Mark, B., French, A., Bury, J., Young, K., & McKenzie, J. (2013). Toward hydro-social modeling: Merging human variables and the social sciences with climate-glacier runoff models (Santa River, Peru). *Journal of Hydrology*, 1-11. doi:http://dx.doi.org/10.1016/j.jhydrol.2013.11.006

Cauvy-Fraunie´, S., Andino, P., Espinosa, R., Calvez, R., Jacobsen, D., & Dangles, O. (2015). Ecological responses to experimental glacier-runoff reduction in alpine rivers. *Nature Communications*, 1-5. doi: 10.1038/ncomms12025

Chang, J., Wang, Y., Istanbulluoglu, E., Bai, T., Huang, Q., Yang, D., & Huang, S. (2014). Impact of climate change and human activities on runoff in the Weihe River Basin, China. *Quaternary International*, 1-11. doi:http://dx.doi.org/10.1016/j.quaint.2014.03.048

Chang, J., Zhang, H., Wang, Y., & Zhang, L. (2017). Impact of climate change on runoff and uncertainty analysis. *Nat Hazards*, 1-19. doi: 10.1007/s11069-017-2909-0

Chen, H., Fleskens, L., Baartman, J., Wang, F., Moolenaar, S., & Ritsema, C. (2020). Impacts of land use change and climatic effects on streamflow in the Chinese Loess Plateau: A meta-analysis. *Science of the Total Environment*, 134989-135003. doi:https://doi.org/10.1016/j.scitotenv.2019.134989

Chen, Z., & Chen, Y. (2014). Effects of climate fluctuations on runoff in the headwater region of the Kaidu River in northwestern China. *Front. Earth Sci.*, 1-10. doi: 10.1007/s11707-014-0406-2

Chen, Z., Chen, Y., & Li, B. (2013). Quantifying the effects of climate variability and human activities on runoff for Kaidu River Basin in arid region of northwest China. *111*, 537–545. doi:DOI 10.1007/s00704-012-0680-4

Croitoru, A.-E., & Minea, I. (2014). The impact of climate changes on river discharge. *Theor Appl Climatol*, 1-14. doi: 10.1007/s00704-014-1194-z

Crossman, J., Futter, M., Oni, S., Whitehead, P., Jin, L., Butterfield, D., Dillon, P. (2013). Impacts of climate change on hydrology and water quality: Future-proofing management strategies in the Lake Simcoe watershed, Canada. *Journal of Great Lakes Research*, 19–32. doi:http://dx.doi.org/10.1016/j.jglr.2012.11.003

D¨oll, P., & Zhang, J. (2010). Impact of climate change on freshwater ecosystems: a global-scale analysis of ecologically relevant river flow alterations. *Hydrol. Earth Syst. Sci*, *14*, 783–799. doi:doi:10.5194/hess-14-783-2010

Daba, M., & You, S. (2020). Assessment of Climate Change Impacts on River Flow Regimes in the Upstream of Awash Basin, Ethiopia: Based on IPCC Fifth Assessment Report (AR5) Climate Change Scenarios. *doi:10.3390/hydrology7040098*, 1-22. doi:doi:10.3390/hydrology7040098

Danneberg, J. (2012). Changes in runoff time series in Thuringia Germany—Mann-Kendall trend test and extreme value analysis. *Adv Geosci*, *31*, 31-56. doi:doi:10.5194/adgeo-31-49-2012

Das, J., & Nanduri, U. (2018). Assessment and evaluation of potential climate change impact on monsoon flows using machine learning technique over Wainganga River Basin, India. *Hydrological Sciences Journal*. doi: 10.1080/02626667.2018.1469757

Delcour, I., Spanoghe, P., & Uyttendaele, M. (2015). Literature review: Impact of climate change on pesticide use. *Food Research International*, 7–15. doi:http://dx.doi.org/10.1016/j.foodres.2014.09.030

Döll, P., & Bunn, S. (2014). Impact of Climate Change on Freshwater Ecosystems due to Altered River Flow Regimes. *Cross-Chapter Box*, 143-146.

Döll, P., & Müller Schmied, P. (2010). How is the impact of climate change on river flow regimes related to the impact on mean annual runoff? A global-scale analysis. *Environ. Res. Lett.*, *7*(1). doi:http://dx.doi.org/10.1088/1748-9326/7/1/014037

Dong, L. H., Xiong, L. H., Yu, K. X., & Li, S. (2012). Research advances in effects of climate change and human activities on hydrology Adv. Water Sci. *2*, 278–285.

Donnelly, C., Greuell, W., Andersson, J., Gerten, D., Pisacane, G., Roudier, P., & Ludwig, F. (2017). Impacts of climate change on European hydrology at 1.5, 2 and 3 degrees mean global warming above preindustrial level. *Climatic Change*, *143*, 13–26. doi:DOI 10.1007/s10584-017-1971-7

Eisner, S., Flörke, M., Chamorro, A., Dasgupta, P., Donnelly, C., Huang, J., . . . Krysanova, V. (2017). An ensemble analysis of climate change impacts on streamflow seasonality across 11 large river basins. *Climatic Change*, *141*, 401–417. doi: 10.1007/s10584-016-1844-5

Fekete, B., Wisser, D., Kroeze, C., Mayorga, E., Bouwman, L., Wollheim, W., & Vörösmarty, C. (2010). Millennium Ecosystem Assessment scenario drivers (1970–2050): Climate and hydrological alterations. *Global Biogeochemical Cycles*, 1-12. doi:doi:10.1029/2009GB003593

Frederick, K. D., & Major, D. C. (1997). Climate change and water resources,. *Climatic Change*, *37*, 7–23.

Giang, P. Q., Toshiki, K., Sakata, M., Kunikane, S., & Vinh, T. Q. (2014). Modeling Climate Change Impacts on the Seasonality of Water Resources in the Upper Ca River Watershed in Southeast Asia. *Hindawi Publishing Corporation The Scientific World Journal*, 1-15. doi:http://dx.doi.org/10.1155/2014/279135

Githui, F., Gitau, W., Mutua, F., & Bauwens, W. (2009). Climate change impact on SWAT simulated streamflow in western Kenya. *Int. J. Climatol*, *29*, 1823–1834. doi: 10.1002/joc.1828

Goulden, M., & Bales, R. (2014). Mountain runoff vulnerability to increased evapotranspiration with vegetation expansion. *Department of Earth System Science, University of California, Irvine*, *111*(39), 14071–14075. Retrieved from www.pnas.org/lookup/suppl/doi:10.

Gupta, P., Panigrahy, S., & Parihar, J. S. (2011). Impact of Climate Change on Runoff of the Major RiverBasins of India Using Global Circulation Model (HadCM3) Projected Data. *J Indian Soc Remote Sens*, *39*(3), 337–344. doi: 10.1007/s12524-011-0101-7

Hagemann, S., Chen, C., Clark, D. B., Folwell, S., Gosling, S. N., Haddeland, I., . . . Wiltshire, A. J. (2013). Climate change impact on available water resources obtained using multiple global climate and hydrology models. *Earth Syst. Dynam*, *4*, 129–144. doi:doi:10.5194/esd-4-129-2013

Hamdi, R., Termonia, P., & Baguis, P. (2011). Effects of urbanization and climate change on surface runoff of the Brussels Capital Region: a case study using an urban soil–vegetation–atmosphere-transfer model. *Int. J. Climatol*, 1959–1974. doi: 10.1002/joc.2207

IPCC. (2007). Climate change 2007. *The Physical Science Basis Report AR4*.

Janzˇa, M. (2013). Impact assessment of projected climate change on the hydrological regime in the SE Alps, Upper Socˇa River basin, Slovenia. *Nat Hazards, 67*, 1025–1043. doi:DOI 10.1007/s11069-011-9892-7

Jeppesen, E., & Kronvang, B. (2009). Climate Change Eff ects on Runoff , Catchment Phosphorus Loading and Lake Ecological State, and Potential Adaptations. *J. Environ. Qual, 38*, 1930–1941. doi:doi:10.2134/jeq2008.0113

Jiang, C., Xiong, L., Wang, D., Liu, P., Guo, S., & Xu, C.-Y. (2015). Separating the impacts of climate change and human activities on runoff using the Budyko-type equations with time-varying parameters. *Journal of Hydrology*, 326–338. doi:http://dx.doi.org/10.1016/j.jhydrol.2014.12.060

Jung, I. W., Moradkhani, H., & Chang, H. (2012). Uncertainty assessment of climate change impacts for hydrologically distinct river basins. *J. Hydrol*, 73–87. doi:http://dx.doi.org/10.1016/j.jhydrol.2012.08.002.

Koch, H., Silva, A. C., Liersch, S., Azevedo, J. G., & Hattermann, F. (2020). Effects of model calibration on hydrological and water resources management simulations under climate change in a semi-arid watershed. *Climatic Change, 163*, 1247–1266.

Kwadjk, J., & Middelkoop, H. (1994). Eastimation of impact of climate change on the peak discharge probability of the river Rhine. *Climatic Change June*, 1-26.

Kumar J.,Biswas B., Walker S *(2020),* Multi-temporal LULC Classification using Hybrid Approach and Monitoring Built-up Growth with Shannon's Entropy for a Semiarid Region of Rajasthan, India, *J. of the Geo. Soc. of India*, Doi: 1 0.1007/s12594-020-1489-x. 95. 626-635

Lei, H., Yang, D., & Huang, M. (2014). Impacts of climate change and vegetation dynamics on runoff in the mountainous region of the Haihe River basin in the past five decades. *Journal of Hydrology*, 786-799. doi:http://dx.doi.org/10.1016/j.jhydrol.2014.02.029

Leppi, J., DeLuca, T., Harrar, S., & Running, S. (2012). Impacts of climate change on August stream discharge in the Central-Rocky Mountains. *Climatic Change, 112*, 997–1014. doi: 10.1007/s10584-011-0235-1

Lettenmaier, D. P., Wood, E. F., & Wallis, J. R. (1994). Hydro-climatological trends in the continental United States1948–88. (7), 586-607.

Li, T., & Gao, Y. (2015). Runoff and Sediment Yield Variations in Response to Precipitation Changes: A Case Study of Xichuan Watershed in the Loess Plateau, China. *Water, 7*, 5638-5656. doi:doi:10.3390/w7105638

Lin, K., Lin, Y., Xiaohong, C., & Fan, L. (2014). Changes in runoff and eco-flow in the Dongjiang River of the Pearl River Basin, China. *Front. Earth Sci.*, 1-11. doi: 10.1007/s11707-014-0434-y

Ling, H. B., Xu, H. L., Shi, W., & Zhang, Q. (2011). Regional climate change and its effects on the runoff of Manas River, Xinjiang, China. *Environ Earth Sci,, 64*(8), 2203–2213.

Luo, Y., Ficklin, D., Liu, X., & Zhang, M. (2013). Assessment of climate change impacts on hydrology and water quality with a watershed modeling approach. *Science of the Total Environment*, 72–82. doi:http://dx.doi.org/10.1016/j.scitotenv.2013.02.004

Lv, X., Zuo, Z., Ni, Y., Sun, J., & Wang, H. (2019). The effects of climate and catchment characteristic change on streamflow in a typical tributary of the Yellow River. *Scintific Report*. doi:https://doi.org/10.1038/s41598-019-51115-x 1

Ma, H., Yang, D., Tan, S. K., Gao, B., & Hu, Q. (2010). Impact of climate variability and human activity on streamflow decrease in the Miyun Reservoir catchment. *Journal of Hydrology*, 317–324. doi:doi:10.1016/j.jhydrol.2010.06.010

Mohammed, R., Scholz, M., Nanekely, A. M., & Mokhtari, Y. (2016). Assessment of models predicting anthropogenic interventions and climate variability on surface runoff of the Lower Zab River. *Stoch Environ Res Risk Assess*, 1-18. doi: 10.1007/s00477-016-1375-7

Narsimlu, B., Gosain, A., & Chahar, B. (2013). Assessment of Future Climate Change Impacts on Water Resources of Upper Sind River Basin, India Using SWAT Model. *Water Resour Manage* , 3647–3662. doi: 10.1007/s11269-013-0371-7

Nijssen, B., Schnur, R., & Lettenmaier, D. P. (2001). Global retrospective estimation of soil moisture using the variable infiltration capacity land surface model, 1980–93. *Journal of Climate, 14*, 1790-1808.

Ning, T., Li, Z., & Liu, W. (2016). Separating the impacts of climate change and land surface alteration on runoff reduction in the Jing River catchment of China. *Catena, 147*, 80–86. doi:http://dx.doi.org/10.1016/j.catena.2016.06.041

Oliveira, V., Mello, C., & Viola, M. (2017). Assessment of climate change impacts on streamflow and hydropower potential in the headwater region of the Grande river basin, Southeastern Brazil. *Int. J. Climatol.*, 1-19. doi: 10.1002/joc.5138

Oni, S., Futter, M., Molot, L., Dillon, P., & Crossman, J. (2014). Uncertainty assessments and hydrological implications of climate change in two adjacent agricultural catchments of a rapidly urbanizing watershed. *Science of the Total Environment*, 326–337. doi:http://dx.doi.org/10.1016/j.scitotenv.2013.12.032

Oti, J. O., Kabo-bah, A., & Ofosu, E. (2020). Hydrologic response to climate change in the Densu River Basin in Ghana. *Heliyon*. doi:https://doi.org/10.1016/j.heliyon.2020.e04722

Papadimitriou, L., Koutroulis, A., Grillakis, M., & Tsanis, I. (2016). High-end climate change impact on European runoff and low flows – exploring the effects of forcing biases. *Hydrol. Earth Syst. Sci, 20*, 1785–1808. doi:doi:10.5194/hess-20-1785-2016

Parry, ML; Canziani, OF;. (2007). Technical summary Climate change: impacts, adaptation and vulnerability, contribution of Working Group II to the Fourth Assessment Report of the Intergovernmental Panel on Climate Change. (M. Parry, O. Canziani, J. Palutikof, J. van der Linden, & C. Hanson, Eds.) *Cambridge University Press, Cambridge, UK*, 23-78.

Peng, D., Qiu, L., Fang, J., & Zhang, Z. (2016). Quantification of Climate Changes and Human Activities That Impact Runoff in the Taihu Lake Basin, China.

Hindawi Publishing Corporation Mathematical Problems in Engineering, 1-8. doi:http://dx.doi.org/10.1155/2016/2194196

Phan, D., Wu, C., & Hsieh, S. (2011). Impact of Climate Change on Stream Discharge and Sediment Yield in Northern Viet Nam1. *Water Resources, 38*(6), 827-236. doi:10.1134/S0097807811060133

Pourmokhtarian, A., Driscoll, C. T., Campbell, J. L., & Hayhoe, K. (2012). Modeling potential hydrochemical responses to climate change and increasing CO2atthe Hubbard Brook Experimental Forest using a dynamic biogeochemical model (PnET-BGC). *Water Resour. Res, 48*(13), 1-14. doi:http://dx.doi.org/10.1029/2011WR011228.

Pumo, D., Arnone, E., Francipane, A., Caracciolo, D., & Noto, L. (2017). Potential implications of climate change and urbanization on watershed hydrology. *Journal of Hydrology*, 80–99. doi:http://dx.doi.org/10.1016/j.jhydrol.2017.09.002

Pumo, D., Caracciolo, D., Viola, F., & Noto, L. (2016). Climate change effects on the hydrological regime of small non-perennial river basins. *Science of the Total Environment*, 76–92. doi:http://dx.doi.org/10.1016/j.scitotenv.2015.10.109

Qiu, J., Shen, Z., Leng, G., Xie, H., Hou, X., & Wei, G. (2015). Impacts of climate change on watershed systems and potential adaptation through BMPs in a drinking water source area. *Journal of Hydrology*, 223-235. doi:https://doi.org/10.1016/j.jhydrol.2019.03.074

Radchenko, I., Dernedde, Y., Mannig, B., Frede, H.-G., & Breuer, L. (2017). Climate Change Impacts on Runoff in the Ferghana Valley (Central Asia). *44*(5), 1-24. doi: 10.1134/S0097807817050098

Scanlon, T., Caylor, K., Levin, S., & Rodriguez-Iturbe, I. (2007). Positive feedbacks promote power-law clustering of Kalahari vegetation. *Nature, 449*, 209-2012.

Schneider, C., Laiz´e, C. L., Acreman, M. C., & Fl¨orke, M. (2013). How will climate change modify river flow regimes in Europe? *Hydrol. Earth Syst. Sci, 17*, 325–339. doi:doi:10.5194/hess-17-325-2013

Shanka, A. S. (2017). Evaluation of Climate Change Impacts on Run-Off in the Gidabo River Basin: Southern Ethiopia. *Environment Pollution and Climate Change, 1*(3), 1-13.

Singh A., Rai P k., Deka G., Biswas B., Prasad D., Rai VK (2021), Management of natural resources through integrated watershed management in Nana Kosi micro watershed, district Almora, India, *Eco. Env. & Cons*, 27(5),259-266.

Solomon, S., Qin, D., Manning, M., Marquis, M., Averyt, K., Tignor, M. B., . . . Chen, Z. (2007). Climate Change 2007: The Physical Science Basis, Cambridge University. *Press, Cambridge, 996*.

Sorg, A., Bolch, T., Stoffel, M., Solomina, O., & Beniston, M. (2012). Climate change impacts on glaciers and runoff in Tien Shan (Central Asia). *Climate Change*, 725-732. doi: 10.1038/NCLIMATE1592

Sorribas, M. V., Paiva, R., Melack, J., Bravo, J., Jones, C., Carvalho, L., . . . Costa, M. H. (2016). Projections of climate change effects on discharge and inundation in the Amazon basin. *Climatic Change*, 1-16. doi: 10.1007/s10584-016-1640-2

Srinivas, R., Singh, A. P., Dhadse, K., & Magner, J. (2020). Hydroclimatic river discharge and seasonal trends assessment model using an advanced spatio-temporal model. *Stochastic Environmental Research and Risk Assessment*, 1-16. doi:https://doi.org/10.1007/s00477-020-01780-6

Stagl, J., & Hattermann, F. (2015). Impacts of Climate Change on the Hydrological Regime of the Danube River and Its Tributaries Using an Ensemble of Climate Scenarios. *Water, 7*, 1-14. doi:6139-6172; doi:10.3390/w7116139

Su, B., Huang, J., Zeng, X., Gao, C., & Jiang, T. (2016). Impacts of climate change on streamflow in the upper Yangtze River basin. *Climatic Change*, 1-14. doi: 10.1007/s10584-016-1852-5

Tang, C., Crosby, B., Wheaton, J., & Piechota, T. (2012). Assessing streamflow sensitivity to temperature increases in the Salmon River Basin, Idaho. *Global and Planetary Change*, 32–44. doi:doi:10.1016/j.gloplacha.2012.03.002

Uniyal, B., Jha, M. K., & Verma, A. K. (2015). Assessing Climate Change Impact on Water Balance Components of a River Basin Using SWAT Model. *Water Resour Manage, 29*, 4767–4785. doi: 10.1007/s11269-015-1089-5

Vano, J., Nijssen, B., & Lettenmaier, D. (2015). Seasonal hydrologic responses to climate change in the Pacific Northwest. *Water Resources Research*, 1-18. doi:10.1002/2014WR015909

Wagner, T., Themeßl, M., Schu¨ppe, A., Gobiet, A., Stigler, H., & Birk, S. (2017). Impacts of climate change on stream flow and hydro power generation in the Alpine region. *Environ Earth Sci, 76*(4), 1-24. doi: 10.1007/s12665-016-6318-6

Wang, D., & Hejazi, M. (2011). Quantifying the relative contribution of the climate and direct human impacts on mean annual streamflow in the contiguous United States. *Water Resour. Res, 47*, 1-16. doi: 10.1029/2010WR010283

Wang, G., Zhang, J., Li, X., Bao, Z., Liu, Y., Liu, C., Luo, J. (2017). Investigating causes of changes in runoff using hydrological simulation approach. *Appl Water Sci, 7*, 2245–2253. Doi: 10.1007/s13201-016-0396-1

Wang, J., Gao, Y., & Wang, S. (2018). Assessing the response of runoff to climate change and human activities for a typical basin in the Northern Taihang Mountain, China. *J. Earth Syst. Sci.*, 1-15. doi:https://doi.org/10.1007/s12040-018-0932-5

Wang, M., Qin, D., Lu, C., & Li, Y. (n.d.). Modeling Anthropogenic Impacts and Hydrological Processes on a Wetland in China. *Water Resour Manage*, 2743–2757. doi: 10.1007/s11269-010-9577-0

Wang, S., Yan, M., Yan, Y., Shi, C., & He, L. (2012). Contributions of climate change and human activities to the changes in runoff increment in different sections of the Yellow River. *Quaternary International*, 66e77. doi:http://dx.doi.org/10.1016/j.quaint.2012.07.011

Worqlul, A. W., Dile, Y. T., Ayana, E. K., Jeong, J., Adem, A. A., & Gerik, T. (2018). Impact of Climate Change on Streamflow Hydrology in Headwater Catchments of the Upper Blue Nile Basin, Ethiopia. *water*, 1-18. doi: 10.3390/w10020120

Wu, J., Gao, X., Giorgi, F., Chen, Z., & Yu, D. (2012). Climate effects of the Three Gorges Reservoir as simulated by a high resolution double nested regional

climate model. *Quaternary Internationa*, 27- 36. doi: 10.1016/j.quaint.2012.04.028

Yang, H., Yang, D., & Hu, Q. (2014). An error analysis of the Budyko hypothesis for assessing the contribution of climate change to runoff. *Water Resources Research*, 9620-9630. doi:doi:10.1002/2014WR015451.

Yang, T., Wang, X., Yu, Z., Krysanova, V., Chen, X., Schwartz, F., & Sudicky, E. (2014). Climate change and probabilistic scenario of streamflow extremes in an alpine region. *Journal of Geophysical Research: Atmospheres*, 8535-8550. doi:10.1002/2014JD021824

Yates, D. (2014). WatBal: An Integrated Water Balance Model for Climate Impact Assessment of River Basin Runoff. *International Journal of Water Resources Development, 12*(2), 121-140. doi: 10.1080/07900629650041902

Yilmaz, A. G., & Imteaz, M. A. (2011). Impact of climate change on runoff in the upper part of the Euphrates. *Hydrological Sciences Journal – Journal des Sciences Hydrologiques, 56*(7), 1265-1279.

Zhang, J. Y., & Wang, G. Q. (2007). Research on Impacts of Climate Change on Hydrology and Water Resources. *Science Press: Beijing, China*, 1-9.

Zhang, J. Y., Wang, G. Q., Pagano, T. C., Liu, C. S., HE, M. R., & Liu, L. I. (2012). Using hydrologic simulation to explore the impacts of climate change on runoff in the Huaihe River basin of China. *Journal of Hydrologic Engineering*, 1-28. doi:doi:10.1061/(ASCE)HE.1943-5584.0000581

Zhang, W., Shaoming, P., Cao, L., Cai, X., Zhang, K., Xu, Y., & Wei, X. (2015). Changes in extreme climate events in eastern China during 1960e2013: A case study of the Huaihe